A METHODOLOGY TO ENABLE CONCURRENT TRADE SPACE EXPLORATION OF SPACE CAMPAIGNS AND TRANSPORTATION SYSTEMS

A Dissertation
Presented to
The Academic Faculty

By

Akshay Prasad

In Partial Fulfillment
of the Requirements for the Degree
Doctor of Philosophy in the
School of Aerospace Engineering

Georgia Institute of Technology

December 2022

A METHODOLOGY TO ENABLE CONCURRENT TRADE SPACE EXPLORATION OF SPACE CAMPAIGNS AND TRANSPORTATION SYSTEMS

Approved By:

Professor Dimitri N. Mavris, Chair
School of Aerospace Engineering
Georgia Institute of Technology

Dr. Bradford E. Robertson
School of Aerospace Engineering
Georgia Institute of Technology

Professor Glenn Lightsey
School of Aerospace Engineering
Georgia Institute of Technology

Dr. Dale C. Arney
Space Mission Analysis Branch
NASA Langley Research Center

Professor Koki Ho
School of Aerospace Engineering
Georgia Institute of Technology

Date approved: November 30, 2022

Somewhere, something incredible is waiting to be known.

Carl Sagan

To my north stars, Anmol and Amli

ACKNOWLEDGMENTS

I would first like to thank Dr. Dimitri Mavris, who has been the foundation of every single one of my accomplishments throughout my ASDL journey. Through all the trials and tribulations that accompany an education at ASDL, you have made me a significantly better engineer, communicator, and most importantly, a better thinker. With your knowledge, wisdom, and guidance, I have been able to start my dream career at NASA so early on. Dr. Bradford Robertson has also been critical to my growth; thank you for all the time and feedback you have given over the years, as well as the opportunity to learn so much more about space than I thought was possible. I would also like to thank committee members Dr. Glenn Lightsey and Dr. Koki Ho, for their extremely valuable feedback regarding my research, which greatly improved its quality to what you see today.

There are so many people who helped me excel throughout my past six years in the ASDL. Without the entire space logistics team, especially Ms. Chloe Downs, the capability would not be where it is today, and by extension, this research itself; same goes for the DYREQT team. Mr. Manny Diaz, I wish we had met way sooner than we did; I consider you a very important mentor and a close friend. The countless hours we have spent talking about anything and everything, were nothing short of integral to me being the aerospace engineer I am today. I hope and cannot wait for our paths cross again in the future. I would also like to acknowledge Dr. Stephen Edwards, who helped me figure out the first steps in my career way back in undergrad.

The Space Mission Analysis Branch also deserves a huge acknowledgment for its role throughout my time in grad school. Dr. Dale Arney, you helped me as I started the process, with identifying potential topics, all the way through helping me polish this dissertation. You have been a great mentor and I look forward to working with you professionally at the branch. Mr. Kevin Earle, and the rest of branch leadership, no number of words can express how much I appreciated all the support I received from you throughout the whole

Ph.D. process. Because of you all, I was able to not only able to start and finish it without any worry, but allowed me to work on exactly what I wanted to work on at the branch throughout. I would also like to thank the rest of the branch, anyone who I have ever talked to about space, anyone who I have ever worked with, and especially anyone who has helped me while I worked on this thesis. I would also like to thank Mr. David R. Komar, who is a key reason for me finding my role and path at Langley.

None of this would have been possible without the monumental support from my family, especially my parents. You two gave me the opportunity to start on this journey by letting me move across the country nine years ago to go to Tech and pushing me to do nothing short of pursuing my passion. I felt nothing but unconditional love and support throughout and I am truly grateful. I haven't said it nearly as much as I should, but I love you.

Every single one of these people helped me along the way, but the only reason I was able to finish is because of my beloved partner, Anmol Sharma. Not a day goes by that I think about how much you have done for me the past few years. I have learned so much about myself and grown so much because of you. You gave me the confidence I needed to push through many tough times and finish strong. You are the absolute love of my life and I can't wait to go on many more adventures now, with you and Amli.

TABLE OF CONTENTS

LIST OF TABLES

LIST OF FIGURES

LIST OF ACRONYMS

ACO Ant Colony Optimization

ADP Approximate Dynamic Programming

AE Ascent Element

AIAA American Institute of Aeronautics and Astronautics

ASDL Aerospace Systems Design Lab

BB Branch and Bound

BC Branch and Cut

BFGS Broyden-Fletcher-Goldfarb-Shanno

BLAST Beyond LEO Architecture Sizing Tool

BLT Ballistic Lunar Transfer

CFM Cryogenic Fluid Management

CLO Campaign Logistics Optimization

CM Command Module

CMG Control Moment Gyros

ConOps Concept of Operations

DDTE Design, Development, Testing and Evaluation

DE Descent Element

DFP Davidon-Fletcher-Powell

DNC Did Not Converge

DoD Department of Defense

DRA 5 Design Reference Architecture 5.0

DYREQT Dynamic Rocket Equation Tool

ECLSS Environmental Control and Life Support Systems

EDL Entry, Descent, and Landing

EGO Efficient Global Optimization

EMC Evolvable Mars Campaign

EXAMINE Exploration Architecture Model for In-space and Earth-to-orbit

FoM Figures of Merit

FPI Fixed Point Iteration

FQ Formulation Questions

FSP Fission Surface Power

GEO Geostationary Orbit

GMCNF Generalized Multi-Commodity Network Flow

GSO Geosynchronous Orbit

HEO High Earth Orbit

HLS Human Landing System

$\mathbf{I_{sp}}$ Specific Impulse

IMF Inert Mass Fraction

IMLEO Initial Mass to Low Earth Orbit

IP Integer Programming

ISRU In-Situ Resource utilization

ISS International Space Station

LCC Life-Cycle Costs

$\mathbf{LCH_4}$ Liquid Methane

LEO Low Earth Orbit

LGA Lunar Gravity Assist

$\mathbf{LH_2}$ Liquid Hydrogen

LLO Low Lunar Orbit

LM Lunar Module

LMO Low Mars Orbit

LOI Level of Interest

LOx Liquid Oxygen

LP Linear Programming

LV Launch Vehicles

M2M Moon to Mars

MAST Mission Architecture Sizing Tool

MAUD Modular Analysis and Unified Derivatives

MAV Mars Ascent Vehicle

MBSE Model-based Systems Engineering

MCP Minimum Cost Problem

MDA Multidisciplinary Analysis

MDAO Multidisciplinary Analysis and Optimization

MDO Multidisciplinary Design Optimization

MEL Master Equipment List

MEO Medium Earth Orbit

MFP Maximum Flow Problem

MGA Mass Growth Allowance

MILP Mixed Integer Linear Programming

MINP Mixed Integer Nonlinear Programming

MIP Mixed Integer Programming

MIQP Mixed Integer Quadratic Programming

MIT Massachusetts Institute of Technology

MLI Multi-Layer Insulation

MOGA Multi-Objective Genetic Algorithm

MPCV Multi-Purpose Crew Vehicle

MPS Main Propulsion System

MT Magnetic Torquers

MTV Mars Transit Vehicle

NAFCOM NASA Air Force Cost Model

NASA National Aeronautics and Space Administration

NDP Network Design Problems

NFL National Football League

NLGS Nonlinear Gauss-Seidel

NLP Nonlinear Programming

NRHO Near Rectilinear Halo Orbit

NTP Nuclear Thermal Propulsion

NTR Nuclear Thermal Rocket

OEC Overall Evaluation Criterion

OFR Oxidizer to Fuel Ratio

PIP Pure Integer Programming

PMF Propellant Mass Fraction

RCS Reaction Control System

RSE Response Surface Equation

SA Simulated Annealing

SEC Space Exploration Campaign

SHAB Surface Habitat

SL Space Logistics

SLS Space Launch System

SM Service Module

SME Subject Matter Experts

SOFI Spray On Foam Insulation

SoI Sphere of Influence

SoS System of Systems

SPP Shortest Path Problem

SR1 Symmetric Rank 1

SSE Error Sum of Squares

STS Space Transportation Systems

sVTOL Small Vertical Takeoff and Landing

T2W Thrust to Weight Ratio

T_{SL}/W_{TO} Minimum Sea-level Static Thrust to Takeoff Weight Ratio

TE Transfer Element

TEGMCF Time-Expanded Generalized Multi-Commodity Flow

THAB Transit Habitat

TLI Trans-Lunar Injection

UAV Unmanned Aerial Vehicles

VSS Vehicle Sizing and Synthesis

W_{TO}/S Wing Loading at Takeoff

SUMMARY

Space exploration campaigns detail the ways and means to achieve goals for our human spaceflight programs. Significant strategic, financial, and programmatic investments over long timescales are required to execute them, and therefore must be justified to decision makers. To make an informed down-selection, many alternative campaign designs are presented at the conceptual-level, as a set and sequence of individual missions to perform that meets the goals and constraints of the campaign, either technical or programmatic. Each mission is executed by in-space transportation systems, which deliver either crew or cargo payloads to various destinations. Design of each of these transportation systems is highly dependent on campaign goals and even small changes in subsystem design parameters can prompt significant changes in the overall campaign strategy. However, the current state of the art describes campaign and vehicle design processes that are generally performed independently, which limits the ability to assess these sensitive impacts. The objective of this research is to establish a methodology for space exploration campaign design that represents transportation systems as a collection of subsystems and integrates its design process to enable concurrent trade space exploration. More specifically, the goal is to identify existing campaign and vehicle design processes to use as a foundation for improvement and eventual integration.

In the past two decades, researchers have adopted terrestrial logistics and supply chain optimization processes to the space campaign design problem by accounting for the challenges that accompany space travel. Fundamentally, a space campaign is formulated as a network design problem where destinations, such as orbits or surfaces of planetary bodies, are represented as nodes with the routes between them as arcs. The objective of this design problem is to optimize the flow of commodities within network using available transport systems. Given the dynamic nature and the number of commodities involved, each campaign can be modeled as a time-expanded, generalized multi-commodity network flow and

solved using a mixed integer programming algorithm. To address the challenge of modeling complex concept of operations (ConOps), this formulation was extended to include paths as a set of arcs, further enabling the inclusion of vehicle stacks and payload transfers in the campaign optimization process. Further, with the focus of transportation system within this research, the typical fixed orbital nodes in the logistics network are modified to represent ranges of orbits, categorized by their characteristic energy. This enables the vehicle design process to vary each orbit in the mission as it desires to find the best one per vehicle. By extension, once integrated, arc costs of ΔV and ΔT are updated each iteration. Once campaign goals and external constraints are included, the formulated campaign design process generates alternatives at the conceptual level, where each one identifies the optimal set and sequence of missions to perform.

Representing transportation systems as a collection of subsystems introduces challenges in the design of each vehicle, with a high degree of coupling between each subsystem as well as the driving mission. Additionally, sizing of each subsystem can have many inputs and outputs linked across the system, resulting in a complex, multi-disciplinary analysis, and optimization problem. By leveraging the ontology within the Dynamic Rocket Equation Tool, DYREQT, this problem can be solved rapidly by defining each system as a hierarchy of elements and subelements, the latter corresponding to external subsystem-level sizing models. DYREQT also enables the construction of individual missions as a series of events, which can be directly driven and generated by the mission set found by the campaign optimization process. This process produces sized vehicles iteratively by using the mission input, subsystem level sizing models, and the ideal rocket equation.

By conducting a literature review of campaign and vehicle design processes, the different pieces of the overall methodology are identified, but not the structure. The specific iterative solver, the corresponding convergence criteria, and initialization scheme are the primary areas for experimentation of this thesis. Using NASA's reference 3-element Human Landing System campaign, the results of these experiments show that the methodology

performs best with the vehicle sizing and synthesis process initializing and a path guess that minimizes ΔV. Further, a converged solution is found faster using non-linear Gauss Seidel fixed point iteration over Jacobi and set of convergence criteria that covers vehicle masses and mission data.

To show improvement over the state of the art, and how it enables concurrent trade studies, this methodology is used at scale in a demonstration using NASA's Design Reference Architecture 5.0. The LH_2 Nuclear Thermal Propulsion (NTP) option is traded with NH_3 and H_2O at the vehicle-level as a way to show the impacts of alternative propellants on the vehicle sizing and campaign strategy. Martian surface stay duration is traded at the campaign-level through two options: long-stay and short-stay. The methodology was able to produce four alternative campaigns over the course of two weeks, which provided data about the launch and aggregation strategy, mission profiles, high-level figures of merit, and subsystem-level vehicle sizes for each alternative. Expectedly, with their lower I_{sp}'s, alternative NTP propellants showed significant growth in the overall mass required to execute each campaign, subsequently represented the number of drop tanks and launches. Further, the short-stay campaign option showed a similar overall mass required compared to its long-stay counterpart, but higher overall costs even given the fewer elements required. Both trade studies supported the overall hypothesis and that integrating the campaign and vehicle design processes addresses the coupling between then and directly shows the impacts of their sensitivities on each other. As a result, the research objective was fulfilled by producing a methodology that was able to address the key gaps identified in the current state of the art.

THESIS STRUCTURE

The logic structure of this dissertation and how it drives the organization of this document is summarized in the following figure. Chapter 1 provides an introduction to Space Exploration Campaigns and the motivations for integration of its design with that of transportation systems using an initial literature review. It identifies the key gap to be filled and the overarching objective of the research. Decomposition of the research objective guides deeper dive into literature for space campaign design and transportation systems design in Chapter 2 and Chapter 3, respectively. Both chapters identify the different pieces required of the overall methodology and state formal questions this research aims to answer. A plan is established in Chapter 4 to formulate hypotheses and answer these questions through experimentation using a small-scale space campaign. The final methodology is assembled using these experimental results, which is used to perform a large-scale Mars campaign design and integrated trade study in Chapter 5. The document concludes with an additional chapter, Chapter 6, to present the specific impacts and contributions of this research and areas for further growth.

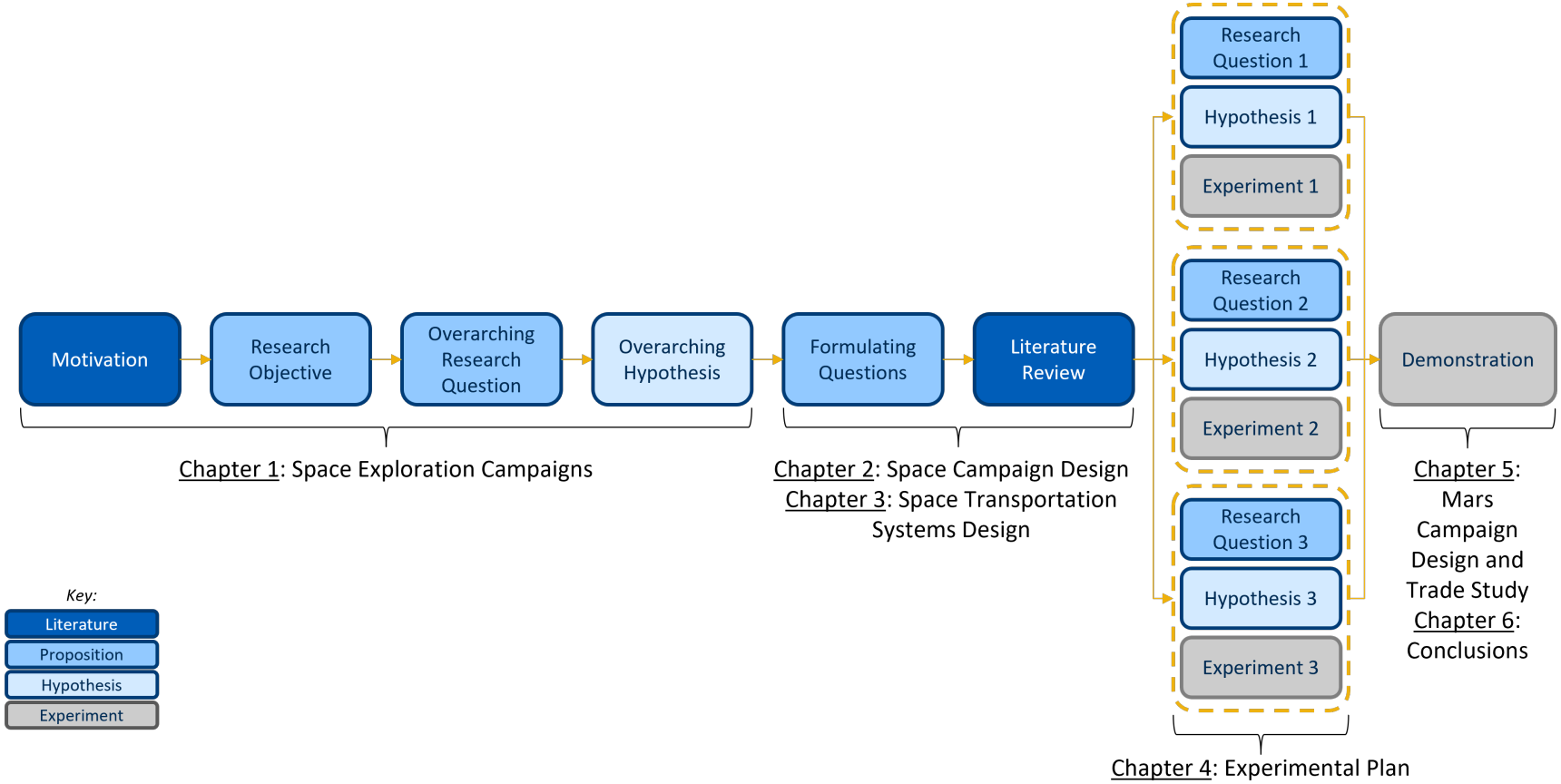
Motivation
Research Objective
Overarching Research Question
Overarching Hypothesis
Formulating Questions
Literature Review
Research Question 1
Hypothesis 1
Experiment 1
Research Question 2
Hypothesis 2
Experiment 2
Research Question 3
Hypothesis 3
Experiment 3
Demonstration
Chapter 1: Space Exploration Campaigns
Chapter 2: Space Campaign Design
Chapter 3: Space Transportation Systems Design
Chapter 4: Experimental Plan
Chapter 5: Mars Campaign Design and Trade Study
Chapter 6: Conclusions
Key:
Literature
Proposition
Hypothesis
Experiment

1
SPACE EXPLORATION CAMPAIGNS

Ever since humans first set foot on the Moon just over 50 years ago, the desire to expand physical presence in space has been growing. The initial completion of the International Space Station (ISS) in 2011 established our permanent presence in Low Earth Orbit (LEO) and since then, space agencies across the world have been setting their sights beyond, to the Moon, Mars and even Near Earth Asteroids [1]. In December of 2017, the United States released Space Policy Directive 1, which states "the United States will lead the return of humans to the Moon for long-term exploration and utilization, followed by human missions to Mars and other destinations" [2]. Although this set lunar exploration as the near term goal, consistent messaging has put Mars as the horizon goal. In response, the National Aeronautics and Space Administration (NASA) has introduced Artemis, the official program to return humans to the Moon by 2024 and set up a lunar base for further exploration. The Moon to Mars (M2M) campaign is a higher-level initiative to use the Moon as a stepping stone for future Mars missions, specifically to demonstrate applicable deep space and surface systems [3, 4].

This Space Exploration Campaign (SEC) is the most recent of many previous attempts at detailing the ways and means to achieve long-term goals of human space exploration. Adapted from NASA and the United States Department of Defense (DoD), a campaign can be defined as "a series of inter-related individual missions performed, aimed at achieving specific strategic goals for space exploration."[5, 6, 7] Space campaigns are significant technical and programmatic investments that involve the planning, design, development, and execution of spaceflights from LEO to Mars. These spaceflights can have many different types of payloads, though always falling in either crew or cargo categories. Payloads drive the design and analysis of space transportation systems and missions, with the goal

of being paired with one or more Launch Vehicles (LV) to put them in orbit. The operations of these transportation systems, hereby referred interchangeably with "vehicles" in this disseration, over the course of many missions achieve the set campaign goals.

A prominent example of a SEC is detailed within NASA's Design Reference Architecture 5.0 (DRA 5), released in 2008 which has been a long-standing reference as one of the most well documented campaigns to date for long duration, crewed Mars Exploration [8]. Within it, engineers at NASA decompose set goals to understand requirements for all elements within the campaign. These requirements provide the basis for designs, trades, and analyses that were performed for the necessary systems and a crew of 6 on a ∼1,500 day roundtrip mission. Figure 1.1 shows the high level Concept of Operations (ConOps) of the DRA 5 mission using a Nuclear Thermal Propulsion (NTP) transportation system. The ConOps is a summarizing visual of the overall campaign architecture, highlighting the different elements within and how they interact with each other [9].

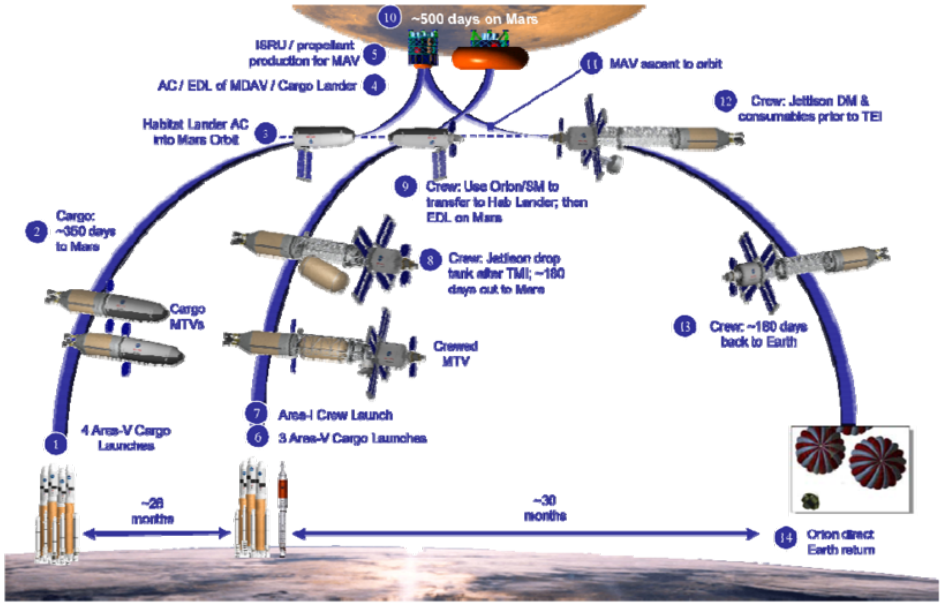

Figure 1.1: Mars DRA 5 ConOps for a nuclear thermal transportation system [8]

The overarching goal of the campaign is stated at the top, of ∼500 days on the Martian surface. Several vehicles are proposed to meet this goal, both crewed and uncrewed, paired

with the sequence of missions they fly. The set of launch vehicles chosen to assemble those vehicles are identified and an overall timeline for the campaign is established. DRA 5's campaign called for a total of 850 metric tons of Initial Mass to Low Earth Orbit (IMLEO) to execute all the necessary missions.

1.1 Challenges of Space Exploration Campaigns

1.1.1 Financial Costs

Given the unprecedented amount of mass required for a crewed Mars mission and the cost of access to LEO, SECs are significant financial investments for many organizations. Although NASA did not publish any official dollar cost estimates for DRA 5, mass can be used as a surrogate metric. LEO departure mass for a single crewed Mars mission is equivalent to 12 International Space Stations, as shown in Figure 1.2, and about 37 Saturn V launches [10].

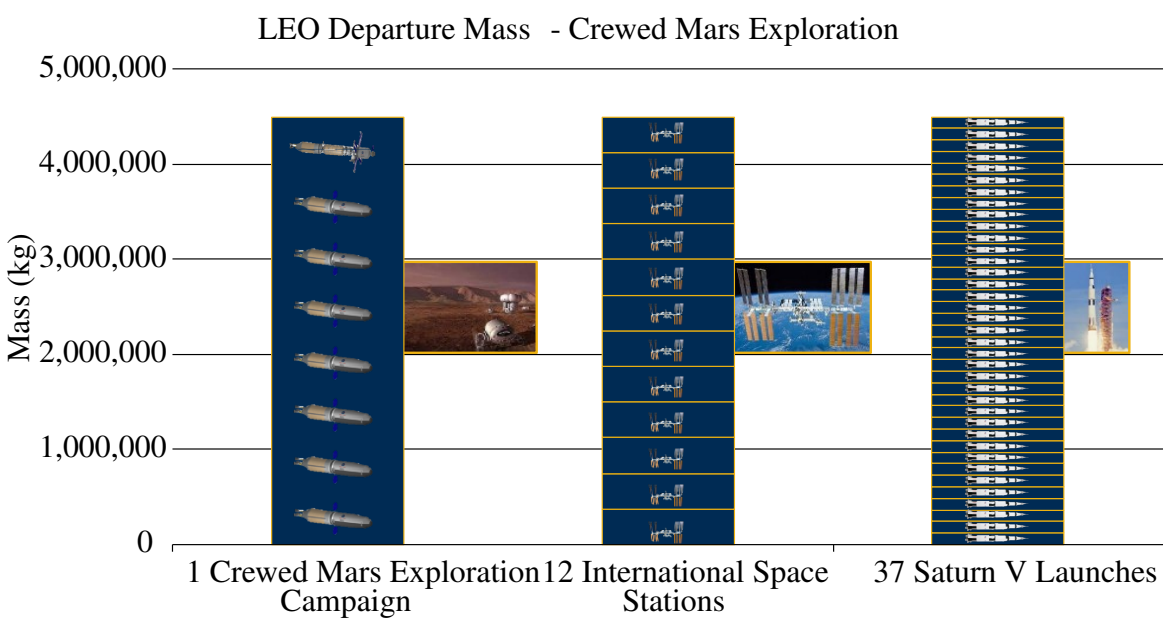

Figure 1.2: Crewed Mars exploration LEO departure mass as compared to the ISS and Saturn V [10].

From the start of the program to a previously projected end date of 2015, the ISS has cost about FY19 $150 billion and a single Saturn V launch costed NASA about FY19 $1.23

billion [11, 12]. Historically, NASA's budget has only been a small fraction of the federal budget, peaking to 4.41% during the Apollo program, shown in Figure 1.3. Recent trends predict that this fraction will stay relatively constant over the next few years, and with a federal budget of FY19 $3.5 trillion, a crewed Mars exploration mission would require a budget orders of magnitude higher.

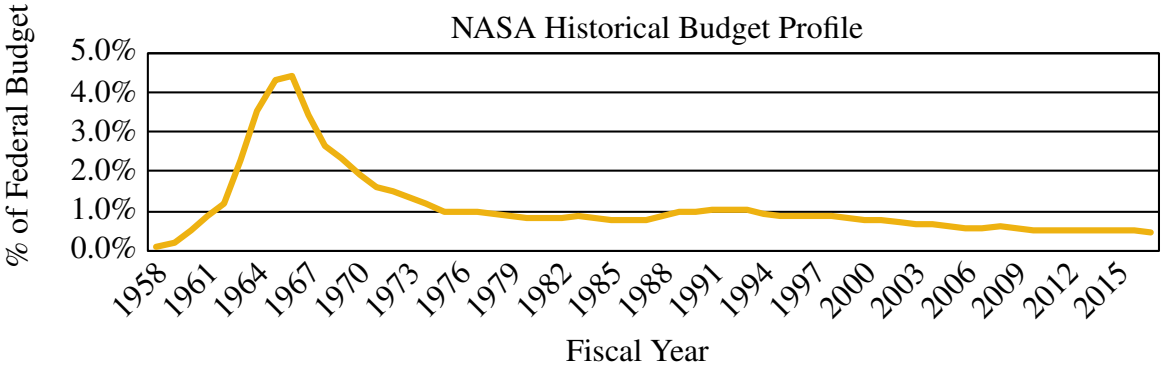

Figure 1.3: NASA's historical budget profile as a fraction of the total federal budget.

Therefore, to execute a SEC, these costs must be justified to stakeholders through details of the campaign and its elements as early in the design process as possible, with many alternatives and their level of "goodness" relative to each other. Efforts to synergize the campaign with other present or future space exploration programs will be important to minimize independent development costs, as seen in the M2M campaign. A key strategy of the lunar exploration campaign is to identify elements and capabilities that can be repurposed or leveraged for Mars, rather than developing new systems from the ground up. This approach will increase affordability and reduce risk of the overall campaign by decreasing reliance on completely new systems.

1.1.2 Campaign Timescales

The financial costs associated with executing SEC are accompanied by temporal costs. DRA 5 estimated its Mars campaign would required 7 years to execute, end-to-end, whereas the M2M is estimated to last more than 10 years [8, 13]. As goals of SECs are achieved long after they are set and development programs for elements have begun, chosen goals

and campaign plans will lock in future investments in required capabilities and assets. The Space Launch System (SLS) is a Space Shuttle-derived, expendable, super-heavy class launch vehicle that has been under development by NASA since 2011. After replacing several previous launch vehicles that were under development at the time, SLS was intended to be at the core of NASA's deep space exploration plans throughout the decade [14]. SLS was also paired with the Orion Multi-Purpose Crew Vehicle (MPCV), a crewed deep space capsule to ferry astronauts between Earth and cis-lunar space. These two elements are critical pieces of the overall M2M campaign that were initially selected a decade ago and now influence any future plans, regardless of the destination.

Technology developments are key enablers of a space campaign, as they help to augment the capabilities of existing assets like SLS and Orion. Viability of the long duration crewed Mars exploration campaign in DRA 5 was dependent on the infusion of 65 key technologies [8]. Development programs for each of these 65 technologies would be on the critical path for successful completion of the campaign, further contributing to the temporal and financial costs.

1.1.3 Increasing Complexities

During the first few decades of space exploration, missions were relatively as simple as placing a satellite into orbit. As human spaceflights began, they followed a similar structure of placing humans into orbit and returning them safely home. They quickly grew more complex in nature, in which each subsequent mission attempted to hit increasingly important goals, such as on-orbit rendezvous and docking, spacewalks, and all the way to:

> *"...landing a man on the moon and returning him safely to the Earth."*
>
> – J. F. Kennedy, *Address to Joint Session of Congress, 1961*[15]

Apollo operated by using the super-heavy launch vehicle, Saturn V, to launch and carry along all elements required for the mission, end-to-end. Apollo 11 launched the crew and the three different elements, Command Module (CM), Lunar Module (LM), Service

Module (SM). The SM housed the power, propulsion, and Environmental Control and Life Support Systems (ECLSS) for the CM and its cabin for three astronauts, which is the only module returned to Earth. The LM integrated the lander and the ascent module for two of the astronauts, while the third stayed in orbit in the CM.

Soon after, NASA designed and built a reusable vehicle, the Space Shuttle, with the purpose of building a modular space station in LEO and establishing a permanent presence. This ISS was built over the course of several decades, and with cooperation of international partners, has been mostly continuously inhabited since then. Regular resupply missions from Earth ensure that the crew, who rotate every few months to year, have all necessary resources.

These two approaches used between Apollo and the ISS are fundamentally different from an operational perspective, in which Apollo can be considered as a "carry-along" strategy and the ISS a "resupply" strategy [16]. Future space exploration missions have the potential to operate on a completely different paradigm, one that is highly dependent on the resources available on other planetary bodies but also a combination of the previous two, as depicted in Figure 1.4. Figure 1.2 shows that a Mars mission is extremely massive, and given that Mars is on average, 200 times as far as the Moon, the level of operational difficulty of future campaigns is apparent.

1.1.4 Campaign-level Decision Making

Compounding these financial expenses, long temporal nature, and increasing complexities of SEC show that they investments into the future of a larger space exploration endeavor. Decision makers are given many alternative campaigns up front to make an informed down-selection, usually at the pre-conceptual to conceptual level of design [17]. Comparing alternatives requires information about each campaign's performance, affordability, and risk. Performance can be summarized by high level Figures of Merit (FoM) that include: number of launches, Life-Cycle Costs (LCC), sustainability, and more. An end-to-end

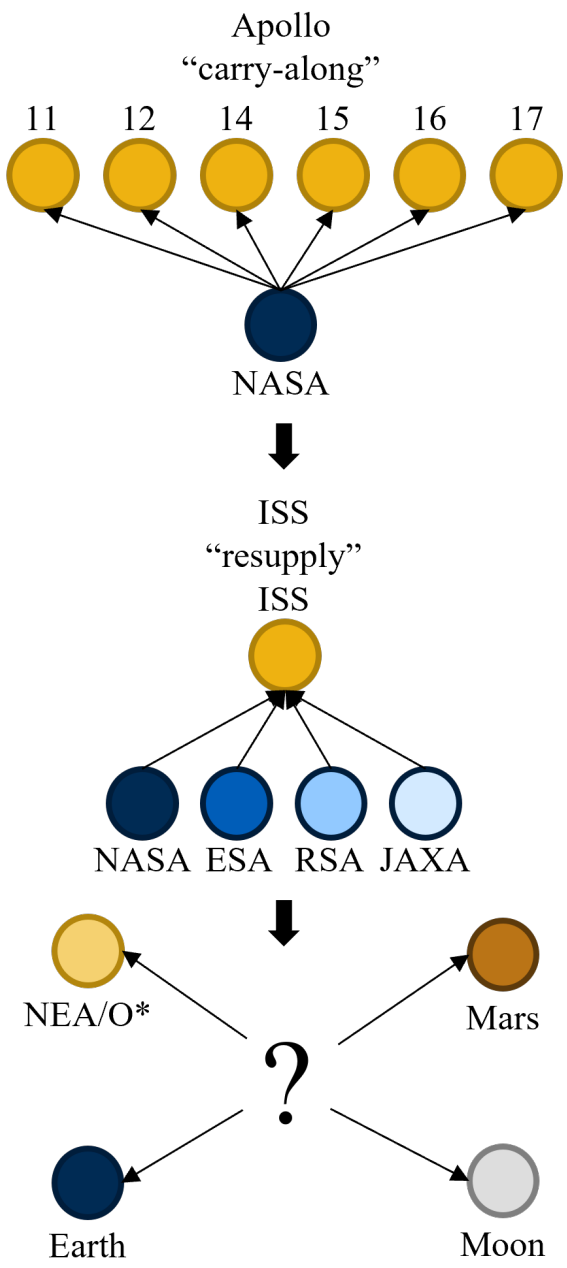

Figure 1.4: Diagram showing the different operational strategies of space campaigns over the years.

campaign design will translate and roll up many technical performance metrics into these higher level metrics. As a result, the campaign must include the design of all elements within it, such as the vehicles, payloads, trajectories, and more.

1.2 Space Campaign Design Problem

As defined previously, a SEC is a series of inter-related individual missions performed, aimed at achieving specific strategic goals for space exploration. Building a space campaign architecture first starts with identifying the highest-level goals and understanding the required set and sequence of missions to achieve them. Thus, missions can be thought of as the first-level decomposition of a SEC, shown in Figure 1.5. Further, each mission will need to transfer payloads to or from destinations, or both ways if the requirement is a roundtrip.

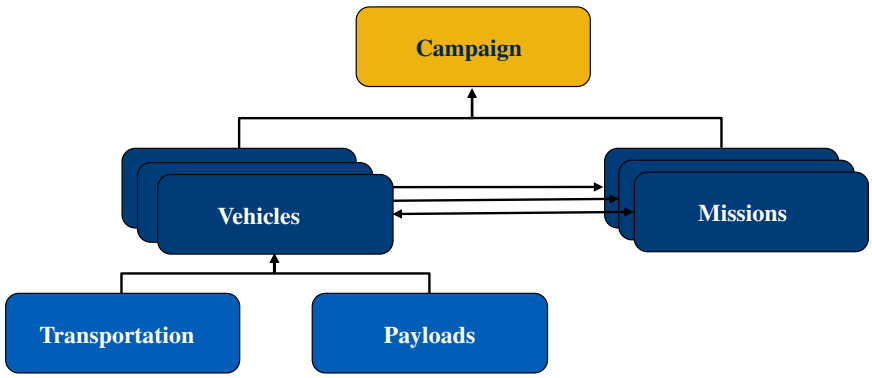

Figure 1.5: Decomposition of a campaign into its physical and functional elements.

These payloads could be crew or cargo, depending on the specific mission being performed, and can be functionally treated as the carried loads that require separate transportation systems to move them. Design of transportation systems depend heavily on the missions they fly but can be categorized into three main types that are shown in Table 1.1.

Regardless of the mission or transportation type, a vehicle can be defined as a paring of a transportation system and a payload. All previous proposed campaigns have called for the use of one or more of these vehicles. Thus, vehicles can be considered key enablers of SECs, and their significance is independent of the campaigns' goals, overall strategy, and payloads within. This leads to the first observation of this thesis:

Observation 1: Vehicle design choices are driven by campaign goals and the mission set within.

Table 1.1: Table of mission types in a campaign, their physical descriptions and the type of vehicle responsible for performing the mission.

Mission Type	**Event**	**Description**	**Transportation Type**
Surface to Space	Launch	Inserting payloads into orbit from the surface of a planetary body	Launch Vehicle
Space to Space	Transfer	Transporting payloads from one orbit to another	In-Space Transportation
Space to Surface	Entry, Descent and Landing	Landing payloads onto the surface of a planetary body	Descent Stage/Capsule

The trade space for vehicle architectures and mission architectures each can contain an exhaustive number of discrete options. [8] For each discrete architecture selection, there exists a continuous design space that can be explored, creating a very computationally expensive design problem. Although setting specific campaign goals can narrow down the available options, it does so only very slightly.

To understand the importance of vehicles within a SEC, the previous decomposition of a campaign in Figure 1.5 can be expanded, as shown in Figure 1.6 [18]. Trent defines campaigns as a group of architectures, which are pairings of missions and the vehicles performing them. This sets campaign design as a systems of systems problem that involves identifying and understanding the interactions and dependencies between elements at all levels. A final solution of this process would be the optimal set and sequence of architectures to achieve set campaign goals.

Decomposing further, each pairing of a mission and vehicle is a complex, systems-level Multidisciplinary Analysis and Optimization (MDAO) problem, requiring the sizing and synthesis of many different individual subsystems [19]. Sizing is highly coupled with mission design due to the underlying physics of orbital mechanics as well as the composition of many individual events within a single mission.

Although the vehicle sizing problem can be analyzed independently, the final selection of mission profiles and in-space vehicles are constrained by available launch vehicles

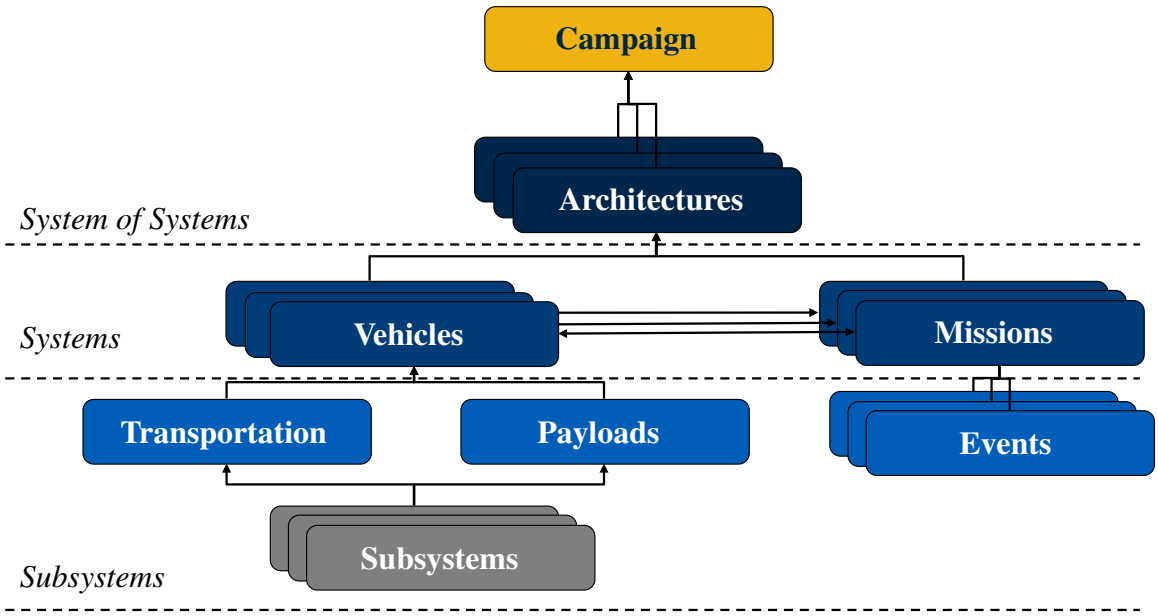

Figure 1.6: Further decomposition of a campaign into its physical and functional elements to show the different levels of systems, adapted from [18].

and their performance capabilities. All campaign problems are additionally constrained by programmatic factors such as design and development timelines, cost and schedules, stakeholder needs and concerns, and commercial and international partnerships. Aggregating these challenges within the campaign design problem can complicate the process for finding one or more potential solutions.

Observation 1 established that the design of a vehicle within the campaign is dependent on the chosen campaign goals. While the previous decomposition of the campaign problem identified the relationship between vehicles and the overall campaign, it is also important to understand the sensitivity of this relationship. For example, crewed vehicles tend to be much heavier than their cargo counterparts, making robotic exploration programs far less costly than crewed ones [10]. Establishing a long-term, surface presence on a planetary body needs many launches, as seen shown by the latest M2M manifest in Figure 1.7 [20].

In contrast, vehicle designs can still vary greatly for a single destination, as seen by previous Mars campaign concepts [21]. Figure 1.8 shows four different transportation ar-

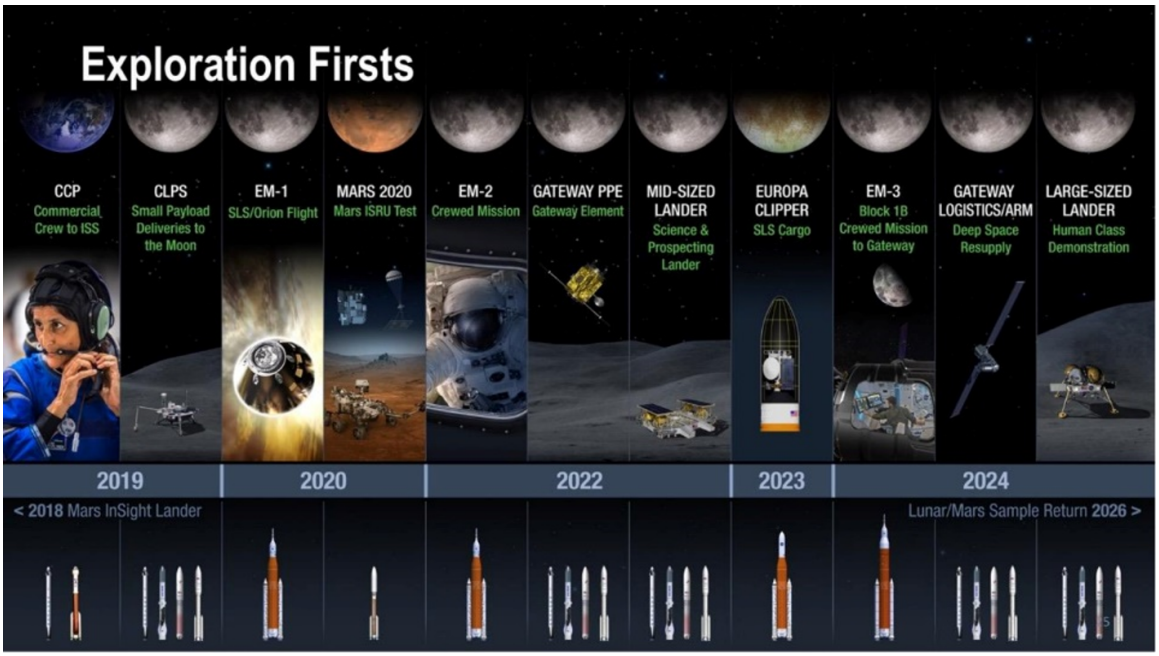

Figure 1.7: Moon 2 Mars program launch manifest through 2026 [20].

chitecture for a Mars campaign, where each one is vastly different from others in terms of design characteristics and performance.

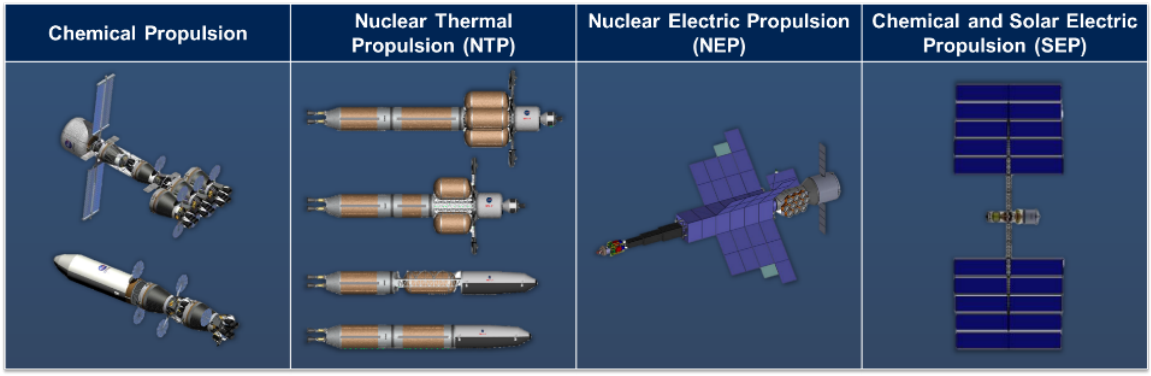

Figure 1.8: Previous Mars transportation architectures and concepts.

Since NASA's SLS had been chosen as the human rated launch vehicle for future crewed missions, its capabilities place limits on how much mass and volume can be thrown to orbit. Similarly, Orion's design does not allow for it fly beyond lunar orbit. Deciding on a vehicle to build will narrow the scope of any future campaign design and planning, leading to the next observation:

Observation 2: Previous vehicle investments constrain campaign design space.

Observations 1 and 2, together, provide the basis for the third observation:

Observation 3: The design of a space campaign is highly coupled with the design of vehicles used within.

Current state of the art for the design of conceptual-level space exploration campaigns describe two main methods, highlighted in Table 1.2

Table 1.2: Two main methods of conceptual campaign design and the organizations utilizing them.

Method	Organizations
Campaign Analysis	NASA
Space Logistics Network Formulation	MIT, Illinois, Georgia Tech

NASA documents their campaign analysis capability as a process that evaluates the performance of exploration scenarios over the full life-cycle of the campaign [7, 17]. The three main areas assessed are system performance, affordability, and risk. Campaign scenarios are driven by past work and trade spaces are filtered by hand through subject matter expertise, resulting in the exploration of only a few alternatives. An example of this process is depicted by the top level transportation architecture trade tree in DRA 5, Figure 1.9. Vehicle design is performed independently, after parts of the trade tree has been trimmed, meaning any changes in the campaign or vehicle designs have to be assessed manually.

This method provides a basis for the identification of a broad gap in the current state of the art:

Broad Gap 1: Space transportation systems are traditionally designed separately, after campaign designers have set individual mission requirements which limits the ability to rapidly assess changes.

Space logistics is a recent area within the space campaign domain that has adopted methods from terrestrial logistics and supply chain research. It applies a network-based

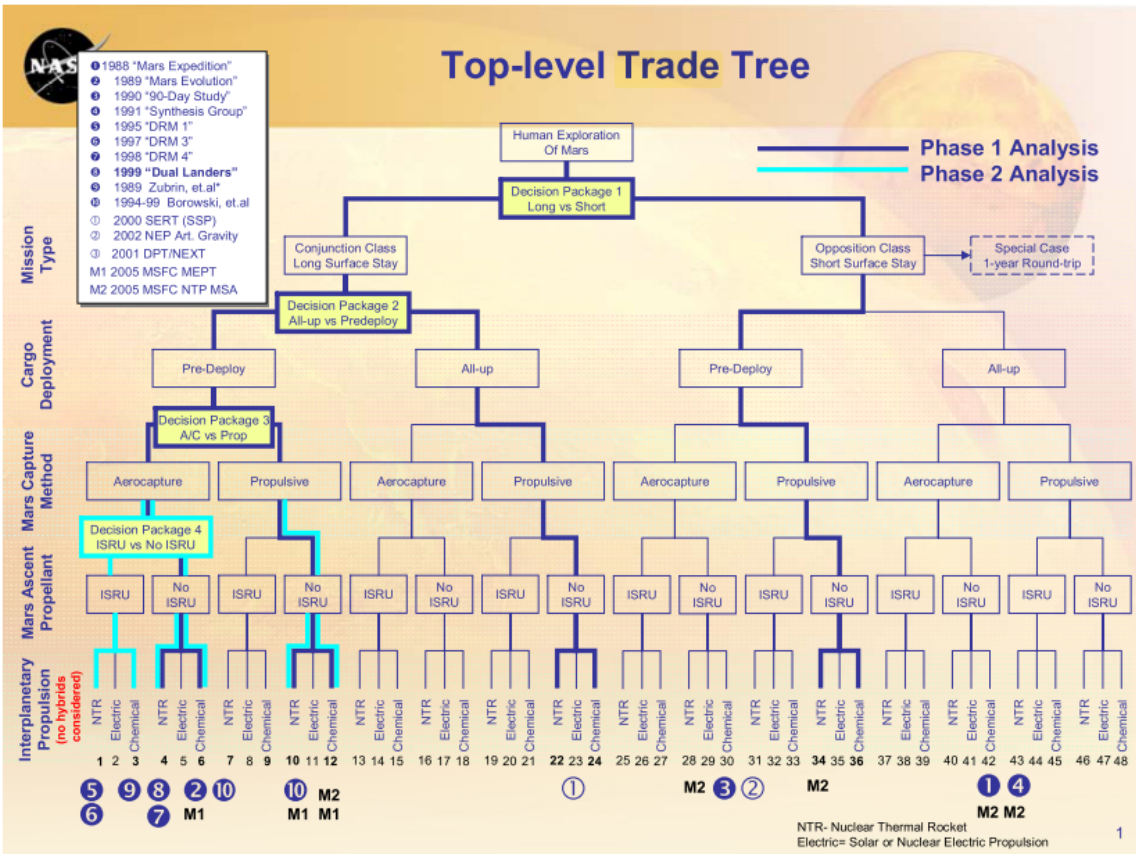

Figure 1.9: DRA 5's top-level in-space transportation architecture trade tree [8].

approach to model destinations as nodes and paths between them as arcs. An example Earth-Moon-Mars network is depicted in Figure 1.10, showing the different orbits, bodies as destinations and the possible transfers between them.

Depending on the network model and problem definition, different mathematical processes are applied to solve the network. These solutions are in the form of necessary flow of resources between the nodes, through their arcs, that satisfy any constraints and achieve high level campaign requirements. Final flows are then used to drive requirements on payloads and accompanying transportation systems.

The Campaign Analysis process by NASA details that vehicle sizing and synthesis is done, but the campaign itself is manifested by hand using generated point designs [22]. This means that the optimal set of architectures may not be explored. Furthermore, the direct impact of the vehicle on the campaign design is unknown without manually updating

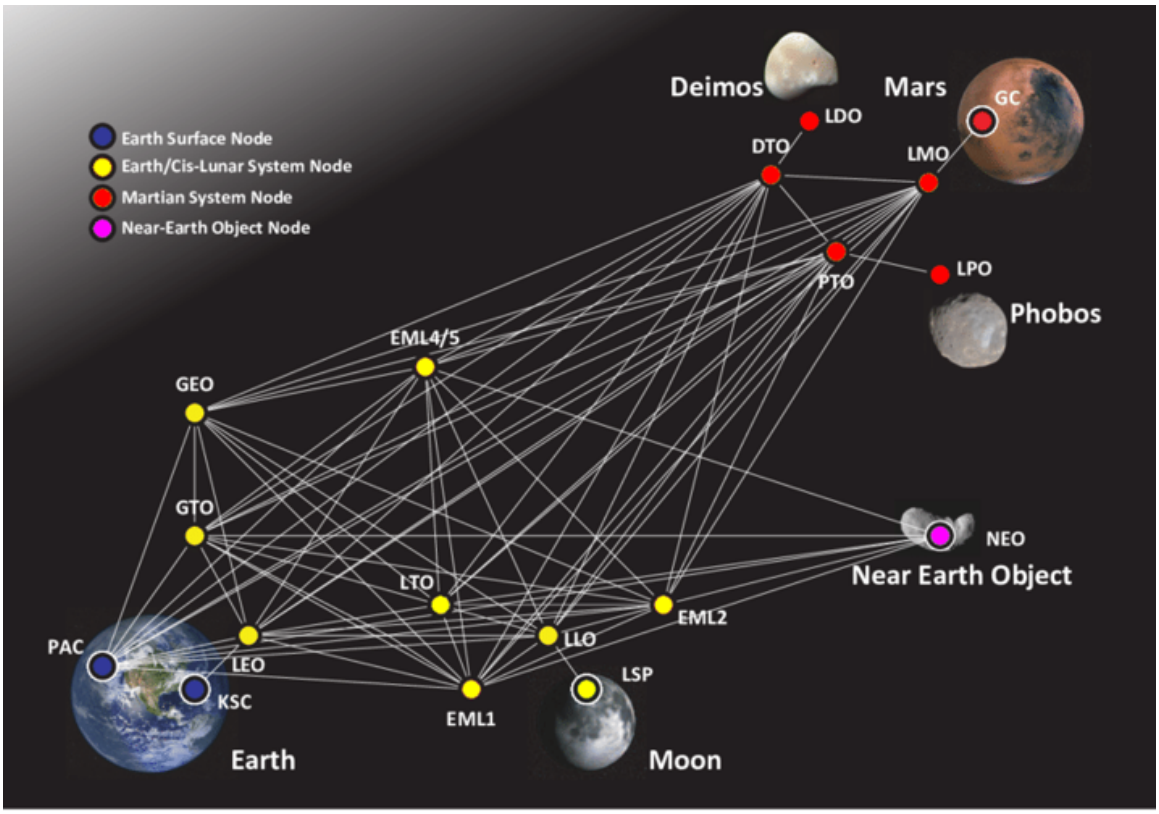

Figure 1.10: An example Earth-Moon-Mars network within a Space Logistics Network Formulation

the campaign. In contrast, the Space Logistics formulations typically use historical regressions or simplified equations to size vehicles as a way to reduce computational time and complexity [23, 24]. The mission design is also simplified using assumptions for similar reasons. In parallel with NASA's method, the direct impact of the campaign on the vehicle design is difficult to assess, leading the to the identification of another broad gap:

Broad Gap 2: Though a space vehicle is made up of many subsystems, processes for conceptual design of space campaigns simplify their representation within the problem to reduce computational complexity and enable rapid generation of campaign alternatives.

1.3 Identified Gaps and Research Objective

The previous sections document the overarching motivations for this research by identifying three key observations and two broad gaps within literature:

Observation 1: Vehicle design choices are driven by campaign goals and the mission set within.

Observation 2: Previous vehicle investments constrain campaign design space.

Observation 3: The design of a space campaign is highly coupled with the design of vehicles used within.

Broad Gap 1: Space transportation systems are traditionally designed separately after campaign designers have set individual mission requirements which limits the ability to rapidly assess changes.

Broad Gap 2: Though a space vehicle is made up of many subsystems, processes for conceptual design of space campaigns simplify their representation within the problem to reduce computational complexity and enable rapid generation of campaign alternatives.

These two broad gaps can be generalized to state an overarching key gap in the current state of the art for campaign and vehicle design:

Key Gap: Although space vehicles are highly coupled to campaigns, their designs are generally performed independently which limits (1) the quality of each campaign solution and (2) the ability to perform integrated trade space exploration.

To fill this gap, the **Research Objective** is formally stated as follows:

Research Objective: Establish a methodology for space exploration campaign design that represents a transportation system as a collection of subsystems and integrates its design process to enable concurrent trade space exploration.

This research aims to assemble a methodology to conduct campaign trades at the vehicle level, supported by sizing at the subsystem level, and shall enable designers to answer questions such as:

- How does a change in the vehicle architecture(s) impact the overall campaign?
- How does a change in campaign strategy affect the required vehicle(s) design?

The thesis structure introduced in the beginning of the document can be broken down and filled in to show the logic used to identify this Research Objective, shown in Figure 1.11.

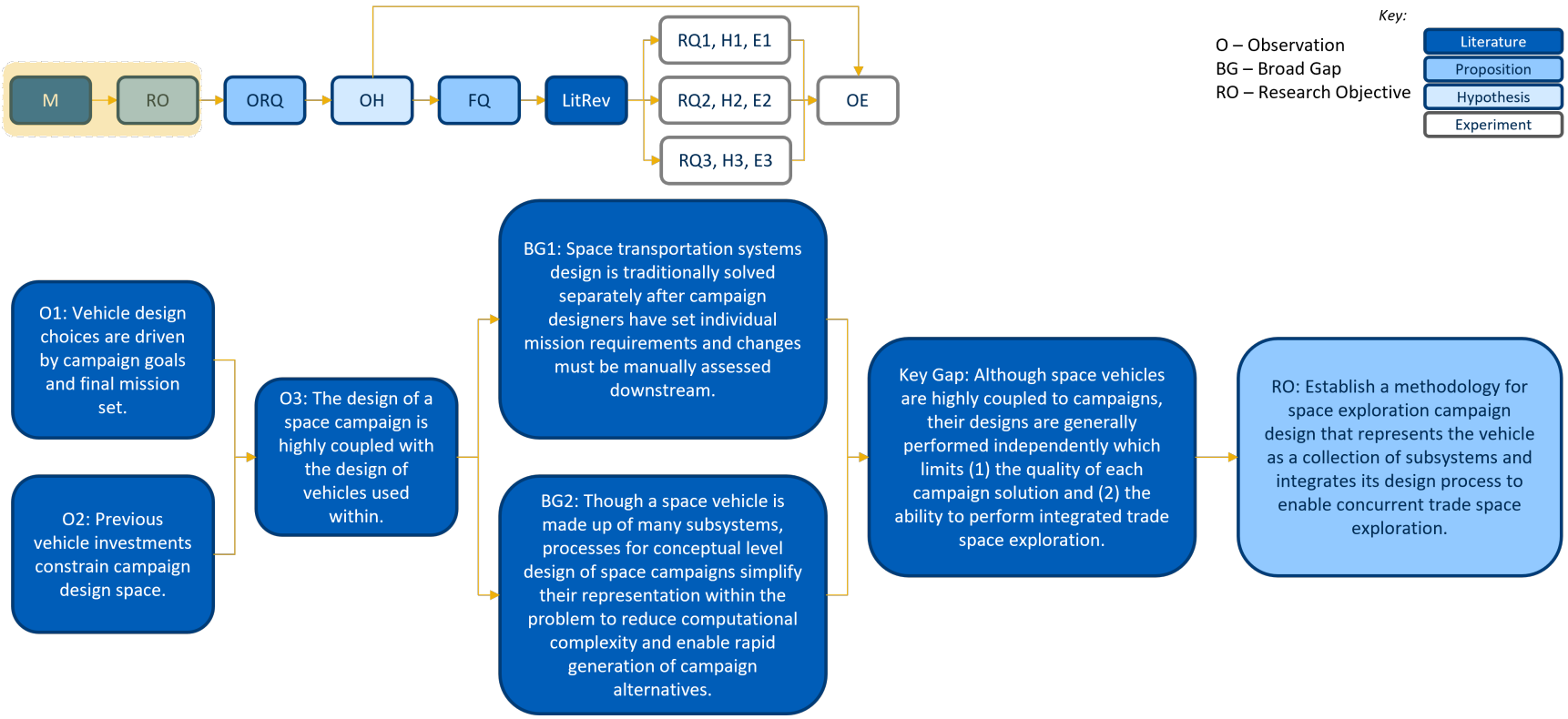

Figure 1.11: Thesis structure up through the Research Objective.

Two main questions need to be answered to fulfill the Research Objective and identify a capable methodology:

Overarching Research Question 1: How can campaign and vehicle design processes be linked to explore the sensitivities of their designs on each other?

Overarching Research Question 2: How does the integrated process improve the current state of the art?

The fully developed methodology will be used to test the overarching hypothesis of this research, stated as:

Overarching Hypothesis: If the Campaign Logistics Optimization (CLO) and Vehicle Sizing and Synthesis (VSS) processes are integrated, then impacts of the vehicle and campaign trades on each other can be directly quantified.

To appropriately fulfill the **Research Objective**, it is necessary to establish the scope of this before proceeding. The goal is to identify individual processes for campaign and vehicle design that addresses most of the challenges surrounding their own problems while also finding the formal methods of integration between them. Figure 1.12 shows a notional, high-level process diagram that describes the main purpose of the campaign and vehicle design processes. Using some stated goals, the identified campaign design processes should be able to find the optimal set and sequence of missions to perform to achieve those goals. The vehicle design process should then take that set and size each vehicle in the campaign individually at the subsystem level.

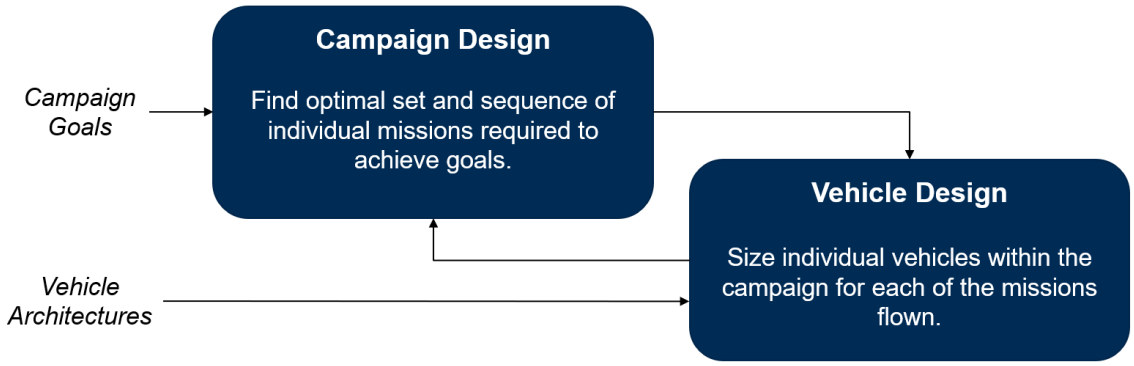

Figure 1.12: Thesis structure up through the Research Objective.

Figure 1.12 can further be used to guide the scope of the literature review by identifying three main resulting questions:

- **Formulation Question 1:** How is the campaign design problem formulated and solved today?
- **Formulation Question 2:** How is conceptual level design of space vehicles done today?
- **Formulation Question 3:** How are the two individual, but coupled problems integrated?

Chapter 2 and Chapter 3 provide a literature review to answer these three questions while the following chapter introduces the formal **Research Questions** of this thesis and the accompanying experimental plan to answer them. Once again, the thesis structure can be updated, shown in Figure 1.13.

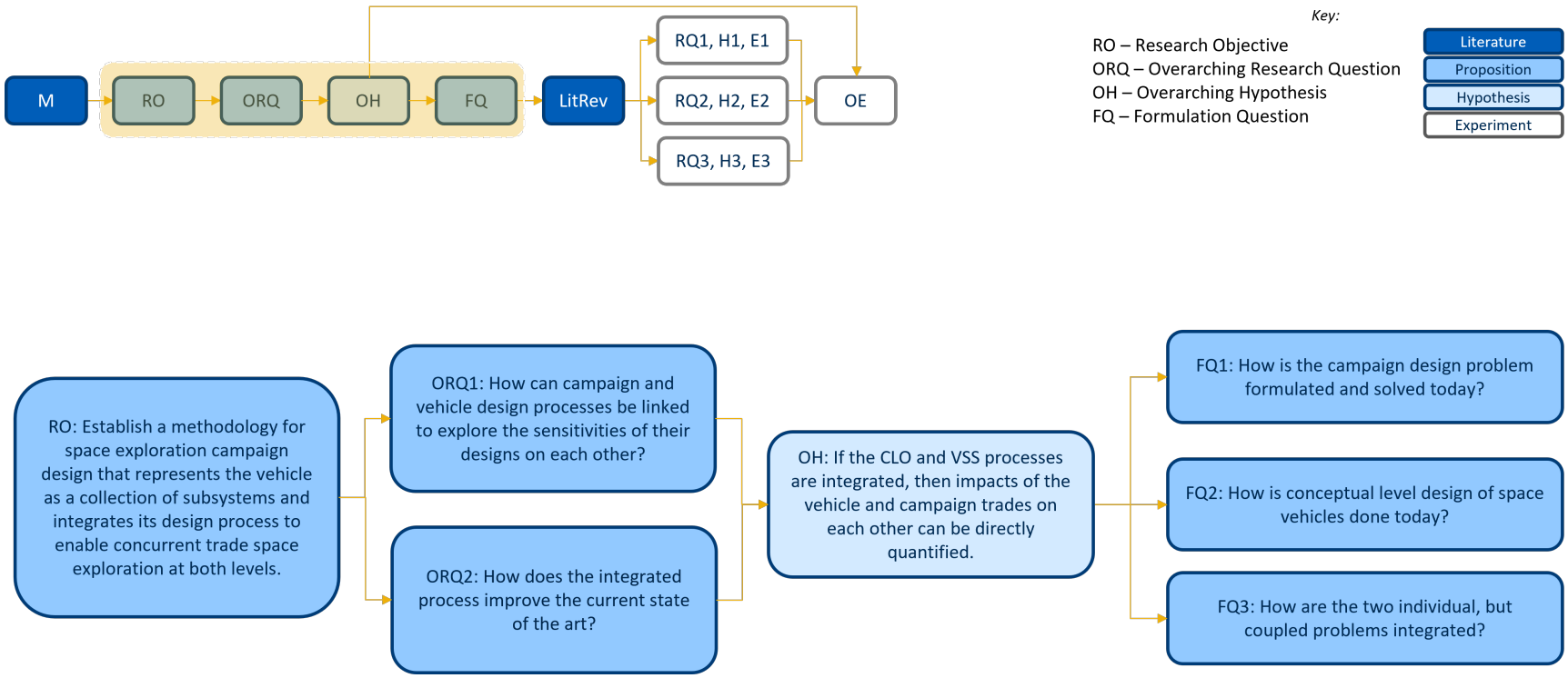

Figure 1.13: Decomposition of the Research Objective to identify the motivating questions for a deep dive literature review.

2
SPACE CAMPAIGN DESIGN

2.1 Requirements for an Integrated Process

Formulating Question 1 sets the scope of this chapter, a review of previous and current methods for SEC design, with the goal of identifying one for integration with vehicle design, either directly or with some modifications. As an initial step in formulating this proposed capability, requirements must be set on the entire method and decomposed to its piece-parts. Driven by decision-makers desiring more information early in the design process, the first key feature is the rapid generation of alternatives at the conceptual level. Rapid implementation of technical- and programmatic-level problem constraints to conduct quick design reassessments would be advantageous for allowing flexibility in decision-maker requests. Among others, examples of technical constraints would include a specific cadence for a launch vehicle and its provider, vehicle aggregation orbits, or the Earth-Mars opportunity windows. Similarly, programmatic constraints could be financial cost, overall timelines, and previous vehicle investments.

Given the critical role of a vehicle within a campaign and in this thesis, a subsystem-level representation would be required to properly perform any vehicle trades and assess their impacts on the overall campaign. Consequently, the integrated methodology should have the ability to explore campaign and vehicle trades space and assess impacts on each other; a requirement that is key to achieving the overall research objective.

2.2 Requirements for Campaign Design

Decomposing the formal set of requirements from Section 2.1 can establish following set for the one of two distinct processes necessary for this method: campaign design. Fore-

most, the purpose of a campaign design process is to find the optimal set and sequence of missions to perform that will achieve all set goals and requirements. These requirements set demands for the flow of many resources throughout the campaign, from payloads to crew and everything necessary to support them. As the scale of space exploration continues to increase, campaigns will need to employ increasingly complex ConOps to reduce overall mass as much as possible. These include, but are not limited to: rendezvous of many elements, in-space refueling, reuse and repurposing of elements. Although it maybe more computationally expensive, those operations would additionally require the use of a dynamic model as opposed to a static one. Finally, as the industry sets its aim towards Mars, this design process should be capable of analyzing operations within Earth and Mars spheres of influence, and transits between them.

2.3 NASA: Campaign Analysis

Although NASA has set the near-term goal for its human spaceflight program to be the Moon, it still considers Mars to be the horizon goal. Along with other organizations, NASA has half-century long history of mission planning for the red planet [25, 26]. Latest iterations are DRA 5, Evolvable Mars Campaign (EMC) and the integrated M2M campaign [3, 8, 27]. Cirillo *et al.* provides and overview of NASA's Strategic Analysis capabilities for Lunar exploration scenarios during their Constellation Program [28]. Three main contributors to assessing the "satisfaction" of a single exploration scenario, or campaign, are: performance, affordability, and risk. A combination of tools that perform separate analyses are linked to generate these metrics for each campaign. These tools allow for definition of the campaign itself, as well as evaluating its risk using probabilistics, affordability modeling, micro-logistics logistics modeling, and sustainability evaluation. A depiction of the relationships between each of these tools is shown in Figure 2.1

It is important to understand how space logistics fits in with NASA's methodology given its focus in this research. The term logistics may refer to different areas of the overall

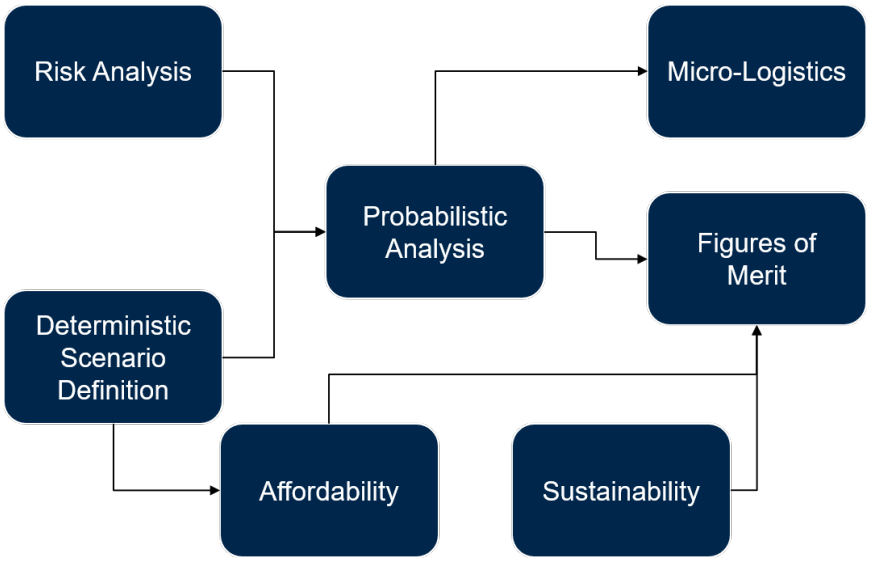

Figure 2.1: Flow diagram of the Strategic Analysis methodology from [28].

SEC design problem, and Cirillo *et al.* provides the definition and distinction between them. Specifically, macro-logistics focuses on the analysis of human space exploration systems as a large-scale logistics network problem, introduced in Section 1.2, whereas micro-logistics is the area of work that aims to understand how to handle the transport, and storage of consumables or goods, use of which by the crew, and eventual disposal of waste, modeled through a systems dynamics methodology [29]. Hereafter, macro-logistics is also referred to as the space logistics network formulation, or space logistics, and will be described further in this chapter. Both logistics concepts are important to understand and include within overall campaign analysis.

Within this campaign analysis methodology, the design and sizing of individual elements within the campaign are not performed, but rather input. Their technical data is used to build individual campaigns iteratively by manually changing campaign-level parameters using subject matter expertise. Volume and mass capacities by available vehicles are the driving constraints on this process, and are fixed throughout the process. Manifesting of payloads is done manually, depending on campaign requirements and available launch vehicles.

The risk of the final campaign design point is evaluated using an event-tree analysis of the probability of each mission within and the reliability of each vehicle. Results are aggregated into high level figures of merit such as probability of loss of crew, mission, or key elements. Affordability is driven primarily by the financial costs of the campaign, modeled through various costing tools and methods that include LCC, cost of spares, launch costs, and more. Identifying the level of sustainability of each campaign is done by analyzing the interactions within, shown in Figure 2.2, and calculating the perceived "Level of Interest (LOI)" by stakeholders. Once each campaign has been built, they are compared through several FoM, described in Table 2.1.

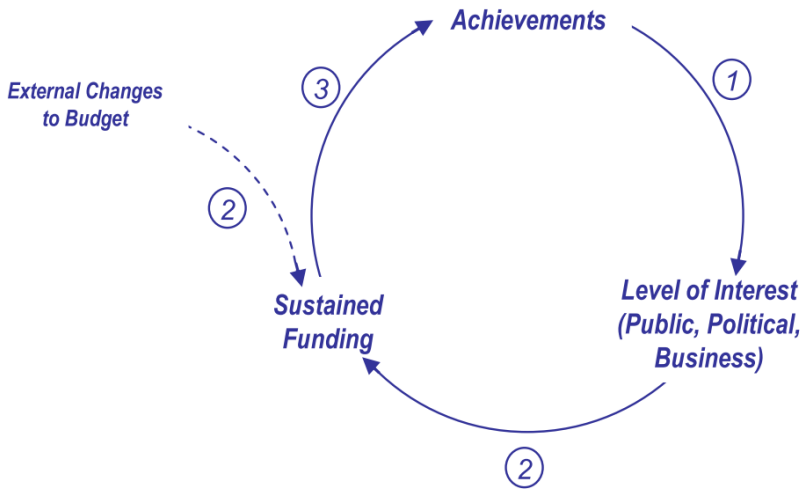

Figure 2.2: Interactions of programmatic sustainability as shown in [28].

Given the method of scenario definition, this campaign analysis does not make any assumptions about the overall trade space, meaning it would allow for broad exploration. The many high-level, strategic FoM also allows for direct comparison of those alternative campaigns. However, the manual nature of this process means not many alternatives are generated over time, and would not be responsive to quick changes in requirements. Additionally, since the sequence of missions or events is modeled by hand, there is no guarantee that the campaign solution is the optimum. Although the level of fidelity of the vehicles within the process is not mentioned, their design process is completely decoupled

Table 2.1: Table of FoM for comparing different exploration scenarios, or campaigns, in the strategic analysis method.

Figure of Merit	**Description**
Affordability	Defined by three types of metrics: Total Budget Delta to 2020 [RY$B], Max Annual Deficit [RY$B], Max Cumulative Difference [RY$B]
Benefit	Measures the value of each campaign across six themes from the Global Exploration Strategy: Exploration Preparation, Scientific Knowledge, Human Civilization, Economic Expansion, Global Partnership, and Public Engagement [30].
Safety and Mission Assurance	Expected losses in the campaign due to uncertainty or unreliability, e.g, loss of crew, mission, and/or elements
Programmatic Risk	Encompassed by mission reliability, which is a roll up of probabilities of loss of crew, loss of mission, missed rendezvous, anomalies, expected delay periods, and contingency plans
Sustainability	Expected LOI below the desired LOI

from campaign analysis, meaning its sensitivity to vehicle design changes would have to be manually processed.

The previous process was utilized for the Lunar Exploration Program, which was a much smaller campaign than the Mars campaign being developed around the same time, DRA 5. For DRA 5, an overall trade space was established, shown in Figure 2.3, and used to explore alternative campaigns, driven mainly by the transportation architecture.

Comparing individual options in this trade space involved the use of high-level models developed using subject matter expertise, with the express goal of removing options that did not meet performance, cost, and risk requirements. Models were also driven by previous experience or existing data to ensure a rapid, comparative down-selection process, as shown in Figure 2.4.

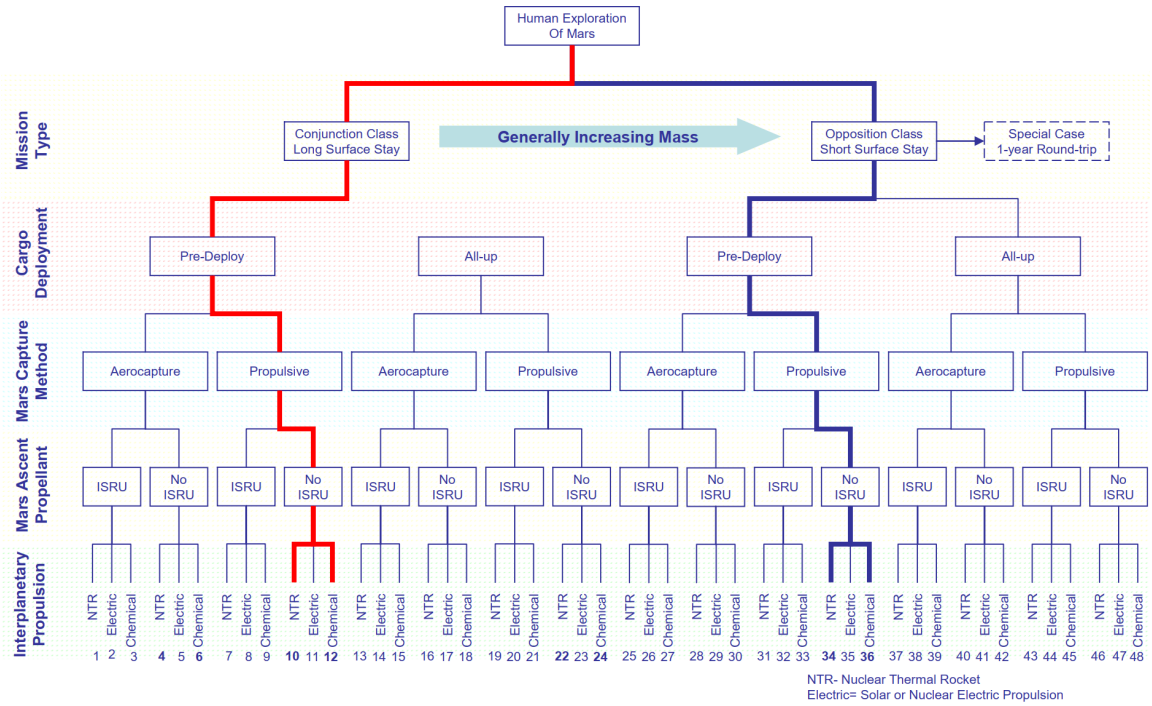

Figure 2.3: The highest level trade tree that was explored in NASA's DRA 5 [8].

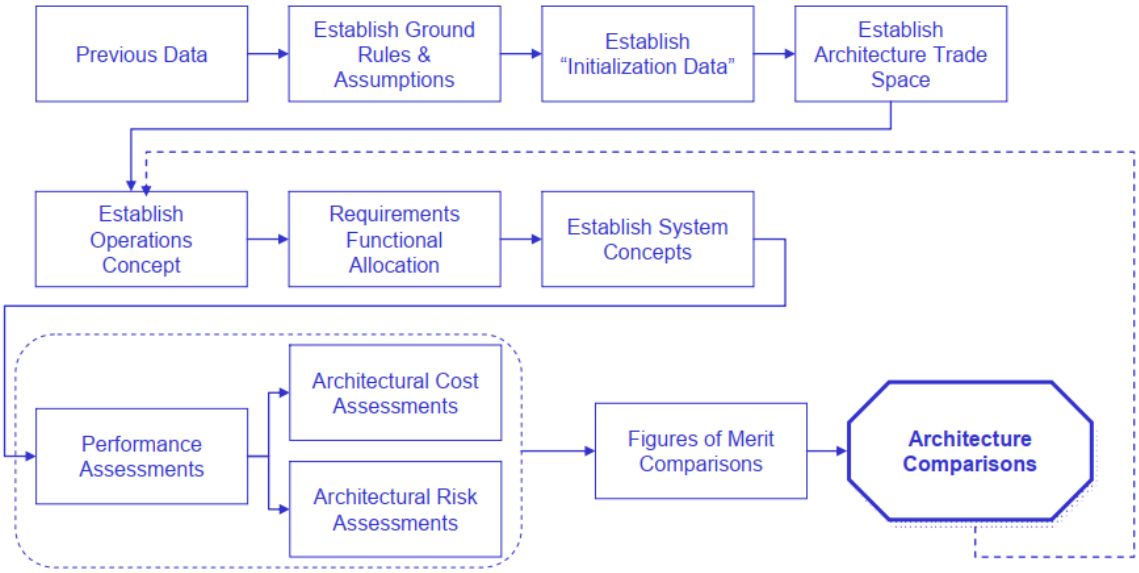

Figure 2.4: Comparative architecture evaluation process used to down-select in NASA's DRA 5 [8].

Out of the 48 architectures in the trade tree, it took many months and over 185 people to filter down to two options, while still leaving many unexplored. The Subject Matter Experts (SME) and past experience-driven approach to exploring alternatives emphasizes

a point-design philosophy and at most, creating clouds around them. Novel designs of vehicles, campaign strategies, or trajectory options would be difficult to assess using this process, potentially leaving more affordable, less risky options untouched. Given the desire to build many alternatives for decision makers, there is a need to identify new processes for designing campaigns at the conceptual level.

2.4 Academia: Space Logistics Network Optimization

Within the past two decades, researchers in the space campaign academic community have focused on applying a specific methodology for their design. By representing space travel as network of destinations and paths, mathematical techniques can be applied to optimize the flow of resources within, with the aim of finding the best logistics scenario. This approach, dubbed Space Logistics (SL), is defined by its American Institute of Aeronautics and Astronautics (AIAA) Technical Committee as, "the theory and practice of driving space system design for operability and managing the flow of material, services, and information needed throughout the system life-cycle" [31]. This definition leads to the fourth observation in this thesis:

Observation 4: Space campaign design is a complex logistics optimization problem.

Terrestrial logistics and supply chain optimization methods are extended to address the complexities that accompany space travel such as: longer timescales, physics of orbital mechanics, high degree of coupling between paths taken and resources used, and the long, high-cost deployment phase for infrastructures. While improving upon each other by filling technical gaps, the goal of each specific method within the field is to identify the optimal flow of all commodities in a apace campaign. **Observation 4** can be decomposed to understand how a logistics formulation can be applied to this research, specifically into the following three formulating questions, also updating the thesis structure in Figure 2.5.

- Formulating Question 4: What type of space logistics problem is to be solved?

- Formulating Question 5: How can complex ConOps be incorporated without increasing the computational complexity?
- Formulating Question 6: Where and how can the vehicle be represented as a synthesis of subsystems in the logistics formulation?

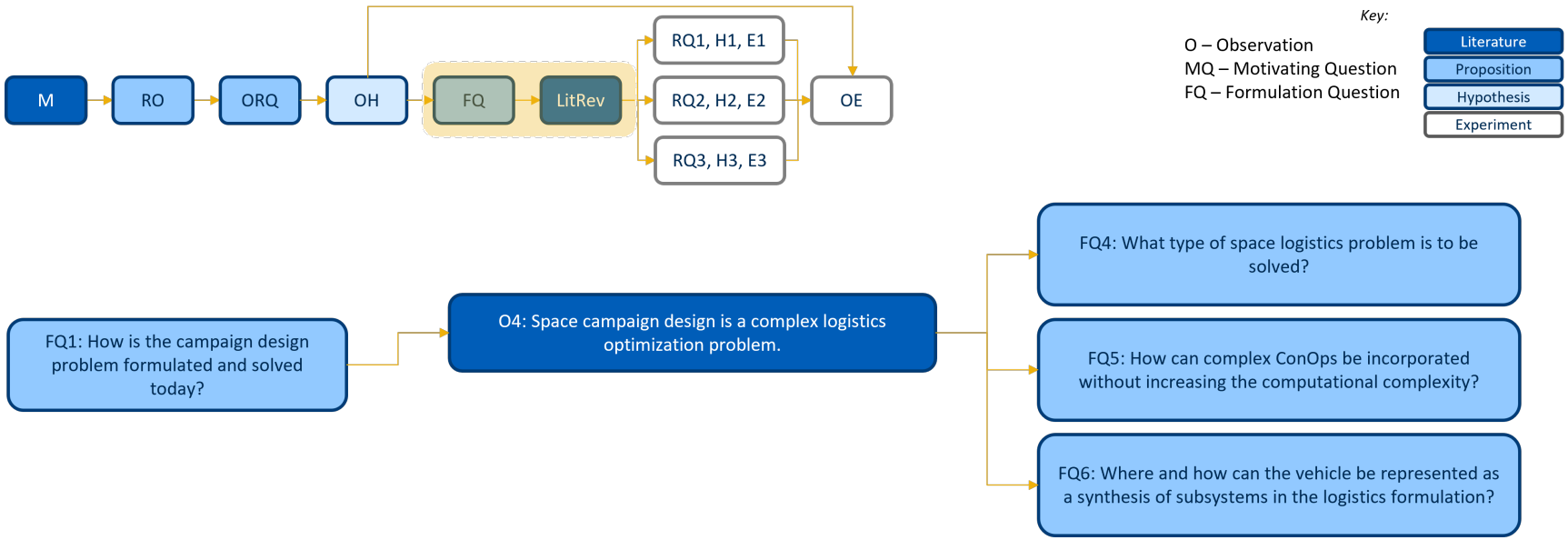

Figure 2.5: Thesis structure updated to show the formulations questions for campaign design.

2.4.1 Network Formulation Theory

Before conducting a review of applications of the logistics optimization problem to space campaigns, it is important to understand the fundamental theories that are used as a foundation. Network flow problems, or Network Design Problems (NDP), were considered as early as the 1950s, initially as purely mathematical constructs, with goal of finding the maximum flow using specific algorithms [32, 33]. Supply chain researchers have used mathematical techniques to optimize the flow of resources for many applications in many different sectors. Networks themselves, also called graphs, are readily apparent across many different domains of humanity, from highway systems, airlines and airports, package delivery services, all the way to the scheduling of football games for the National Football League (NFL) [34]. The United States Air Force conducted research to identify the proper locations of new Air and Sea Ports augmenting existing goods distribution centers to meet demands [35]. Fedex developed an algorithm to efficiently routes all of their express packages within the United States in a single day while also scheduling the optimal vehicles for those packages [36]. Although summarized here, Smith *et al.* provides a thorough introduction to these types of problems as well as their applications and potential solutions [37].

Of all of the ones mentioned above, the Minimum Cost Problem (MCP) is the problem that is most fundamental to all NDP. The goal is to determine the cheapest transportation strategy that meets all the demands at certain locations, while constrained by the supply at others. Let G be a network with $G = (N, A)$, where N is a set of n nodes and A is a set of m directed arcs. Nodes represent locations where arcs represent routes of transport between them. A directed arc is one in which commodities can flow in a single direction. Each arc, $(i, j) \in A$ in this generalized network, can be assigned a cost of travel, c_{ij}, that defines the how expensive it is to travel along that arc. In this case, the cost is assumed to scale linearly with the amount of commodity flow on the arc. Arc capacities, u_{ij} and l_{ij}, define the maximum or minimum amount of flow on the arc, respectively, to model those

on physical transportation systems. Integer variables, $b(i)$, for each node, $i \in N$, represent the supply or demand of each node, where $b(i) > 0$ is a supply node i, $b(i) < 0$ is a demand node i, and $b(i) = 0$ is neither. The latter is defined as a transshipment node by [37]. With these components, the final MCP can be formulated as follows:

$$\begin{aligned}
\text{min} \quad & \textstyle\sum_{(i,j)\in A} c_{ij} x_{ij} && && (2.1)\\
\text{s.t.} \quad & \textstyle\sum_{j:(i,j)\in A} x_{ij} - \sum_{j:(j,i)\in A} x_{ji} = b(i) && \text{for all } i \in N && (2.2)\\
& l_{ij} \leq x_{ij} \leq u_{ij} && \text{for all } (i,j) \in A && (2.3)\\
\text{where} \quad & \textstyle\sum_{i=1}^{n} b(i) = 0 && && (2.4)
\end{aligned}$$

The objective function, Equation 2.1, defines the total cost of traveling through arcs with, in this case a single commodity, x. Equation 2.2 are called mass balance constraints which serve to ensure the flow of the commodity through the node is continuous. The difference between the outflow and inflow, terms 1 and 2 respectively, must be equal to the supply or demand at that node. If the node does not have either, the total outflow of the node is then equal to the inflow. Capacity constraints on the commodity are represented by flow bound constraints in Equation 2.3. Finally, Equation 2.4 enforces that total amount of commodity within the network is conserved. Most notable NDP are variations of this fundamental problem. Table 2.2 summarizes these variations and their mathematical formulations, introduces generalizations of the problem itself, and other NDP problems of note.

Table 2.2: A summary of variations, generalizations of the MCP and other network problems, adapted from [37].

Group	**Title**	**Descriptions**	**Example**
Variations	Shortest Path Problem (SPP)	The simplest NDP that aims to find the minimum cost or length path from one destination to another, using arc length c_{ij} for $(i, j) \in A$. There are no flow bounds on a SPP	Traffic Flow
	Maximum Flow Problem (MFP)	Similar to the SPP but the flows are capped along each arc while costs are zero.	Electrical Grid

Table 2.2: A summary of variations, generalizations of the MCP and other network problems, adapted from [37].

Group	**Title**	**Descriptions**	**Example**
Variations	Assignment Problem	A collections of pairings of individuals from two larger, but equally sized, sets, N_1 and N_2, have an associated cost. The goal is to find the set of pairings that minimize the total cost.	Class Scheduling
	Transportation Problem	Similar to the MCP but node set N is divided into two smaller subsets, N_1 and N_2, where one is set of supply nodes and the latter a set of demand nodes.	Package Delivery Services

Table 2.2: A summary of variations, generalizations of the MCP and other network problems, adapted from [37].

Group	**Title**	**Descriptions**	**Example**
Variations	Circulation Problem	The MCP with only transshipment nodes, $b(i) = 0$ for all $i \in N$	Commercial Airline Scheduling
Generalization	Convex Cost Flow Problems	MCP assumes a linear cost model, whereas here, the cost is simply a convex function of the amount of flow. The flow costs varies for different reasons in the network.	Power losses in an electrical grid

Table 2.2: A summary of variations, generalizations of the MCP and other network problems, adapted from [37].

Group	**Title**	**Descriptions**	**Example**
Generalization	Generalized Flow Problems	Arcs can consume or generate flow with rates μ_{ij} for each arc $(i, j) \in A$. If $0 < \mu_{ij} < 1$, the arc is lossy, whereas if $\mu_{ij} > 1$ the arc is gainy.	Pipeline flows with leaks
Other Problems	Multi-Commodity Flow Problems	Simply the MCP with more than one commodities.	Food Distribution
	Minimum Spanning Tree Problem	Identification of the minimum length path from one end of a connected graph to the other in an undirected network.	Highway Construction

Table 2.2: A summary of variations, generalizations of the MCP and other network problems, adapted from [37].

Group	**Title**	**Descriptions**	**Example**
Other Problems	Matching Problems	In a network $G = (N, A)$, a matching is a set of arcs where every node is incident to at most one arc. A single node is matched with at most, another single node. The problem is dependent on some certain criteria being optimized to.	Roommate matching in dorms

As stated previously, these fundamental problems have many applications and each individual problem is modified to include its own set of objectives, constraints, costs, capacities, and other parameters. Finding a numerical solution to these problems generally require the use of some optimization algorithm.

2.4.2 Network Optimization Theory

Selection of an optimization method to solve network flow problems depend on the type of problem and its parameters. Integer Programming (IP) is a type of optimization algorithm that is reserved for problems where one or more of the decision variables can only be integers [38]. A Pure Integer Programming (PIP) problem is a subset of IP where all of the variables are integers, whereas it is otherwise referred to as Mixed Integer Programming (MIP) if they are not. If the objective function and all of the constraints are linear, they can be considered as Linear Programming (LP), or if not, then as Nonlinear Programming (NLP) As an example, the standardized Mixed Integer Linear Programming (MILP) formulation represented as a MCP in matrix form is shown in Equation 2.5, Equation 2.6, and Equation 2.7.

$$\min_{\mathbf{x},\mathbf{y}} \qquad z = \mathbf{c^T x} + \mathbf{d^T y} \tag{2.5}$$

$$\text{s.t.} \quad \mathbf{Ax} + \mathbf{Ey} = \ or \ \leq \ or \ \geq \mathbf{b} \tag{2.6}$$

$$\mathbf{x}_{min} \leq \mathbf{x} \leq \mathbf{x}_{max} \qquad \mathbf{y} \in \{0,1\}^{n_y} \tag{2.7}$$

The objective function in Equation 2.5 represents the total costs of the problem where $\mathbf{c}$,$\mathbf{d}$ are the cost matrices for the linear and integer variables, $\mathbf{x}$ and $\mathbf{y}$, respectively. Similarly, $\mathbf{A}$ and $\mathbf{B}$ are the matrices of coefficients, representing the balance constraint, analogous to Equation 2.2. For purely LP problems, $\mathbf{d}$ and $\mathbf{E}$ are effectively zero as there are no integer variables, $\mathbf{y}$. If a LP problem has only two variables, x_1, x_2, and n inequality

constraints, the feasible region can be shown visually as a convex polygon with n sides [39]. Figure 2.6 shows an example problem with 5 inequality constraints.

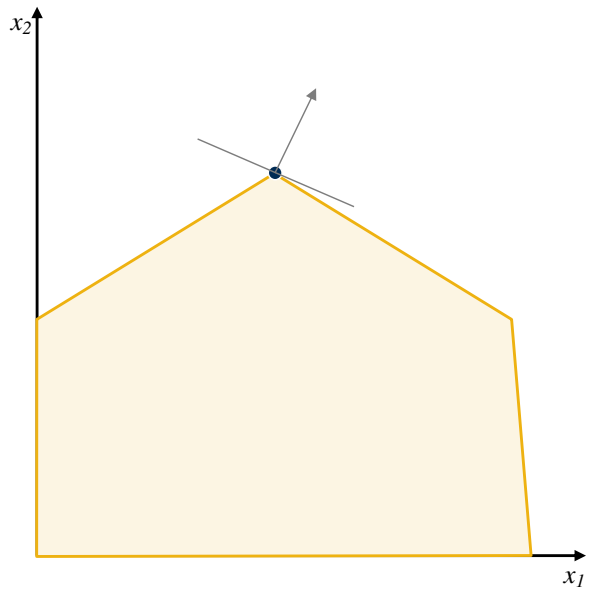

Figure 2.6: The feasible region of a LP problem with two variables and 5 inequality constraints.

For some small set of problems like this, a geometric solution can be found. The optimal point exists at the intersection of two inequality constraints, or the corners, specifically called extreme points. The coefficients of the objective function define the direction to move within the feasible region towards the optimal point, in this example case, $-\mathbf{c}$ or $(-c_1, -c_2)$, which is shown in gray.

Depending on the constraints and objective function there are several other cases of the type of optimal solution. Although the example case gave a unique optimal solution, the feasible region in Figure 2.6 was bounded completely. A unique solution can still exist on a corner point even if the feasible region is unbounded as shown in Figure 2.7. If the direction of the anti-normal of the objective function is at an angle of 180° to that of one of the constraints, there can exist a set of alternative optimal solutions, bounded or not, as shown in Figure 2.8. Similarly, if the anti-normal is at an angle of 90°, and the region is unbounded, there is no optimal solution, shown in Figure 2.10. Finally, if the constraints

are inconsistent, the feasible region is said to be empty. For all cases, an n-variable problem will have a feasible region that is an n-dimensional convex polyhedron.

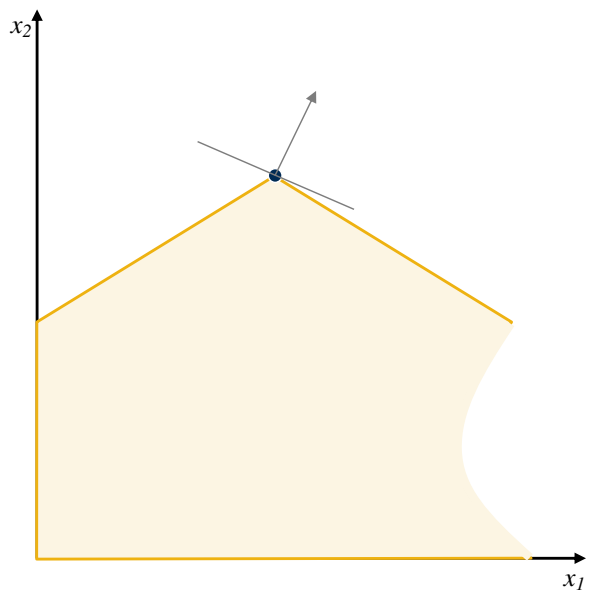

Figure 2.7: Example of a unique solution of a LP with an unbounded feasible region.

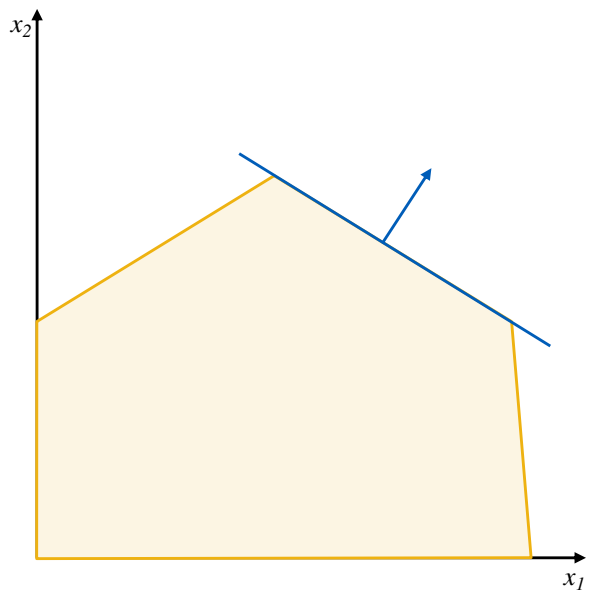

Figure 2.8: Example of a alternative optimal solutions of a LP for both, bounded and unbounded, feasible regions.

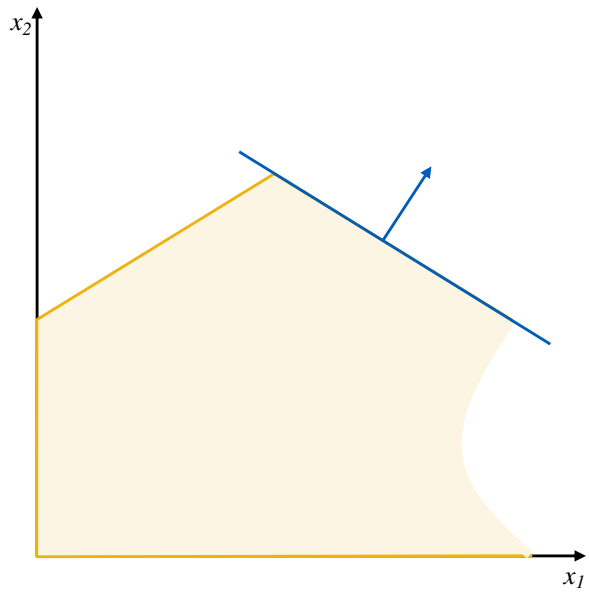

Figure 2.9: Example of LP where there is no optimal solution.

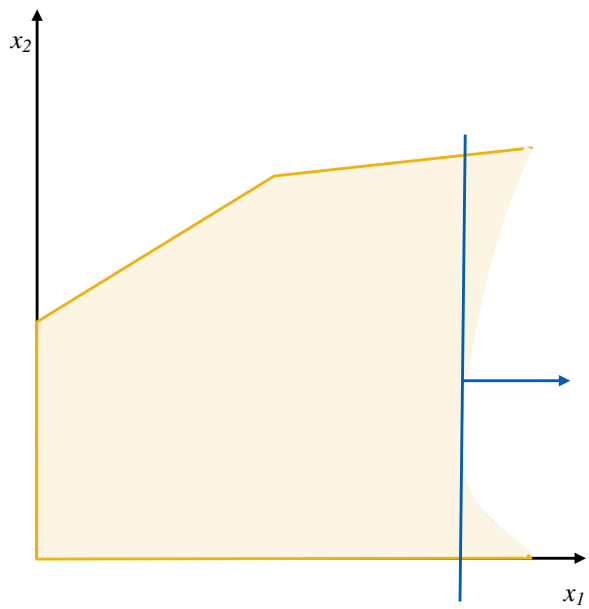

Figure 2.10: Example of LP where there is no optimal solution.

General algorithms for finding the optimal points in LP have roots as early as 1936 through mathematician Leonid Kantorovich [40]. However, his specific computational algorithm was never complete and it was only nearly a decade later until which George Dantzig developed the simplex method, one of the most popular for solving LPs [41]. The simplex method is still considered a valuable approach and only a few modifications have

been made since its introduction. Klee and Minty showed that the method's worst case performance is solved in exponential time, $\mathcal{E}$, but it was not soon after that Hansen and Zwick introduced the interior-point method which was able to solve the problem in polynomial time, $\mathcal{P}$ [42, 43]. Simplex methods identify the optimal point by moving from vertex to vertex along the edges of the feasible polyhedron region bounded by the constraints. In contrast, interior-point methods search within the feasible region itself until the optimal point is found [44].

The inclusion of integer variables in the problem reclassifies it as a MIP and requires different methods to find a numerical solution. In comparison, the feasible region of a MIP is no longer just defined by the constraints, but by the nearest integer feasible point, which may be just inside the edge of the polyhedron. As a result, the simplex and interior-point methods by themselves are inadequate to solve a MIP which resulted in the introduction of the cutting plane and Branch and Bound (BB) methods [45, 46, 47, 48, 49, 50].

The cutting plane method works very similarly to the simplex method in that it tries to identify a new edge of the polyhedron using the integer points. Near the region of the optimal point of the LP, it uses the integer points to add constraints to the problem to create a new edge with the integer points as the vertices, as shown in Figure 2.11. Similarly, to Figure 2.6, the shaded area represents the feasible region of a generic, two variable LP problem and the points are added to represent the integer variables. Since the optimal solution must be an integer, it rules out the vertex created by the edges of the polygon, which would have been the solution to the pure LP problem. Instead, the actual edges of the polygon are the ones created by connecting the integer points closest to the that of the larger one, shown in green. Cutting planes are added as constraints to the problem to identify one of those new vertices as the optimal integer point, shown as dashed lines. However, applying the right cutting planes is often considered as its own separate problem and as a result, becomes computationally expensive.

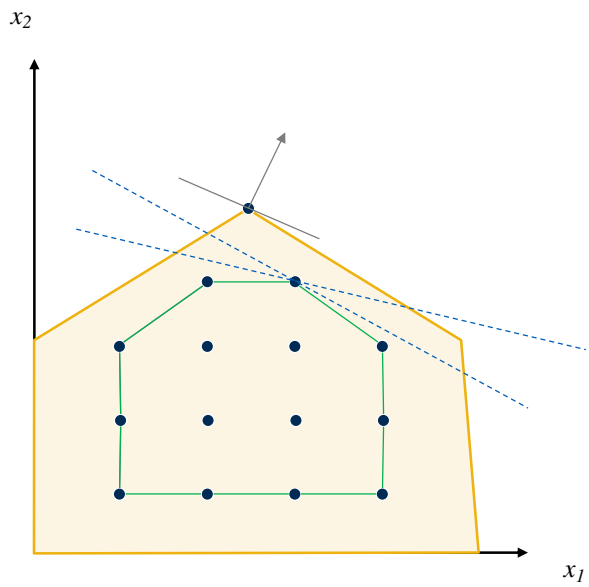

Figure 2.11: The addition of constraints on the LP problem to identify a the new edges for the MIP problem using the cutting plane method.

The BB method may seem very similar to a brute force algorithm which explores every feasible point to identify optimality, but rather searches for points in an intelligent manner. [51] It partitions the entire feasible sections in to smaller sets to identify upper and lower bounds to a new, smaller problem and repeats until the optimum is found, notionally shown in Figure 2.12 [52].

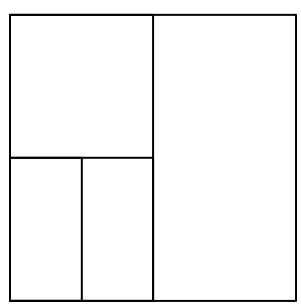

Figure 2.12: Notional depiction of the BB algorithm of a 2-d feasible region of a MIP problem, adapted from [52].

To further improve this technique, it was extended to include parts of the cutting plane method, creating Branch and Cut (BC) [53]. By combining the benefits of both of the previous methods, BC was considered to be very effective at solving MIP problems.

Up until now, the methods and techniques reviewed previously have been simple implementations at solving basic problems. Commercial software solutions have used them

as a foundation to create advanced packages that increase the general performance of these optimizers to solve much larger, more complex network problems. Anand *et al.* provides a summary of open source and commercial optimizers as well as comparison of their performance [54]. Although there are plenty of options, CPLEX, Gurobi, and XPRESS are the top performers and the final selection of the specific package will depend on the characteristics of the problem being solved [55, 56, 57].

Formulating the space logistics network optimization problem involves extending these fundamental concepts to account for the complexities of space travel. The following section will provide an overview of previous attempts at solving the space logistics network problem, their specific formulations, and their gaps when considering the requirements for campaign design in this thesis.

2.4.3 Space Logistics Network Optimization Processes

Christine Taylor, from Massachusetts Institute of Technology (MIT), formulated a process that connected the transportation systems design optimization problem to the network flow [23]. Specifically, the overall systems definition of a transportation architecture was expanded to include the network of destinations it travels through and the resulting integrated problem is solved through concurrent optimization of both elements. Though both aircraft and spacecraft were considered, the problem decomposition of the integrated interplanetary logistics model is show in Figure 2.13.

The integration of the vehicle and network problems is handled through the operations model via two sets of constraints: capacity and capability. As vehicles are assigned to specific arcs to perform their mission, their maximum mass capacity is translated to total commodity mass on each arc. Capability constraints define whether or not that vehicle is capable of traveling on that arc, ensuring their available fuel is more than what is required. Further, vehicles are modeled to hold the commodities and propel them through the network. As a result, the design of the vehicle is modeled as three main components: structural

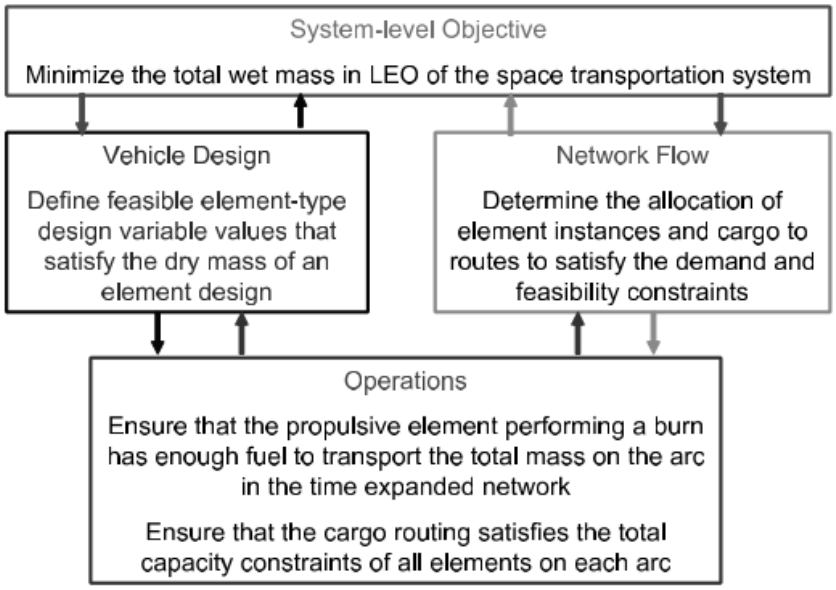

Figure 2.13: Functional decomposition of the integrated interplanetary logistics problem.

mass, propellant mass, and the required payload, shown in Figure 2.14 The structural mass is estimated through a mathematical regression from empirical data while the propellant mass is a design variable.

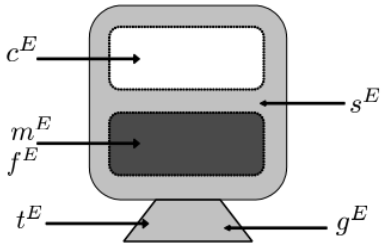

Figure 2.14: Vehicle representation within Taylor and Weck's integrated design framework.

Though Taylor was able to integrated both the vehicle and campaign design processes, the simplification of the vehicle model and its implementation though a regression means vehicle-level trades cannot be performed without major modifications. Additionally, the transportation network considered was an Earth-Moon system, and crewed missions were not considered, closing of a large portion of the campaign design space.

Arney presented a methodology to explore the space systems design space using graph theory and a rule-based algorithm [58]. This methodology was split into three main parts:

graph generation, design space exploration, and evaluation. Graph generation is a user driven process where they define a set of nodes and edges of a graph using a tabular format, representing the missions being considered. The nodes represent specific locations or steady states and the edges the paths between them. With this formulation, the user can define the system architectures with as many nodes and edges as desired, depending on the complexity of the problem. Link nodes are specific nodes in the graph that represent locations that are static in nature, such that assets can be pre-positioned. Edges are also defined by specific metadata that represent information about the type of transfer and how it relates to the sizing of associated systems. For example, a propulsive maneuver edge includes ΔV, Thrust-to-Weight, Engine Type, Time of Flight, and Planet, whereas a In-Space Habitation edge only includes a scenario and a stay time. During the design space exploration stage, a system map is a matrix representation of how each system travels through the graph indicating the order of events used for sizing tools. Enumerating all the available paths for each system shows an exhaustive number of options to explore which necessitated the need for the rule-based traversal algorithm. A total of ten rules were established, split in two groups of Existence and Functional rules, all of which are shown in Table 2.3.

Table 2.3: Rules established by Arney for the traversal of a system architecture graph [58].

Category	Rule	Description
Existence Rule	Crew Instance	Surface Habitat OR In-Space Habitat OR Crew
Functional Rule	Earth Launch	Launch Vehicle
	Propulsive	Propulsive Stage OR Descent Stage OR Ascent Stage
	Planetary Ascent	Descent Stage OR Ascent Stage
	Planetary Descent	Descent Stage
	In-Space Habitation	In-Space Habitat
	Surface Habitation	Surface Habitat OR Crew Capsule
	Planetary EDL	Crew Capsule
	Refuel	Propellant Depot
	Orbit Capture	Aerocapture System OR Crew Capsule

Existence rules force the existence of a specific system on an edge if another one also exists there; if an edge contains crew, then the edge must also contain a type of habitation. Functional rules force a system on an edge if the traversal of that edge requires the function provided by that system; the Earth launch edge requires the use of a LV. Ant Colony Optimization (ACO) is used to find the optimal set of system assignment to edges such that all systems and all edges have satisfied the rules. Up until now, the algorithm has only assessed functional feasibility, but not physical feasibility. Evaluation of each architecture is done through sizing of each system using the graph and estimating the dollar costs. A system

hierarchy is first established prior to sizing of systems to ensure each one is being sized in the proper order. The sizing itself is depends on the specific system but each model is either a Response Surface Equation (RSE) or using photographic scaling. Finally, costing estimation is broken down into Design, Development, Testing and Evaluation (DDTE) and flight unit costs using NASA Air Force Cost Model (NAFCOM) or Transcost depending on the system type. A process diagram of this methodology is shown in Figure 2.15.

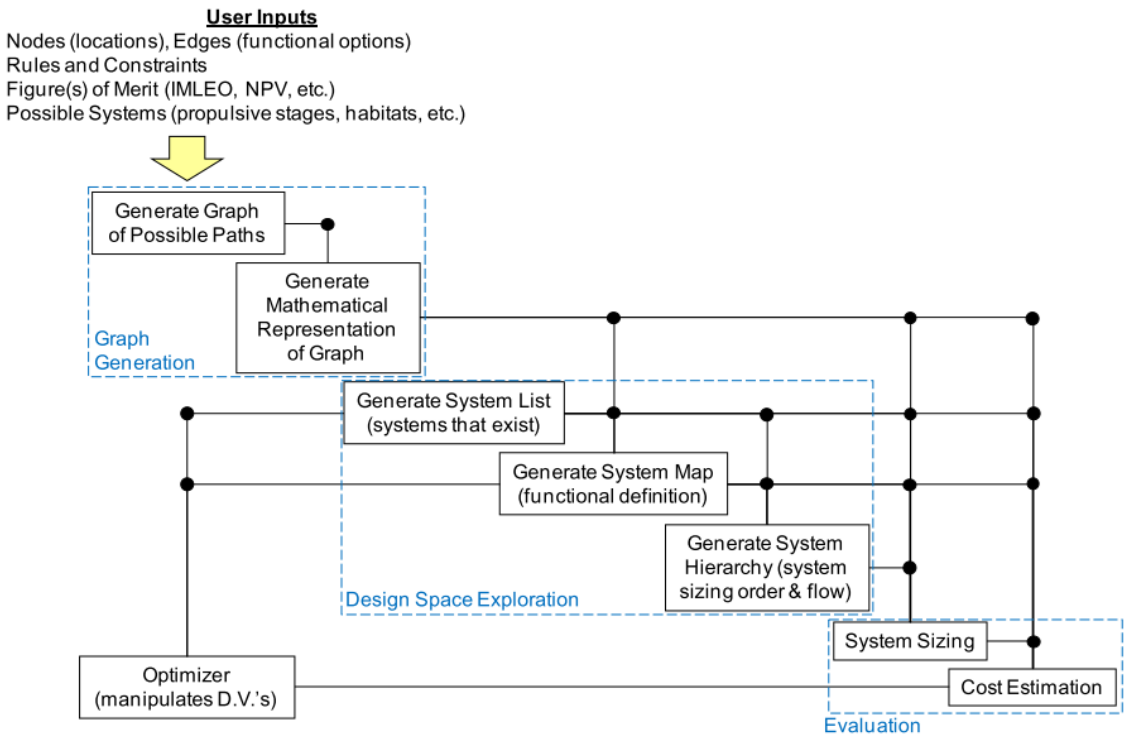

Figure 2.15: Process diagram of the graph theory-based system architecture design space exploration method presented by Arney [58].

Since the definition of the graph is user-input and given its flexibility to node and edge definition, many exploration scenarios can be assessed using this method. Complex ConOps could be represented using the link nodes and the ability define as many nodes as necessary. The rule-based traversal algorithm will automatically assign systems to certain edges based on the functionality that is required on that edge, enabling very little user interaction after graph generation. However, the strength of this method is also its limitation: the user-driven definition of exploration scenarios. Defining the graph also means defining

the transportation strategy of the payloads and the vehicles that push those payloads. This means that certain exploration strategies may not be explored, potentially leaving the optimal one on the table. Additionally, vehicle design was included in this method, but its limitations are discussed in the next chapter.

To build off of the success of the space logistics network formulation from Taylor, MIT created SpaceNet through their Space Logistics Research Project [59]. This was an open-source tool developed in part with NASA, with the goal of allowing campaign designers to evaluate how the crew and cargo transportation systems will be used as a supply chain problem. A discrete event simulation was used as the framework for this software, enabling an analysis of alternatives for various campaign architectures and trades [60, 16]. Although various complex operations were considered and modeled, such as reusability, reconfigurability, commonality, and repairability, it requires an input transportation network and mission sequence [61]. As such, it only finds the optimal logistics flow and manifest for that given scenario, not exploring broad trade spaces.

In response to the previous gaps, Ishimatsu *et al.* formulated an optimization process that allows for modeling of larger, and longer-term human exploration campaigns using the Generalized Multi-Commodity Network Flow (GMCNF) model. Also adopting a network approach, the author states that a space mission objective can be translated into demands for a flow of cargo or commodities throughout. These commodities can be sourced from different destinations, whether it be Earth, or even Mars using In-Situ Resource utilization (ISRU), which results in a multi-commodity network. Further, the author formulates that due to the complexities of space travel, flow on an arc is not conserved; some commodities may be generated or consumed during the course of an arc. Propellant is used to by the spacecraft to transfer from one node to another, and if the mission is crewed, they can consume food and generate waste. Additionally the rate of consumption or generation of one commodity may depend on another or even transform: propellant used by the spacecraft is directly dependent on how much mass it is pushing, food turns into waste through the

crew. This property allows the problem to be classified as one with generalized flow. To address these modeling gaps, the concepts of a self-loop and multi-graphs were introduced, as depicted in Figure 2.16 and Figure 2.17.

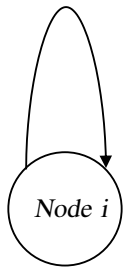

Figure 2.16: Fundamental depiction of a self loop on a node [60].

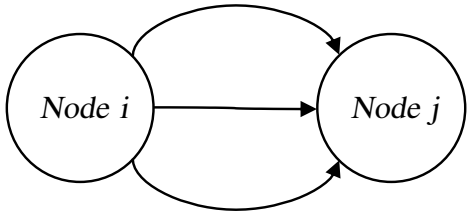

Figure 2.17: Fundamental depiction of a multi-graph between two nodes [60].

With the objective of minimizing flow costs throughout the network, the problem is fully formulated as follows:

$$\min \quad \mathcal{J} = \sum_{(i,j)\in\mathcal{A}} (\mathbf{c}_{ij}^{+^T}\mathbf{x}_{ij}^{+} + \mathbf{c}_{ij}^{-^T}\mathbf{x}_{ij}^{-}) \tag{2.8}$$

$$\text{s.t.} \quad \sum_{j:(i,j)\in\mathcal{A}} \mathbf{A}_{ij}^{+}\mathbf{x}_{ij}^{+} - \sum_{j:(j,i)\in\mathcal{A}} \mathbf{A}_{ji}^{-}\mathbf{x}_{ji}^{-} \leq \mathbf{b}_i \quad \forall\, i \in \mathcal{N} \tag{2.9}$$

$$\mathbf{x}_{ij}^{-} = \mathbf{B}_{ij}\mathbf{x}_{ij}^{+} \quad \forall\, (i,j) \in \mathcal{A} \tag{2.10}$$

$$\mathbf{C}_{ij}^{+}\mathbf{x}_{ij}^{+} \leq \mathbf{d}_{ij}^{+} \quad \text{and} \quad \mathbf{C}_{ij}^{-}\mathbf{x}_{ij}^{-} \leq \mathbf{d}_{ij}^{-} \quad \forall\, (i,j) \in \mathcal{A} \tag{2.11}$$

$$\mathbf{l}_{ij}^{+} \leq \mathbf{x}_{ij}^{+} \leq \mathbf{u}_{ij}^{+} \quad \text{and} \quad \mathbf{l}_{ij}^{-} \leq \mathbf{x}_{ij}^{-} \leq \mathbf{u}_{ij}^{-} \quad \forall\, (i,j) \in \mathcal{A} \tag{2.12}$$

Self-loops model resource gain or loss at a single node, whereas multi-graphs model different transportation options between nodes. Fully formulated, this process gives the optimal commodity flow that meets all demands. Due to the use of linear programming

optimization, the problem is guaranteed and optimal solution if a solution is found. However, there is one fundamental assumption or simplification within this process that is a key limitation: the static nature of the network. It does not handle the flow of resources over time, which constrains the campaign design space considerably. Various operations and missions cannot be considered such as: phased infrastructure build-up, ISRU stockpile tracking, launch or departure windows, and more. Additionally, the vehicle design within this framework is accomplished through Inert Mass Fraction (IMF) based sizing. The ideal rocket equation, shown in Equation 2.13 is used to calculate the structures mass based on an input ΔV and an assumed IMF of 0.08 for LOx/LH_2 and 0.3 for NTP systems.

$$\Delta V = g_0 I_{sp} \ln(\frac{m_i}{m_f}) \tag{2.13}$$

As a direct improvement to this limitation, Ho *et al.* extends the network formulation to include unit timesteps [62]. The author shows that the full network is instantiated at each timestep, creating a full time-space network of nodes and arcs, depicted in Figure 2.18.

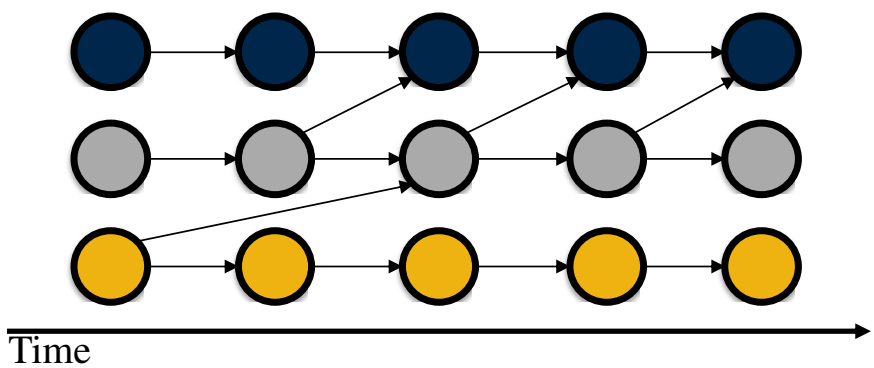

Figure 2.18: A notional time-expanded network.

A key assumption with this formulation is that each timestep, as well as any specific times and windows, are rational numbers to ensure that overall timescales can be multiples of the step. However, interplanetary missions introduce specific departure windows for transportation systems and can complicate this network. The previous two properties dramatically increase the computational complexity of the resulting optimization problem

by linearly increasing the number of overall variables and constraints. The bi-scale network to alleviate this issue by heuristically clustering nodes such that travel between any node within a cluster can be done at any time. Although the computational efficiency was greatly increased with this formulation, the author states it comes at the cost of linearization and a lower level of fidelity. Within space vehicle design, these simplifications can have a significant impact as their design is very tightly coupled with its mission [63].

In response to **Formulating Question 1**, the previous theories and formulations lead to another observation on the type of formulation:

Observation 5 : Due to the characteristics of a space campaign, it is represented through a dynamic, generalized, multi-commodity network.

Following Ho *et al.*'s dynamic formulation of the space logistics network, several researchers have added multiple levels of functionality to this fundamental formulation, with the purpose of addressing different areas of complexity in space campaign design. Improvements were made the modeling of the campaign itself and accompanying logistics formulation, the design of spacecraft and infrastructure elements, or integrated design of trajectories. The rest of this sections will detail these specific contributions and key limitations using the requirements set in Section 2.1 and Section 2.2.

Chen and Ho extends the bi-scale, time-expanded GMCNF by including an alterable timestep within the clusters themselves [24]. Rather than having a constant timestep within each cluster, those for holdover arcs are calculated based on the interval for the time window. Shown in Figure 2.19, the time windows for node k is only open at t, t + 2, and t + 8. As a result, the length of the timestep can be analytically found by calculating the difference between the times, 2 and 6, respectively.

Nonlinear sizing models for the ISRU and spacecraft are included as well, and the resulting optimization problem is a Mixed Integer Nonlinear Programming (MINP) dealt with in two main ways. The first linearizes each model and converts the entire problem

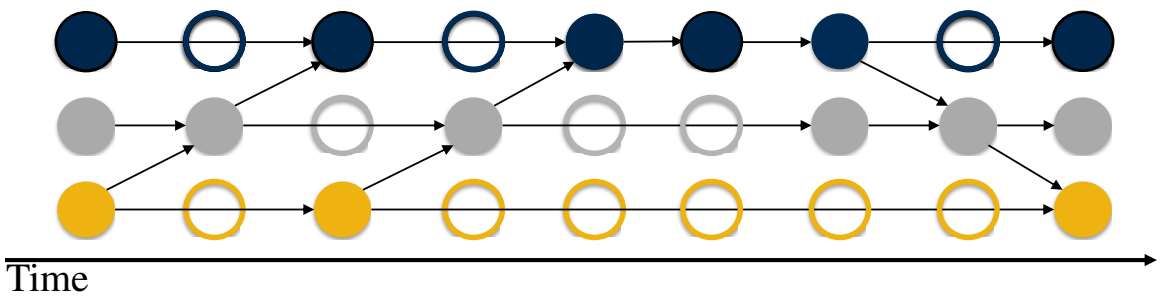

Figure 2.19: A time-expanded network with variable timesteps, adapted from Chen and Ho [24].

into a MILP using a piecewise approximating method. The other utilizes the same approximating method for the ISRU sizing, but includes the full, nonlinear spacecraft model using Simulated Annealing (SA). Specifically, the structural mass, S, is calculated using Equation 2.14, where $f(C)$ is the linear function, based on payload capacity, C, and $g(M)$ is the nonlinear function, based on propellant capability M.

$$S = f(C) + g(M) \tag{2.14}$$

With it being external to the campaign optimization problem, the model can have as many design variables as necessary and the following MILP can use only the relevant design parameters for its optimization, as shown in Figure 2.20.

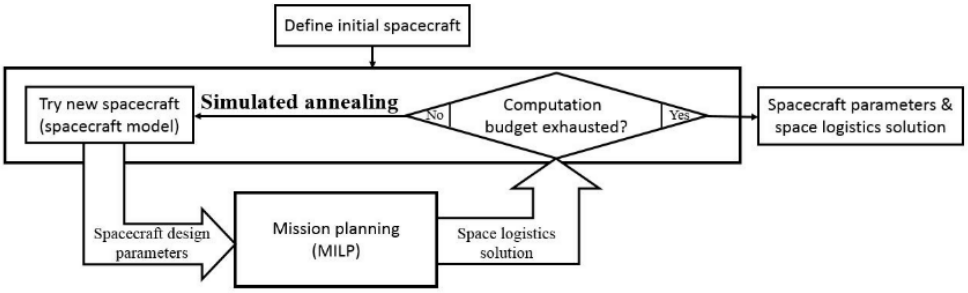

Figure 2.20: Campaign logistics optimization with nonlinear spacecraft design using SA [24].

Though the latter method allows for a higher fidelity spacecraft model, the author states if the vehicle is represented as it is in Figure 2.14, the MILP method is always the better

choice as the SA algorithm cannot guarantee an optimal solution. Regardless, the vehicle model itself is the key gap, which will be discussed further in Chapter 3.

Chen *et al.* developed an analytical model to simplify and guide the complex network formulation process [64]. A bootstrapping deployment strategy for infrastructure is used to identify the optimal number of stages needed for different exploration scenarios. The main contribution of the paper was aimed at improving the campaign level model and although vehicle design was included, the process was the same as [60].

Following the integrated space infrastructure and spacecraft design method from Chen and Ho, the same author added improvements to account for the uncertainty with rocket launches and staging events [65]. However, the formulation of the space campaign is fundamentally the same time-expanded, GMCNF model and is optimized using MILP. This formulation is changed in [66] with the inclusion of a partially periodic time-expended network. Chen *et al.* models a campaign scenario that is executed in two main phases: a setup phase for infrastructure and a periodic, steady phase afterwards. The first phase can be considered as a smaller scale campaign with sole goal of deploying and setting up infrastructure that will be used in regular intervals during later missions. These regular intervals define the periodic nature of the second phase, where a single transportation scenario is duplicated many times. As a result, only two separate optimization problems are required to be solved, one for each phase, shown in Figure 2.21, rather than solving a large integrated one, or many smaller ones.

Although this formulation is key in simplifying the computational complexity of modeling this much longer-term campaign scenario, it is only applicable to that specific scenario. Only this two phase campaign can be solved using this formulation, which does not meet the requirements for this thesis of enabling broad trade space exploration.

Large space campaigns can be difficult to model using the methods presented previously, as the number of missions within can significantly increase the computational expense of the optimization problem. Although the last method addresses that issue directly,

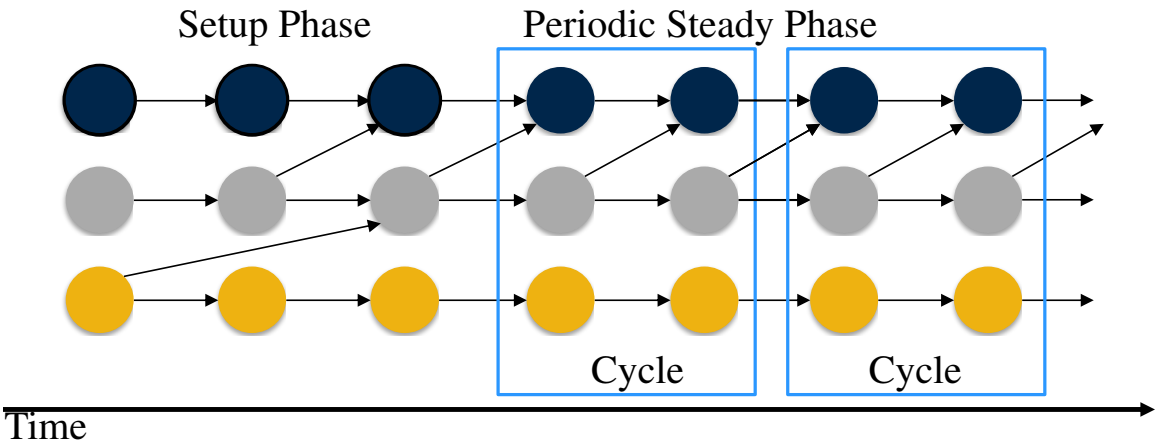

Figure 2.21: A partially periodic time-expanded network, with a setup phase and regular transportation missions, as depicted in [66]

it does so at the cost of constraining the types of campaigns that could be considered. Chen *et al.* attempts to address this scalability issue by implementing Approximate Dynamic Programming (ADP) within the network formulation [67]. This solves the logistics optimization problem in a forward manner, rather than the traditional backward of considering all possible traversable paths at each timestep. It approximates the value, or performance, of the initial missions and changes future ones based on that information.

In a similar manner, Chen and Ho reformulates the space logistics optimization problem as a Markov decision process [68]. Within each mission in the campaign, design decisions are made as a hierarchy, from spacecraft design to infrastructure design, and finally scheduling. Using a value function approximation, the optimal spacecraft design is found and drives the infrastructure design via a deep deterministic policy gradient algorithm. Once the spacecraft and infrastructure designs are optimized, the resulting logistics problem is solved.

Additional improvements have been made with the logistics formulation to include subsystem level sizing of ISRU elements within the campaign [69, 70]. This is to address limitations in previous formulations where ISRU sizing was done, but subsystem designs are selected a priori to logistics optimization, compromising on the level of fidelity of the designs themselves. Infrastructure design is out of the scope of this thesis, but the method-

ology of integrating subsystem level sizing within the logistics formulation is analogous to inclusion of that for the vehicle problem. Chen *et al.* considers a broad trade space for ISRU sizing by treating each subsystem as a different commodity, thereby leaving the overall formulation of the optimization problem the same, just with different constraints. Specifically, the mass balance constraint in a time-expanded, GMCNF model is expanded to include the resource production process. Additionally, the capacity constraints for spacecrafts have to be extended to include storage and flow of these resources.

Since the formulation of the logistics problem is the same, these additional constraints increase the computational complexity of the resulting optimization problem. The author addresses this issue by introducing constraint aggregation and variable packing. Ultimately, a full-scale subsystem level sizing problem is integrated with the space logistics network optimization by including additional constraints on the problem. As the author states, that addition only adds to the computational expense, requiring simplifying methods within the optimization problem. To avoid this issue, and given the high degree of coupling between vehicle sizing and missions, this thesis aims to link the logistics optimization with vehicle design, each their own distinct process, similar to [24].

Researchers at Aerospace Systems Design Lab (ASDL) added capabilities to account for the complex operations performed in some campaigns [71]. NASA's Human Landing System (HLS) requires the rendezvous and docking of three different propulsive elements at the Gateway in a Near Rectilinear Halo Orbit (NRHO) and subsequent staging of each one at different times [72]. Gateway's goals within the M2M program also introduces several unique issues within the logistics framework. Although it itself is a vehicle, designed as one and assembled in orbit, it will serve as a staging point for HLS, future Mars mission vehicles, and other deep space elements [73]. McBrayer *et al.* states, within the logistics formulation, these and other complex operations can be modeled using the path-arc formulation.

Pre-defining specific paths for certain vehicles in the campaign can save computational expenses by forcing the optimizer to chose those paths rather than having it spend resources to find it on its own, as shown in [24]. The latter is technically feasible within the bi-scale, time-expanded GMCNF formulation presented previously. However, it is not guaranteed the optimizer will find it without adding many constraints and thereby increasing computational complexity greatly. This formulation addresses the fifth **Formulating Question** through the following observation:

Observation 6: Vehicles can be assigned to specific nodes within the network without the use of constraints.

Isaji *et al.* describes a methodology that integrates the coupled mission planning and vehicle design problems using a decomposed optimization problem and Lagrangian coordination [74]. The mission planning, or campaign problem is represented and solved as a single Mixed Integer Quadratic Programming (MIQP) problem while each vehicle in the campaign is solved using NLP and a piecewise linear approximation , notionally shown in Figure 2.22 This structure is proposed due to the characteristics of each problem, where the campaign side is linear with integer variables, while each vehicle problem is nonlinear, but with only continuous variables.

In this formulation, the coupled subproblems are integrated using the master problem which minimizes the Lagrangian penalty function of each vehicle problem and updates all shared variables for each iteration. Using this decomposition, two loops connect the subproblems, where the outer loop updates the penalty parameters while the inner loop tries to solve the master problem as well as each subproblem. The former is considered solved when each subsolution is feasibly within the tolerance and the change in consistency constraints are below a tolerance as well. An initial guess is generated by solving the full integrated campaign and vehicle design problem, where each nonlinear vehicle model is approximated using a piecewise linearization. The solution to this problem may

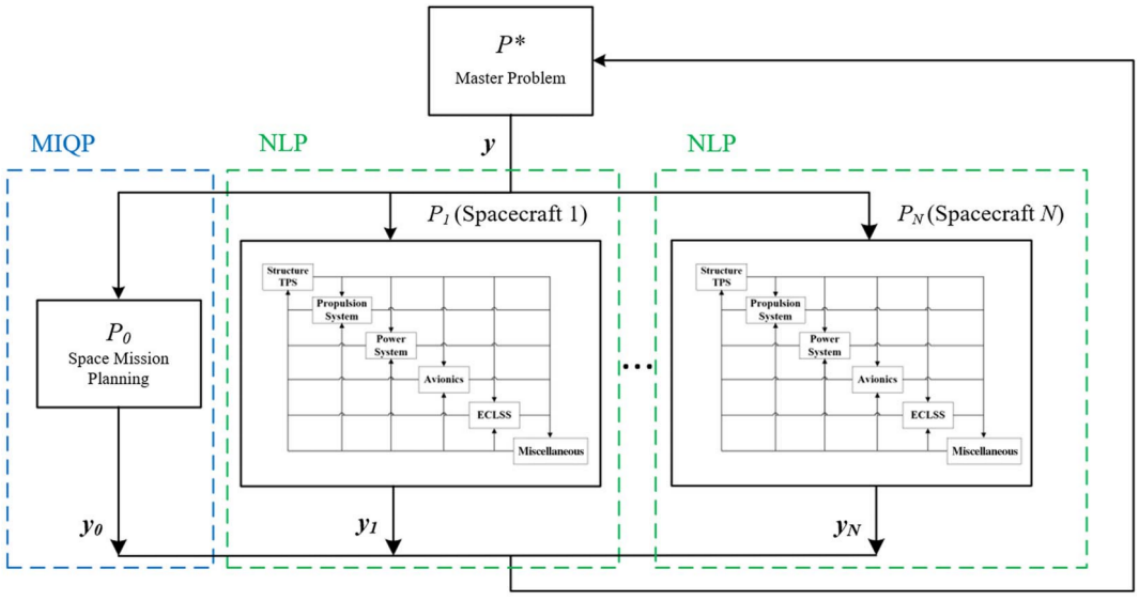

Figure 2.22: Process structure for the integrated mission planning and vehicle design optimization problem proposed by Isaji *et al.* [74].

not be the global optimum, but provides a good initial guess for the iterative method proposed; the overall decomposed process structure is shown in Figure 2.23. This method was demonstrated on an exploration scenario with two individual missions, but a single vehicle model of a single-stage lander was used for each vehicle. The author showed a significant improvement in computational performance compared to an embedded optimization problem, extended from [23], where the overall problem is solved in a matter of seconds to minutes. This methodology does address the coupling between the individual campaign and vehicle design problems, where each vehicle within is sized at the subsystem level for its mission. Further, it is possible to assess changes in the campaign and vehicle designs on each other, and although nonlinear approximations were used for this specific case study, the author states the method can be easily extended to include more complex formulations of vehicle design models.

However, there are several key limitations to be highlighted both for the campaign and vehicle subproblems. It is unclear how complex ConOps such as integrated vehicle stacks, aggregating, staging, payload transfers, and more can be formulated using this method,

with the separation of each vehicle design problem into individual NLP problems. Further, although more complex vehicle models can be included, as the author also states, all variables within must be continuous. This means changes in discrete variables such as number of tanks, number of engines on the overall problem cannot be assessed without a reformulation of the methodology. Overall this limits the type of trades that can be assessed using this methodology.

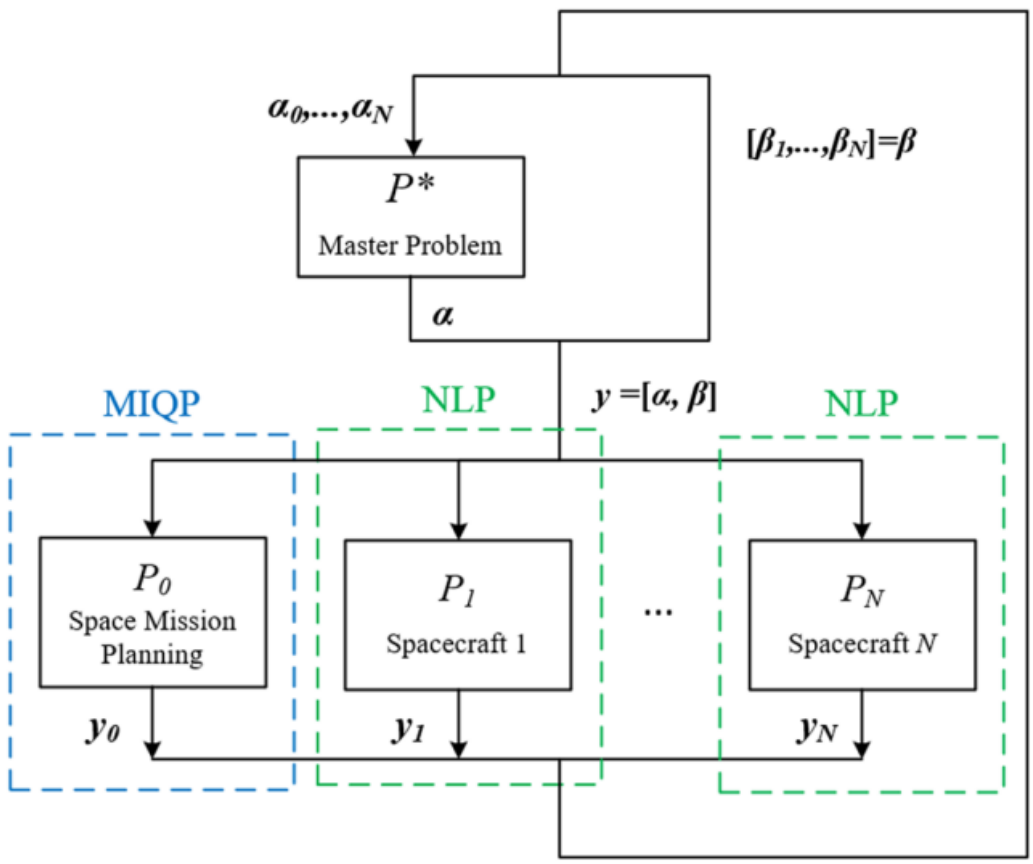

Figure 2.23: Decomposed optimization problem structure for the integrated mission planning and vehicle design problems proposed by Isaji *et al.* [74].

Table 2.4 provides a summary of the major CLO formulations presented in this chapter, which provide the basis for the formulation to be used in this research.

Table 2.4: Summary of major Space Logistics formulations introduced in recent years and described in this chapter.

Formulation	**Description**	**Strengths**	**Weaknesses**
Integrated Network-Vehicle Design	Solved the concurrent network flow-vehicle design problems using a systems-level and operational constraints of capacity and capability.	Full integration of both individual problems	Simplified vehicle design
Rule-based Space Systems Architecting using Graph Theory	Generation, evaluation of space system architecture alternatives using a graph of locations and transfers with rules to assign campaign elements.	Flexibility to many different, complex scenarios, Vehicle design in the loop, little user interaction	Simplified Vehicle Design, User-defined exploration scenarios limit options.

Table 2.4: Summary of major Space Logistics formulations introduced in recent years and described in this chapter.

Formulation	Description	Strengths	Weaknesses
SpaceNet	Integration of discrete event simulation to enable modeling of complex ConOps using input networks and transportation scenarios.	Ability to model many different complex ConOps	Input network and transportation scenarios limit broad trade space exploration
GMCNF	Models the many resources in the problem as individual commodities and adds generalized flows: consumption of commodities along arcs. Finds an optimal flow of commodities using linear programming.	Can model all propellant burned, Crew consumables, ISRU	Simplified vehicle design, Time-related inconsistencies

Table 2.4: Summary of major Space Logistics formulations introduced in recent years and described in this chapter.

Formulation	**Description**	**Strengths**	**Weaknesses**
Time-Expanded Generalized Multi-Commodity Flow (TEGMCF)	Duplication of static network of t timesteps	Accurately model campaigns with vehicles and crew using resources over time	Simplified vehicle design, computational complexity with larger problems
Path-arc	Introduction of paths as a sets of arcs and vehicles	Ability to model complex ConOps	Simplified vehicle design
Integrated Mission Planning and Spacecraft Design	Optimization coupled campaign and vehicle problems using a decomposed problem architecture	Subsystem-level vehicle design integrated with campaign optimization	May not be able to model complex ConOps and assess certain trades

2.5 Integrated Methodologies within Other Fields

Though this thesis focuses on SEC and the integration of vehicles within the campaign design process, a review of analogous methods in other fields is presented in this section. As Subsection 2.4.1 mentioned, the applications for NDPs are numerous, but each individual formulation is built upon the fundamental concepts. This section does not focus those other applications of NDPs by themselves, but rather the methods that integrated vehicle design and their processes for doing so.

2.5.1 Air Transportation Networks and Aircraft

Taylor and Weck was mentioned in Subsection 2.4.3 to have an integrated methodology for space campaigns and vehicles, which was built on the previous work of the same for air transportation networks and aircraft [23]. Both problems extended the systems design control volume to include both the NDP and vehicle design. The difference in the method of integration of each individual process is negligible, leading to the same fundamental technical gaps. With the control volume of the system-level optimizer being around both processes, each one was simplified to reduce the overall computational complexity. As a result, subsystem level sizing was not included in either formulation.

More in line with the objective of this thesis, Mane *et al.* used a System of Systems (SoS) approach to integrated the aircraft design and fleet allocation problem [75]. An initial aircraft design optimization problem was solved first based on an required range and payload capacity. The resulting design was used to identify the new optimal routing with the rest of the fleet using a MINP approach. However, this research focused assessing the impact of a singular new aircraft design into an already existing fleet, rather than the design of many architectures.

Bower and Kroo presented a methodology for the design of one or more aircraft that are optimized to fly a given route network [76]. A Multi-Objective Genetic Algorithm

(MOGA) was used on the aircraft design space to minimize direct operating costs, CO_2 and NOx emissions for a test problem with 4 cities and 8 routes. Each aircraft was design independently using a simplified, system level design model. Although the fleet assignment problem was solved, the network itself was input and its design was not considered. Similar methods have been proposed in [77, 78, 79].

Concurrent design optimization of air networks and aircraft design using economic trends was presented in [80, 81]. The author captures the impact of specific aircraft configurations on the market itself, as well as demands for routes. Again, each aircraft was designed using a systems level design tool, and subsystem information was not represented.

Hwang and Martins extended the concurrent design problem by using surrogate models for the aerodynamics and propulsion subsystems with a mission analysis tool [82, 83]. A gradient-based optimization technique was used initially on a single aircraft configuration, but was extended soon after for a full 128 route network. Though the aircraft design process did not represent every subsystem individually, the author showed that the concurrent aircraft-mission-allocation design problem is an important formulation with a 27% increase airline expected profit.

Roy and Crossley formulated an optimization framework that drives the design of aircraft using fleet level objectives as a MINP problem [84]. The author states that previous methods have used a sequential strategy for the combined problem, which does not address the coupling that exists between the two individual problems. An Efficient Global Optimization (EGO) based framework was used to solve the integrated problem, but the design of the aircraft was done at the systems level.

Most recently, Alexandre *et al.* proposed a methodology to determine the optimal air transportation network concurrently with the optimal fleet for the network [85]. Passenger demand information was used to identify the optimal network which drove the design of the optimal set of aircraft for that network, analogous to the objective of this research. The integrated framework is shown in Figure 2.24. Although not directly represented by a

collection of subsystems, each aircraft had a total of 46 design variables that were selected to ensure each design point adhered to FAR requirements.

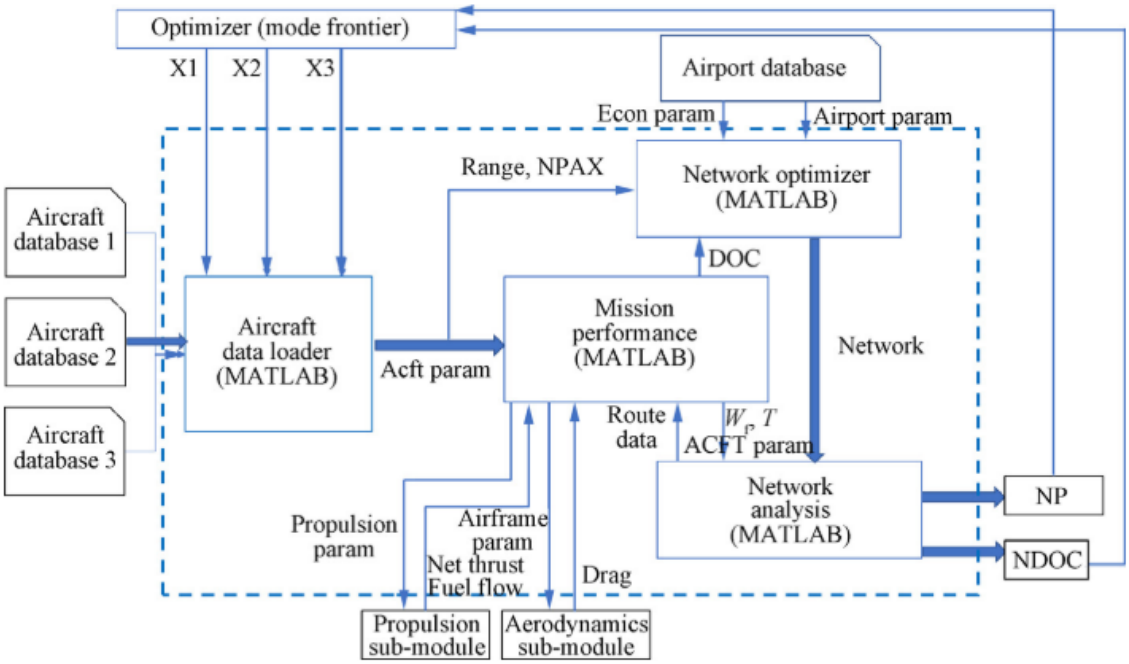

Figure 2.24: An integrated aircraft-network optimization framework presented in [85].

2.5.2 Concurrent Network Design and Sizing of Unmanned Aerial Vehicles

Choi presents a methodology for the concurrent design and optimization of Unmanned Aerial Vehicles (UAV) and their networks for delivery systems, also shown in Figure 2.25 [86, 87]. An initial urban flight network is generated using map data which is used to solve an endurance constrained vehicle routing problem. This first optimization problem does not size any individual vehicles but uses a reference set represented by payload capacity, velocity, endurance, and a fixed cost. Endurance constraints are used to account for effects of take-off and landing during delivery, which range constraints cannot do. The endurance constrained problem is solved to identify an initial set of optimal network routes for the UAV design process, represented by a Small Vertical Takeoff and Landing (sVTOL) UAV sizing and synthesis process. A worst-case route is chosen as the sizing mission for each UAV in the network using sVTOL UAV sizing and synthesis, as shown in Figure 2.26. The

updated vehicle set is re-represented in the network using energy based parameters to solve a new, energy-constrained vehicle routing problem, generating a new set of optimal routes. Convergence is assessed using vehicle design parameters and the updated routes and the process is repeated using Fixed Point Iteration (FPI) if necessary. The resulting converged solution is an optimal network with each UAV sized as a collection of subsystems.

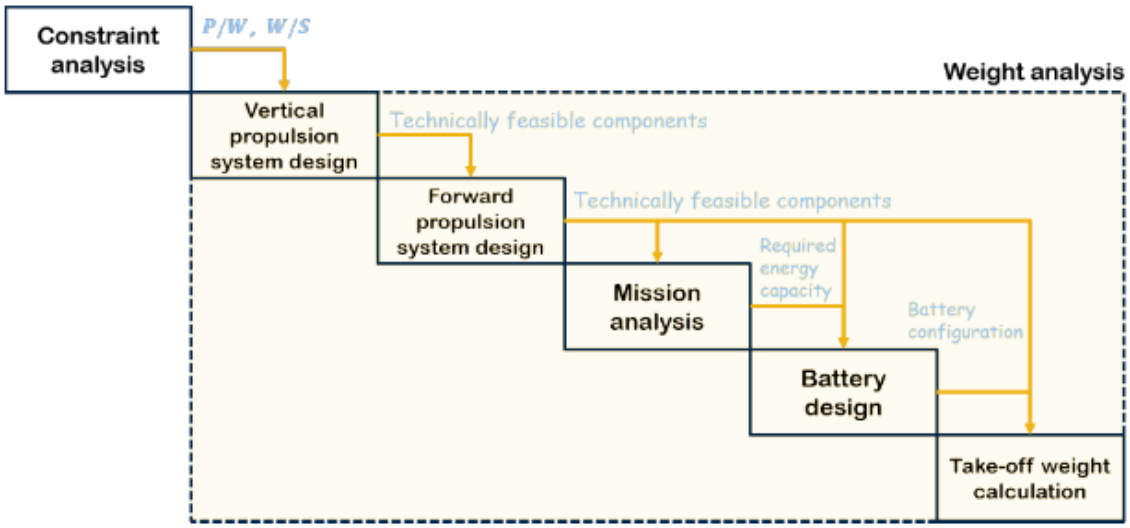

Figure 2.25: Integrated framework for network design and UAV sizing and synthesis from [86].

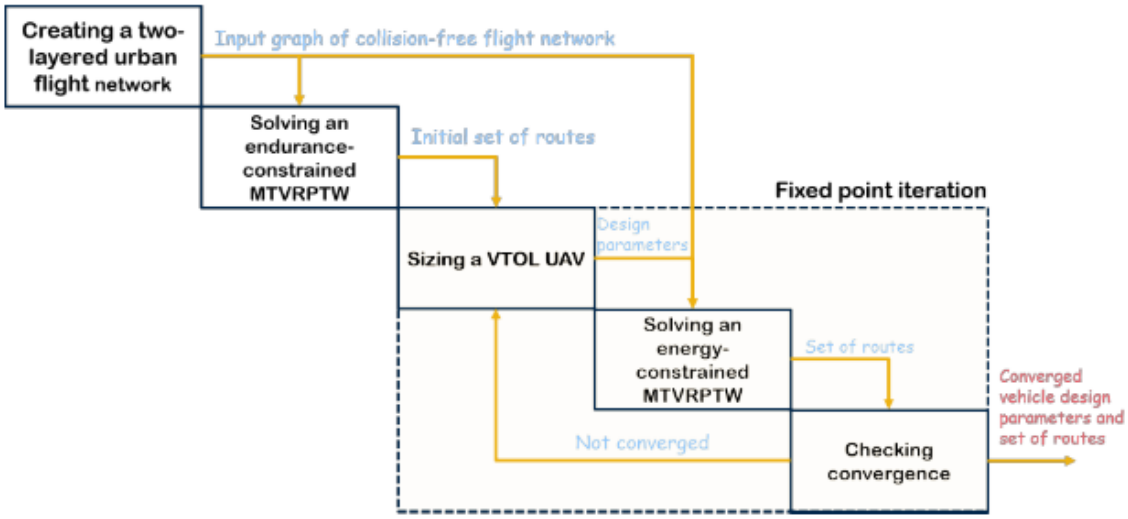

Figure 2.26: Sizing and synthesis process of a sVTOL UAV in the integrated design framework presented in [86].

After reviewing these campaign logistics formulations, the following observation can be stated regarding the representation of in-space transportation systems and their subsystems:

Observation 7: Given logistics optimization processes require a set of vehicle capabilities, the set can be extended to include subsystem information.

The information presented in this chapter and the observations made with regards to specific CLO processes are used to construct hypotheses on the formulation of the campaign design process for the proposed methodology. These hypotheses are shown below and in the updated thesis structure in Figure 2.27.

- Formulation Hypothesis 1: If Mixed Integer Programming is used to optimize a time-expanded, generalized multi-commodity network, broad areas of the campaign trade space can be explored.
- Formulation Hypothesis 2: If certain paths are specified in the logistics formulation, complex ConOps could be included without a significant increase in computational load.
- Formulation Hypothesis 3: If the assumed vehicle capabilities in the logistics formulation includes a set of subsystems, it could be updated on each iteration using the sizing and synthesis process.
- Formulation Hypothesis 4: If the optimal mission set from campaign optimization is used to drive vehicle design, each vehicle in the campaign will be sized individually for its own mission.

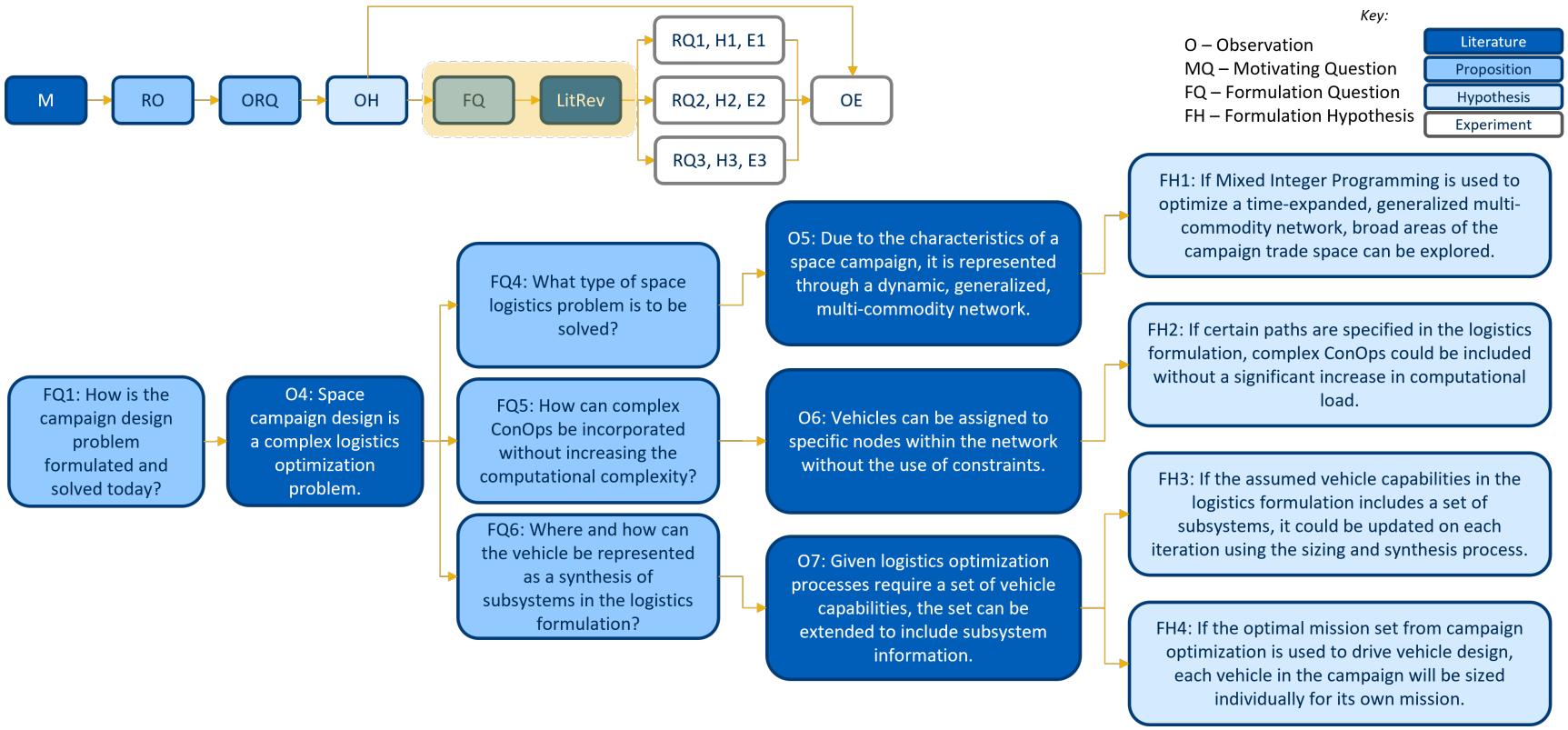

Figure 2.27: Thesis structure updated to show the formulation hypotheses for campaign design.

2.6 Network Formulation and Optimization

The previous sections of literature review found that campaign design is a complex logistics optimization problem that can be represented as a TEGMCF and that complex ConOps can be modeled using paths. This section uses these findings as a basis and details the specific technical formulations of the network considered for this thesis, the accompanying improvements necessary to properly model in-space transportation systems, and any other data required.

2.6.1 Nodes

The introduction of chapters 2 and 3 set one of the requirements of the network formulation to be an Earth-Moon-Mars network. This enables analysis of many different campaigns, from smaller cis-lunar aggregation to much larger crewed Mars exploration campaigns like DRA 5. Within the TEGMCF, each planetary node can be extended to its own sphere of influence to include orbital destinations within it. Each orbit in space is unique, parameterized, and defined by several continuous orbital elements, summarized in Table 2.5 and visually represented in Figure 2.28 [88].

Table 2.5: Summary of the classical parameters used in orbital mechanics.

Orbital Element	**Variable**	**Description**
Radius at Apoapsis	r_a	Distance from the center of the orbital body to the farthest point in orbit (apoapsis).

Table 2.5: Summary of the classical parameters used in orbital mechanics.

Orbital Element	**Variable**	**Description**
Radius at Periapsis	r_p	Distance from the center of the orbital body to the closest point in orbit (periapsis).
Eccentricity	e	Ratio of the radii of the orbit that defines the shape of the orbit.
Altitude	h	The distance of a point in orbit above the surface of the central body. The radius of the orbit minus the radius of the central body
Semimajor Axis	a	Half of the sum of the Apo and Periapsis radii.
Inclination	i	The angle of the orbital plane with respect to the reference plane
Longitude of Ascending Node	Ω	Angle in the reference plane of the ascending node, the point at which the orbit passes upward through the reference plane.

Table 2.5: Summary of the classical parameters used in orbital mechanics.

Orbital Element	**Variable**	**Description**
Argument of Periapsis	ω	Angle that defines the orientation of the orbit about its own axis.
True Anomaly	θ	Angle of the body in the orbit with respect to periapsis.
Specific Orbital Energy	ξ	Total energy state of the orbit.
Characteristic Energy	$C3$	Amount of energy required to escape the gravity of a central body.
Period	T	The amount of time it takes to perform one full revolution of an orbit.

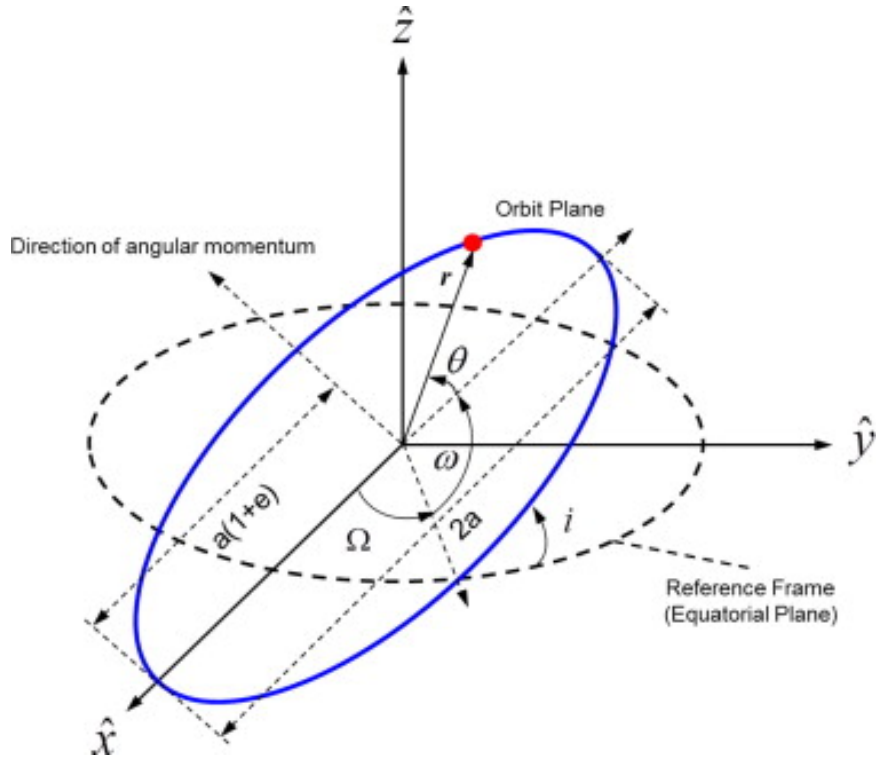

Figure 2.28: Visual representation of the main orbital elements used to define locations, movements, and orbits in space [89].

Given the number of design variables, and dependence of reference frame and time, full-scale orbital mechanics problems are very complex, with some taking many days to arrive at a numerical solution even with high performance computing resources. Adding travel to other bodies only exacerbates the problem, especially for Mars as the amount of energy to reach is cyclical in nature, as Earth and Mars move about the Sun at different speeds, closest every 26 months. Different types of transportation systems assumed can also affect the closure and runtime of trajectory analysis. For these reasons, at the pre-conceptual to conceptual level of design, full-scale trajectory analysis is either replaced by surrogate models or simplified using assumptions [90]. For the scope of this research, the latter is chosen to minimize runtime, while the former is left as a future area of growth.

Given the significance of vehicles in this thesis and their highly coupled nature to their sizing missions, locking these degrees of freedom closes off parts off the design space. However, to not significantly increase the computational with a large scale tra-

jectory optimization problem, the orbital mechanics and mission analysis considered in this research will be simplified. Each orbit will be parameterized semimajor axis (a), and by extension, characteristic energy ($C3$), where the latter is defined by Equation 2.15. The constant, μ, is the gravitational parameter, a product of the gravitational constant, $G = 6.67430 * 10^{-11} \frac{m^3}{kg*s^2}$, and the mass of the central body.

$$C3 = -\frac{\mu}{a} \tag{2.15}$$

Although the orbital parameters are continuous, they can be grouped based on their distance from the central body. Highly elliptical orbits may have a perigee in LEO but an apogee in High Earth Orbit (HEO) which can complicate this schema. As a mitigation, orbits can instead be grouped by their $C3$, as a measure of the distance from the central in an energy perspective. That is, higher orbits will have higher $C3$s, and vice versa.

Earth Sphere

For the Earth Sphere of Influence (SoI), or Earth Sphere, there are five main orbital nodes: Surface, LEO, Geosynchronous Orbit (GSO), Medium Earth Orbit (MEO), and HEO, categorized by their $C3s$ in Table 2.6 [91]. The surface node is the most important, as every campaign and mission has its origin at Earth during launch. LEO, MEO, and HEO are parametric orbits where many operations occur, from launch staging, to refueling, and more. GSO is a specific circular orbit, where the period is exactly 24 Earth hours, corresponding to an altitude of about 35,786 km. Geostationary Orbit (GEO) is a special case of GSO with an inclination of zero and a groundtrack of a point rather than the figure eight of GSO. Although departure for interplanetary missions can occur from anywhere, given the vehicle has enough ΔV capability, most campaign concepts call for departure at higher orbits, after refueling, as the vehicle would be far out from Earth's gravity well. Departure opportunities for the Moon are less complicated and much less energetically expensive.

Table 2.6: Summary of the Earth Sphere nodes formulated this research, categorized by their $C3$s.

Node	**Minimum** $C3$ (km^2/s^2)	**Maximum** $C3$ (km^2/s^2)
Earth Surface	Undefined	Undefined
LEO	-60	-47.578
MEO	-47.58	-9.4536
GSO or GEO	-9.4536	-9.4536
HEO	-9.4536	-1.02106

Lunar Sphere

The Moon itself is within the Earth Sphere, but is treated as its own planetary node. Similar to Earth, the Lunar surface node is very significant both as a goal destination for some campaigns and as ISRU option for others. There are two orbits considered in the Lunar Sphere: NRHO, Low Lunar Orbit (LLO). NRHO serves as the location of Gateway and as a staging orbit for other vehicles, while LLO can serve as an intermediate orbit for Lunar surface access, analogous to LEO. However, for problems involving cislunar space, orbits are harder to parameterize as the Moon's gravitational pull is not as strong as Earth's, limiting the range of stable orbits in its sphere of influence. As a result, within the lunar sphere, the ΔVs will be varied directly, rather than the semimajor axis.

Mars Sphere

Mars is important to include in the network to assess longer, more complex campaigns, and given its status as the horizon goal. Although it has two moons of its own, Phobos and Deimos, they are not included in this formulation to reduce computational complexity and given the focus of Mars as the destination. Adding them for future studies is possible with little extra work. As a result, nodes within the Mars Sphere is similar to those in the Earth Sphere, summarized in Table 2.7, although with different nomenclature. Orbits called n-sol refer to their periods in integer number of Earth-days. For example, a 5-sol orbit is an elliptical Mars orbit with a period of 5 Earth days.

Table 2.7: Summary of the Mars Sphere nodes formulated this research, categorized by their $C3$s.

Node	**Minimum** $C3$ (km^2/s^2)	**Maximum** $C3$ (km^2/s^2)
Mars Surface	Undefined	Undefined
Low Mars Orbit (LMO)	-11.75	-11
n-sol	-2.13 (1-sol)	-0.58 (7-sol)

2.6.2 Arcs

Typically in within the logistics network formulation, each node is given an assumed orbit and the arc cost to transfer from one node to another has set values of ΔV and ΔT. This is an input data set that the optimizers uses to associate the cost of traveling on an arc in the form of an energy and time penalty for the vehicle. With the nodal parameterization mentioned in Subsection 2.6.1, that formulation needs to be augmented as the ΔV and ΔT of each arc can vary with the specific orbit of the node. The specific method for calculating those values for each transfer will be discussed in the mission analysis portion of the VSS section. That data table of network costs is updated at each iteration using the this calculation, meaning the CLO process does not use them as additional design variables within the optimizer. This reduces the computational load on the campaign side, which is expected to be more computationally expensive than the VSS process. Vehicles traveling on an arcs are denoted by binary variable, $b_{v,a}$, for all vehicles and arcs in the network.

Interplanetary Arcs

Earth and Mars move about the Sun at different speeds, approaching each other at their closest point about every 26 months. This means the energy required to transfer between them is cyclical in nature, where the peaks signify transfers where the planets are not optimally aligned and the valleys are opportunities. Interplanetary trajectories to Mars are typically split into two classes: conjunction or opposition. Conjunction class missions are transfers between the two planets while they are on the same side of the Sun, while op-

position trajectories have them on opposite sides. The former is characterized by longer trip times and surface stays for relatively lower energy requirements. [92, 93] Opposition class trajectories trade higher energy requirements for lower trip times and surface stays. Although both are considered for cargo and crew missions, opposition trajectories are considered to reduce the crew exposure to the deep space radiation environment, while conjunction missions can offer much lower propulsive requirements. Figure 2.29 shows the cyclical nature of Earth-Mars trajectories over time and the quantitative difference in the energy requirements between conjunction and opposition. Planetary flybys are often considered to reduce the energy requirements for opposition missions without a major increase in trip times, which are also shown in Figure 2.29.

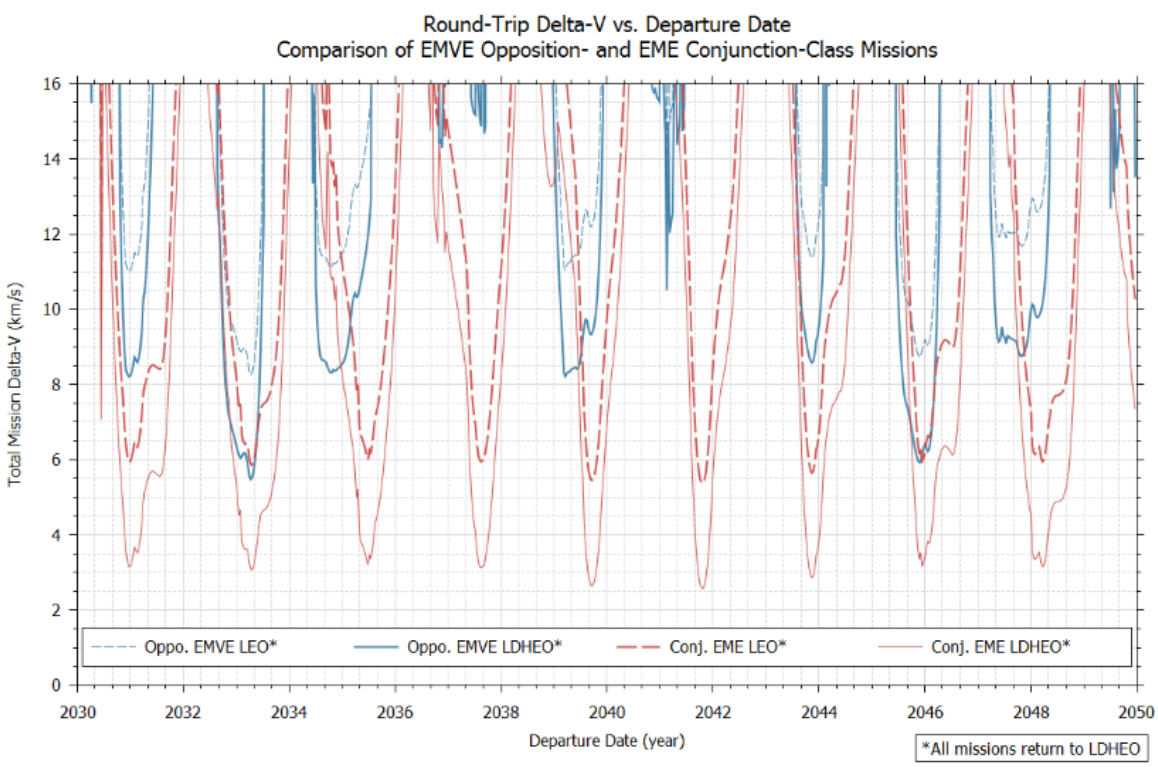

Figure 2.29: A plot of the ΔV requirements for Earth-Mars transfers between 2030 and 2050 [94].

The peaks in ΔV required for an interplanetary transfer when Earth and Mars are not aligned can be over a 400% increase. As a result, Mars missions are typically conducted at every valley, also called a transfer opportunity or transfer window.

Another way of showing the trends depicted in Figure 2.29 and estimating the ΔV is using a porkchop plot. They parameterize the total ΔV required by the departure and arrival dates of the planets, creating a 2-D contoured version of Figure 2.29 [95]. An example porkchop plot for a 2018 Earth-Mars opportunity is shown in Figure 2.30.

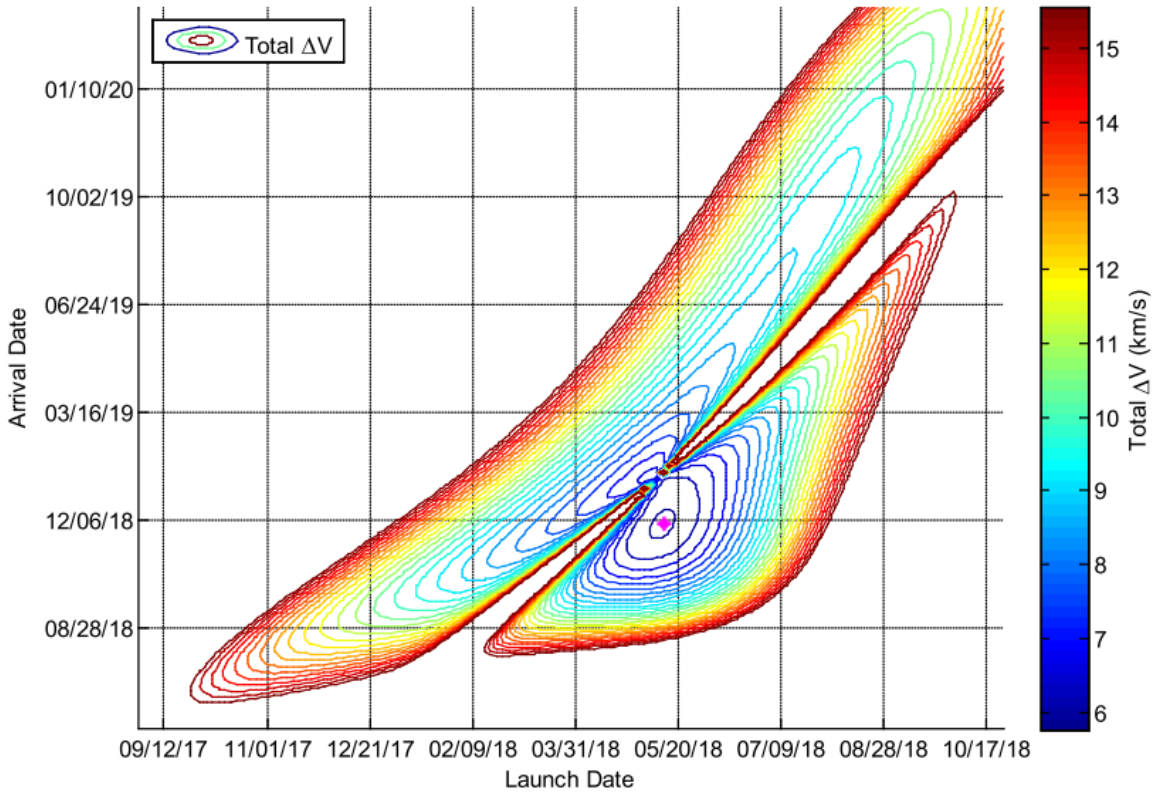

Figure 2.30: Porkchop plot of the 2018 Earth-Mars opportunity [95].

A single porkchop plot can be generated for many opportunities to show the cyclical nature described previously. Each single porkchop will show the same trends, but the values of the minimums will change with respect to the dates, shown in Figure 2.31.

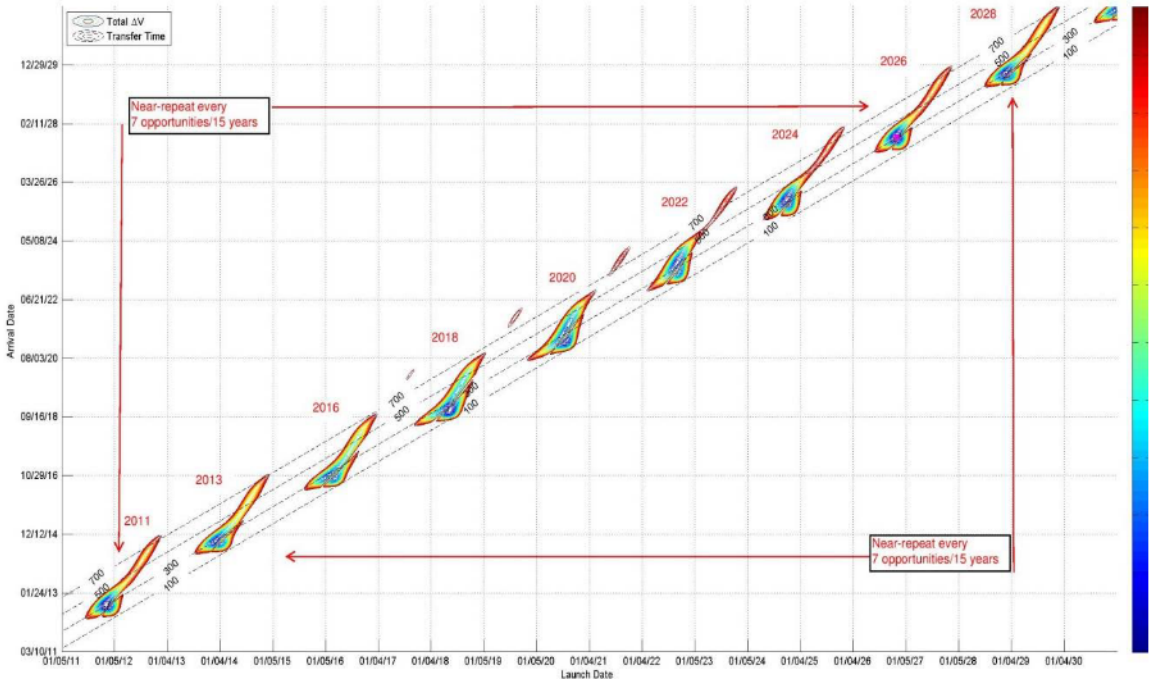

Figure 2.31: Porkchop plot extended to show different transfer opportunities [95].

For this research, transfers between Earth and Mars will be calculated using porkchop data and parameterized by dates. That is, each interplanetary arc will be generated based on the departure and arrival dates of generated porkchop data, shown notionally in Equation 2.16. This enables CLO to vary the dates as needed to find the best one for each vehicle and size them accordingly.

$$\Delta V, \Delta T = porkchop(date_{departure}, date_{arrival}) \tag{2.16}$$

2.6.3 Paths

As introduced in Subsection 2.4.3, the path-arc formulation is an addition to the overall logistics formulation. It defines a path as a pre-specified set of arcs for a vehicle or crew to travel through within the network so as to model certain complex ConOps. These ConOps can be modeled without paths, by adding more, proper constraints on the overall optimization problem at the cost of drastically increasing the computational expense and runtime.

Since the paths are pre-specified, the optimizer does not have to find it by itself, but rather it has been defined as a part of the optimization problem itself. The implementation presented by McBrayer *et al.* was used to model the launch, aggregation, and mission execution of the 3-element government reference HLS mission. This approach included a crew launch to the Gateway in NRHO via SLS and Orion.

Fundamentally, paths are the assignment of vehicles or crew to specific arcs and each one is problem dependent and user driven. A notional example of a path for a generic vehicle is shown in Figure 2.32. Note that while a path is defined as a series of events for a vehicle, throughout the network, there may be several valid sets of these series of events, depending on when the events initialize; these are called arc-sets. This distinction between a path and arc-set is significant, where a path is chosen for use by the optimizer through a binary variable, b_p, it must select at most one of those valid arc-sets, governed by the constraint in Equation 2.17.

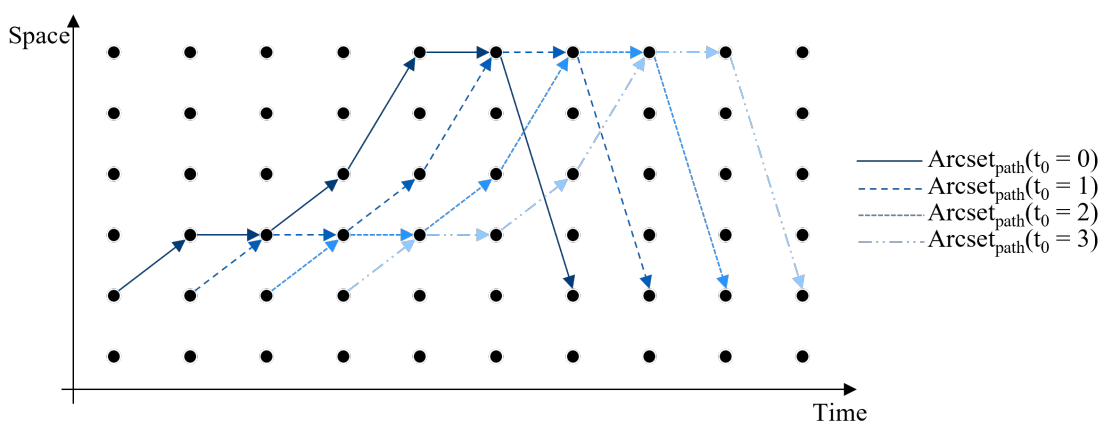

Figure 2.32: Notional depiction of the path arc formulation showing a path as a set of different, valid arc-sets that start at various times.

$$b_p = \sum_{arcset \in p} b_{arcset,p} \quad \forall\, p \in P \tag{2.17}$$

Each path is defined as a series of events for a vehicle by specifying the departure and arrival locations for each event and the event type. Table 2.8 summarize the different

allowable path event types. Valid arcsets are built using these event definitions over the time domain of the network, each assigned a binary variable, $b_{arcset,p}$. This binary variable further constrains the use of the vehicles on each arc in the arc-set, through Equation 2.18.

Table 2.8: List of path event types and their descriptions.

Event Type	Description
ΔV	Burn event that specifies a vehicle moving from one spatial location to another
ΔT	Time passage event that specifies how long the vehicle stays at a spatial location
Δm	A mass change event that specifies a docking or undocking of a vehicle, payload over the course of a single time step

$$b_{arcset,p} = 1 \implies \sum_{a \in arcset} \sum_{v \in arcset} b_{v,a} = \sum_{a \in arcset} \sum_{v \in arcset} 1 \tag{2.18}$$

2.6.4 Vehicles

Vehicles within this formulation are split into three types: launch vehicles, space vehicles, and vehicle stacks. Launch vehicles govern the movement of space vehicles on every arc leaving the Earth's surface, and are defined by the parameters in Table 2.9. The dimensions of each space vehicle constrain the valid set of available launch vehicles for it and which launch arc chosen is constrained by the total mass of that space vehicle at the origin. Each launch vehicle has some dollar costs associated with it, which can be used in the objective function as a minimization term. The cadence constrains how many of that launch vehicle can be used within a range of timesteps, corresponding to real operational constraints.

Similarly, space vehicles have their own set of design parameters, summarized in Table 2.10. The main design variables in the optimization process is the amount of fuel and oxidizer for each space vehicle, constrained by the vehicles' I_{sp}, OFR, and the arcs it ends up traveling on. Within the CLO process, the inert mass is a fixed parameter, although it may be updated during each iteration of the integrated process, produced by the VSS pro-

Table 2.9: List of parameters and their descriptions that define a launch vehicle within this network formulation.

Parameter	Description
Throw Mass	Maximum mass to LEO, GEO, HEO
Maximum Diameter	Maximum allowable payload diameter
Maximum Height	Maximum allowable payload height
Launch Cost	Cost for each launch
Cadence	Minimum time between consecutive launches

cess. It is important to note that the inert mass here is the total mass of the vehicle minus the consumables, payloads, and propellants. For this research, in the CLO process, it is assumed that there is a single main propulsion system on board for all burns, and no Reaction Control System (RCS) is used. However, it is assumed to be accounted for in the inert mass of each vehicle. If crew is involved in the campaign, variables for each consumables are included to ensure they are on board.

To properly model transportation systems in SECs, the concept of vehicle stacks is introduced to model the integration of multiple vehicle elements for larger transportation systems and longer missions. Stacks are defined as a set of individual space vehicles that travel together, with active element that provides propulsion for itself and the passive elements. Implementation of vehicle stacks within the network is enabled solely because of paths. As each path event is defined, the full stack and active element can be specified, and the usage of all corresponding vehicles is enforced through Equation 2.19 and Equation 2.20. Of course, the amount of propellant burned differs between that of the passive and active vehicles in the stack, as well as if each vehicle was flying independently. Constraints to ensure the proper amount of propellant is accounted for is presented in the following subsection.

Table 2.10: List of parameters and their descriptions that define a space vehicle within this network formulation.

Parameter	Description
Inert Mass (kg)	Total mass of all non-propellants in the vehicle. Includes RCS propellant.
Diameter (m)	Overall diameter of the vehicle, used to assign valid launch vehicles
Height (m)	Overall height of the vehicle, used to assign valid launch vehicles
Fuel	Main fuel for the space vehicle
Oxidizer	Main oxidizer for the space vehicle
I_{sp} (s)	Specific impulse of the propellant
OFR	Mass ratio of the oxidizer and fuel
Max Payload Diameter (m)	Maximum available diameter for potential payloads
Max Payload Height (m)	Maximum available height for potential payloads
Max Payload Mass (kg)	Maximum available mass for potential payloads
Boiloff$_{fuel}$ (kg/day)	Boiloff rate of the fuel
Boiloff$_{ox}$ (kg/day)	Boiloff rate of the oxidizer
Fuel Mass (kg)	Design variable for the fuel mass for the vehicle, set as a range
Oxidizer Mass (kg)	Design variable for the oxidizer mass for the vehicle, set as a range
Water Mass (kg)	Design variable for the amount of water for crew, if on board, set as a range
Oxygen Mass (kg)	Design variable for the amount of oxygen for crew, if on board, set as a range
Food Mass (kg)	Design variable for the amount of food for crew, if on board, set as a range

$$b_{arcset} = 1 \implies \sum_{a \in arcset} \sum_{v \in arcset} b_{v,a} + \sum_{a \in arcset} \sum_{stack \in arcset} b_{stack,a} = \sum_{a \in arcset} \sum_{v \in arcset} 1 + \sum_{a \in arcset} \sum_{stack \in arcset} 1 \quad (2.19)$$

$$b_{stack,a} = 1 \implies \sum_{v \in stack} b_{a,stack} = \sum_{v \in stack} 1 \quad (2.20)$$

2.6.5 Payloads and Crew

Payloads are key to each campaign as they directly relate to the mission objectives. Within this formulation, payloads are divided in to crew and cargo, while the latter is further divided into pathed and un-pathed. Fundamentally, all payloads must be attached to either a vehicle or a location to model their transport and delivery to their target destinations. All crew missions are pathed, as typically their ConOps are known a priori. Table 2.11 summarizes the different parameters that define a payload in this network formulation.

Table 2.11: List of parameters and their descriptions that define the different payload types.

Parameter	**Description**
Type	Crew or Cargo
Pathed	Whether or not the payload is path defined
Final Destination	Location where the payload is intended to reach
Diameter (m)	Diameter of the payload
Height (m)	Height of the payload
Mass (kg)	Mass of the payload
Setup Time (days)	The time it takes for the payload to be initialized before it can be used (ex. ISRU)
Number of Crew	Number of crew being transported
Commodities	The commodities related to this payload
Capacity	The capacity for each related commodity
Production Rate (kg/day)	The rate of production of each related commodity

For payloads that are not pathed, the optimizer is able to select the vehicle that each one is attached to based on the payloads configuration and vehicle's capacities. The final destination drives the optimizer to choose vehicles and arcs to deliver each payload while minimizing the objective.

Pathed payloads operate in a simpler manner by defining the source vehicle for that payload during a path definition. With constraints that enforce payloads are connected to vehicles at all times, this ensures pathed payloads stick with the accompanying vehicle on the path. Paths also enable transfer of payloads from one vehicle to another, assumed to

occur over the course of a single timestep holdover arc. The constraints governing payload transfer are covered in the subsequent sections.

2.6.6 Commodities

Commodities are categorized mainly by type: fuels, oxidizers and consumables and are defined primarily by density. Crew consumables require one more parameter: consumption rate of the commodity per timestep, per crew member. Each vehicle has a minimum and maximum available commodity storage capacity, defined as a design variable for the optimizer. Constraints are applied such that these commodities are being used at the proper rates. Propellant usage, or arc burn constraints are defined later, but crew consumable constraints are simply driven by the previously mentioned rates and the number of crew on the associated vehicle.

2.6.7 Constraints

Constraints bind the overall optimization problem to ensure the optimizer finds a numerical solution that not only satisfies the objective, but is in fact feasible. These constraints can be used to represent physical laws, such as mass conservation, or even external factors like launch cadence, operations, and more. Two groups of constraints will be considered for this research: technical and programmatic, each one covering a different subset, described in the following subsections.

Technical Constraints *- Vehicle Movement*

The main set of technical constraints enforce that vehicles are moving properly and using the correct amount of propellants. These are broken down into three main subsets: launches, in-space transfers, and paths. Although vehicles can be sourced in-space, to model assets that have already launched, Earth-sourced vehicles must be launched by launch vehicles and thus, no propellants are used by vehicles for these arcs. Valid launch

vehicles are assigned to each vehicle based on their type and input dimensions and the specific launch arc chosen depends on the mass of the vehicle and launch vehicle throw capabilities. For the set of all launch vehicles, LV, and all vehicles, V, variable $b_{v,lv}$ represents the use of launch vehicle lv for vehicle v. These launch operations are enforced through the constraints in Equation 2.21 and Equation 2.22, where A_{launch} is the set of all launch arcs.

$$\sum_{lv \in LV} b_{v,lv} = \sum_{a \in A_{launch}} b_{v,a} \leq 1 \quad \forall\, v \in V \tag{2.21}$$

$$b_{v,a} = 1 \implies$$
$$\sum_{lv \in LV} b_{v,lv} \; * \; throw\, mass_{lv,a,arrival\, location} \geq total\, mass_{v,a,departure\, location}$$
$$\forall\, a \in A_{launch}, v \in V \tag{2.22}$$

Once launched and in-space, vehicles are conserved at the node level, where all vehicles flowing into a node must leave it. Since the act of a vehicle traveling on an arc is associated with binary variable, $b_{v,a}$, this constraint is written in Equation 2.23, where N is the set of all nodes, $A_{n,arrival}$ is the set of all arcs that arrive at node n, and $A_{n,departure}$ is the set of all arcs that depart node n.

$$\sum_{a \in A_{n,arrival}} b_{v,a} = \sum_{a \in A_{n,departure}} b_{v,a} \quad \forall\, v \in V, n \in N \tag{2.23}$$

Technical Constraints *- Payload Movement*

Payloads must always be attached to either a vehicle, or a node, depending on where it is in its mission. For non-pathed payload elements, there are several constraints necessary to ensure continuity and model these operations. Each payload in the set of all payloads,

$\rho \in \mathcal{P}$, has a binary variable, b_v^ρ that denotes whether or not it is attached to vehicle v. Similar to the relationship between vehicles and launch vehicles, invalid payload-vehicle pairings are prefiltered based on the input parameters of mass and dimensions of each. Payloads also have binary variables indicating which vehicle it is attached to at each node, $b_{v,i,m}^\rho$ and another to indicate whether it has been dropped off at a node, d_m^ρ. If a payload is detached, both variables are 0; otherwise they are 1. Equation 2.24 shows the logic of the constraints around these variables.

$$z_{v,i,m}^\rho \begin{cases} = 1 & z_v^\rho = 1 \text{ and } d_m^\rho = 1 \text{ and } b_{v,a} = 1 \\ = 0 & z_v^\rho = 1 \text{ and } b_{v,a} = 1 \text{ and } (i = \text{final destination or } d_m^\rho = 0) \end{cases} \tag{2.24}$$

$$\forall \rho \in \mathcal{P}, v \in V_{valid}^\rho, a \in A$$

Further, the dropoff indicators can also be constrained to:

$$d_m^\rho \begin{cases} = 1 & \sum_{s \in S} \sum_{v \in V} z_{v,s,m}^\rho = 1 \text{ or } \sum_{v \in V} z_v^\rho = 0 \\ = 0 & \sum_{s \in S} \sum_{v \in V} z_{v,s,m}^\rho = 0 \text{ and } \sum_{v \in V} z_v^\rho = 1 \end{cases} \quad \forall \rho \in \mathcal{P}, m \in T \tag{2.25}$$

Finally, for payloads like ISRU that are dropped off but are still utilized afterwards, they are attached to nodes themselves through binary variable, $b_{i,m}^\rho$ and constraints in Equation 2.26

$$z_{i,m}^\rho \begin{cases} = 1 & d_m^\rho = 0 \\ = 0 & d_m^\rho = 1 \end{cases} \quad \forall \rho \in \mathcal{P}, i \in S, m \in T \tag{2.26}$$

Pathed payloads, however, follow a different set of constraints, with all of them being sourced at $t = 0$, as defined in Equation 2.27.

$$b_{\rho,p} = 1 \implies \sum_{v \in V} b^{\rho}_{v,m_{source},0} = 1 \quad \forall\, p \in, \rho \in \mathcal{P} \tag{2.27}$$

Binary variable, $b_{\rho,p}$, is the path variable for the payload and P_ρ is the set of all payload paths. To conserve the movement of these payloads, Equation 2.28 is written to ensure all payloads are attached to the same vehicle at every node, unless otherwise specified.

$$\begin{gathered} b_{\rho,p} = 1 \implies b_{arcset} = 1 \implies b^{p}_{v,a_1,departure\,node} + \sum_{i=1}^{n} z b^{p}_{v,a_i,arrival\,node} \\ where\ n = number\ of\ arcs\ in\ arcset \quad \forall\, v, a \in arcset \end{gathered} \tag{2.28}$$

Payload transfers are implemented in this formulation using paths. That is, during path definition, a payload can be transferred from one vehicle to another over the course of a single timestep holdover arc. Subsequently, this means that both the source and sink vehicles must also be on the path and used on the arc, at least for the transfer event itself. These operations are modeled through constraints in Equation 2.29 and Equation 2.30, where b_p corresponds to the path that the transfer is occurring on.

$$\begin{gathered} b_p = 1 \implies b_{arcset} = 1 \implies b^{\rho}_{v_{source},a_{transfer},departure\,node} + b^{\rho}_{v_{sink},a_{transfer},arrival\,node} = 2 \\ \forall\, a_{transfer}, v_{source}, v_{sink}, \rho \in arcset \end{gathered} \tag{2.29}$$

$$\begin{gathered} b_p = 1 \implies b_{arcset} = 1 \implies b_{v_{source},a_{transfer}} + b_{v_{sink},a_{transfer}} \\ \forall\, a_{transfer}, v_{source}, v_{sink} \in arcset \end{gathered} \tag{2.30}$$

Although payloads should also be conserved at the node and vehicle levels, the inclusion of payload transfer in the network formulation subsequently breaks this conservation.

As a result, an additional set of variables and constraints are implemented to ensure continuity. Table 2.12 summarizes the variables and Equation 2.31-Equation 2.34 are the constraints themselves. The last equation ensures that continuity constraints are only applied for payloads on vehicles on specific arcs that are not transfer arcs. The auxiliary variables help indicate whether or not those arcs have transfers through the logic shown.

Table 2.12: List of variables used to model payload transfers.

Variable	Description
$b_{a,v}^{transfer}$	Binary variable that indicates whether or not vehicle v on arc a is used for a payload transfer
$d_{a,v}^{transfer_1}$	Auxiliary binary variable 1 that indicates if a vehicle v is used, not part of a path on arc a, and therefore does not have a transfer
$d_{a,v}^{transfer_2}$	Auxiliary binary variable 2 that indicates a pathed vehicle v on arc a is used and does not have a transfer.

$$b_p = 1 \implies b_{arcset} = 1 \implies b_{a,v_{source}}^{transfer} + b_{a,v_{sink}}^{transfer} = 2 \quad \forall \rho \in \mathcal{P}_{transfers} \tag{2.31}$$

$$d_{a,v}^{transfer_1} = b_{v,a} - b_{a,v}^{transfer} \quad \forall v \in V \tag{2.32}$$

$$d_{a,v}^{transfer_2} = AND(b_{v,a}, d_{a,v}^{transfer_1}) \quad \forall v \in V \tag{2.33}$$

$$d_{a,v}^{transfer_2} = 1 \implies b_{v,a,departure\,node}^{\rho} = b_{v,a,arrival\,node}^{\rho} \tag{2.34}$$

Technical Constraints *- Commodity Usage and Conservation*

Burns

As stated previously, commodities in the network are mainly divided into propellants and crew consumables. Propellant usage is defined using the arc costs of ΔV and ΔT

through engine burns and boiloff. Burns are performed by vehicles on all arcs that are not holdover arcs, excluding launch arcs, which are performed by launch vehicles. The amount of propellant burned depends on the vehicle configuration, propellant used, and ΔV through the ideal rocket equation, Equation 2.13

$$\Delta V = g_0 I_{sp} ln(\frac{m_{initial}}{m_{final}}) \tag{2.35}$$

Rearranged, the mass ratio of $\frac{m_{final}}{m_{initial}}$, or K, for a vehicle on an arc can be calculated using Equation 2.36.

$$K = e^{-\frac{\Delta V}{g_0 I_{sp}}} \tag{2.36}$$

Finally, using the input OFR for each vehicle, the amount of fuel and oxidizer burned for each arc can be calculated, where the amount burned is the difference between the initial and final total masses of a vehicle on an arc. A summary of the amount of propellants burned for all arcs and vehicles in the network is shown Equation 2.37, where y_{total} is the total mass of each vehicle at the beginning of the arc.

$$x_{fuel,burned,a,v} = \begin{cases} (1-K)(y_{total})\frac{1}{1+OFR} & a \in A_{transfer,discard} \text{ and } v = v_{burn} \\ 0 & a \in A_{holdover,launch} \text{ or } v \neq v_{burn} \end{cases} \tag{2.37}$$

$$\forall a \in A, v \in V \tag{2.38}$$

$$x_{ox,burned,a,v} = \begin{cases} (1-K)(y_{total})\frac{1}{1+1/OFR} & a \in A_{transfer,discard} \text{ and } v = v_{burn} \\ 0 & a \in A_{holdover,launch} \text{ or } v \neq v_{burn} \end{cases} \tag{2.39}$$

$$\forall a \in A, v \in V \tag{2.40}$$

If a vehicle is burning on its own, the amount of propellant burned is different than that of vehicles that are part of a stack, whether they are passive or active. Several auxiliary variables are introduced and constrained to indicate the vehicle configuration for all burn constraints; Table 2.13 summarizes these variables.

Table 2.13: List of variables used to model vehicle configurations for burn constraints.

Variable	Description
$y^{total}_{a,m_{departure},v}$	Continuous variable for the total mass of a vehicle v on arc a, at the departure node, $m_{departure}$
$b^{stack}_{a,v}$	Binary variable that indicates vehicle v on arc a is part of a vehicle stack.
$b^{stack,active}_{a,v}$	Binary variable that indicates vehicle v on arc a is the active vehicle in the stack
$b^{stack,passive}_{a,v}$	Binary variable that indicates vehicle v on arc a is a passive vehicle in the stack
$b^{stack,passive,aux}_{a,v}$	Auxiliary binary variable that helps indicates vehicle v on arc a is a passive vehicle in the stack

Rather than directly modify the burn constraints in Equation 2.37 to reflect the different burn amounts, the initial total mass can be modified to reflect the vehicle configuration on the arc. That is, continuous variable, $y^{total}_{a,m_{departure},v}$, can be constrained to the proper mass depending on the vehicle, which will result in the proper mass change over the arc. For vehicles flying on their own, their initial total mass is simply their own total mass. Passive vehicle elements in stacks don't burn any propellant even if the stack is burning, meaning their initial total mass is effectively 0. The active element, however, has to push the rest of the stack, meaning the initial total mass is the total mass of the entire stack. This logic is summarized in Equation 2.41.

$$y^{total}_{a,m_{departure},v} = \begin{cases} y_{v,i,m} & if\ vehicle\ v\ is\ not\ in\ a\ stack \\ \sum_{v \in V_{stack}} y_{v,i,m} & if\ vehicle\ v\ is\ active\ in\ a\ stack \\ 0 & if\ vehicle\ v\ is\ passive\ in\ a\ stack \end{cases} \tag{2.41}$$

Since vehicles stacks can only be modeled through paths, they are also used to constrain the variables in Table 2.13 to indicate the vehicle configuration for each vehicle on each arc. If a vehicle is a part of a stack, Equation 2.42 constrains the stack indicator variable for that vehicle and Equation 2.43 constrains the passive or active indicators. Equation 2.44 is applied to ensure $b_{a,v}^{stack} = 0$ and subsequently, $b_{a,v}^{stack,active} = 0$ for vehicles that are flying on their own in a path.

$$b_p = 1 \implies b_{arcset,p} = 1 \implies b_{a,v}^{stack} = 1 \quad \forall\, v \in V_{stack},\, a \in arcset \tag{2.42}$$

$$b_{a,v}^{stack} = 1 \implies \begin{cases} b_{a,v}^{stack,active} = 1, b_{a,v}^{stack,passive} = 0 & v\, is\, active \\ b_{a,v}^{stack,active} = 0, b_{a,v}^{stack,passive} = 1 & v\, is\, passive \end{cases} \tag{2.43}$$

$$b_p = 1 \implies b_{arcset,p} = 1 \implies b_{a,v}^{stack} = 0,\, b_{a,v}^{stack,active} = 0 \quad v\, is\, not\, in\, stack \tag{2.44}$$

For arcs that aren't used, these variables are all constrained to 0 in Equation 2.45 since vehicles aren't burning on those arcs.

$$b_{a,v} = 0 \implies b_{a,v}^{stack} + b_{a,v}^{stack,active} + b_{a,v}^{stack,passive} = 0 \quad \forall\, v \in V,\, a \in A \tag{2.45}$$

Finally, $b_{a,v}^{stack,passive,aux}$ is constrained Equation 2.46 to indicate that a vehicle is in a stack and the passive element. This is the variable used as the indicator for the final initial mass constraints, shown in Equation 2.47.

$$b_{a,v}^{stack,passive,aux} = AND(b_{a,v}^{stack}, b_{a,v}^{stack,passive}) \quad \forall\, v \in V,\, a \in A \tag{2.46}$$

$$y^{total}_{a,m_{departure},v} = \begin{cases} y_{v,i,m} & b^{stack}_{a,v} = 0 \\ \sum_{v \in V_{stack}} y_{v,i,m} & b^{stack,active}_{a,v} = 1 \\ 0 & b^{stack,passive,aux}_{a,v} = 1 \end{cases} \tag{2.47}$$

Boiloff

Given the significance of vehicle modeling for this research, there is a commodity that is passively consumed as time passes by the vehicle that needs to be accounted for. Boiloff is the passive vaporization of cryogenic propellants that are not stored at the optimal temperature or pressure, in addition to the propellant used during a burn. Technologies for minimizing or completely preventing boiloff is on the critical path for long-term space exploration, but the proper modeling of boiloff at the conceptual design level is a challenge of its own [96]. Within the space logistics network formulation, Deguignet presents a method for modeling boiloff for a TEGMCF. Two initial approaches were considered, with boiloff implementations at the arc or node levels. The former was ruled out as the specification of propellant loss due to a burn and boiloff cannot be set simultaneously. Instead, they should be treated separately, where boiloff is accounted for at the nodes, tracking both the fuel and oxidizer boiloff separately flowing into and out of each one. To track the amount of boiloff loss through a node, two further methods of implementation were assessed: absolute and relative boiloff modeling. Absolute boiloff calculates the propellant loss rate as a fixed mass over time, meaning the boiloff mass towards the end of the mission is the same as of that in the beginning. The rate itself, can be calculated using the enthalpy of vaporization of the propellant, h_{vap}, and the heat entering the tank, q:

$$\text{boiloff rate} = \frac{q}{h_{vap}} \tag{2.48}$$

In contrast, relative boiloff models the rate of vaporization as a fixed percentage of the remaining propellant over time, which means the daily boiloff mass is changing as the amount of propellant left in the tank is changing. Using this formulation, the calculated rate of decay is:

$$\text{boiloff rate} = \frac{q}{h_{vap}} * \frac{86400}{m_{fulltank}} \tag{2.49}$$

where $m_{fulltank}$ is the mass of the propellant initially.

These two methods are shown comparatively in Figure 2.33, with a notional tank of starting propellant mass of 2,000 kg and tracked over the course of 30 days. The absolute boiloff method as a constant slope of 30 kg/day, while the slope of the relative boiloff model decreases over time as the propellant left in the tank decreases. At the end of 30 days, the former method leaves 1,100 kg of propellant in the tank while the latter leaves 1270.92 kg.

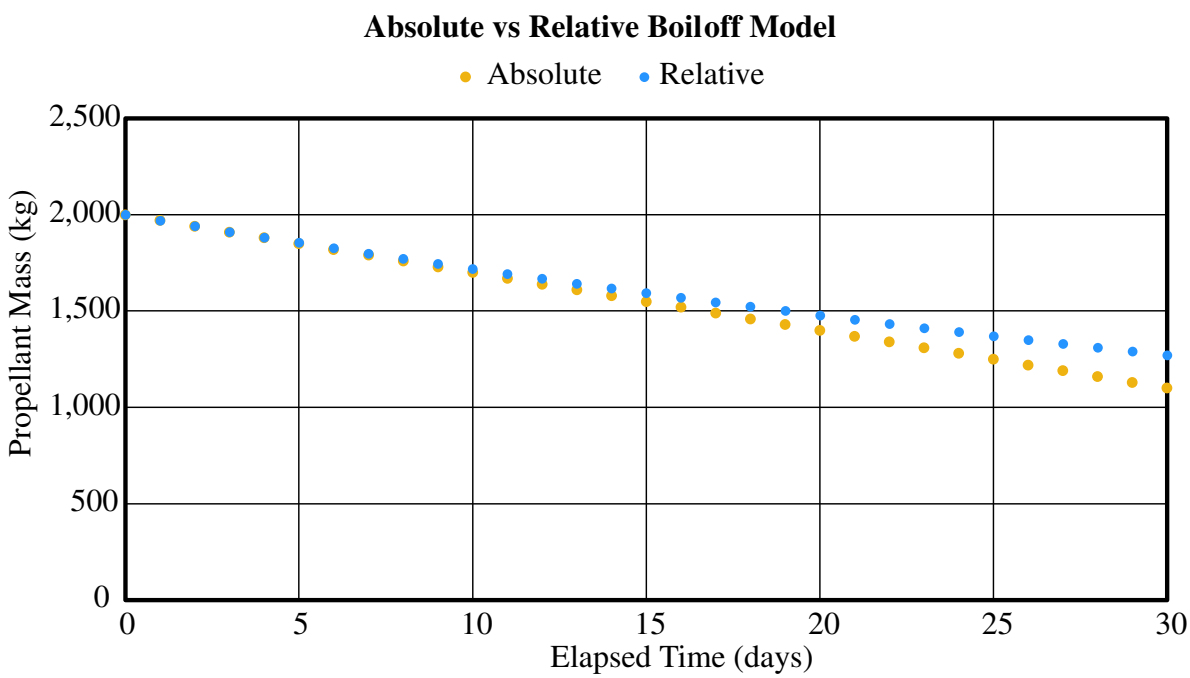

Figure 2.33: Comparison of absolute and relative boiloff modeling using a notional propellant and tank system, adapted from [97].

Fundamentally, since the propellant in the boiloff model sees losses as a fraction of each load everyday, it will theoretically never reach zero if boiloff is the only factor. Over

time, the relative model predicts a total boiloff mass that is lower than that of an absolute model. In addition, the half-life is longer, meaning the propellant modeled will last longer, leading to a less conservative estimate than the absolute model.

Within the network formulation, the absolute boiloff model can be represented as:

$$\mathrm{m}_{boiloff,fuel} = rate_{fuel}\Delta T \tag{2.50}$$

$$\mathrm{m}_{boiloff,ox} = rate_{ox}\Delta T \tag{2.51}$$

Similarly, the relative model can be represented as:

$$\mathrm{m}_{boiloff,fuel} = rate_{fuel}f_{in,fuel}\Delta T \tag{2.52}$$

$$\mathrm{m}_{boiloff,ox} = rate_{ox}f_{in,ox}\Delta T \tag{2.53}$$

Both formulations were implemented using an example case to provide a direct comparison in conjunction with burn events. The results showed very different campaigns for each of the two methods. Campaigns with the highest relative rates had cumulative boiloff masses only slightly more than that of the lowest absolute rates. That is, the relative model is much less conservative in calculating the overall boiloff mass. Although both methods are shown in other literature, rates for existing cases of boiloff reduction look to be constant in nature, leading to the selection of an absolute boiloff model [98].

Within the network formulation, boiloff occurs on all arcs for both the fuel and oxidizer, except for holdover arcs on the Earth's surface and arcs to a discard node. For the former, it is assumed that the boiled off propellants are refueled immediately as the resource is readily available. For the latter, since the vehicle is discarded, modeling boiloff is unnecessary. Each vehicle is given an input rate per day of boiloff for the fuel and oxidizer, and if the timesteps of the problem are greater than 1, this rate is scaled appropriately. The total

propellant boiled off is calculated as the product of the rate and the ΔT on the arc and if the arc is a burn arc, then the total propellant used is the sum of the boiled off and burned propellant. A summary of these constraints is shown in Equation 2.54 and Equation 2.56.

$$x_{fuel,bo,a,v} = \begin{cases} \frac{bo\_rate_{fuel}\Delta t}{t_{step}} & a \in A_{transfer,non-Earth\ holdover,launch} \\ 0 & a \in A_{Earth\ holdover,discard} \end{cases} \quad \forall a \in A, v \in V \quad (2.54)$$

$$x_{ox,bo,a,v} = \begin{cases} \frac{bo\_rate_{ox}\Delta t}{t_{step}} & a \in A_{transfer,non-Earth\ holdover,launch} \\ 0 & a \in A_{Earth\ holdover,discard} \end{cases} \quad \forall a \in A, v \in V \quad (2.55)$$

$$x_{v,fuel,j,l} = x_{v,fuel,i,m} - x_{fuel,burned,a,v} - x_{fuel,bo,a,v} \ \forall a \in A, v \in V \quad (2.56)$$

$$x_{v,ox,j,l} = x_{v,ox,i,m} - x_{ox,burned,a,v} - x_{ox,bo,a,v} \ \forall a \in A, v \in V \quad (2.57)$$

Crew Consumables

Crew consumables are modeled very similarly to boiloff, just for arcs and vehicles that have crew. Since crew are modeled as a type of payload, they must be attached to a vehicle at all times. As a result, it is assumed that crew can only consume the resources that is on the same vehicle. Using input rates of consumption and the number of crew attached to a vehicle, $n_{crew,v}$, the total amount of consumables can be calculated using Equation 2.58, for all consumables, C_{cons}. Just like boiloff, it also assumed that no consumables are used on Earth and discard arcs.

$$x_{c,cons,a,v} = \begin{cases} \eta_{crew,v} rate_{cons} \Delta t & a \in A_{transfer,non-Earthholdover,launch} \text{ and } \eta_{crew,v} \geq 1 \\ 0 & a \in A_{Earthholdover,discard} \text{ or } \eta_{crew,v} = 0 \end{cases} \tag{2.58}$$

$$\forall a \in A, v \in V_{crew}, c \in C_{cons}$$

$$x_{v,c,j,l} = x_{v,c,i,m} - x_{c,cons,a,v} \; \forall a \in A, v \in V_{crew}, c \in C_{cons} \tag{2.59}$$

Programmatic Constraints

Some constraints can be added on the campaign from the perspective of a decision maker or stakeholder. As they are not usually technical in nature, they can be considered programmatic level constraints. If overall costs are being modeled within the campaign, the optimizer can be constrained to a maximum dollar costs, so as to not build a campaign alternative that is cost prohibitive. Although launch cadence is a technical constraint, launch rates are usually programmatic ones, dictated by costs. For example, the launch rate for NASA's SLS is expected to be only one per year [99, 100]. Additionally, some campaigns have set dates for specific goals, such as NASA's 2024 target for the next Moon landing. Again, constraints like these are largely campaign-dependent, so for this formulation, no blanket programmatic constraint is applied. Instead, they will be discussed when utilized in the mathematical formulation for each use case.

2.6.8 Objective Function

Finding a numerical solution using an optimization algorithm requires the definition of an objective function. Although they can vary depending on the specific problem, just like constraints, a base function can be defined. Additionally, there are many FoMs to track when comparing campaigns, but there is only a single objective function. An Overall

Evaluation Criterion (OEC) can be used to represent all of these factors in a single, tracked metric. That is, a weighted sum function where each FoM is normalized and weighted by its importance relative to others.

Propellant Mass

The ideal rocket equation governs mass minimization of any SEC, as the amount of propellant it takes to push extra mass around the solar system grows in an exponential manner. There for it is important to track and minimize the amount of propellant used, or in other words minimize the energy expenditure of all vehicles in the network. Since propellant is burned over time, the max amount will be at all nodes at $t = 0$. This can be calculated by summing up the fuel and oxidizer at the origin for each vehicle in the network, as shown in Equation 2.60, where S is the set of all spatial nodes. An OEC objective term can then be constructed by normalizing by a maximum propellant amount for all vehicles, $m_{prop} * num_{veh}$ and applying weight, w_{prop}, shown in Equation 2.61

$$mass_{total,propellant} = \sum_{v \in V} \sum_{s \in S} (x_{v,fuel,s,0} + x_{v,ox,s,0}) \tag{2.60}$$

$$\frac{w_{prop}}{m_{prop} num_{veh}} \sum_{v \in V} \sum_{s \in S} (x_{v,fuel,s,0} + x_{v,ox,s,0}) \tag{2.61}$$

Campaign Execution Time

In addition to mass, campaign execution time should be minimized to ensure the optimizer choose the slowest paths and minimize energy expenditure. This also ensures the crew is not spending too much time in space, which could be detrimental to their health. It is challenging to properly estimate when the campaign can be considered "done", so to approximate this, execution time is calculated as the sum of the final arc time for each vehicle, $t_{v,final}$. The final arc is a user defined location that represents where the vehicle

has completed its mission. The objective term is shown in Equation 2.62, where w_{time} is the corresponding weight, t_{final} is the final time for the campaign, and V_d is the subset of vehicles that have been given a final location.

$$\frac{w_{time}}{t_{max} num_{veh}} \sum_{v \in V_d} t_{v,final} \tag{2.62}$$

Launch Costs

Financial costs are also significant, as discussed in Chapter 1, but estimating the total cost of a campaign is out of the scope of this thesis. Rather, a surrogate for cost will be overall campaign propellant mass, which is already included in the objective function. However, launch costs can be minimized by assigning each launch vehicle a dollar cost per use. This will discourage the optimizer from consistently choosing the most powerful launch vehicles. Total launch cost for each campaign is simply the sum of the cost of all launch vehicles used. This, and the accompanying objective term is shown in Equation 2.63, where κ_{max} is the max launch cost of all available launch vehicles, and κ_{lv} is each cost.

$$\frac{w_{cost}}{\kappa_{max} num_{veh}} \sum_{lv \in LV} \sum_{a \in A_{launch}} b_{lv,a} \kappa_{lv} \tag{2.63}$$

Burn Count

The final term in the objective function accounts for the total number of burns performed throughout the campaign. Although this may seem the same as minimizing propellant mass, the inclusion of this term avoids situations where a discard node is included in the campaign and the optimizer choosing to discard vehicles as soon as possible to do so. Total burn count is simply the sum of all arcs used that aren't holdover arcs, and the full objective term is shown in Equation 2.64, where $num_{maxburns}$ is an input number of maximum burns.

$$\frac{w_{burns}}{num_{maxburns} num_{veh}} \sum_{a \in A_{burns}} \sum_{v \in V} b_{v,a} \tag{2.64}$$

Therefore, the full objective function is written as:

$$\begin{aligned} min \quad & \frac{w_{prop}}{m_{prop} num_{veh}} \sum_{v \in V} \sum_{s \in S} (x_{v,fuel,s,0} + x_{v,ox,s,0}) + \frac{w_{time}}{t_{max} \eta_{veh}} \sum_{v \in V_d} t_{v,final} + \\ & \frac{w_{cost}}{\kappa_{max} num_{veh}} \sum_{lv \in LV} \sum_{a \in A_{launch}} b_{lv,a} \kappa_{lv} + \frac{w_{burns}}{num_{maxburns} num_{veh}} \sum_{a \in A_{burns}} \sum_{v \in V} b_{v,a} \end{aligned} \tag{2.65}$$

2.6.9 Reference Data

In addition to vehicle capabilities, the CLO process requires some reference data to properly execute: LV set and performance, arc costs, and consumable rates. In-space arcs costs are discussed in Subsection 2.6.2, but for launch arcs, the throw capabilities for various LVs are used to identify the farthest node each payload can be inserted into. This information is typically tabulated for specific orbits by each LV provider, whether it be commercial or NASA. Since the formulation of nodes in the CLO is parameterized, these points need to be extended to include intermediate points, which can be accomplished by creating a regression based on that existing data set. During each iteration of the CLO process itself, however, the nodes are fixed.

The product of this regression will be a continuous curve of payload capacity vs $C3$ achieved by each LV being considered. During each iteration, the achievable $C3$ can be calculated using these curves and a post-launch ΔV based on the closest orbital node's $C3$. Additionally, the volume capacity of each one will be included by way of max diameter and max height of the fairing. Table 2.14 lists the providers and specific LVs that are being considered for this research, and their estimated performance capabilities from manufacturer provided data. An approximate 10% performance hit was assumed for the crew versions

of launch vehicles, if data was unavailable. All launch vehicles performance curves are of the form shown in Equation 2.66, and Table 2.15 lists the constants found from the throw capabilities data points and the R^2 values.

$$C3 = -\frac{1}{a} \ln \frac{m_{payload}}{b} \tag{2.66}$$

Table 2.14: List of launch vehicles considered for their study and their estimated throw performance [101, 102, 103, 104, 105].

C3	-60	-47.56	-16.36	-9.46	-2
SLS 1B Crew	94,500				38,000
SLS 2B Crew	135,000				43,000
Falcon 9 Crew	20,520		7,470		2,826
Starship Crew	90,000		18,900		
New Glenn Crew	34,983	20,272.5		8,707.5	6,376.5
SLS 1B Cargo	105,000				42,000
SLS 2B Cargo	150,000				46,000
Falcon 9 Cargo	22,800		8,300		3,140
Falcon Heavy Cargo	63,800		26,700		15,310
Starship Cargo	125,000		21,000		
New Glenn Cargo	45,000		13,600	9,675	7,085
Centaur Cargo	27,910	21,200		12,650	11,215

Table 2.15: List of launch vehicles considered, the coefficients found for the exponential form, and their R^2 values.

Launch Vehicle	a	b	R^2
SLS 1B Crew	0.016	36825	1
SLS 2B Crew	0.02	41337	1
Falcon 9 Crew	0.032	3313.9	0.9758
Starship Crew	0.036	10529	1
New Glenn Crew	0.027	6263.5	0.9728
SLS 1B Cargo	0.016	20694	1
SLS 2B Cargo	0.02	44163	1
Falcon 9 Cargo	0.032	3682.1	0.9758
Falcon Heavy Cargo	0.024	16042	0.9902
Starship Cargo	0.036	11698	1
New Glenn Cargo	0.031	1474.1	0.9968
Centaur Cargo	0.015	10859	0.9882

The rates of consumption of commodities used by the crew can be defined using data from ISS, shown in Table 2.16 [106, 71].

Table 2.16: Rates of consumption of consumables by the crew.

Commodity	**Density (kg/m^3)**	**Rate (kg/crew/day)**
Water	1,000	2.42
Oxygen	1,140	0.84
Food	500	1.77

3

SPACE TRANSPORTATION SYSTEMS DESIGN

3.1 Requirements for Vehicle Design

The requirements set for the integrated process in Section 2.1 can also be used to decompose vehicle design specific ones. Enabling vehicle level trade space exploration with integrated campaign design requires the vehicle design process to have subsystem level representation. Sizing of space transportation systems within the campaign means sizing of each of the individual subsystems that make up that transportation system. The specific set of subsystems depends on the type of cargo, the type of mission, and high level architecture decisions such as propulsion type. Exploring broad ranges of the trade space would require flexibility in the ability to model many different subsystems, and integrate them with a conceptual-level design process.

As the campaign design process finds the optimal set and sequence of mission events, the vehicle design process should aim to size each of those transportation systems to that set of missions. Depending on the subset of missions, the order may matter for sizing, as a single vehicle could perform more than one mission.

3.2 Sizing and Synthesis Process

3.2.1 Aircraft Conceptual Design

Sizing and synthesis traditionally refers to the conceptual-level aircraft design problem through constraint, mission, and weight analyses, described in [107, 108] and depicted in Figure 3.1. The overall design process is driven by aircraft requirements, usually indicating the level of performance, design characteristics, and types of missions to be conducted. Constraint analysis establishes a feasible design space by converting these re-

quirements into mathematical expressions and parameterizing them by Minimum Sea-level Static Thrust to Takeoff Weight Ratio (T_{SL}/W_{TO}) and Wing Loading at Takeoff (W_{TO}/S). These are generalized scaling parameters that enable sizing of many different aircraft types within this process. Following the identification of a feasible design point, the scale of the aircraft can be calculated through mission analysis, which is driven by the specific mission the aircraft is to fly. Breaking this mission down in to different segments allow for estimation of fuel burn through physics-based expressions and propulsion and aerodynamic design characteristics. The total weight of the aircraft is also discretized into smaller components that are individually estimated using different techniques. In addition to the fuel burn mentioned above, the empty weight is traditionally calculated through historical regressions [109]. Payload and crew weights are either set as requirements or given by the manufacturer. Weights of subsystems such as aerodynamics, propulsion, and structures can be estimated through fundamental expressions and are highly coupled to each other. The difference between the design point chosen through constraint analysis and the aggregated take-off gross weight from mission analysis is iterated upon until converged. Within this process, sizing can be defined as calculation of the physical scale of the conceptual-level aircraft design point, whereas synthesis is the integration of different coupled subsystems throughout [110]. This enables a physics-based analysis that is able to generate many valid, feasible design points of aircraft as well as explore their trade spaces with the inclusion of corresponding, higher fidelity subsystem analyses.

3.2.2 Spacecraft Conceptual Design

Researchers within the space systems community have been able to apply similar processes for the conceptual design of spacecraft by extending the previous methods to account for the challenges of space travel. Spacecraft, or space vehicles, used interchangeably in this thesis, are defined as "devices, manned or unmanned, which are designed to be placed into an orbit about the earth or into a trajectory to another celestial body" [111]. Using

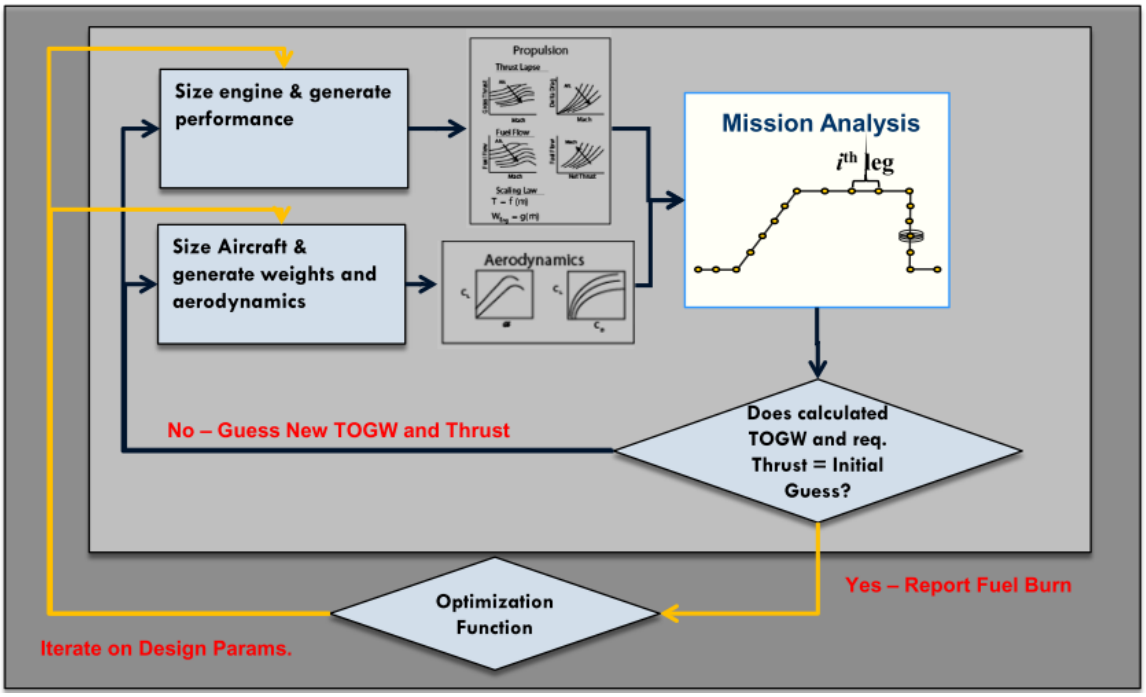

Figure 3.1: Flow diagram of the conceptual-level aircraft sizing and synthesis process [110].

the decomposition posed in Figure 1.5, a space vehicle can be represented by two main components, the transportation system and the payload. As Table 1.1 established, different type of missions required different vehicle architectures, but each one has fundamentally the same goal of transporting a payload from one destination to another. Regardless of the type of payload, usually either crew or cargo, each vehicle is made up many individual but interdependent subsystems. Each subsystem usually performs a specific function, and are coupled to others as well as the mission being flown, notionally shown in Figure 3.2 [112, 113].

Specific design characteristics of the vehicle and its subsystems are defined by decomposing goals into mission requirements. Analogous to the mission analysis portion of the aircraft sizing and synthesis process in Subsection 3.2.1, a space mission can be broken down into individual events that establish an overall ConOps each vehicle can be sized to. Regardless of the complexity of the ConOps, spacecraft sizing is driven primarily by the ideal rocket equation, Equation 2.13. It defines the exponential relationship between the

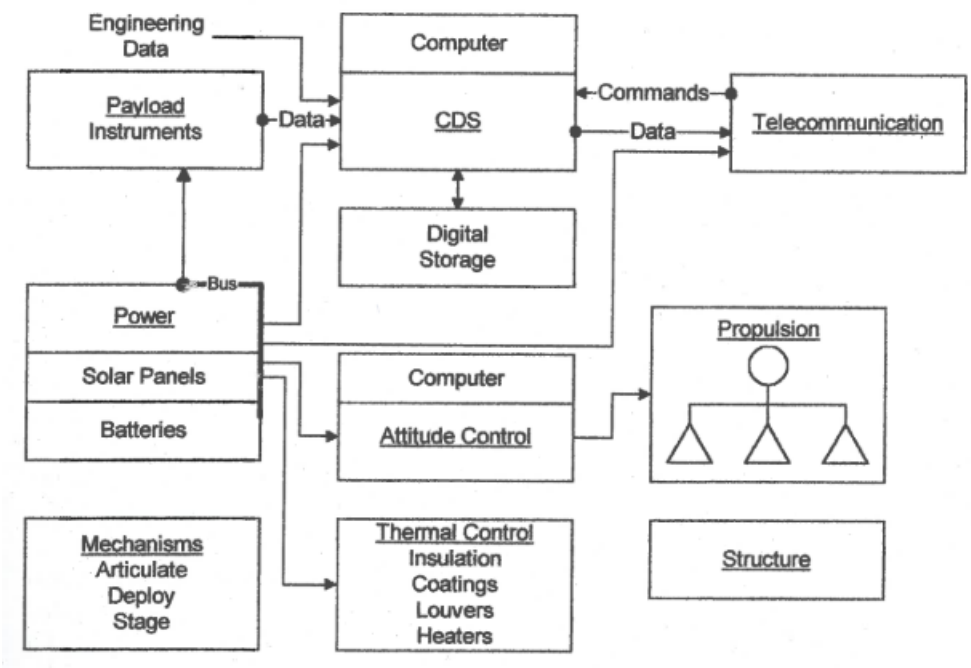

Figure 3.2: Notional breakdown of an uncrewed spacecraft into its subsystems and their specific functions [114].

spacecraft's mass and the amount energy required to transfer between orbits, ΔV. Traditionally, a set of ΔVs are used to calculate the overall propellant required to perform the mission which further drives the sizing of the required systems to carry the propellant and the payload. Sizing of the spacecraft can be as high a level of assuming an IMF, defined in Equation 3.1, and calculating the inert mass based on the propellant loading.

$$IMF = \frac{m_{inert}}{m_{inert} + m_{propellant}} \tag{3.1}$$

This is done mostly during pre-conceptual phase of design or for proof-of-concept assessments. Higher fidelity formulations attempt to estimate the mass of each subsystem for a more holistic estimate of the size of the vehicle, as notionally shown in Equation 3.2, where the mass of payloads, $m_{payload}$ is typically an input.

$$
\begin{aligned}
m_{inert} = m_{avionics} + m_{engines} + m_{tanks} + m_{structures} \\
+m_{engines} + m_{power} + m_{thermal} + m_{payload} + ... \\
m_{total} = m_{inert} + m_{propellant} \\
where\ m_{propellant} = f(mission)
\end{aligned}
\tag{3.2}
$$

The specific methods for estimating the mass of individual subsystems depends on some input design characteristics of the vehicle and the mission and their level of fidelity typically depends on the purpose of the analysis. For example, a high fidelity, parametric finite-element analysis for the structures subsystem can be used to assess propulsive loads on-orbit. However, at the conceptual level, subsystem models use historical regressions, physics-based first principles and scaling parameters, or similar, with the goal of estimating the mass, volume, and power consumption [115]. Even at this level, however, models can be linear or non-linear, with most having many inputs and outputs.

The overall sizing process is iterative in nature, where the mission informs the required size of the vehicle and the vehicle size informs what missions it can fly. Using the input mission, ideal rocket equation, and initial m_{inert} guess, the total mass of the spacecraft is estimated by calculating the overall propellant required to perform the mission. Based on the subsystems considered, their sizing may be dependent on the mission, other subsystems or independent. As a result, the inert and subsequent total mass produced by the subsystem sizing models may be different than what is required by the mission, necessitating some iteration between the mission and vehicle problems. With more complex mission and vehicle architectures, there can be many links between the many design variables and the entire process can take many iterations between the sizing itself and the mission analysis to produce a converged solution. Identifying a process for creating these links and generating a converged solution in a reasonable amount of time is key as this research aims to solve this problem for each vehicle in the campaign.

The following observations can be made regarding the vehicle design process, which further prompt some Formulation Questions (FQ)s and the update of the thesis structure in Figure 3.3.

Observation 8: Space vehicle design is a complex MDAO problem that requires the sizing of many subsystems.

Observation 9: Space vehicles are traditionally sized to individual missions.

- Formulation Question 5: How can the sizing and synthesis (S&S) problem be solved in a rapid manner without simplifying the vehicle and constraining the overall trade space?
- Formulation Question 6: How can campaign parameters drive the design of the vehicles within?

When considering the exhaustive, integrated vehicle and mission design trade space, this problem can become intractable, even at the conceptual level. There have been many attempts at formulating the VSS problem, with main differences usually being the assumptions made to simplify the problem, either on the mission or vehicle side. The goal of the rest of this chapter is to identify if an existing VSS method for in-space transportation systems can be integrated to a campaign logistics optimization process. Although the last chapter showed a few campaign design methods do address vehicle design, the next section will provide a brief overview of the limitations of those processes within the context of VSS. Following, a review of existing methods for VSS will be provided with the goal of identifying one that meets the requirements presented in Section 3.1.

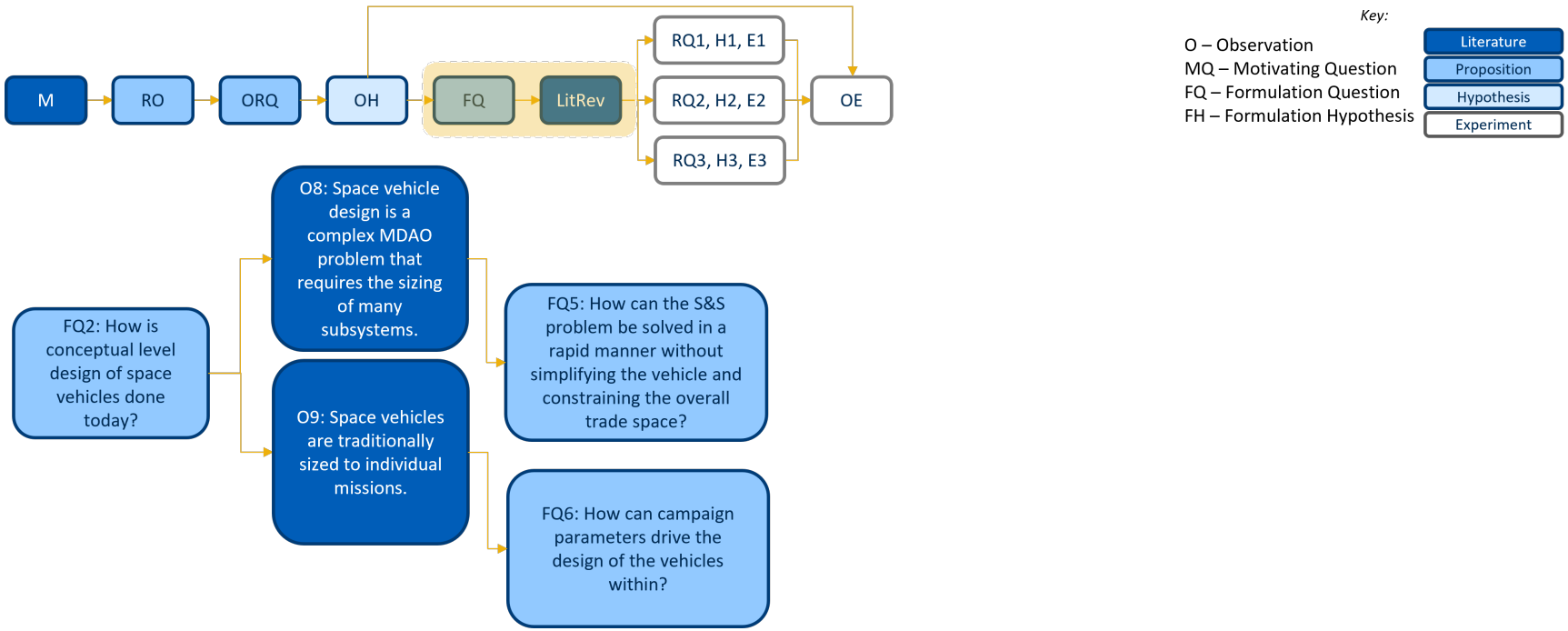

Figure 3.3: Thesis structure updated to show observations from the literature of Space Transportation Systems (STS) design.

3.2.3 Transportation Systems Design in Previous Space Campaign Logistics Formulations

Several of the space logistics network formulations presented in Chapter 2 included vehicle design within. Taylor and Weck established a concurrent design process where the space vehicle was represented as a sum of three masses: dry, propellant, and payload. Fuel type, f^E, is the first design variable, which prompts a look-up table function to grab the Specific Impulse (I_{sp}) and structural fraction, α, for it. For each element, E, the second design variable is the maximum fuel available for the vehicle, m^E, which is bounded between 0 and an upper mass, m_{UB}. Similarly, the final design variable is payload mass capacity, c^E, is also bounded between 0 and an upper mass, c_{UB}. The dry mass was the sum of the structures mass and engine mass, where the latter is calculated through Equation 3.3, defined in Hofstetter and Maschinenwesen [116].

$$g^E = \frac{0.4189(t^E)^{0.7764}}{g_0} \tag{3.3}$$

$$where \quad t^E = \frac{m^E I_{sp}(f^E) g_0}{t_b} \tag{3.4}$$

The mass of the engine is driven by the thrust, calculated using Equation 3.4, and the selected fuel type, where t_b is the engine burn time set to 120s, and g_0 is the sea-level gravitational acceleration of Earth. The structural mass is split into two parts, the mass required to support the propellant and the mass required to support the payload. The latter is represented by the structural ratio, α, and the former by Equation 3.5, a least squares fit of various different space vehicles and their mass data, shown in their appendix.

$$s^E = 2.3931c^E + \alpha(f^E)m^E(1 - \frac{0.2m^E}{m_{UB}}) \tag{3.5}$$

Therefore, the full vehicle mass is represented as:

$$vehicle = m^E + 2.3931c^E + \alpha(f^E)m^E(1 - \frac{0.2m^E}{m_{UB}}) + \frac{0.4189(\frac{m^E I_{sp}(f^E)g_0}{t_b})^{0.7764}}{g_0} \quad (3.6)$$

The upper bound on the allowable fuel mass is set as 500,000 kg. Although this is a nonlinear equation, it is a singular nonlinear equation that could be rapidly calculated given the set of inputs for every function call, which is significant when the computational complexity of the overall CLO process is relatively high. Given the high upper bound for the propellant mass, a potentially wide range of mission scenarios and vehicle designs can be accounted for. Additionally, this relationship is integrated within the optimization problem, where the optimizer is concurrently varying campaign and vehicle level design parameters.

Although computationally efficient and representative of space vehicle design, this process limits the types of trades that can be assessed. Given the simplification of the vehicle architecture, assessing changes in the subsystem level design parameters on the rest of vehicle and campaign becomes challenging. Variation of the fuel type propagates the effect of changing propellant species, but only on the mass of the vehicle. Propellant selection also drives the sizing and configuration of storage systems, mostly limited by the volume of the LVs being used. As a result, a propellant change that is expected to change the number of launches due to volume limitations may not be captured by this representation. If cryogenic propellants are considered, the necessary thermal control systems could also be affected in conjunction with the thermal environment throughout the mission. Additionally, vehicle architecture level trades, such as NTP vs all-chemical, can only be represented through the fuel type variable. The effect of these different architectures on the operations within the campaign may not be captured. These links between subsystems and the mission is what makes the vehicle design a complex MDAO problem, one that may not be addressed using the previous formulations.

Most of the methods presented in Subsection 2.4.3 make significant improvements to the space logistics network formulation, and some include vehicle design [24, 66, 68]. However, they also integrate Equation 3.6 from Taylor and Weck into the optimization problem, leading to the same limitations.

Arney presented a method of a space systems architecting using graph theory and integrates systems sizing [58]. Within this methodology, the modeling method for the sizing of the system depends on the system itself, summarized in Table 3.1.

Table 3.1: System sizing methods for the graph theory-based space systems architecting method [58].

System	**Modeling Method**
Crew Capsule	Photographic Scaling
Lunar Descent Stage	Photographic Scaling
Launch Vehicle	Photographic Scaling
Lunar Ascent Vehicle	Photographic Scaling
Propellant Depot	Regression, RSE
Propulsive Stage	Regression, RSE
Surface Habitat	Photographic Scaling
In-Space Habitat	Photographic Scaling

Photographic scaling is the resizing of a baseline vehicle using a single characteristic while keeping the rest, such as layout, configuration, tank pressure, and engine performance, the same. Habitation systems are scaled using mission duration, number of crew, or a combination, while propulsive systems are mainly driven by propellant mass. RSE modeling involves fitting a 2nd order, multivariate, quadratic equation, shown in Equation 3.7, to a set of existing data points to create a regression that could be used to size elements. Data points can be generated using higher fidelity models a priori using as many input variables as necessary.

$$y = b_0 + \sum_{i=1}^{k} b_i x_i + \sum_{i=1}^{k} b_{ii} x_i^2 + \sum_{i=1}^{k-1} \sum_{j=i+1}^{k} b_{ij} x_i x_j + \varepsilon \tag{3.7}$$

Though RSEs can be very useful for representing subsystem level sizing models or even the entire system using subsystem level inputs, photographic scaling may not accurately represent the scaling of in-space transportation systems. For propulsive stages scaled by propellant, larger systems may not fit inside fairings of LVs due to volume constraints. Additionally the interdependencies between subsystems may not be captured.

3.3 Existing Capabilities

Mission Architecture Sizing Tool (MAST)

MAST was developed by Johnson Space center to perform integrated trajectory design and spacecraft sizing of exploration architectures [117]. The main advantage of MAST was the generalized logic of the code to enable assessment of mission architectures with any number of vehicle. An entire exploration architecture is stored within a single array, which contains any and all vehicles as well as their specific trajectory maneuvers, as shown in Figure 3.4.

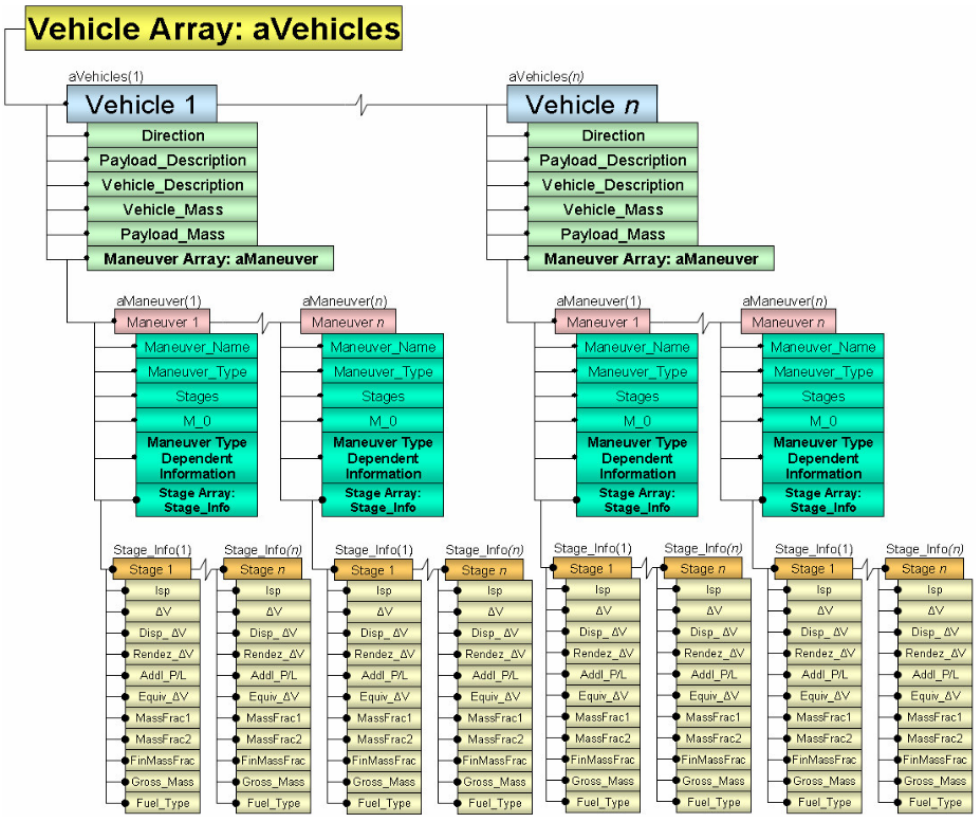

Figure 3.4: Schematic of the data storage structure of exploration architectures in MAST [117].

Using this hierarchy, each vehicle is sized using the ideal rocket equation and user input performance data. Although integration with a trajectory analysis tool was planned, it was not implemented due to time constraints. Additionally, because the sizing was simplified to use the ideal rocket equation, the capability does not meet the requirement of modeling subsystems.

Beyond LEO Architecture Sizing Tool (BLAST)

The BLAST was developed by Zero Point Frontiers with NASA Johnson Space Center to enable rapid generation of design points for transportation systems and human exploration architectures [118, 18]. It estimates the mass of each architecture using regressions built off of historical data from the Apollo era up until 2012. Although it has a user-friendly

interface that is setup to run trade space exploration, the underlying regressions themselves are hard coded, which makes assessing new or revolutionary architectures challenging.

Exploration Architecture Model for In-space and Earth-to-orbit (EXAMINE)

In response to the growing need for rapid generation of alternatives for decision makers, Komar *et al.* formulated a framework for parametric modeling of space exploration architectures at NASA Langley Research Center. The author identifies processes at the time, focused on establishing a few point designs with many teams developing different components, with the advantage of having SME level knowledge in the design loop itself. However, these processes were ad-hoc, with verification of the systems design to meet requirements being done manually. This limits the ability to generate many different alternatives without the necessity of many engineers and designers. EXAMINE was established with the goal of having an integrated framework of many different models to assess relative sensitivities of space exploration architectures in a very rapid manner. It accomplishes this goal by allowing the user to define the system to model, as a collection of subsystem models that are available in the tool itself, which is not limited to any specific group of space architectures. EXAMINE has subsystem models that can be used for transportation systems, surface systems, and even entry and hypersonic vehicles. A high level program is used to manage all of the data between the subsystems and control any convergence needed but the linking of coupled design parameters between subsystems is up to the user. It is important to note that since system definition and linking of design parameters is entirely user driven, it is up to that user to verify the system itself is being modeled properly and the model is set up properly. A full N^2 diagram of the EXAMINE framework is shown in Figure 3.5, which depicts the overall data flow in the framework.

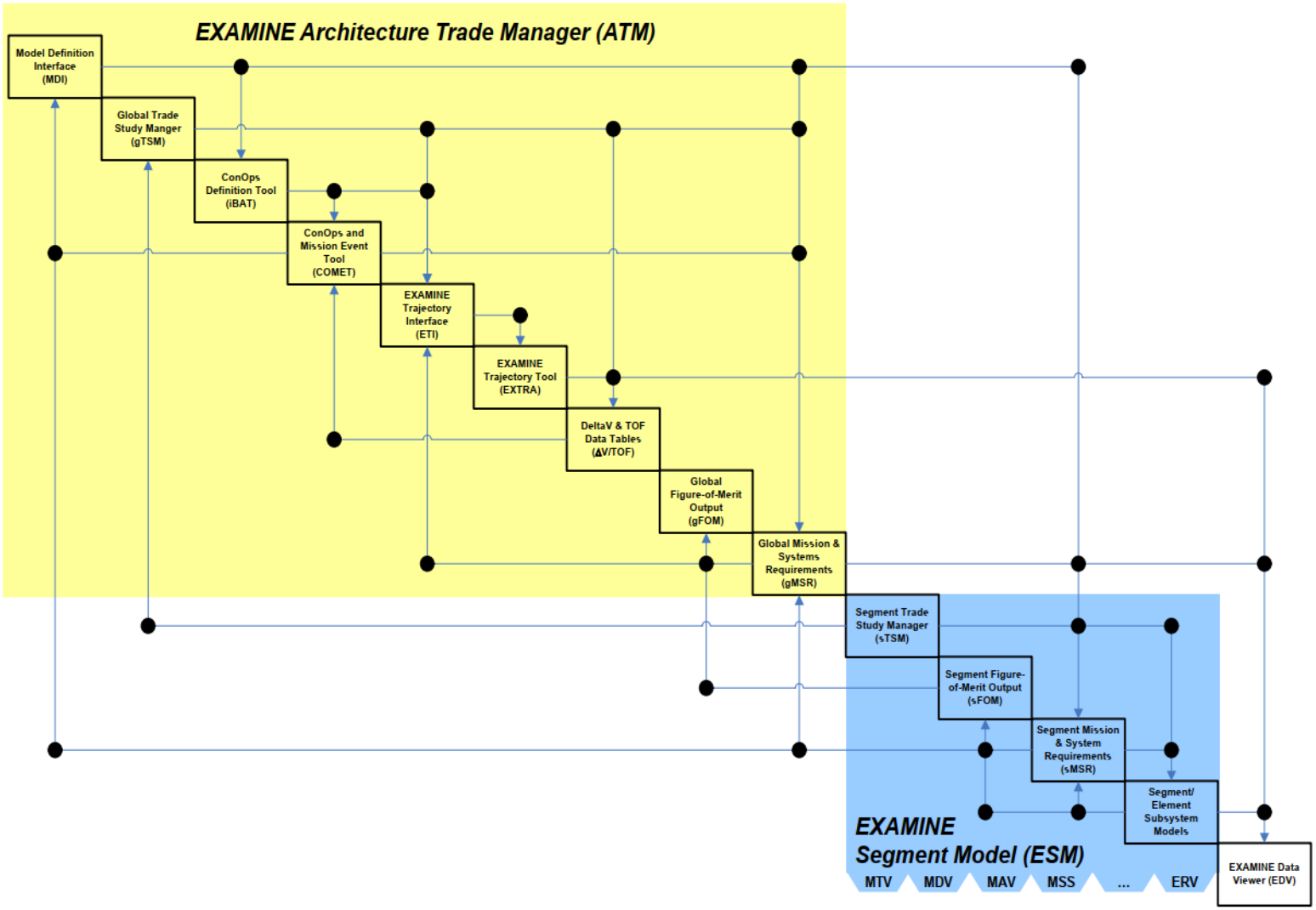

Figure 3.5: N^2 diagram of the EXAMINE framework [119].

The entire framework is built in Microsoft Excel and Visual Basic, with individual sheet performing different modeling functions from convergence methods to mission analysis and trade space exploration. The underlying engine for the framework and the hierarchical formulation enables broad trade space exploration of many different space architectures. Additionally, it is very traceable, as each mathematical expression is visible in the populated cells and the values of design parameters are shown in each sheet. EXAMINE's modularity also enables a user to create their own subsystem model on the fly and integrate it into the system model in the event that the existing set does not include the desired functional capabilities. Although Excel enables EXAMINE to be modular, traceable, and evolvable, it also limits the capability to integrate the entire framework with other tools. For this thesis, EXAMINE would be able to size and synthesize space transportation systems, but the level of ease of integration with the campaign optimization process may be difficult and overall runtimes for the vehicle design process may be long. The latter is significant as the integrated process may involve the design of many vehicles with each iteration.

Dynamic Rocket Equation Tool (DYREQT)

Researchers at ASDL have formulated a python-based framework for rapid synthesis of STS architectures using a Model-based Systems Engineering (MBSE) paradigm [19, 120, 121]. MBSE is an engineering philosophy that aims to apply specific modeling techniques and standardized, automated processes to the augment current systems engineering principles. DYREQT is specifically formulated as an architecture synthesis tool to numerically solve the complex MDAO problem of space transportation systems design for each enumerated architecture in the trade space. It automates the overall linking process of the many design parameters across the problem using NASA's OpenMDAO framework and an established ontology of vehicle specification. Shown in Figure 3.6, an architecture is defined as a pairing of a vehicle with the mission it is flying. Further, each mission can

be made up of many individual events, with each one covering a different function for the vehicle, such as: burn, idle, or mass change.

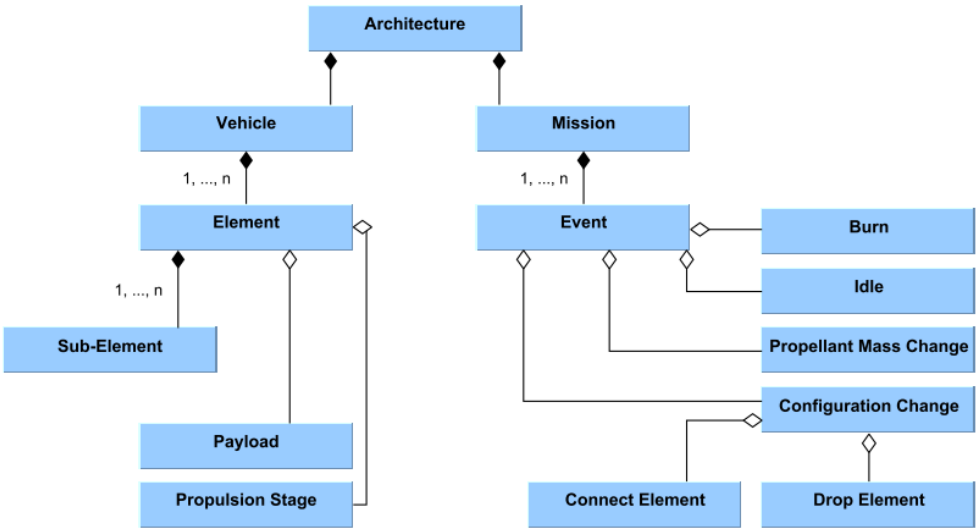

Figure 3.6: An ontology of the space transportation system design problem as defined within DYREQT [19].

Analogously, the vehicle is made up of one or more elements, which can either be the propulsion stage or the payload. Each of those two can be further defined as a collection of any number of sub-elements, usually corresponding to specific subsystems for the vehicle. Users are able to select existing or integrate external subsystem models, regardless of format or fidelity, into DYREQT for that representation. The specific models themselves contain their own inputs and outputs, either coupled with other systems, the overall vehicle, or the mission.

Given the flexibility in mission and vehicle definition, DYREQT enables the definition of many different, and potentially complex, mission scenarios and vehicle designs. Sizing of the design point itself is driven by mapping the vehicle stages to mission events to create virtual stages, as shown in Figure 3.7. This mapping is called the ConOps, which establishes the order of events and which specific vehicle and vehicle element is performing the event.

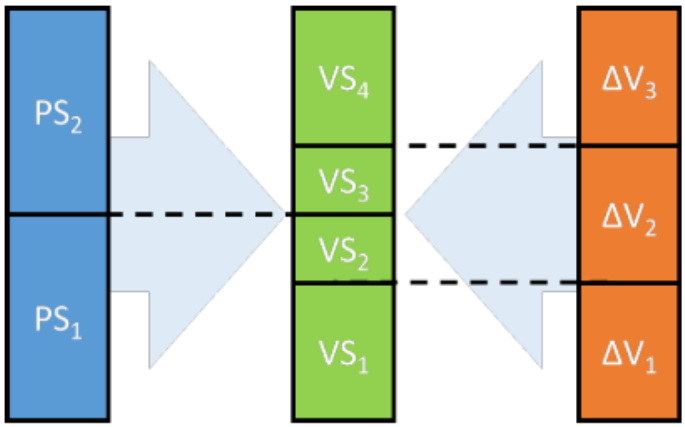

Figure 3.7: Then notional mapping of physical vehicle stages, or elements, to mission events to create virtual stages [19].

The mission definition is then used to generate a mass for the vehicle using the ideal rocket equation and propagates sizing down to the subsystem level. Given the multidisciplinary nature of the vehicle, DYREQT uses the Modular Analysis and Unified Derivatives (MAUD) Multidisciplinary Design Optimization (MDO) architecture to represent the sizing problem and finds a converged solution using a Nonlinear Gauss-Seidel (NLGS) iterative solver. Runtimes vary depending on the architecture, but the case studies presented in [19] took less than a second to converge each design point.

The flexible, modular nature of DYREQT lends itself well to solving the vehicle sizing and synthesis problem for the integrated methodology in this thesis. Although subsystem models are not included within it, DYREQT does not make assumptions about the format of each model, only interfacing with its inputs and outputs. As a result, it can be supported with an external library of subsystem models that can enable broad trade space exploration of vehicle designs. Similarly, each mission can be defined flexibly using information from the campaign logistics optimization process, with some translation of data products. Additionally, a python-based framework is much more easily integrable, both with the campaign process as well as individual subsystem models.

Considering the current state of the art for conceptual design of STS, the following observations can be stated:

Observation 10: The rocket equation can be used to iteratively drive the sizing of the vehicle through mission events, regardless of what the subsystems are.

Observation 11: Missions parameters are a product of campaign design and are key inputs for the vehicle design problem.

Further, for the design of STS in the integrated methodology, the following hypothesis is constructed using the literature presented in this chapter. A summary of the logic structure for this literature review is shown in Figure 3.8.

- Formulation Hypothesis 5: If DYREQT is used as the synthesis capability, broad areas of the vehicle trade space can be explored in a rapid manner with external subsystem sizing models.

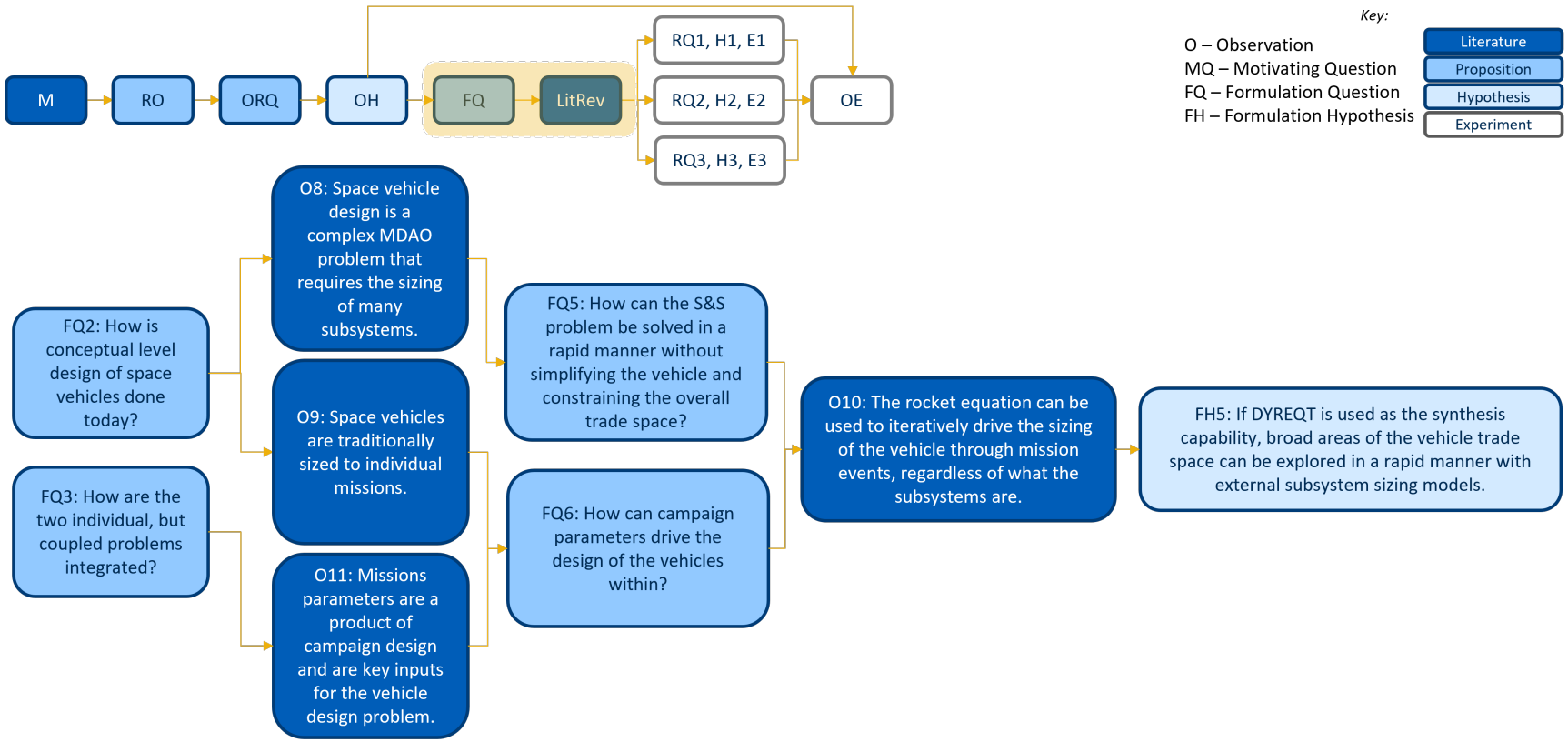

Figure 3.8: Thesis structure updated to show the formulation hypothesis for STS design and the integration with CLO.

3.4 Space Transportation System Sizing and Synthesis

As stated in Chapter 3, conceptual design of space transportation systems is a complex MDAO problem that requires the sizing and synthesis of many subsystem. FH4 states that if DYREQT is used as the synthesis capability, this problem can be solved in a rapid manner for each vehicle in the campaign without closing off parts of the vehicle trade space. Integration with the CLO process presented in the previous sections is done throughout the overall optimal mission set it finds. This set drives the VSS process as the sizing missions for each of those individual vehicles.

3.4.1 Mission Analysis

Subsection 2.6.1 described the parameterization of nodes within the CLO process, which was added to the formulation to allow additional degrees of freedom for the VSS. Since those additional degrees of freedom are not handled by the CLO, it needs to be addressed elsewhere. DYREQT automates the linking and sizing of each subsystem in a vehicle using an input sizing mission in the form of a set of individual events. These can be ΔV, ΔT, Δm events or a combination of them. Given the parameterization of orbits by semimajor axis (a), eccentricity (e), and inclination (i), the ΔV and ΔT to transfer between orbits must be calculated using these variables. This process can be split into two routes, where transfers between Earth and Mars are handled separately from any other one.

Planetary Transfers

With the proper assumptions, planetary transfers can be calculated analytically without the use of external tools and optimization processes. Specifically, this research assumes minimum energy transfers for these cases. Hohmann transfers are the most common type, using an elliptical transfer orbit to travel between two coplanar, circular orbits, either ascending or descending. Although, they can be generalized for cases where the initial and final or-

bits can be either circular or elliptical. A Hohmann transfer between two circular orbits, shown in Figure 3.9, is executed by performing a series of burns to put the vehicle on an elliptical transfer orbit [88]. For the case of a lower initial orbit, the first burn is used to speed of the vehicle to match the periapsis velocity of the transfer orbit and the 2nd burn is used to slow down once it has arrived in the higher, slower orbit. If the lower orbit is the destination, the process is simply reversed. Between two elliptical orbits, the geometry can be specific to the problem, but there are still two burns required [122]. A special case of a Hohmann transfer that is typically used for large transfers is the bi-elliptic transfer, shown in Figure 3.10

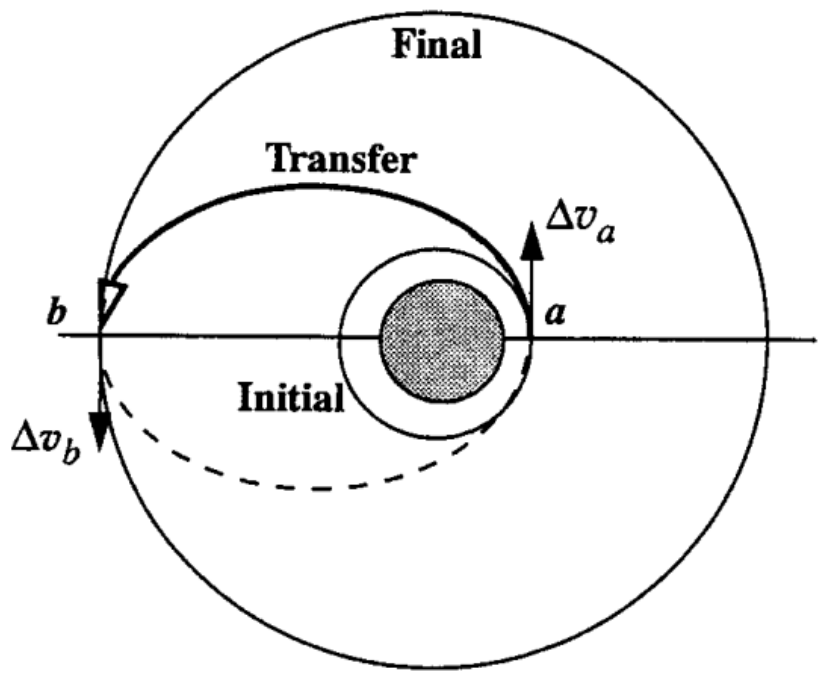

Figure 3.9: A Hohmann transfer between two circular orbits [122].

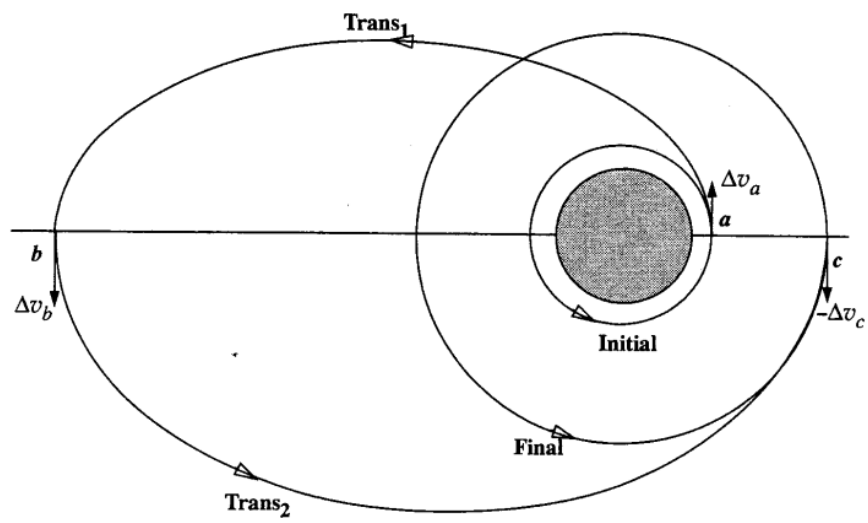

Figure 3.10: A bi-elliptic transfer between two circular orbits [122].

In this case, the transfer is split into two different elliptical orbits rather than just one. There is a third burn at the apoapsis of the first elliptic orbit to change the vehicle's velocity to match the 2nd elliptic orbit. A bi-elliptic transfer can be lower in energy requirements than a Hohmann transfer in some cases.

Earth-Moon Transfers to NRHO

Transfers between the Earth and Moon can be assessed using the equations introduced in the previous section. However, to simplify the mission analysis for these cases, a special case of transferring from Earth to NRHO is discussed in this section. Depending on the payload mass, pushing it to a trajectory aimed at the moon, called Trans-Lunar Injection (TLI), is performed either by the LV itself or by the in-space transportation stage. From TLI, the vehicle can perform a minimal energy transfer into other lunar orbits, but transfers into NRHO are accomplished using a Ballistic Lunar Transfer (BLT), of which there are two types: fast or slow [123]. These options can reduce the overall ΔV requirements by 200-400 m/s depending on the dates and targeted transfer time. For this research the fast option is assumed to be a fixed ΔV of 450 m/s with a time of flight of 5 days, whereas the slow option is 30 m/s for 100 days. Departure from NRHO assumes the same values.

3.4.2 Vehicle Trade Space Synthesis

Sizing each vehicle for missions first requires the synthesis of the individual subsystems based on the choices of vehicle architectures to explore. The latter is intended to be inputs so that the methodology could be used to explore vehicle trade spaces. DYREQT's formulation allows the user to define the vehicle as they wish, using the hierarchical ontology in Figure 3.6. That is, a vehicle can be defined as a collection of elements that are further individually defined as a collection of subelements. An example setup of a vehicle architecture is shown in Figure 3.11, with a propulsive stage and a payload.

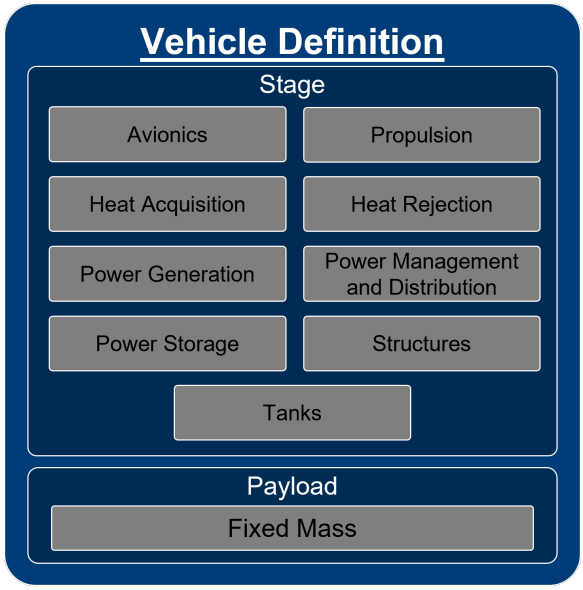

Figure 3.11: An example 2 element vehicle architecture defined using DYREQT's ontology

The vehicle is made up of elements: the propulsion or transportation stage and the payload. In this case, the payload element is simply a fixed mass that is assigned by user input. Payload masses can be either vehicles or mission payloads depending on mission itself. For the scope of this research, only in-space transportation systems are being designed so the propulsion stage can be represented as a set of subelements, with each one corresponding to a specific subsystem. This specification of each vehicle is up to the user for the initial setup phase, after which those vehicles designs are updated at each iteration.

3.4.3 Subsystem Sizing Models

As DYREQT is just the synthesis tool for the VSS process, it is up to the user to bring the necessary subsystem models that are required to represent the vehicle as subelements. Though DYREQT is built in python, a subsystem model does not have to be, as the user only has to specify the inputs and outputs of the model within DYREQT. It will treat each model as a black box, regardless of the format or fidelity. The specific set of models to use is driven by the vehicle architecture definition, discussed previously. It can be expected that each model would have many inputs and outputs, even at the conceptual level of design. Inputs can either be continuous or discrete values depending on the model which creates a design space within each vehicle architecture selection to explore as well. Setting the values for each one can either be user driven, or can be assigned as a design variable for DYREQT. All subsystem models used are detailed in Appendix A.

3.4.4 ConOps Definition

DYREQT automates the process of linking the necessary design variables across the complex MDAO problem and synthesizes a design point using the sizing missions from CLO. Generation of a numerical solution is starts by defining the mission as a series of events and assigning them to the physical elements of the vehicle, as shown in Figure 3.7. There are different types of events to choose from to build each mission, summarized in Table 3.2

Table 3.2: Mission event types within DYREQT.

Event Type	**Description**
ΔV	Burn event to change in energy state of the vehicle. Performed by either the main propulsion system or RCS.
ΔT	Coast event that models a passage of time but the vehicle is not executing an operation.

Table 3.2: Mission event types within DYREQT.

Event Type	Description
$\Delta m_{continious}$	A continuous change in mass of the vehicle over time, typically to model propellant refueling.
$\Delta m_{discrete}$	A discrete change in mass instantaneously, typically to model a dock or undock event.

Given the example Mars transport vehicle from section Subsection 3.4.2, the Table 3.3 provides a corresponding example mission to pickup a crewed habitat of 45t in orbit around Earth for delivery to Mars. This assumes the Mars transport vehicle is already in the same orbit as the payload at the start of the mission; that is, both elements are assumed to be launched directly to the aggregation orbit.

Table 3.3: Example mission for a Mars transportation system.

Event	Event Type	Value
Phasing	ΔV	45 $\frac{m}{s}$
Dock to Payload	$\Delta m_{discrete}$	+45,000 kg
Earth Departure Burn	ΔV	3,000 $\frac{m}{s}$
Interplanetary Coast	ΔT	500 days
Mars Arrival Burn	ΔV	2,000 $\frac{m}{s}$
Payload Drop	$\Delta m_{discrete}$	-45,000 kg

The transportation stage pickups up the crewed habitat in the aggregation orbit and performs the departure burn from Earth and an arrival burn at Mars after a long coast period. The stage then drops off the payload which then performs its own individual mission. ConOps definition within DYREQT is the assignment of each event in the mission to a element that executes it. Thus, Table 3.3 can be extended to show which part of the vehicle corresponds to the event in Table 3.4. For propulsion stages, this is especially important as most have two individual propulsion stages on board, a Main Propulsion System (MPS) and

RCS, where the former is used for larger burns and the latter for smaller ones or proximity operations.

Table 3.4: Example ConOps definition in DYREQT for a Mars transportation system.

Event	**Event Type**	**Value**	**Element**
Phasing	ΔV	45 $\frac{m}{s}$	Stage, RCS
Dock to Payload	$\Delta m_{discrete}$	+45,000 kg	Habitat
Earth Departure Burn	ΔV	3,000 $\frac{m}{s}$	Stage, MPS
Interplanetary Coast	ΔT	500 days	Vehicle (Stage + Habitat)
Mars Arrival Burn	ΔV	2,000 $\frac{m}{s}$	Stage
Payload Drop	$\Delta m_{discrete}$	-45,000 kg	Habitat

Using the ConOps, DYREQT iteratively calculates the mass of the vehicle with the ideal rocket equation and the individual subsystem models and finds a converged solution between the two. If design variables are provided for either the mission or vehicle, the integrated OpenMDAO framework within DYREQT will automatically find the values that satisfies the mission and any additional objectives. This process finds a converged solution for a typical conceptual vehicle stage and mission on the order of a few seconds. When linked to the CLO, it is repeated for each vehicle in the campaign at every iteration.

4
EXPERIMENTATION AND RESULTS

4.1 Research Plan and Questions

Although the different pieces of a methodology have been identified in the previous chapters, the specific structure of it has yet to be defined. The primary tool for producing a converged solution between the CLO and VSS is the numerical iterative solver. Within the field of numerical methods, there are many solvers, each one varying in their specific mathematical formulation for converging one or more coupled systems. The need to find an appropriate iterative solver for the proposed methodology is formally stated as the first **Research Question** of this thesis:

Research Question 1: What iterative solver is best for converging the CLO and VSS processes?

The selection of specific stopping criteria is closely tied to the choice of the iterative solver. Stopping criteria, or convergence criteria, is the set of coupled variables that can be used to assess the relative difference between values produced by each process, which once low enough, can tell the iterative algorithm the solution is valid. This motivates the second **Research Question**:

Research Question 2: What is the proper set of convergence criteria for the chosen iterative process?

Additionally, since there are two individual processes, either one could be executed first, and this initialization could affect the performance of the overall methodology. As a result, the final **Research Question** is stated as follows:

Research Question 3: Which individual process should be executed first given a starting guess from the other?

This chapter chapter discusses in detail the experimental plan developed to answer these questions and the individual tests that will be conducted through the use of a small-scale SEC.

4.2 Canonical Small-scale Campaign: Human Landing System 2024 Crewed Mission

4.2.1 Concept of Operations

To properly answer the research questions, a sample SEC is required as an experimental apparatus to test different potential structures for the integrated design methodology. The scale for this campaign should be relatively smaller in comparison to the one used for a final demonstration, in terms of overall time and number of elements, to minimize computational complexity for experimentation. As such, a lunar campaign would be more ideal for this purpose, as opposed to a Mars-focused alternative. Further, it should still be relevant within academia and industry, include complex ConOps for the path-arc formulation, and multiple vehicles to size and synthesize. It is important to also require crew within the campaign to set demands and drive the commodity flows within the network. These requirements guided a literature review and ultimate selection of the Government Reference HLS 2024 Crewed Lunar Landing as the canonical small-scale space campaign for the experimentation, shown in Figure 4.1

Although NASA is planning on selecting a commercial lunar lander to perform the mission, it released a reference campaign with a 3 element architecture. To return the next humans to the Moon in 2024, NASA chose to design separate elements, each performing as the propulsive element for a different portion of the overall campaign. That is, once all three elements have aggregated at Gateway and the crew have arrived via SLS and

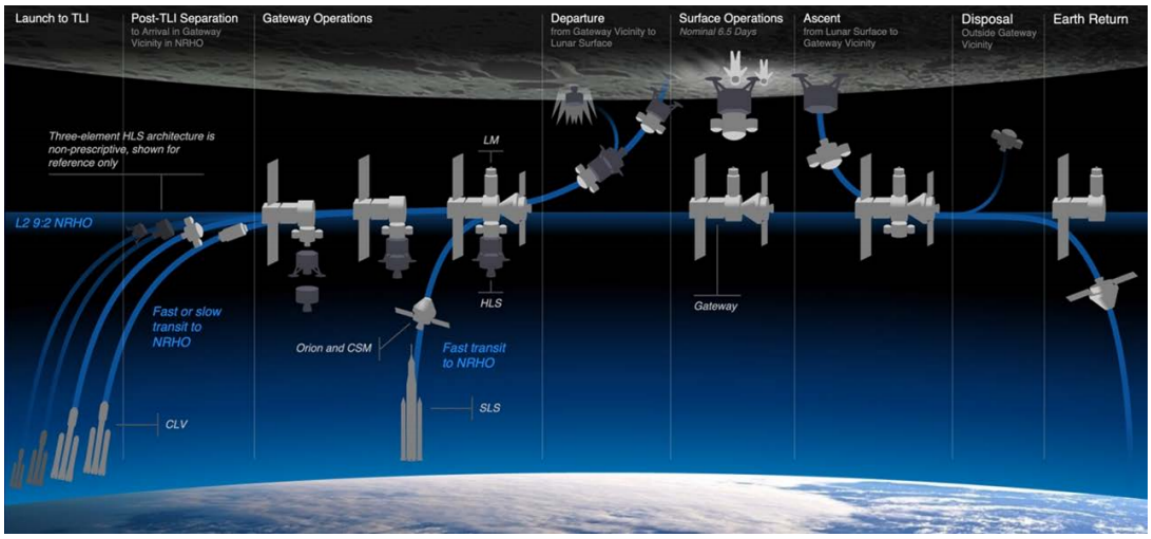

Figure 4.1: Concept of operations of the 3 element, government reference, HLS crewed lunar landing mission in 2024 [73].

Orion, the Transfer Element (TE) will perform the transfer burn from NRHO to LLO and be disposed. Following, the Descent Element (DE) will provide a powered landing to the surface and after a 7 day surface stay, the Ascent Element (AE) will leave the DE behind on the surface to push the crew back up to Gateway. The crew will then depart on Orion and return to Earth following a lunar flyby. The 6.5-day surface stay duration will set the commodity flow demands for the network optimization and each HLS element can be sized individually.

4.2.2 Campaign Optimization Problem Setup

Degrees of Freedom

As stated previously, the goal for CLO process is to be able to handle higher-level, campaign ConOps trades while the VSS process sizes the vehicles. The baseline architecture for HLS is to have all 3 propulsive elements and the crew aggregate at Gateway in NRHO. Therefore, this aggregation location can be selected as the main degree of freedom for this campaign, allowing the optimizer to choose between different orbits, or spatial nodes. For the following experiments, in addition to NRHO, a HEO is used as an alternative aggrega-

tion orbit. By aggregating closer to Earth, the optimizer may be more inclined to choose less powerful, cheaper, launch vehicles that throw to lower orbits, and pushing more of the propulsive load onto the elements themselves.

Another degree of freedom that can be opened up is the split of burns between the elements, specifically, the TE and DE. Since the AE will solely be used for ascent back to NRHO, the TE can potentially be used to share part of the descent burn with the DE. These two degrees of freedom are implemented through the use of paths, where each path represents a different set of ConOps.

Network Data

The list of spatial nodes considered for this campaign and their specific orbits are shown in Table 4.1. Several Earth orbits were included as different throw locations for the launch vehicles, while NRHO, LLO, and the lunar surface are required for the surface mission. An LLO_{low} orbit was included to represent a theoretical lower LLO that signifies where the TE burns to for the shared descent option. A set of ΔVs and ΔTs is required to represent the costs of traveling on each arc between the spatial nodes. For each transfer, there exists a range of possible values ΔVs, depending on how fast the transfer is. However, for the purposes of this campaign, only two energy levels of transfer are considered, minimum energy and minimum time, also only for specific arcs, which enables an additional degree of freedom for the optimizer without significantly increasing the computation complexity. These arc cost values are listed in Table 4.2 and Table 4.3, respectively, using data from Deguignet, Ishimatsu *et al.*, Sloss, Collins. Values denoted with an asterisk were calculated analytically using a Hohmann transfer assumption.

Vehicle and Payload Data

Design traits for the configuration, propulsion systems, and optimization design variables for each of the 4 in-space vehicles are summarized in Table 4.4, pulled from [126, 127,

Table 4.1: The different spatial nodes considered for the problem and their corresponding orbits.

Node	**Orbit/Surface**	**C3/Orbit**
ES	Earth Surface	-
LEO	Low Earth Orbit	-60
GEO	Geosynchronous Orbit	-9.454
HEO	High Earth Orbit	-2
NRHO	Near Rectilinear Halo Orbit	-
LLO	Low Lunar Orbit	100 km Circ
LS	Lunar Surface	-

128, 129]. The inert mass and dimensions for each vehicle are left for Experiment 3. A fixed set of launch vehicles for this problem was chosen, split into crew and cargo variants; their parameters for the CLO process are listed in Table 4.5 and Table 4.6 [101, 102, 103, 130, 104]. Each of the 4 crew members are assumed to be 75 kg and 1.5 m in both diameter and height [126]. They are the only payloads considered in the campaign, but only 2 of the 4 go down to the surface while the other pair stay at Gateway.

Table 4.2: ΔVs and ΔTs for minimum energy arc costs, where the row headers are the departure location and column headers are the arrival location.

ΔTs [d]

	ES	**LEO**	**GEO**	**HEO**	**NRHO**	**LLO**	**LS**
ES	0	1	1	1			
LEO	1	0	0.21*	5.41*			
GEO		0.21*	0	6.12*			
HEO		5.41*	6.12*	0	100	100	
NRHO					0	1	
LLO	5				1	0	1
LS						1	0

ΔVs [m/s]

	ES	**LEO**	**GEO**	**HEO**	**NRHO**	**LLO**	**LS**
ES	0	0	0	0	0	0	0
LEO	950	0	4,508*	3,089*			
GEO		4,508*	0	1,314*			
HEO		3,089*	1,314*	0	30	640	
NRHO					0	750	
LLO	180				750	0	1,870
LS						1,870	0

Table 4.3: ΔVs and ΔTs for minimum time arc costs, where the row headers are the departure location and column headers are the arrival location.

ΔTs [d]

	ES	**LEO**	**GEO**	**HEO**	**NRHO**	**LLO**	**LS**
ES	0	1	1	1			
LEO	1	0	0.2*	5.41*			
GEO		0.2*	0	6.12*			
HEO		5.41*	6.12*	0	5	3	
NRHO					0	1	
LLO	5				1	0	1
LS						1	0

ΔVs [m/s]

	ES	**LEO**	**GEO**	**HEO**	**NRHO**	**LLO**	**LS**
ES	0	0	0	0	0	0	0
LEO	950	0	5,581*	3,089*			
GEO		5,581*	0	1,314*			
HEO		3,089*	1,314*	0	450	900	
NRHO					0	750	
LLO	180				750	0	1,870
LS						1,870	0

Table 4.4: Design parameters and range input for the CLO process for each of the HLS in-space vehicles.

Design Parameter	**Parameter Type**	**TE**	**DE**	**AE**	**Orion**
Inert Mass (kg)	Fixed Input	-	-	-	-
Diameter (m)	Fixed Input	-	-	-	-
Height (m)	Fixed Input	-	-	-	-
Fuel	Fixed Input	LH_2	LH_2	LCH_4	MMH
Oxidizer	Fixed Input	LOx	LOx	LOx	MON
I_{sp} (s)	Fixed Input	449	449	341	319
OFR	Fixed Input	6.0	6.0	1.74	2.27
Max Payload Diameter (m)	Fixed Input	4	4	4	4
Max Payload Height (m)	Fixed Input	6	6	6	6
Max Payload Mass (kg)	Fixed Input	5,000	10,000	5,000	10,000
Boiloff$_{fuel}$ (kg/day)	Fixed Input	6	10	0	0
Boiloff$_{ox}$ (kg/day)	Fixed Input	0	30	0	0
Fuel Mass [0,max] (kg)	Design Variable	10,000	10,000	10,000	9,000
Oxidizer Mass [0,max] (kg)	Design Variable	60,000	60,000	60,000	9,000
Water Mass [0,max] (kg)	Design Variable	5,000	5,000	5,000	5,000
Oxygen Mass [0,max] (kg)	Design Variable	5,000	5,000	5,000	5,000
Food Mass [0,max] (kg)	Design Variable	5,000	5,000	5,000	5,000

Table 4.5: Crew launch vehicle data set for the CLO process.

Type	**Vehicle**	**Max Diameter (m)**	**Max Height (m)**	**Launch Cost**	**Cadence (days)**	**Throw Mass (kg)**
Crew	SpaceX Falcon 9	5.2	13.9	$80,000,000	90	LEO: 22,800, GEO: 8,300, HEO: 7,500
	SpaceX Starship	9	18	$150,000,000*	30	LEO: 63,800, GEO: 15,000, HEO: 35,000
	Blue Origin New Glenn	7	21.9	$130,000,000*	45	LEO: 45,000, GEO: 13,000, HEO: 10,000
	NASA SLS 1B Crew	5	8	$3,000,000,000	365	LEO: 105,000, GEO: 75,000, HEO: 55,000
	NASA SLS 2B Crew	5	8	$4,100,000,000	365	LEO: 150,000, GEO: 75,000, HEO: 55,000

Table 4.6: Cargo launch vehicle data set for the CLO process.

Type	Vehicle	Max Diameter (m)	Max Height (m)	Launch Cost	Cadence (days)	Throw Mass (kg)
Cargo	SpaceX Falcon 9	5.2	13.9	$67,000,000	90	LEO: 22,800, MEO: 20,000, GEO: 8,300, HEO: 7,500
	SpaceX Falcon Heavy	5.2	13.9	$97,000,000	90	LEO: 63,800, MEO: 45,000, GEO: 26,700, HEO: 20,000
	SpaceX Starship	9	18	$150,000,000*	30	LEO: 100,000, MEO: 60,000, GEO: 40,000, HEO: 35,000
	Blue Origin New Glenn	7	21.9	$120,000,000*	45	LEO: 45,000, MEO: 30,000, GEO: 13,000, HEO: 10,000
	Northrop Antares	3.9	9.5	$80,000,000	90	LEO: 8,000, MEO: 6,000, GEO: 5,000, HEO: 4,000
	ULA Vulcan Atlas V	5.4	23.4	$137,000,000	90	LEO: 12,030, MEO: 5,000, GEO: 1,935, HEO: 1,700
	ULA Vulcan Centaur	5.4	15.5	$150,000,000	90	LEO: 19,000, MEO: 3,900, GEO: 2,600, HEO: 2,500
	NASA SLS 1B Cargo	5	8	$2,700,000,000	365	LEO: 105,000, MEO: 90,000, GEO: 75,000, HEO: 55,000

Problem Specific Constraints

In addition to the technical constraints detailed in Section 2.6, constraints on the launch and aggregation of the vehicles are necessary to accurately model those operations. These include the cadence of each launch vehicle, the sequencing of each of the vehicles, as well as the minimum processing time for ground operations at the launch site. Although each launch vehicle has a different cadence, it is assumed that Kennedy Space Center can handle a launch every 30 days, defined by the indicator constraints in Equation 4.1 and Equation 4.2. Variable b_{v_i,v_j} indicates the launch sequencing between vehicle pair, v_i, v_j; whether vehicle v_i launches before or after vehicle v_j. Variable b_{v_i} indicates whether or not vehicle i launches in the campaign and t_{launch,v_i} is the time of launch of that vehicle.

$$b_{v_i,v_j} = 0 \implies t_{launch,v_i} - t_{launch,v_j} \leq (b_{v_i} + b_{v_j} - 1) * (-30) \tag{4.1}$$

$$b_{v_i,v_j} = 1 \implies t_{launch,v_i} - t_{launch,v_j} \leq (b_{v_i} + b_{v_j} - 1) * (30) \tag{4.2}$$

$$for \quad i,j \quad in \quad combination(v \in V), i \neq j \tag{4.3}$$

Since the launch vehicle chosen for each vehicle is a variable, the cadence constraints for those launch vehicles are more involved and require the introduction of several binary variables, summarized in Table 4.7 These variables need to be constrained further to ensure they relate to each other properly. Equation 4.4 constrains $b_{lv,t}$ to be the equal to the sum of all launch vehicles used for all vehicles, $b_{lv,v}$. Binary variable $b_{v,t}$ is constrained to be equal to any vehicle used variable, $b_{v,a}$, for all launch arcs at that timestep to denote whether or not vehicle v is launched at timestep t. Equation 4.6 constraints variable $b_{lv,v,t}$ to be true if vehicle, v is launched at time t and launch vehicle, lv is used for that vehicle. Subsequently, $b_{lv,t}$ can be true at time t if any of the variables, $b_{lv,v,t}$ are used at that time. The final cadence constraint for each launch vehicles is shown in Equation 4.9, which identifies a range of

timesteps based on the specific cadence and restricts a launch of that launch vehicle to be a maximum of one.

Table 4.7: Summary of binary variables related to launch vehicle cadence constraints.

Variable	Description
$b_{v,lv}$	Launch vehicle, lv, used for vehicle v
$b_{lv,t}$	Launch vehicle, lv, used at time t
$b_{v,t}$	Vehicle, v, launched at time, t
$b_{lv,v,t}$	Vehicle, v, launched at time, t, on launch vehicle lv

$$\sum_{t=0}^{t_{final}} b_{lv,t} = \sum_{v \in V} b_{v,lv} \quad \forall\, lv \in LV \tag{4.4}$$

$$b_{v,t} = OR(b_{v,a,t}, ...) \quad \forall\, v \in V,\ t \in [t_0, t_{final}],\ a \in A_{launch} \tag{4.5}$$

$$b_{lv,v,t} = AND(b_{v,lv}, b_{v,t}) \quad \forall\, v \in V,\ t \in [t_0, t_{final}],\ lv \in LV \tag{4.6}$$

$$b_{lv,t} = OR(b_{v_1,lv,t}, b_{v_i,lv,t}, ...) \quad for\ i = 1, .., n_{vehicles}, \forall\, v \in V,\ t \in [t_0, t_{final}],\ lv \in LV \tag{4.7}$$

$$\begin{aligned} t_{range,lv} = [max((t - cadence_{lv}), 0), min((t + cadence_{lv}), t_{final})] \\ \forall\, t \in [t_0, t_{final}],\ lv \in LV \end{aligned} \tag{4.8}$$

$$\sum_{t=t_{range,low}}^{t_{range,high}} b_{lv,t} \leq 1 \quad \forall\, lv \in LV \tag{4.9}$$

NASA's reference HLS architecture requires a specific launch sequence for each of the 4 vehicles to minimize boiloff; the AE is launched first, followed by the DE and TE, respectively. Orion will only launch once all 3 propulsive elements have already reached the aggregation location. The former sequence is implemented using a single constraint

that relates the launch times for each of the vehicles, in Equation 4.10. The latter operational constraint requires the use of an additional integer variable, $t_{loc,v}$, which indicates the aggregation time at location, loc for vehicle v, constrained using Equation 4.12. Finally Orion's launch time, $t_{launch,Orion}$ can be constrained to be greater than the aggregation time for each of the vehicles. However, this is augmented using an indicator constraint, to ensure that the aggregation time corresponds to the proper location, dependent on the path chosen in the campaign, shown in Equation 4.13.

$$t_{launch,v} = \sum_{a \in A_{launch}} m(b_{v,a_{im,jl}}) quad \forall v \in V \tag{4.10}$$

$$t_{launch,Orion} > t_{launch,TE} > t_{launch,DE} > t_{launch,AE} \tag{4.11}$$

$$t_{loc,v} = min(a_{loc,loc,t}) \quad \forall t \in [0, t_{final}] \tag{4.12}$$

$$b_{path,agg\_loc} = 1 \implies t_{launch,Orion} \geq t_{loc,v} \quad \forall v \in V \tag{4.13}$$

Process Parameters

The maximum runtime for CLO was set at 4 hours and the MIP gap was set to 0.001. The convergence tolerance is set at 5%, and the maximum number of iterations to 10. The table below lists the weights used for the OEC objective function.

Table 4.8: Objective weights for the HLS campaign CLO problem.

Objective Term	**Weight**	**Max Value**
Propellant Mass	0.05	10,000
Number of Burns	0.65	5
Execution Time	0.22	270
Launch Costs	0.18	4,100,000,000

4.2.3 Vehicle Sizing and Synthesis Problem Setup

Vehicle Architecture Definition

Only the 3 main propulsion elements will be sized for this lunar campaign, as Orion's mission is fixed as a crew transport to the aggregation location. Table 4.9 defines the subsystems used for each of the vehicles and a high level description of each subsystem model and Table 4.10 details the main design parameters, with a blanket Mass Growth Allowance (MGA). Due to the type of campaign, each of the propulsion elements are functionally identical, comprised of the same subsystems. Further the differences in each of their sizes, which will be determined through the whole VSS process and depending on their individual missions.

Table 4.9: The different subsystems used for each of the 3 propulsive elements in the HLS campaign.

Subsystem	**Description**
Sensors	Aggregation of different sensor components required for navigation using a bottoms-up approach
Communications	Models the communications equipment using a bottoms-up approach
Structures	Estimates the mass of all structural components in the vehicle, excluding the propulsion system, as a fraction of the inert mass of the vehicle
Radiator	Sizes a radiator to reject the vehicle heat load
Power	Sizes a photovoltaic array and accompanying power storage and distribution systems
Tanks	Sizes the tanks and estimates the thermal characteristics of the propellant depending on the environment
Main Engines	Sizes an input number of engines and defines the propulsive capabilities for mission analysis
Reaction Control System	Modeled as a fraction of the inert mass of the vehicle

Table 4.10: Key design parameters used in VSS for each of the propulsive elements.

Subsystem	Design Parameter	AE	DE	TE
Propulsion	Cryocooler	20K	none	none
	Tank l/d	1	1	1
	Tank Config	2x2	2x2	2x2
	Tank Pressure [MPa]	0.207	0.207	0.207
	Tank Temperature [K]	20	20	20
	Tank Material	AL2195	AL2195	AL2195
	Num Engines	3	3	3
	Engine Thrust [kN]	34	34	34
	I_{sp}	341	449	449
Avionics	n_{gyros}	3	3	3
	$n_{star\ sensors}$	3	3	3
	$n_{horizon\ sensors}$	1	1	1
	Comms Package	Deep Space	Deep Space	Deep Space
Structures	Structures Fraction	0.30	0.30	0.30
RCS	RCS Fraction	0.25	0.25	0.25
Power	η_{cell}	0.33	0.33	0.33
	Array Density [kg/m^2]	18.2	18.2	18.2
	Operations Distance [AU]	1.5	1.5	1.5
	Battery specific capacity [W*hr/kg]	125	125	125
	Depth of Discharge	0.5	0.5	0.5

Mission Analysis

Within the mission analysis portion of the VSS, the goal is to allow degrees of freedom in some mission parameters to ensure each vehicle is flying its most optimal mission. Although the orbital nodes are parameterized in mission analysis, for the HLS campaign, each vehicle will have to fly from its launch dropoff location to the aggregation point. This means varying orbits below those points within this problem is unnecessary and the main mission degrees of freedom should be within cislunar space. Due to the small sphere of influence of the moon and its low gravitational pull, it is more difficult to specify concrete orbits. As such, the degrees of freedom for this problem will be the ΔV splits between the elements, constrained by the total ΔV between the aggregation location and return of the AE. By defining these ΔVs as design variables within DYREQT, they are allowed to

vary while the vehicle is being sized. Each variable is given a range of $\pm 25\%$ from the baseline values defined in Table 4.2 and Table 4.3, giving some room for the mission to play around without allowing too much variation that may cause the integrated process to diverge. These degrees of freedom are summarized in Table 4.11, for each of the campaign paths being considered. Note that for the TE Shared Descent path, there is one less degree of freedom: AE's ascent ΔV.

Table 4.11: The mission degrees of freedom defined in DYREQT for the VSS process.

Campaign Path	**Variables**	**Constraint**
Baseline	$\Delta V_{NRHO,LLO}$, $\Delta V_{LLO,LS}$, $\Delta V_{LS,LLO}$, $\Delta V_{LLO,NRHO}$	$\Delta V_{NRHO,LLO} + \Delta V_{LLO,LS} + \Delta V_{LS,LLO} + \Delta V_{LLO,NRHO} = 5240$
TE Shared Descent	$\Delta V_{NRHO,LLO}$, $\Delta V_{LLO,LS}$	$\Delta V_{NRHO,LLO} + \Delta V_{LLO,LS} = 2882$
HEO Aggregation	$\Delta V_{HEO,LLO}$, $\Delta V_{LLO,LS}$, $\Delta V_{LS,LLO}$, $\Delta V_{LLO,HEO}$	$\Delta V_{HEO,LLO} + \Delta V_{LLO,LS} + \Delta V_{LS,LLO} + \Delta V_{LLO,HEO} = 5188$

4.3 Iterative Methods

4.3.1 MDO vs MDA

MDO is a field that aims to solve optimization problems of complex systems in which multiple disciplines, or subsystems, are coupled. They are notably used within aerospace systems design, where different aircraft or spacecraft subsystems are optimized to achieve a specific objective, usually the minimization of mass. Distinct from a traditional optimization problems, the design variables of the problem are no longer just input to a single analysis, but rather can be input to multiple ones. The objective function can also depend on a single analysis or multiple ones, depending on the problem. Figure 4.2 shows a notional MDO problem with three coupled disciplines, A, B, and C. In this case, although there is still only one set of design variables and one objective function, each variable are inputs to multiple subsystems, with no structured scheme. An analogous problem in space systems

design would be a coupled propulsion, structure and power sizing code, where there are interdependencies between the variables, and the objective is to minimize mass of the vehicle, very similar to the process used in DYREQT. Multidisciplinary Analysis (MDA), however, is the definition of the process by which the coupled disciplines are solved numerically, as shown in Figure 4.3, usually requiring the use of iterative methods to do so.

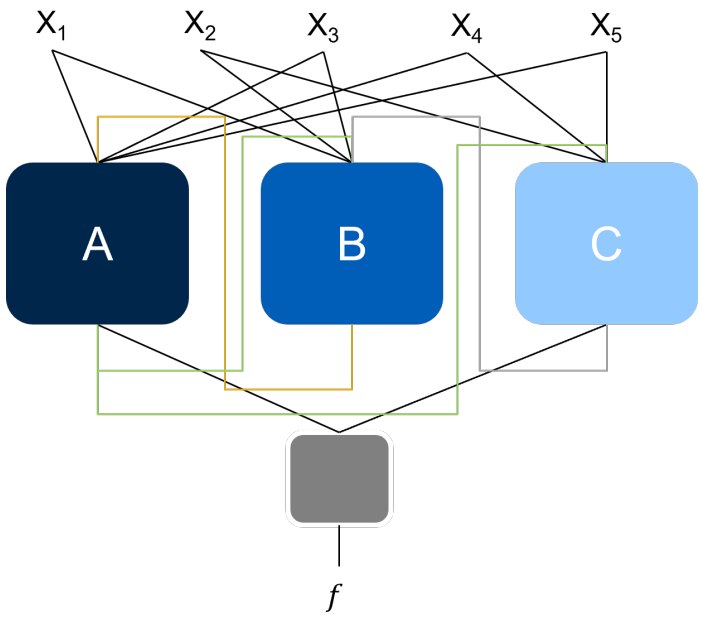

Figure 4.2: Notional MDO problem with 3 systems and 5 design variables [131].

With the methodology proposed in this chapter, the two integrated disciplines are CLO and VSS, with the latter being a full MDAO problem by itself, as described in Subsection 3.2.2. Following the conventions of MDO, this problem is classified as a highly coupled, single level system as changes in one can have large impacts on the other and there is no parent problem to solve [132]. However, this research objective is to establish integrated design methodology and as such, optimization of the integrated system is outside the scope of this research The resulting problem is only MDA, rather than MDO

Solvers are numerical methods used to converge two or more coupled systems in the MDA problem, and can be linear or non-linear. Non-linear solvers are iterative in nature

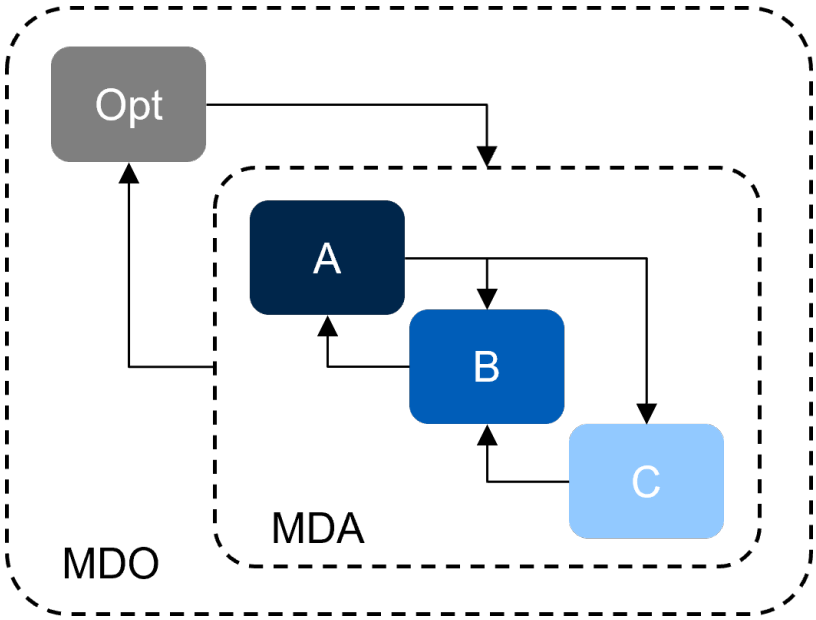

Figure 4.3: Notional MDA problem within the overall MDO problem [131].

as the solution to the systems of equations is difficult to find analytically. A taxonomy of iterative solvers reviewed for this experiment is shown in Figure 4.4

4.3.2 Newton-like Methods

Given a system with i design variables each, $f(x_1, x_2, x_3, ..., x_i)$, the Jacobian and Hessian matrices is defined as the first and second order gradients. Matrix elements of the Jacobian and Hessian are defined by Equation 4.14 and Equation 4.15, respectively.

$$(J_f)_i = \frac{\partial f}{\partial x_i} \tag{4.14}$$

$$(H_f)_{ij} = \frac{\partial^2 f}{\partial x_i \partial x_j} \tag{4.15}$$

Newton methods use either Jacobian or Hessian information to calculate each step size in the iteration, which can be ruled out immediately as each process is treated as a black box for integration and neither is available. Quasi-newton methods were introduced for those cases by either approximating the Jacobian (first order gradient) or the Hessian (second or-

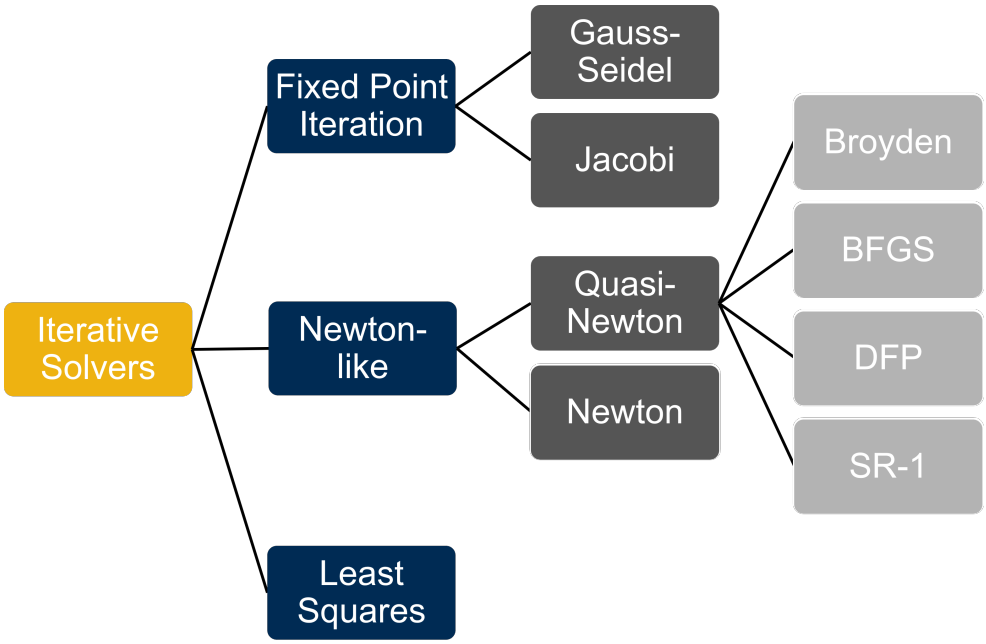

Figure 4.4: Taxonomy of iterative solvers reviewed for this research.

der gradient). The Broyden-Fletcher-Goldfarb-Shanno (BFGS), Davidon-Fletcher-Powell (DFP), and Symmetric Rank 1 (SR1) methods approximate the Hessian matrix using the Jacobian, which also can be rules out for the same reason as above. The Broyden method, however, approximates the Jacobian using the secant equation at each iteration in the process. With the characteristics of the campaign logistics optimization process being driven by integer design variables, calculating the derivatives may become problematic. For this reason, the Broyden method was also ruled out as an iterative solver for the methodology.

4.3.3 Fixed Point Iteration

FPI is the process by which successive substitution is used to identify the fixed point of two or more systems [133]. Given a single, non-linear equation of the form, $f(x) = 0$, it can be transformed into the form, $x = g(x)$ [134]. An initial guess, x^0, a series of successive substitution values can be computed:

$$x^{k+1} = g(x^k) \quad k = 0, 1, 2, ... \tag{4.16}$$

If the function $g(x)$ is continuous and maps an interval, I, into itself, then there exists a point, x^* in $g(x)$, called a fixed or stationary point, that satisfies x^* = $g(x^*)$. Further this implies that x^* is a solution of f, or $f(x^*) = 0$. This single variable, single system procedure can be generalized to cover a problem with i systems, each with j variables:

$$f_1(x_1, x_2, ..., x_j) = 0 \tag{4.17}$$

$$f_2(x_1, x_2, ..., x_j) = 0 \tag{4.18}$$

$$\vdots \tag{4.19}$$

$$f_i(x_1, x_2, ..., x_j) = 0 \tag{4.20}$$

Or simply in vector form in:

$$\mathbf{F}(\mathbf{x}) = \mathbf{0} \tag{4.21}$$

In this case, output variables from one system that are used as inputs to another are called coupling variables. The analogous process of iteration is defined by transformation into $\mathbf{x} = \mathbf{G}(\mathbf{x})$ and an initial guess, $\mathbf{x}^0$:

$$\mathbf{x}^{k+1} = \mathbf{G}(\mathbf{x}^k) \quad k = 0, 1, 2, ... \tag{4.22}$$

Similarly, the existence of a fixed point, $\mathbf{x}^*$ can be proven if the domain, $\mathbf{D}$ of $\mathbf{G}$ can be mapped into $\mathbf{D}$ via $\mathbf{G}$ itself. A more detailed proof of this is presented in [133, 134]. If $\mathbf{G}$ is

continuous on $\mathbf{D}$, then there exists a point, $\mathbf{x}^*$ such that $\mathbf{F}(\mathbf{x}^*) = \mathbf{0}$. Using these concepts, there are two main methods of implementation for real systems: NLGS or Jacobi iteration [135]. NLGS for multiple systems is run in series, where the inputs for one system are the outputs from another in the previous iteration [136]. In contrast, Jacobi iteration uses parallel execution by turning the problem into matrix form and the outputs for each system are calculated simultaneously using a full set of inputs from the previous iteration. Given a good starting point, NLGS generally converges faster than Jacobi and is relatively easier to implement [137]. Specific formulations for these to iterative methods will be discussed during the design of experiment 1.

4.3.4 Hypothesis Development and Experiment Design

In terms of computational complexity, CLO is more intensive than VSS, given the potentially highly constrained mixed-integer optimization problem. However, if many design variables are included, the latter could become expensive as well. Since the integrated process is iterative, the number of function calls drives the runtime of the whole process. Between the two FPI methods, NLGS is expected to finish faster, which leads to the hypothesis: [138]

Hypothesis 1: If non-linear, Gauss-Seidel iteration is used to iteratively converge the two processes, then the solution will be found with minimal runtime.

An experiment to test this hypothesis should be the direct comparison of available iterative methods to identify whether or not NLGS provides the best performance. From the literature review of iterative solvers, since only the two FPI are valid for this problem, this experiment should and will only have one independent variable with a total of two tests. The dependent variables for this experiment are the number of iterations, and subsequently the overall runtime it takes to produce a converged solution. These are necessary to directly compare the performance of the two iterative solvers and identify the better performing one.

This will enable the assessment of the validity of **Hypothesis 1**. The equations below provide the problem formulation of the overall experiment to test the performance of iterative solvers.

$$Veh_{out}, Veh_{out,c} = \mathbf{VSS}(Veh_{in}, Camp_{out,c}) \tag{4.23}$$

$$Camp_{out}, Camp_{out,c} = \mathbf{CLO}(Camp_{in}, Veh_{out,c}) \tag{4.24}$$

$$VSS \equiv Vehicle\ Sizing\ and\ Synthesis \tag{4.25}$$

$$CLO \equiv Campaign\ Logistics\ Optimization \tag{4.26}$$

$$Veh_{out} = VSS\ Specific\ outputs \tag{4.27}$$

$$Veh_{in} = VSS\ Specific\ inputs \tag{4.28}$$

$$Veh_{out,c} = VSS\ outputs\ coupled\ to\ CLO \tag{4.29}$$

$$Camp_{out} = CLO\ Specific\ outputs \tag{4.30}$$

$$Camp_{in} = CLO\ Specific\ inputs \tag{4.31}$$

$$Camp_{out,c} = CLO\ outputs\ coupled\ to\ VSS \tag{4.32}$$

Jacobi Iteration - Test 1

$$Veh_{out}, Veh_{out,c}^{k+1} = \mathbf{VSS}(Veh_{in}, Camp_{out,c}^{k}) \tag{4.33}$$

$$Camp_{out}, Camp_{out,c}^{k+1} = \mathbf{CLO}(Camp_{in}, Veh_{out,c}^{k}) \tag{4.34}$$

$$k = iteration \tag{4.35}$$

$$Veh_{out}, Veh_{out,c}^{k+1} = \mathbf{VSS}(Veh_{in}, Camp_{out,c}^{k}) \tag{4.36}$$

$$Camp_{out}, Camp_{out,c}^{k+1} = \mathbf{CLO}(Camp_{in}, Veh_{out,c}^{k+1}) \tag{4.37}$$

$$k = iteration \tag{4.38}$$

4.4 Convergence Criteria

This section discusses **Research Question 2**:

What is the proper set of convergence criteria for the chosen iterative process?

Regardless of the final choice of iterative solver, a proper set of convergence criteria is required to identify the when to stop the algorithm. The criteria could affect the performance of the solver itself as well as the validity of the solution after convergence. For problem of one or more systems, the convergence, or stopping criteria are defined by the coupling variables between the systems. Depending on the coupled system, the magnitude of the variables could be very large or very small, and identifying a specific tolerance could be difficult. A normalized Error Sum of Squares (SSE) is typically used to mitigate this issue, shown in Equation 4.39, for n design variables.

$$SSE = \sum_{i=1}^{n} \frac{(x_i - \overline{x})^2}{x_0} \tag{4.39}$$

4.4.1 Hypothesis Development and Experiment Design

Two main disciplines, CLO and VSS, are linked for this thesis mainly through the overall mission set provided by the former and the vehicle capabilities provided by the latter. The mission set information is used to drive the VSS process through the overall number of missions and ΔV, ΔT for each event in each mission. Vehicles in the CLO process are updated at each iteration by VSS mainly through its inert mass.

Since both sets of information, mission and vehicle, are updated at each iteration, both could be used as convergence criteria. Considering the flow of resources throughout the campaign are constrained by what vehicles are available to move those resources, the hypothesis for **Research Question 2** is stated as follows:

Hypothesis 2: If only vehicle masses is used as the convergence criteria, the errors will be minimized.

To test this hypothesis, the convergence criteria can be first grouped by their information: mission, vehicle, or a combined set. These are required as the main coupling variables between the campaign and vehicle problems. The independent variables of this experiment are the different set of criteria, while the dependent variables are the overall error magnitudes, runtime, and number of iterations. Tracking the errors is important as the converged solution needs to be a closed design. That is, differences in magnitudes of the coupling variables imply that a campaign requires nearly identical vehicle sizes than what the VSS is providing. Runtime and number of iterations allow to characterize the performance of each criteria, enabling identification of sets that may take too long to converge, if at all. Equation 4.40 is the 2-norm error of the gross masses of each individual vehicle in the campaign and Equation 4.41 is the same for propellant masses of each vehicle. Similarly, the main mission parameters are ΔV and ΔT, the arc costs in the CLO formulation. The 2-norm errors for those are shown in Equation 4.42 and Equation 4.43, respectively. Finally, a combination of vehicle or mission parameters could be used, shown in Equation 4.45. Each of these equations are an individual test for the convergence criteria experiment of **Research Question 2**.

$$\sum_{i=1}^{n} \frac{\|m_{gross,k+1} - m_{gross,k}\|_2^2}{m_0} < \varepsilon \tag{4.40}$$

$$\sum_{i=1}^{n} \frac{\|m_{inert,k+1} - m_{inert,k}\|_2^2}{m_0} < \varepsilon \tag{4.41}$$

$$\sum_{j=1}^{n} \frac{\|\Delta V_{k+1,j} - \Delta V_{k,j}\|_2^2}{\Delta V_0} < \varepsilon \tag{4.42}$$

$$\sum_{j=1}^{n} \frac{\|\Delta T_{k+1,j} - \Delta T_{k,j}\|_2^2}{\Delta T_0} < \varepsilon \tag{4.43}$$

$$\sum_{j=1}^{n} \frac{\|\Delta V_{k+1,j} - \Delta V_{k,j}\|_2^2}{\Delta V_0} + \frac{\|\Delta T_{k+1,j} - \Delta T_{k,j}\|_2^2}{\Delta T_0} < \varepsilon \tag{4.44}$$

$$\sum_{j=1}^{n} \frac{\|m_{gross,vss,i} - m_{gross,clo,i}\|_2^2}{m_0} + \frac{\|\Delta V_{k+1,j} - \Delta V_{k,j}\|_2^2}{\Delta V_0} < \varepsilon \tag{4.45}$$

4.5 Method Initialization

When fully integrated, regardless of the structure of methodology, the CLO process requires vehicle capabilities to execute and the VSS process requires missions to size to. The initialization of the integrated process requires one to be executed first, with a starting guess of the other, with a total of two possible structures, shown in Figure 4.5.

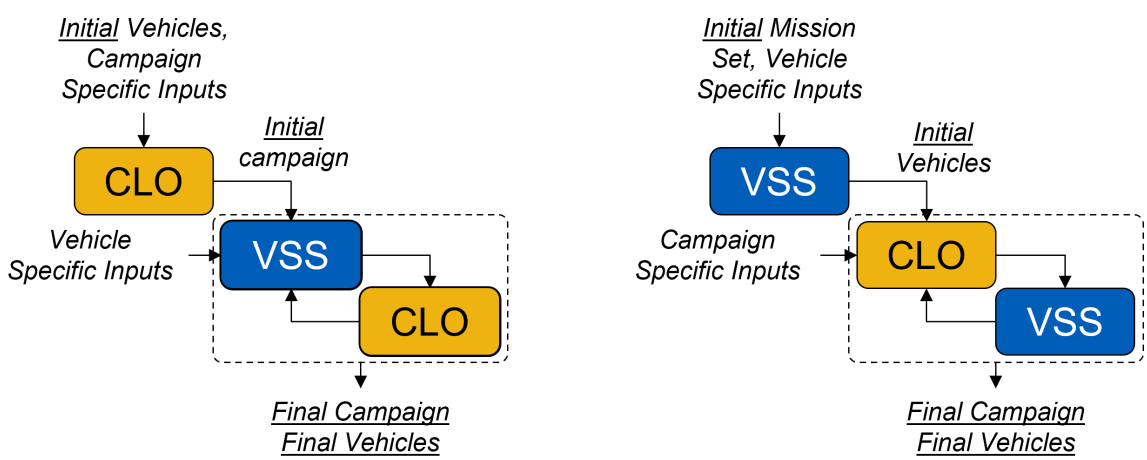

Figure 4.5: Process diagrams of the two possible execution structures of the integrated methodology.

The converged solution may depend on this sequence of execution, where the initial guess may drive the optimal campaign solution, necessitating the tracking of the technical FoMs, through the objective value of provided by the CLO process.

4.5.1 Hypothesis Development and Experiment Design

With only two options available for initialization, a direct comparison can be made between the two processes as the initial one to develop the hypothesis for this research question.

If a converged solution exists and the problem is setup correctly, either process structure should theoretically find that solution. Vehicles in the CLO process primarily require a inert mass to properly calculate the propellant burned throughout the network and VSS requires the missions flown by the vehicles. Regardless of how that initial inert mass guess is given if CLO starts, it drives the mission chosen by the optimizer as higher inert masses may preclude certain missions. However, once a mission is chosen, the following VSS run is expected to update the CLO input with the correct inert mass, opening up the proper options in the CLO problem. Therefore, **Hypothesis 3** can be stated as:

Hypothesis 3: If the CLO problem is solved first, the campaign will be at a minimum without an appreciable change in runtime.

To test this hypothesis a simple experiment is setup that runs the integrated process with both CLO and VSS. Similar to **Experiment 1**, since there are only two possible methods of initialization, there is only one independent variable for this experiment, with a total of two tests. Directly comparing these tests will identify which one provides better performance of the overall methodology and subsequently the validity of **Hypothesis 3**. Since the initial mass guess and initial process may drive the converged solution, it is necessary to track the objective values as a dependent variable in addition to the performance parameters of number of iterations and runtime. But two subsequent questions arise with the execution of this experiment that need to be answered first; defined as **Research Question 3.1** and **Research Question 3.2**:

Research Question 3.1: If CLO is executed first, how is the inert mass guess generated?

Research Question 3.2: If VSS is executed first, how is the mission event sequence guess generated?

CLO Initialization

Starting with **Research Questions 3.1**, regardless of how that initial inert mass guess is given if CLO starts, it drives the mission chosen by the optimizer as higher inert masses may preclude certain missions. There are several ways to estimate the inert mass of an in-space transportation system, whether information about its mission is available or not. An IMF can be set such that the inert mass of each spacecraft is simply a fraction of the total mass at the origin, the latter ensuring the inert mass does not change throughout the mission. Since the CLO process does not account for RCS burns or propellant residuals and reserves, but the inert mass does, the "inert mass" in CLO should include these masses. In other words, the inert masses for each vehicle in CLO accounts for all masses that is not used propellants by that vehicle.

All spacecraft are constrained by the mass and volume throw capabilities of available launch vehicles. Depending on the density of the propellant and the type of vehicle, the volume can be more constraining than the mass. Therefore, vehicles can be sized to maximize these constraints and the inert mass from this sizing can be used as the initial guess. This provides the additional benefit in that there will be valid launch vehicles for each vehicle for the CLO optimizer to chose from.

For the latter guess type, it could be possible that the inert masses are too high for the mission required of each vehicle by CLO, creating an infeasible solution space. The hypothesis for this research question is stated as follows:

Hypothesis 3.1: If CLO is solved first with an initial inert mass guess that is a fraction of total mass, then the converged solution will be a minimum.

Experiment 3.1 will test this hypothesis by running the integrated process with both inert mass guess types with CLO running first. A blanket IMF of 0.45 is used for test 1, which corresponds to a Propellant Mass Fraction (PMF) of 0.55. For in-space transportation systems, and especially for larger ones, this is a conservative estimate by design.

Sizing of each of the three propulsive elements in the HLS campaign for launch vehicles in test 2 of this experiment uses the launch vehicles provided in Table 4.5 and Table 4.6. The volume of each fairing was calculated as a cylinder based on the allowable diameter and height, as $V_{lv} = \pi \frac{d_{lv}^2}{4} h_{lv}$. Then, using the density of the fuel and oxidizer, $\rho_{fuel}, \rho_{oxidixzer}$, of each vehicle along with the Oxidizer to Fuel Ratio (OFR), the total mass of propellant that maximizes volume can be calculated as:

$$m_{fuel,v} = \frac{0.60 * V_{lv} \rho_{fuel,v} \rho_{oxidizer,v}}{OFR_v * \rho_{fuel,v} + \rho_{oxidizer,v}} \tag{4.46}$$

$$m_{oxidizer,v} = OFR_v * m_{fuel,v} \tag{4.47}$$

$$\tag{4.48}$$

where it was assumed that all other systems of the spacecraft take up 40% of the volume. Finally, the inert masses are calculated by using the PMF for each vehicle, which are shown in Table 4.12 [126]. For this experiment, the minimum inert masses are used as the initial guess so that it does not preclude the optimizer from using a different launch vehicle, if it chooses to. That is, if a higher inert mass is chosen, it would filter out some other launch vehicles for that vehicle.

Table 4.12: Table of inert masses for each vehicle in the HLS campaign sized to maximize the volume of each launch vehicle fairing.

	Ascent Element	**Descent Element**	**Transfer Element**
Falcon 9	51,143	20,730	21,916
Falcon Heavy	51,143	20,730	21,916
New Glenn	86,816	35,190	37,203
Antares	28,626	11,603	12,267
Atlas V	50,478	20,461	21,631
Vulcan Centaur	82,418	33,407	35,319
SLS 1B	220,426	89,346	94,459
SLS 2B	220,001	89,174	94,277

VSS Initialization

Addressing **Research Question 3.2** requires an initial guess of a mission sequence for the VSS to size to. Given a main user input for the CLO process is the path set for the problem, this can be used to tackle this problem. Specifically, since a path is a user input set of events for a vehicle to follow, it can double as the sizing mission in the VSS. For problems with multiple paths, the question arises of which path to choose from as the initial guess. The hypothesis for this research question is stated as:

Hypothesis 3.2: If VSS is solved first with an initial path guess that minimizes ΔV, then the integrated solution will be a minimum.

There are two available options for a path guess experiment, **Experiment 3.1**, to test this hypothesis: the minimum ΔV path and a random guess. Test 1, with the former, is as the name says, choosing a path with the minimum overall ΔV, where the overall ΔV is the sum of ΔVs that each vehicle goes through. Test 2 is a simple random selection from all available paths, and is run three times to ensure repeatability.

4.6 Experimental Matrix and Plan Summary

Looking at the set of research questions and subsequent experiments, it could be said they are all are interdependent. The convergence criteria set and initialization process could directly affect the performance of the solvers. The initial guess could be good, but the specific set of convergence criteria may not let the problem converge. All of the above could affect the overall validity of the final campaign and vehicle solution. Therefore, it is necessary to assess different combinations of tests to identify the best process, much like an experimental trade space exploration. This experimental matrix of tests is shown in Table 4.13, with a total of 42 different compatible combinations. As Jacobi iteration is parallel in execution, both CLO and VSS need an initial guess, requiring two fewer tests than the full combination set.

With a total of five research for this thesis, the overall research plan to address them, presented in this chapter, is summarized in Figure 4.6. Once fully constructed using the results from these experiments, the integrated methodology can be applied to a large-scale Mars campaign to show the improvement over the state of the art.

Table 4.13: A matrix of interdependent tests for all of the experiments.

Solver	Jacobi	NLGS		
Convergence Criteria	Mission	Vehicle	Both	
Initial Process	CLO	VSS		
Initial Guess for VSS	Minimum ΔV Path	Random Path 1	Random Path 2	Random Path 3
Initial Guess for CLO	Inert Mass Fraction	Launch Vehicle Sized Vehicles		

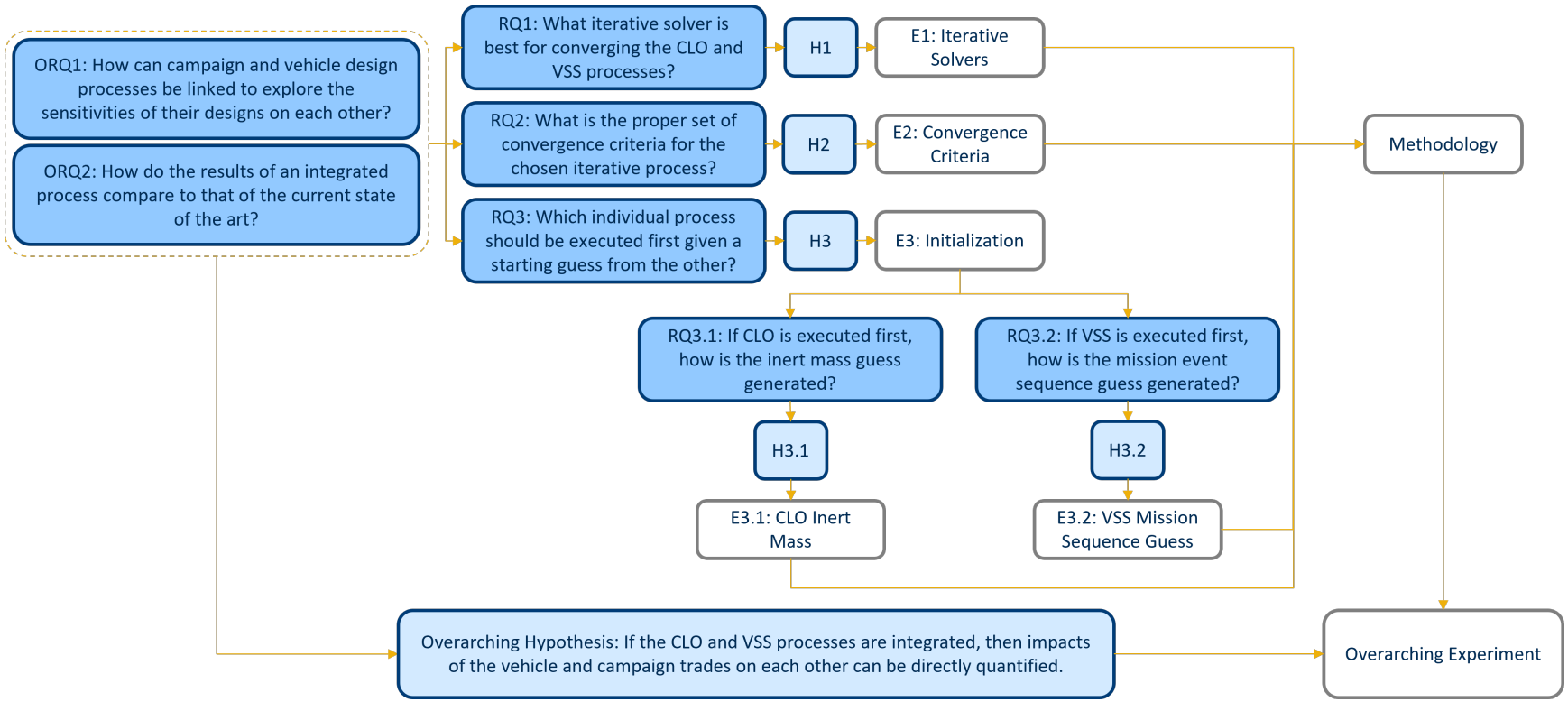

Figure 4.6: Thesis structure updated to show a summary of the experimental plan for this research.

4.7 Experiment Results

4.7.1 Experiment 2: Convergence Criteria

Before proceeding to the rest of the results, it is necessary to examine those for **Experiment 2**, run with a NLGS, CLO running first, and a IMF initial guess. The convergence criteria for this combination of tests were the inert and gross mass errors, but the errors for the cislunar arcs were also calculated, the former using Equation 4.49 and the latter using Equation 4.50, where k is the number of iterations and n is the number of vehicles.

$$\sum_{i=1}^{n} \frac{\|m_{gross,vss} - m_{gross,clo}\|_2^2}{m_0} + \sum_{i=1}^{n} \frac{\|m_{inert,k+1} - m_{inert,k}\|_2^2}{m_0} < \varepsilon \tag{4.49}$$

$$\sum_{j=1}^{n} \frac{\|\Delta V_{k+1,j} - \Delta V_{k,j}\|_2^2}{\Delta V_0} < \varepsilon \tag{4.50}$$

Three plots follow, the first two showing the inert and gross mass errors, respectively, over the course of the 10 allowed iterations, while the third shows the ΔV errors for the cislunar arcs. It is a converged solution, by iteration 10, as the vehicle parameters of inert and gross mass were chosen as the criteria for this combination of tests. However, at iterations 7 and 8, all cislunar arc errors are below the tolerance.

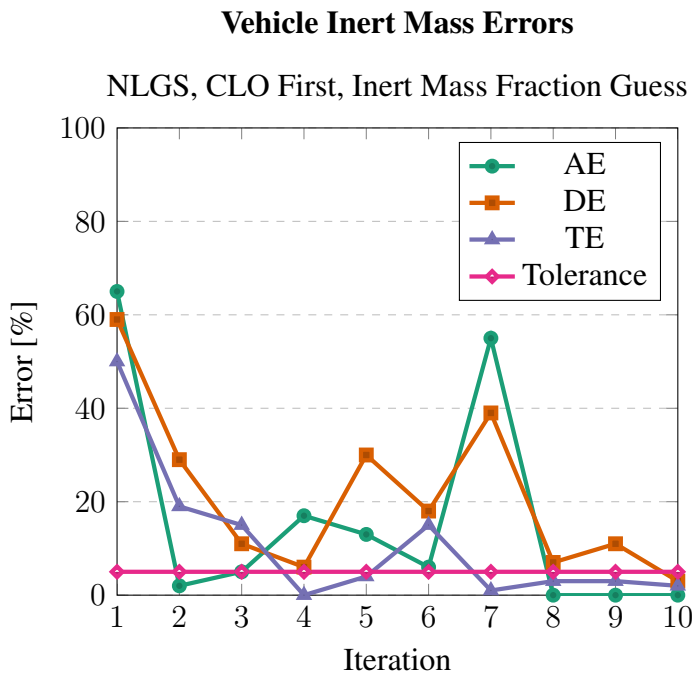

Figure 4.7: Errors for the vehicle inert masses per iteration.

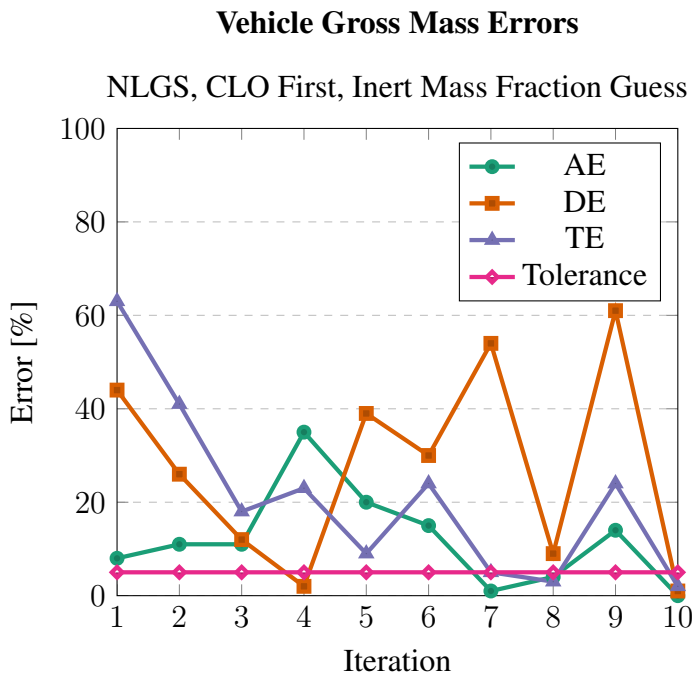

Figure 4.8: Errors for the vehicle gross masses per iteration.

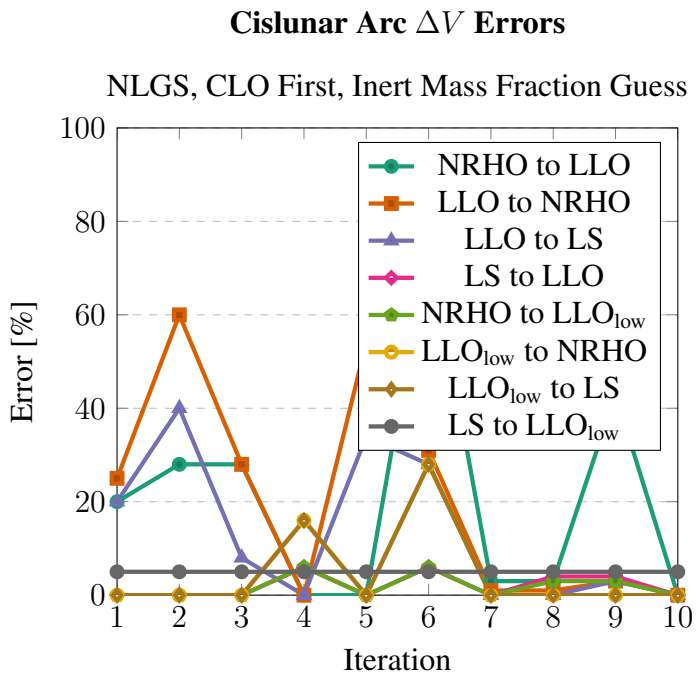

Figure 4.9: Errors for the vehicle gross masses per iteration.

If only the mission parameters, these ΔV, were chosen as the criteria rather than the masses, the process would be considered converged by iteration 7, but because the masses are not below the tolerance, the resulting solution would not be valid. This behavior leads to the first significant finding among the experimentation results, that it does not make sense to consider either mission or vehicle parameters solely as convergence criteria. That is, a converged solution should mean that both sets of parameters are below the tolerance. Therefore, **Hypothesis 2 is rejected**, and the rest of the combinatorial test space that don't use both sets can be skipped, resulting in only 14 remaining combinations, Equation 4.51 shows the required final convergence criterion.

$$\varepsilon \geq \sum_{i=1}^{n} \frac{\|m_{gross,vss} - m_{gross,clo}\|_2^2}{m_0} + \sum_{i=1}^{n} \frac{\|m_{inert,k+1} - m_{inert,k}\|_2^2}{m_0} + \sum_{j=1}^{n} \frac{\|\Delta V_{k+1,j} - \Delta V_{k,j}\|_2^2}{\Delta V_0} + \sum_{j=1}^{n} \frac{\|\Delta T_{k+1,j} - \Delta T_{k,j}\|_2^2}{\Delta V_0} \tag{4.51}$$

4.7.2 Experiment 1: Iterative Solvers

Experiment 1 tests the performance of the different solvers for the integrated process. Including the other tests in the combinatorial space, there a total of 14 different combinations, 7 for NLGS and 7 for Jacobi iteration. Figure 4.10-Figure 4.19 show that all Jacobi iteration cases Did Not Converge (DNC) in the 10 iteration limit, whereas all but a single NLGS case converged. Although there is not enough information to say if Jacobi iteration does close past 10 iterations, ignoring the one DNC case, NLGS converges in 10 iterations or less. Therefore, **Hypothesis 1 is accepted**, and NLGS is the selected iterative solver for the final methodology.

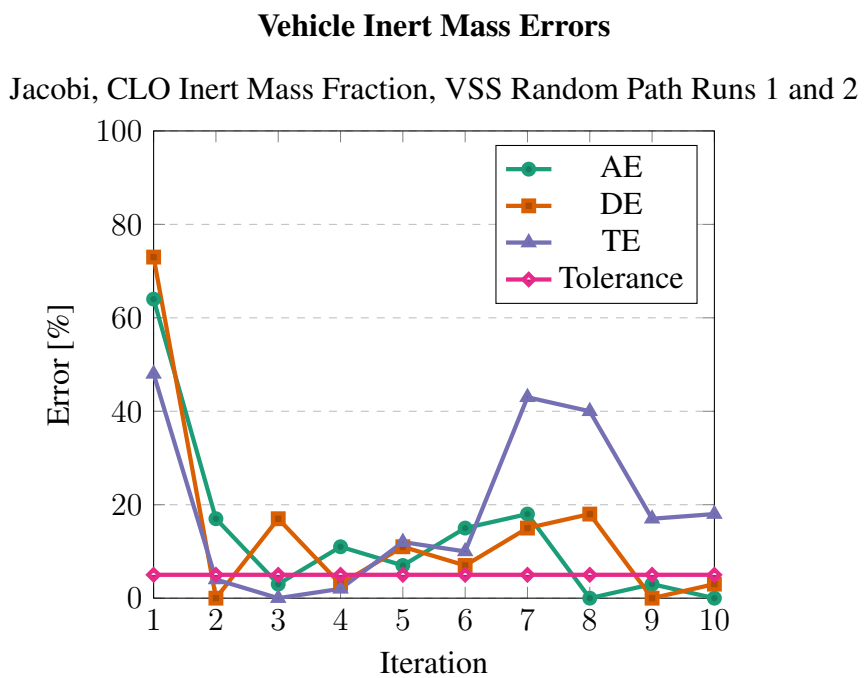

Figure 4.10: Errors for the vehicle inert masses per iteration for Experiment 1, with Jacobi iteration, CLO inert mass fraction guess and VSS Random Path Runs 1 and 2 - Baseline.

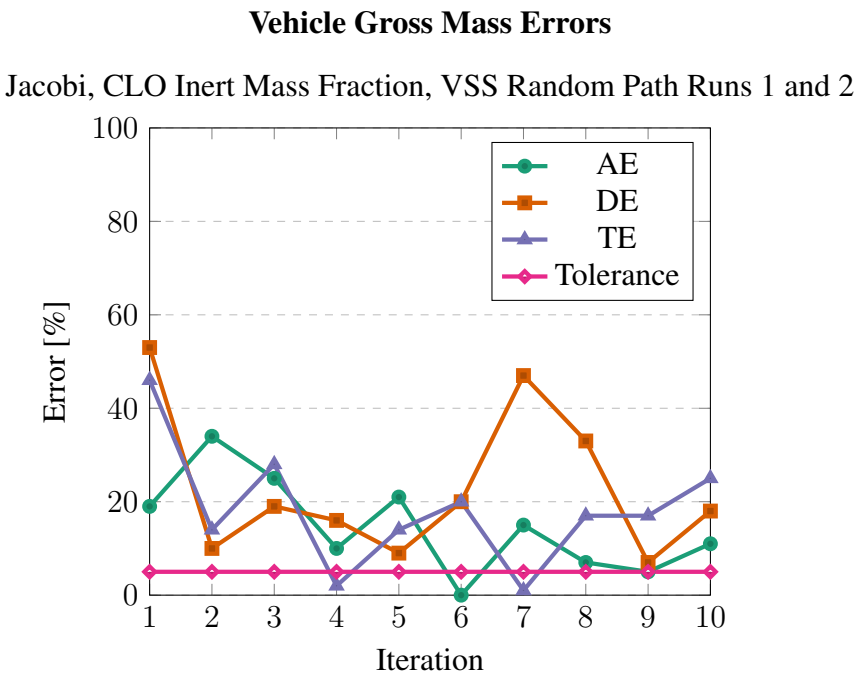

Figure 4.11: Errors for the vehicle gross masses per iteration for Experiment 1, with Jacobi iteration, CLO inert mass fraction guess and VSS Random Path Runs 1 and 2 - Baseline.

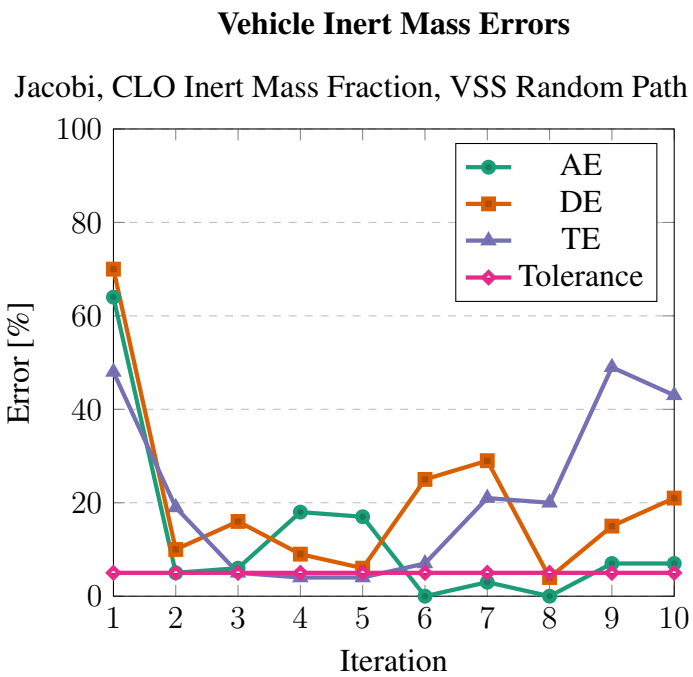

Figure 4.12: Errors for the vehicle inert masses per iteration for Experiment 1, with Jacobi iteration, CLO inert mass fraction guess and VSS Random Path Run 3 - TE Shared Descent.

Figure 4.13: Errors for the vehicle gross masses per iteration for Experiment 1, with Jacobi iteration, CLO inert mass fraction guess and VSS Random Path 3 - TE Shared Descent.

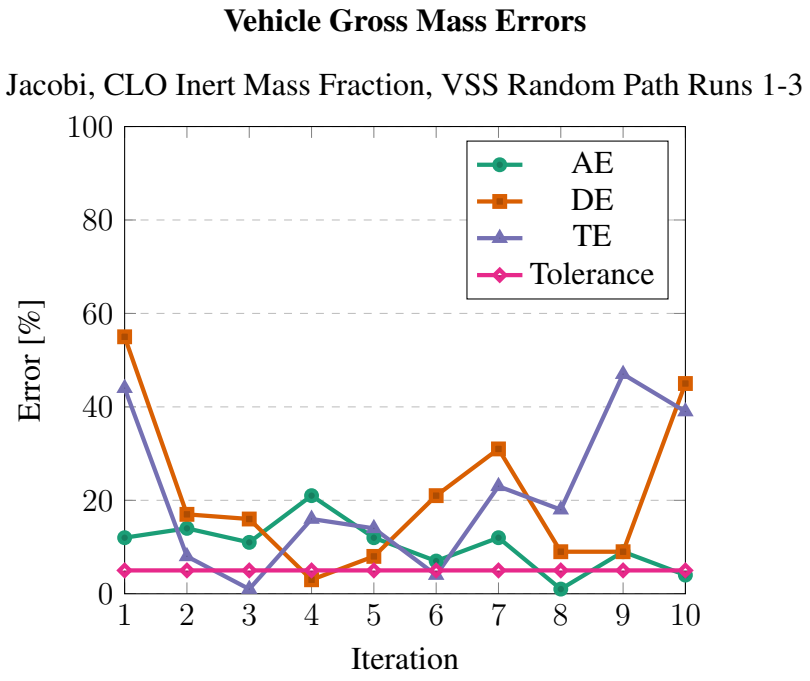

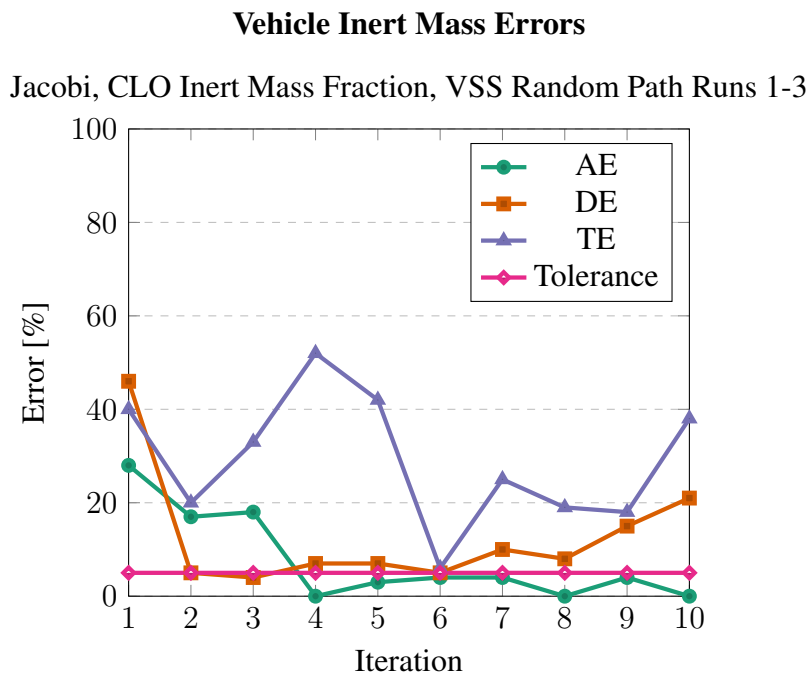

Figure 4.14: Errors for the vehicle inert masses per iteration for Experiment 1, with Jacobi iteration, CLO LV sized vehicles and VSS Random Path Runs 1-3 with Baseline initialization.

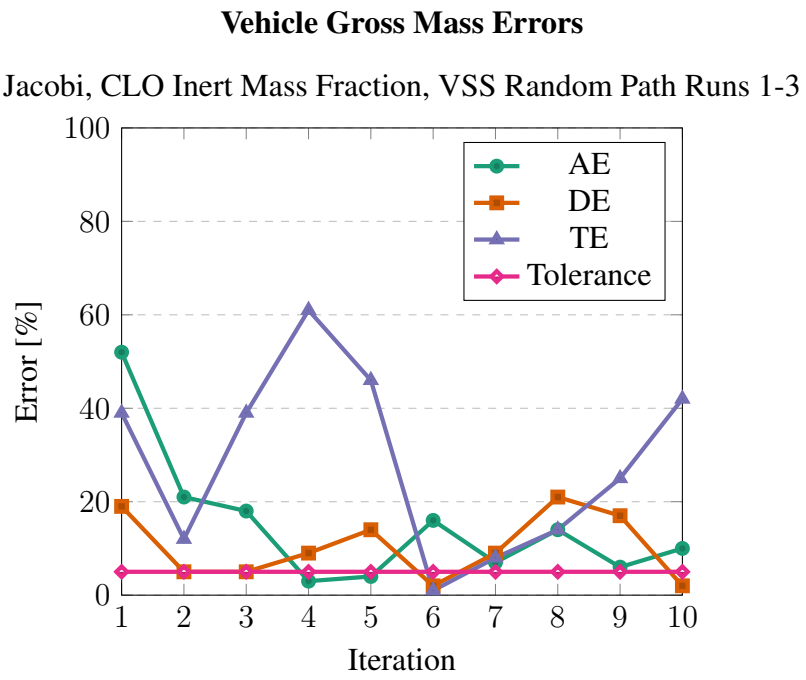

Figure 4.15: Errors for the vehicle gross masses per iteration for Experiment 1, with Jacobi iteration, CLO LV sized vehicles and VSS Random Path Runs 1-3 with Baseline initialization.

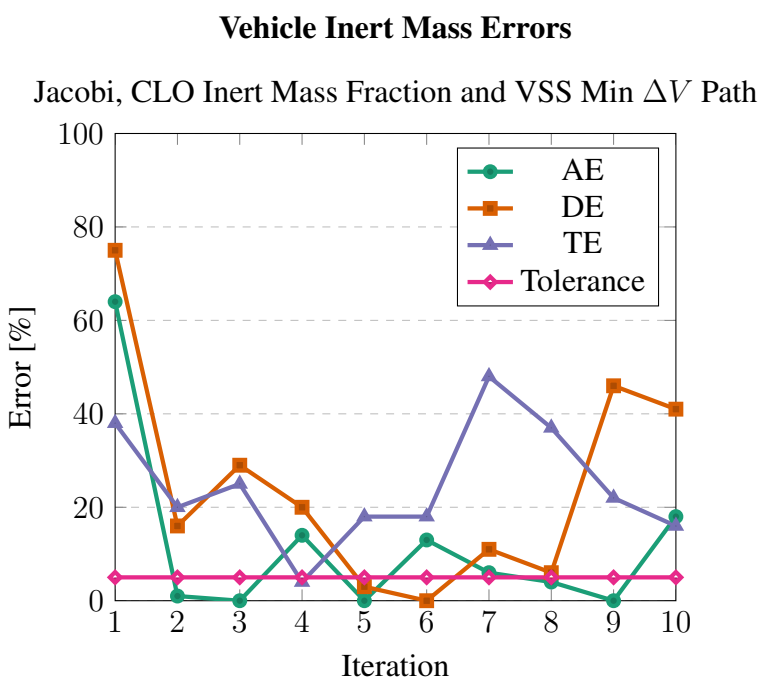

Figure 4.16: Errors for the vehicle inert masses per iteration for Experiment 1, with Jacobi iteration, CLO Inert Mass Fraction and VSS Min ΔV Path.

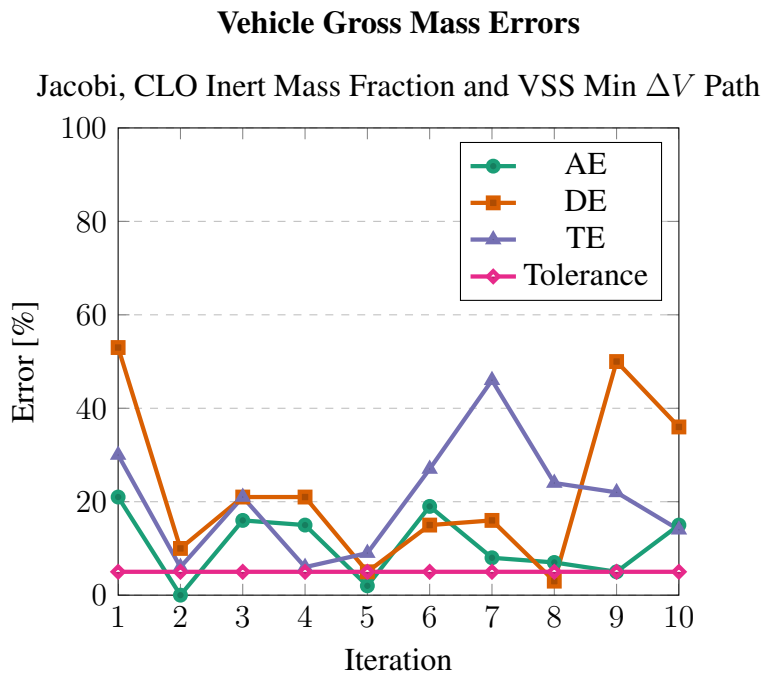

Figure 4.17: Errors for the vehicle gross masses per iteration for Experiment 1, with Jacobi iteration, CLO Inert Mass Fraction and VSS Min ΔV Path.

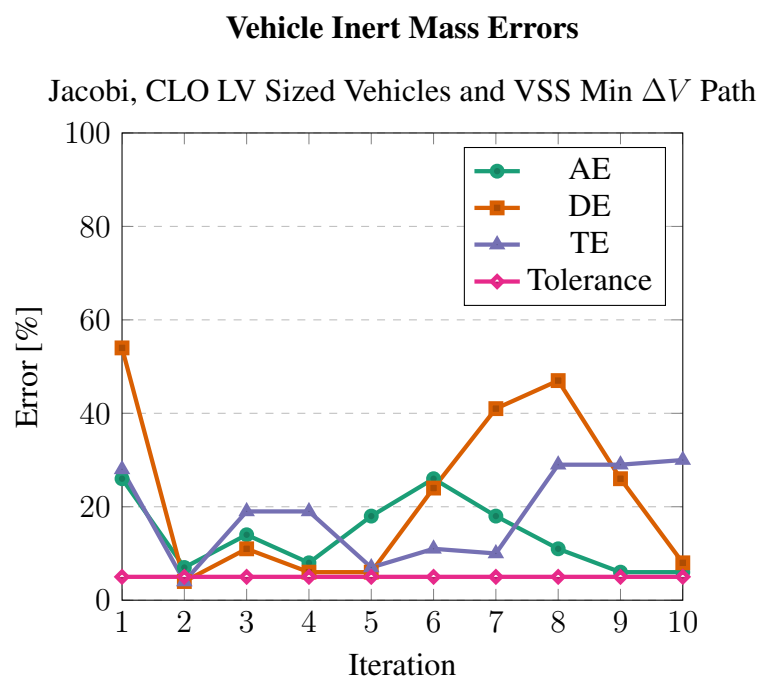

Figure 4.18: Errors for the vehicle inert masses per iteration for Experiment 1, with Jacobi iteration, CLO LV Sized Vehicles and VSS Min ΔV Path.

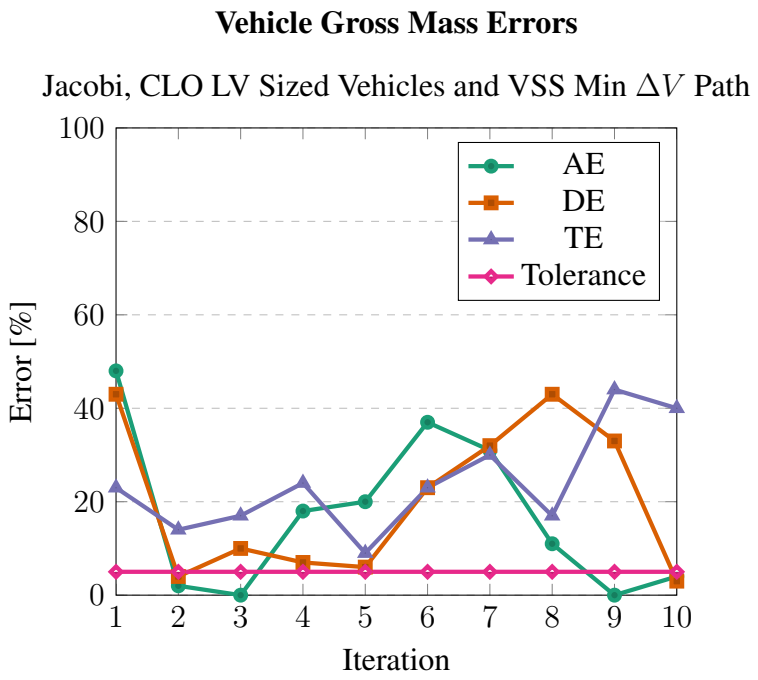

Figure 4.19: Errors for the vehicle gross masses per iteration for Experiment 1, with Jacobi iteration, CLO LV Sized Vehicles and VSS Min ΔV Path.

4.7.3 Experiment 3: Initialization

Experiment 3.1: CLO Initialization and Inert Mass Guess Type

Before addressing **Hypothesis 3**, **Hypothesis 3.1** and **Hypothesis 3.2** are assessed first through their respective experiments. Since Jacobi iteration has been removed from consideration, **Experiment 3.1** has only two set of results to investigate with the different inert mass guess types. Figure 4.20 - Figure 4.25 show the errors and mass convergence performance for the IMF guess case, while Figure 4.26 shows the inert mass errors for LV sized vehicles. The results of this experiment are relatively clear as the LV sized vehicles cause the process to diverge, specifically in that CLO could not find a feasible campaign with the inert masses given. This could be due to a number of different reasons, from propellant loads that are too much to launch, even with super heavy class vehicles, to infeasible cadence constraints. Specifically, with the inert masses being so high and the three elements operating as stack from NRHO, the propellant required on the TE would be relatively high.

If it did not exceed the mass limits for any LV it may have required multiple LVs that did not fit with its cadence; for example, three SLS launches in the first 100 days. In contrast, the IMF guess produces much lower inert masses for the initial CLO run with the AE, DE, and TE having inert masses of 1,984 kg, 1,587 kg, and 2,654 kg, respectively. These masses are much lower than those of the closed solution at iteration 10, which is acceptable as the less conservative estimate for inert mass likely allows this closure. Synthesizing all this data, the main findings show that the IMF guess for CLO initialization produces a converged solution and therefore, **Hypothesis 3.1 is accepted**.

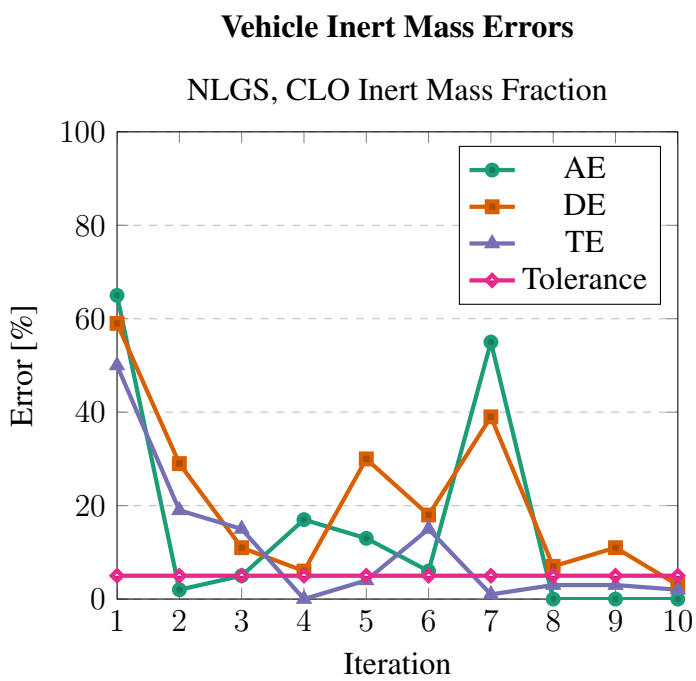

Figure 4.20: Errors for the vehicle inert masses per iteration for Experiment 3.1, with NLGS iteration, CLO First with Inert Mass Fraction Guess.

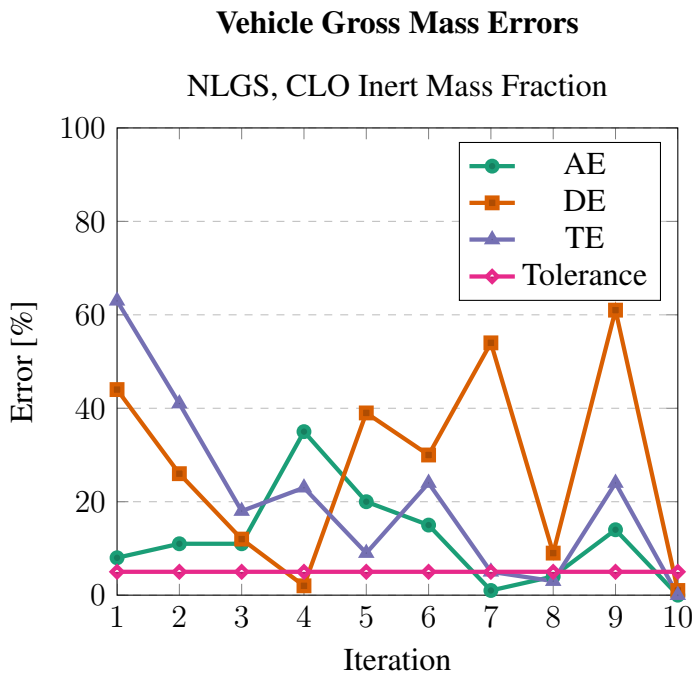

Figure 4.21: Errors for the vehicle gross masses per iteration for Experiment 3.1, with NLGS iteration, CLO First with Inert Mass Fraction Guess.

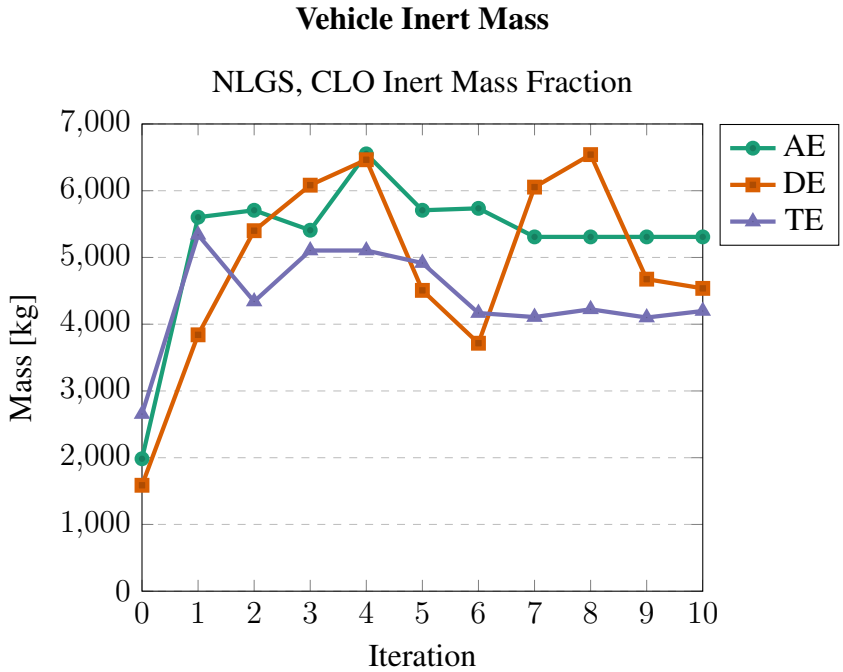

Figure 4.22: Vehicle inert masses per iteration for Experiment 3.1, with NLGS iteration, CLO First with Inert Mass Fraction Guess.

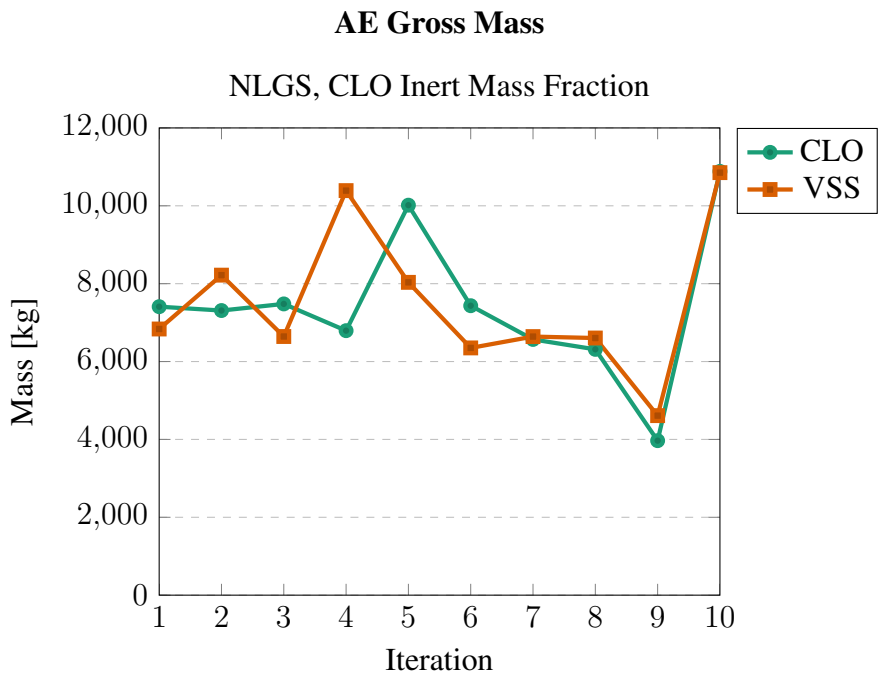

Figure 4.23: Ascent Element gross mass per iteration for Experiment 3.1, with NLGS iteration, CLO First with Inert Mass Fraction Guess.

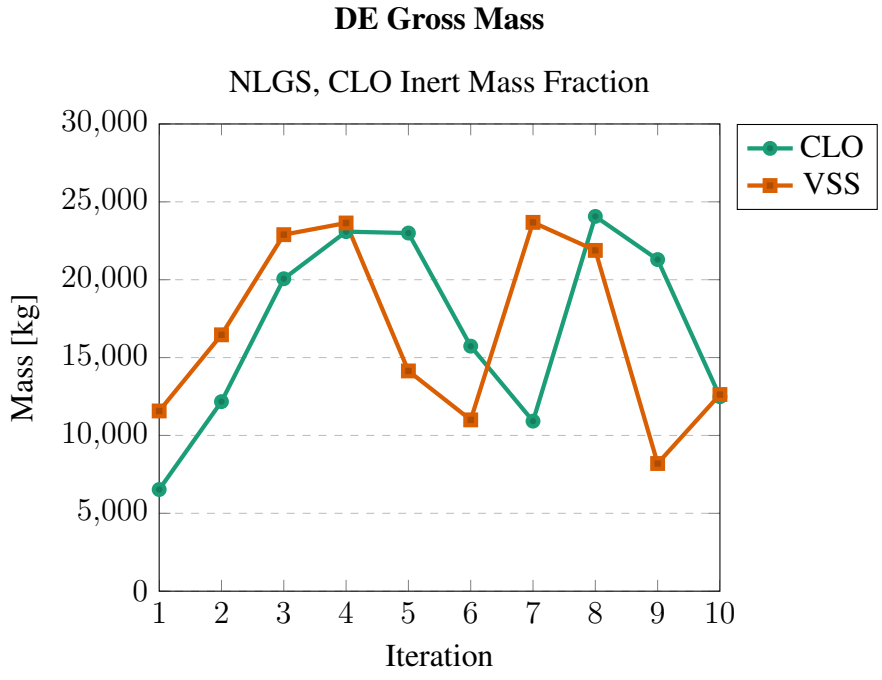

Figure 4.24: Descent Element gross mass per iteration for Experiment 3.1, with NLGS iteration, CLO First with Inert Mass Fraction Guess.

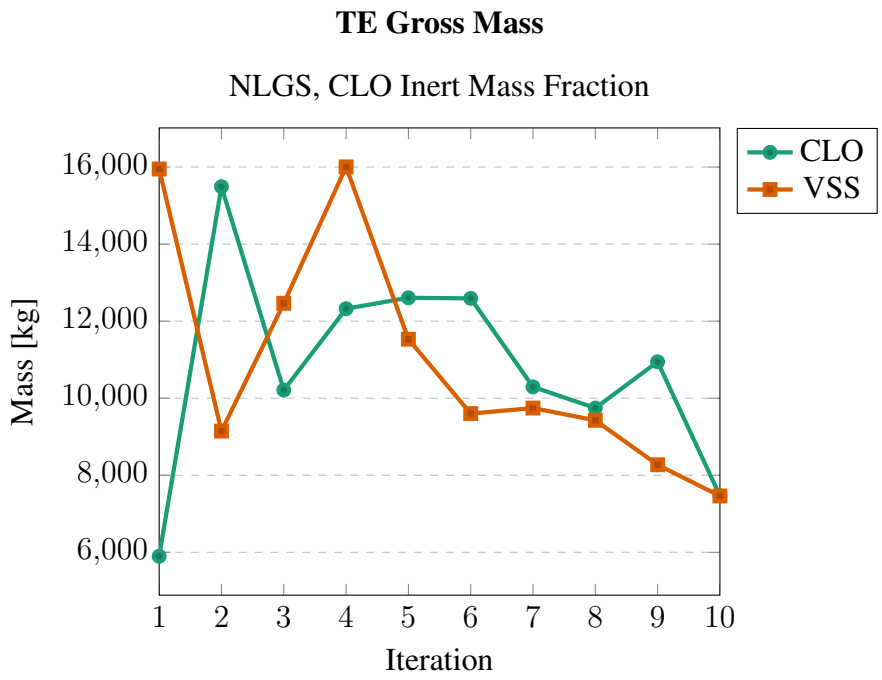

Figure 4.25: Transfer Element gross mass per iteration for Experiment 3.1, with NLGS iteration, CLO First with Inert Mass Fraction Guess.

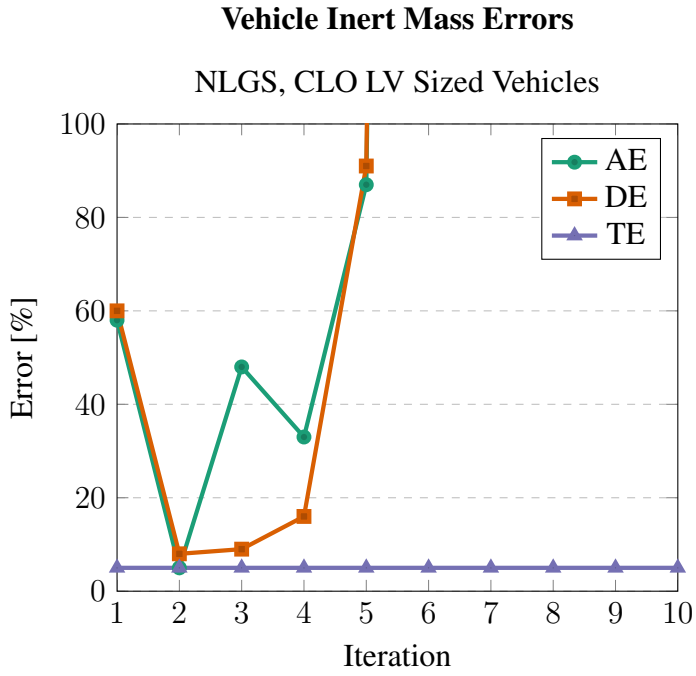

Figure 4.26: Errors for the vehicle inert masses per iteration for Experiment 3.1, with NLGS iteration, CLO First with LV Sized Vehicles.

Experiment 3.2: VSS Initialization and Mission Sequence Guess Type

Since test 2 for **Experiment 3.2** requires a random selection, it was run three times to ensure repeatability, giving a total of four sets of results to investigate for **Experiment 3.2**. Figure 4.27-Figure 4.32 show the convergence for VSS initialization with a minimum ΔV path, while Figure 4.33-Figure 4.38 show that of VSS initialization with random path choice. For the latter, runs 1 and 3 were both chosen as Baseline path initialization and performed exactly the same, while run 2 started with a HEO aggregation, which also performed exactly the same as the previous set of charts. From the set of all paths, the minimum ΔV path is the HEO aggregation one, with a total of 4,690 m/s. Although it may be intuitive to think that the higher aggregation orbits mean lower overall ΔVs, it also means each vehicle must burn individually to that aggregation location, if they are dropped off by the launch vehicle at a lower location. With the three random tests, the baseline NRHO aggregation path was chosen twice and the HEO aggregation path once. Both sets of results are exactly the same, meaning that this process structure is repeatable. Cases with the HEO aggregation initial guess close in 6 iterations and an overall runtime of just over 24 hours, while cases with the baseline NRHO aggregation close in 1 more iterations and 4 more hours.

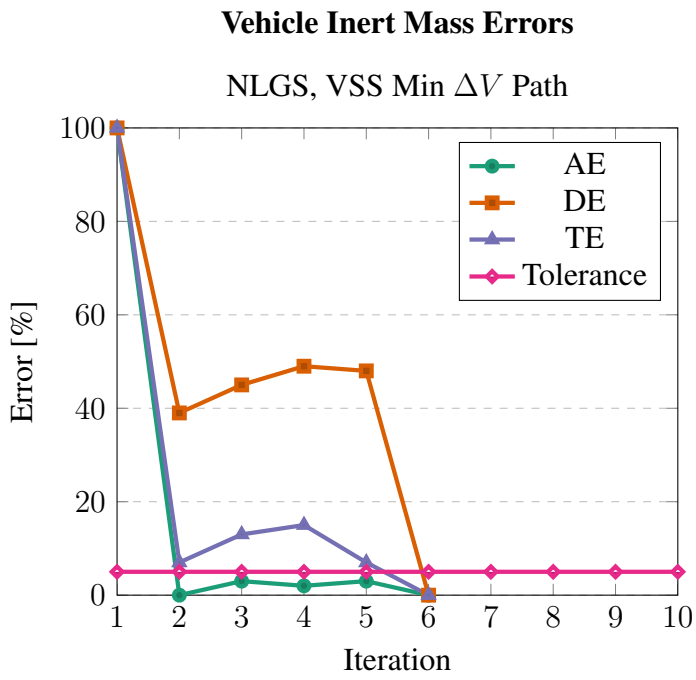

Figure 4.27: Errors for the vehicle inert masses per iteration for Experiment 3.2, with NLGS iteration, VSS First with Min ΔV Path.

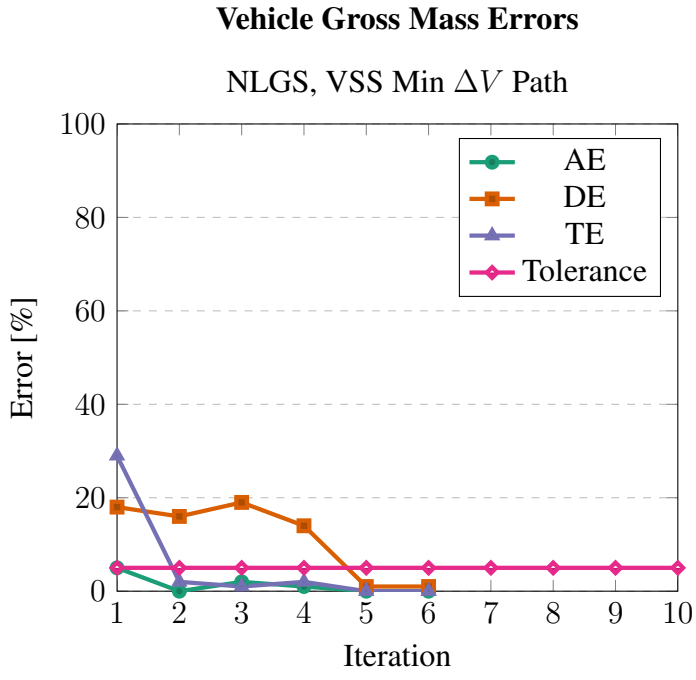

Figure 4.28: Errors for the vehicle gross masses per iteration for Experiment 3.2, with NLGS iteration, VSS First with Min ΔV Path.

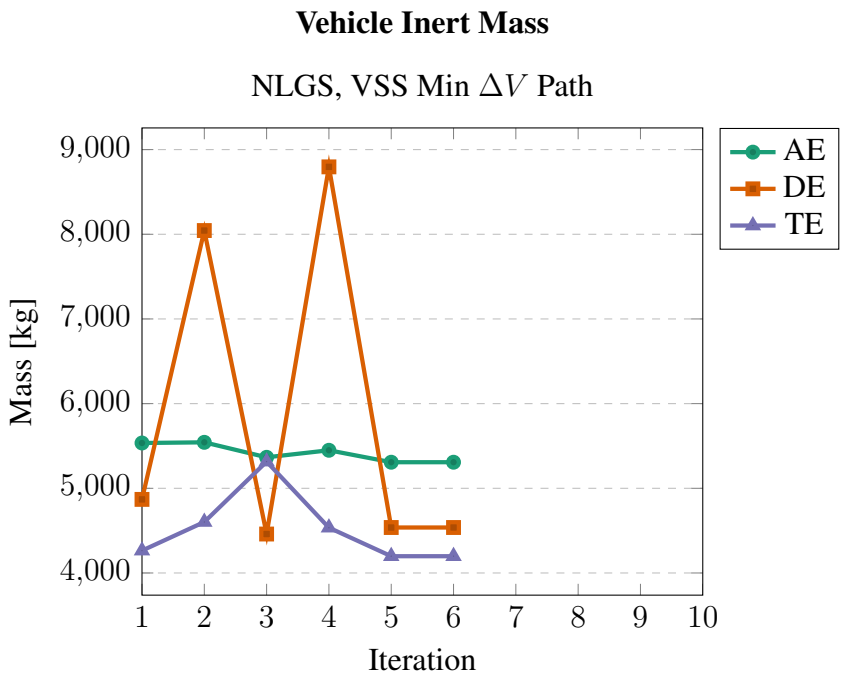

Figure 4.29: Vehicle inert masses per iteration for Experiment 3.2, with NLGS iteration, VSS First with Min ΔV Path.

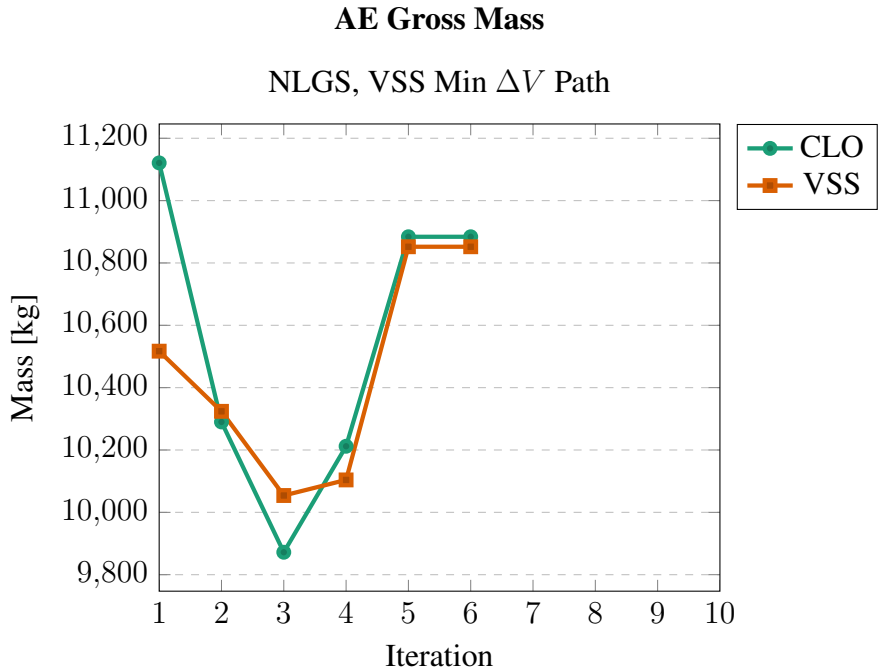

Figure 4.30: Ascent Element gross mass per iteration for Experiment 3.2, with NLGS iteration, VSS First with Min ΔV Path.

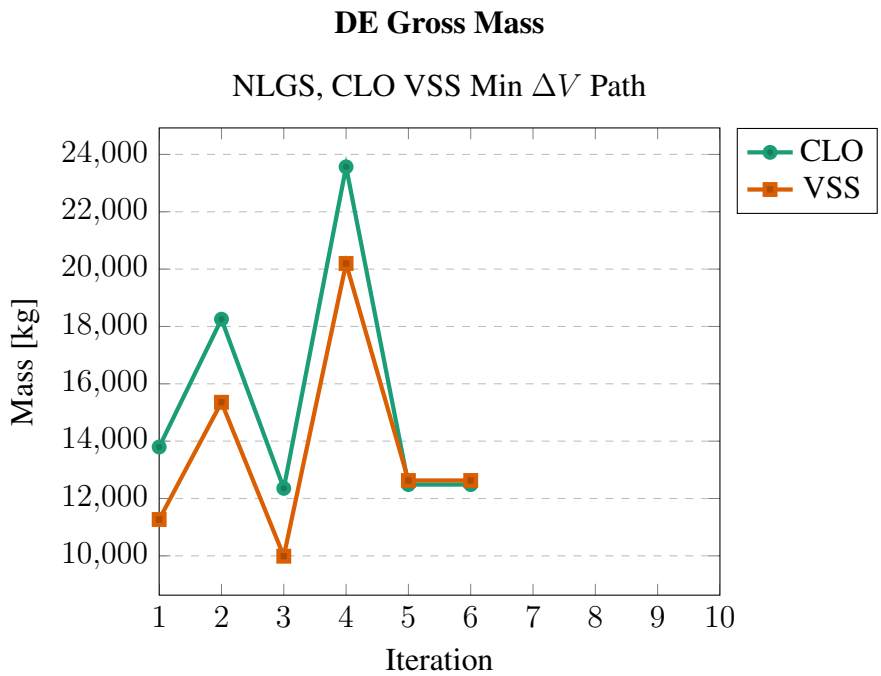

Figure 4.31: Descent Element gross mass per iteration for Experiment 3.2, with NLGS iteration, VSS First with Min ΔV Path.

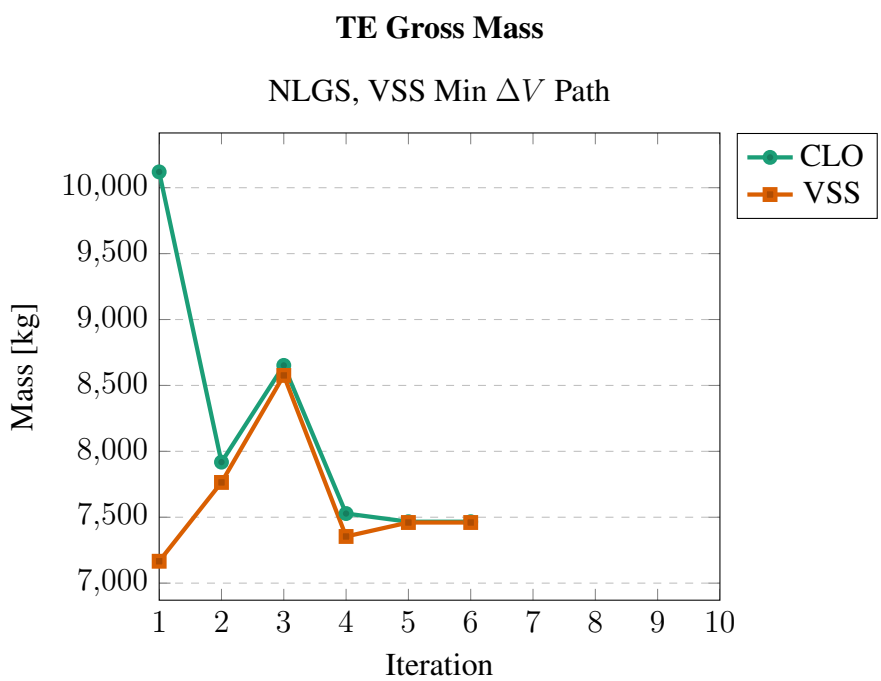

Figure 4.32: Transfer Element gross mass per iteration for Experiment 3.1, with NLGS iteration, VSS First with Min ΔV Path.

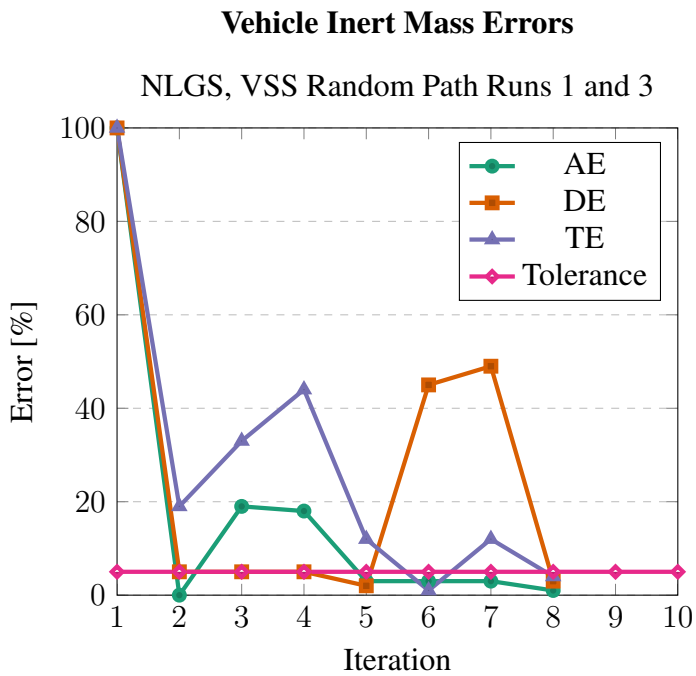

Figure 4.33: Errors for the vehicle inert masses per iteration for Experiment 3.2, with NLGS iteration, VSS First with Random Path Runs 1 and 3.

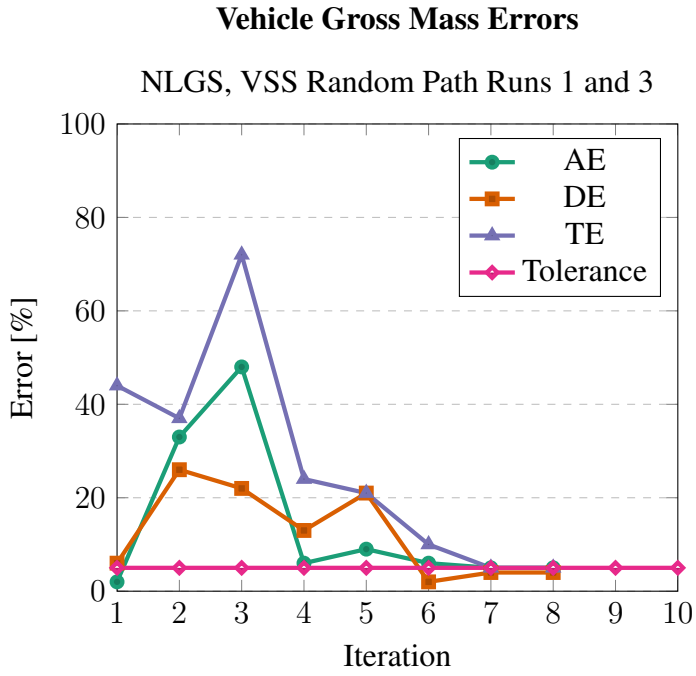

Figure 4.34: Errors for the vehicle gross masses per iteration for Experiment 3.2, with NLGS iteration, VSS First with Random Path Runs 1 and 3.

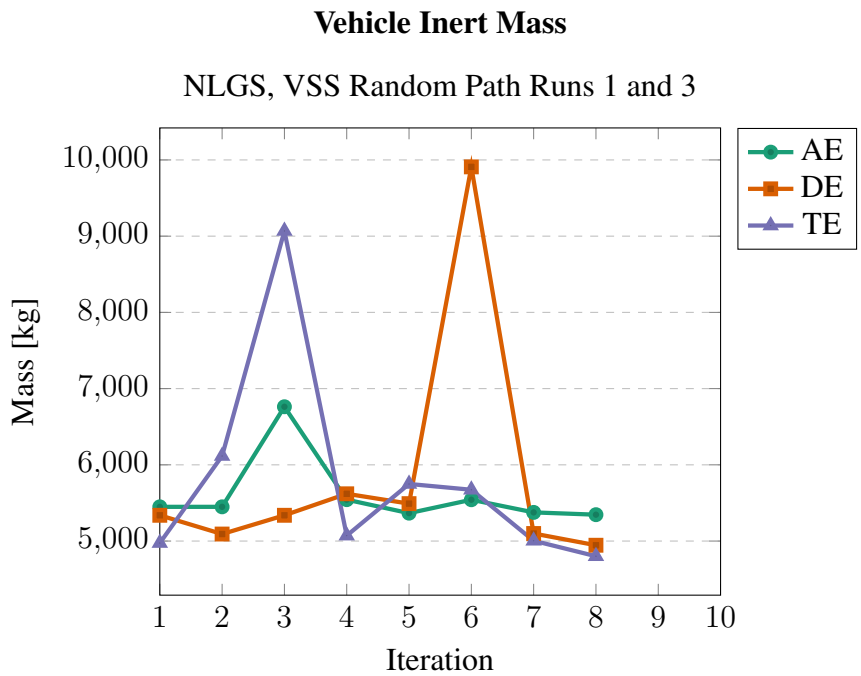

Figure 4.35: Vehicle inert masses per iteration for Experiment 3.2, with NLGS iteration, VSS First with Random Path Runs 1 and 3.

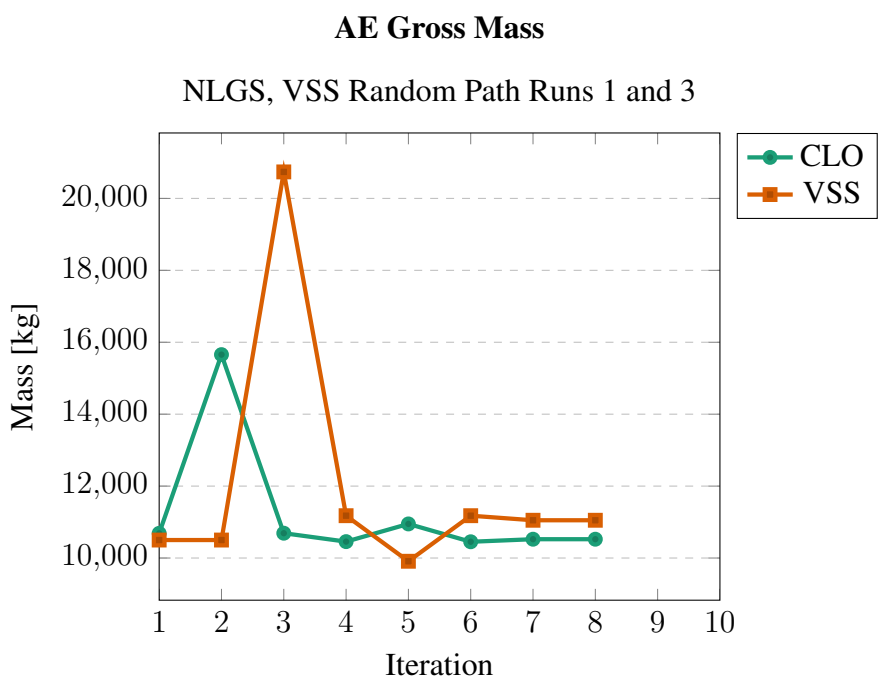

Figure 4.36: Ascent Element gross mass per iteration for Experiment 3.2, with NLGS iteration, VSS First with Random Path Runs 1 and 3.

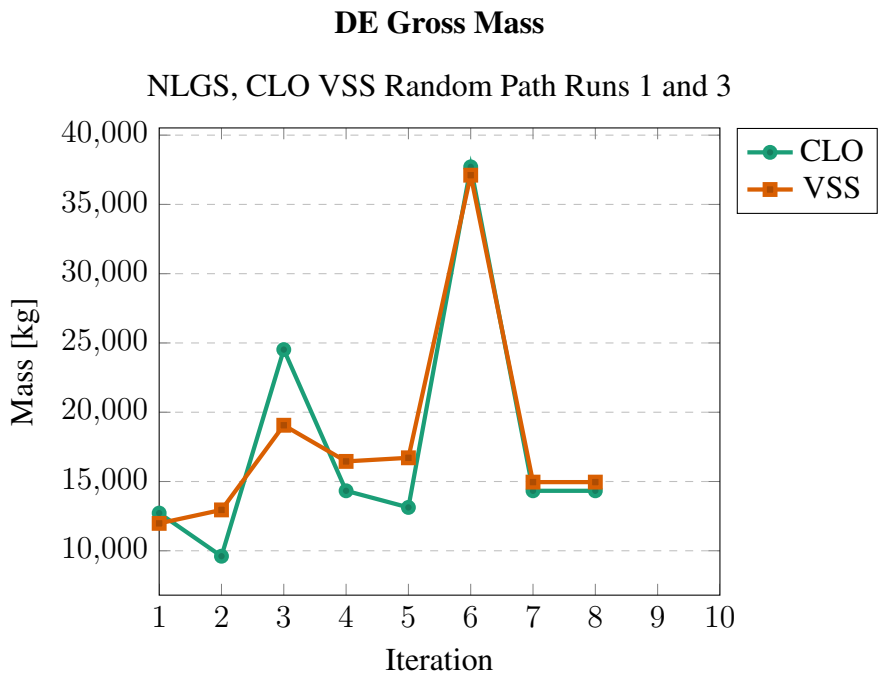

Figure 4.37: Descent Element gross mass per iteration for Experiment 3.2, with NLGS iteration, VSS First with Random Path Runs 1 and 3.

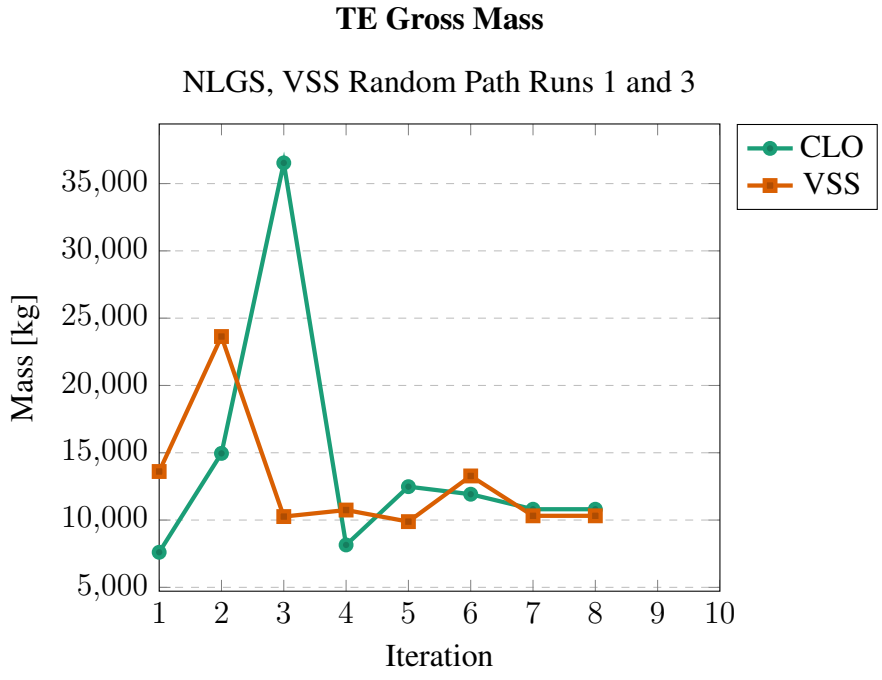

Figure 4.38: Transfer Element gross mass per iteration for Experiment 3.2, with NLGS iteration, VSS Random Path Runs 1 and 3.

The two different initial guesses converge to two different final solutions. The minimum ΔV path guess produces a solution with an objective value of 0.724 and the other with an objective value of 0.752. Examining the vehicle paths for both campaigns, which are shown in Figure 4.39 and Figure 4.40, respectively, show the main difference between the two is the TE taking a slow transfer to the aggregation location after being dropped off in HEO. Both campaigns converge to the baseline NRHO aggregation location option, but Table 4.14, shows that the TE shared descent option was chosen for a few iterations, implying the optimizer is not only considering the ConOps trades, but actively changing the optimal one based on updates from VSS. Since the TE is taking the slow transfer to NRHO and it does not have any active Cryogenic Fluid Management (CFM) systems to mitigate boiloff, the amount of propellant it loses during the slow transfer is greater than if it just burned through a faster transfer. These findings show that a random path guess does not always converge to the minimum solution, and therefore, **Hypothesis 3.2 is accepted**.

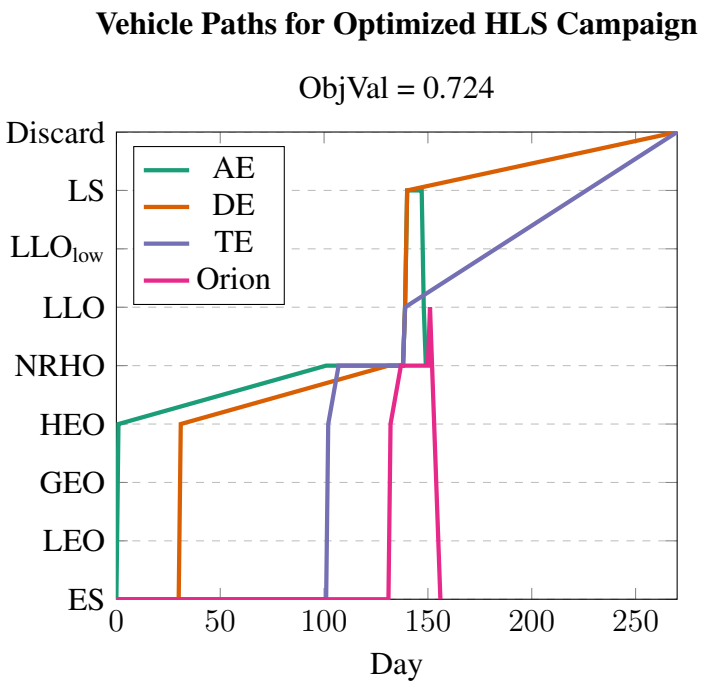

Figure 4.39: Vehicle paths for the HLS campaign solution with objective value of 0.724.

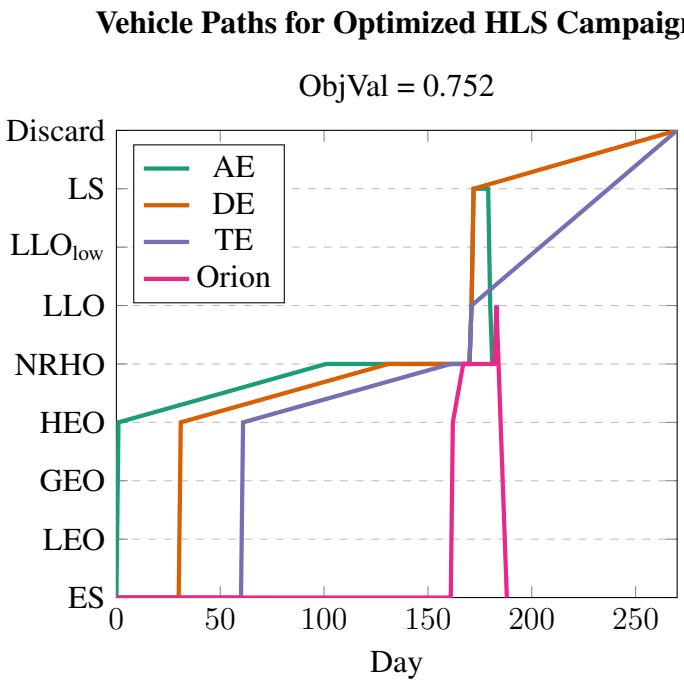

Figure 4.40: Vehicle paths for the HLS campaign solution with objective value of 0.752.

Iteration	Path Chosen by CLO
1	TE Shared Descent
2	Baseline
3	Baseline
4	TE Shared Descent
5	Baseline
6	Baseline

Table 4.14: Table showing the chosen path by CLO for each iteration for the final solution with an objective value of 0.724.

With the findings from **Experiment 3.1** and **Experiment 3.2**, the higher level **Experiment 3** can be addressed. Filtering out combinations of tests that have been ruled out, there remains only two: CLO initialization with an IMF guess and VSS with the minimum ΔV path. The results of this experiments have already been shown in Figure 4.20 - Figure 4.25 and Figure 4.27-Figure 4.32. The difference in performance, and therefore findings for this experiment, in these two process structures is relatively clear. Both final solutions are exactly the same optimal campaign, with an objective value of 0.724. However, running VSS

first requires four fewer iterations, and thereby 16 hours less runtime. As a result, **Hypothesis 3 is rejected**, and a process structure with VSS initialization would be preferred.

4.7.4 Summary of Results and Final Methodology

Figure 4.41 shows the experiment structure for this research and the accompanying results presented in the previous sections. Synthesizing all of the results, the final structure of the concurrent trade space exploration methodology is shown in Figure 4.42

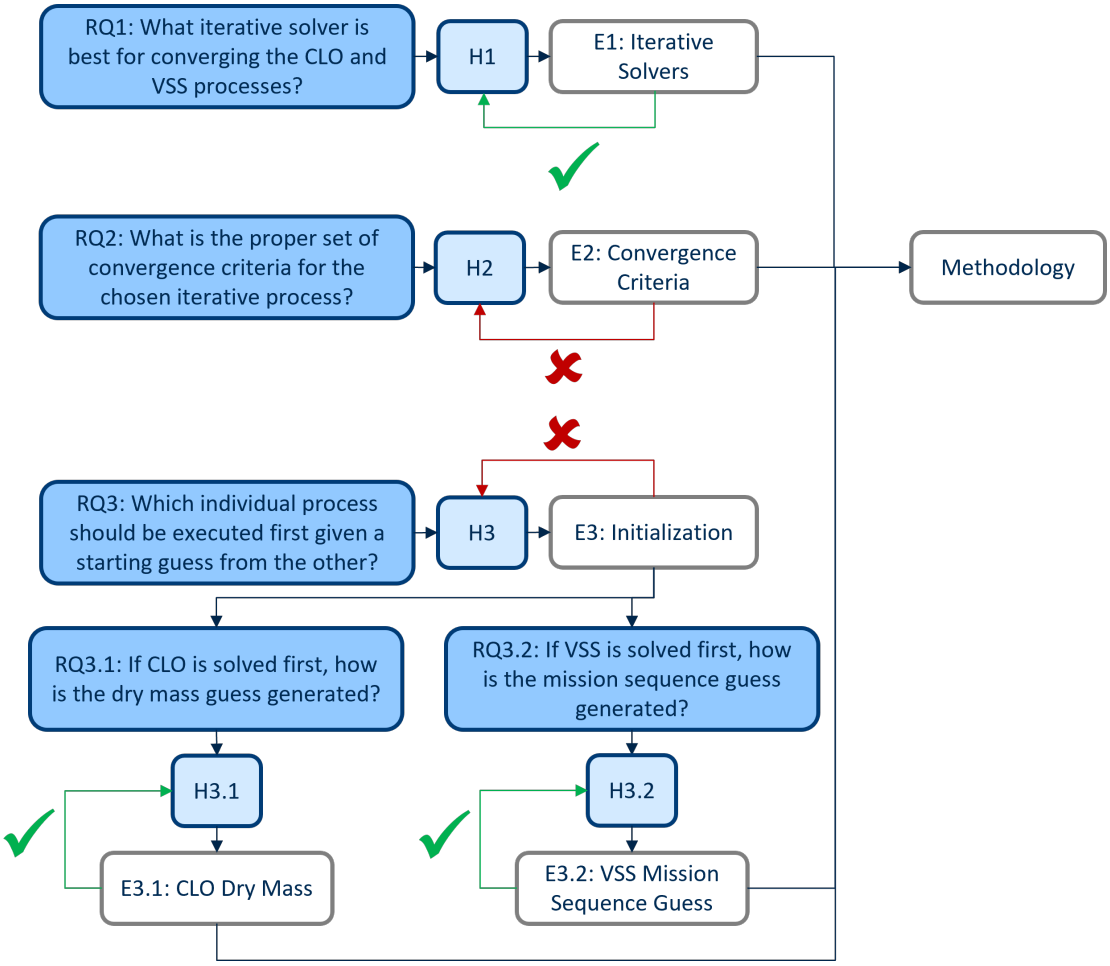

Figure 4.41: Summary of the experimentation structure for this thesis with the results of the experiments.

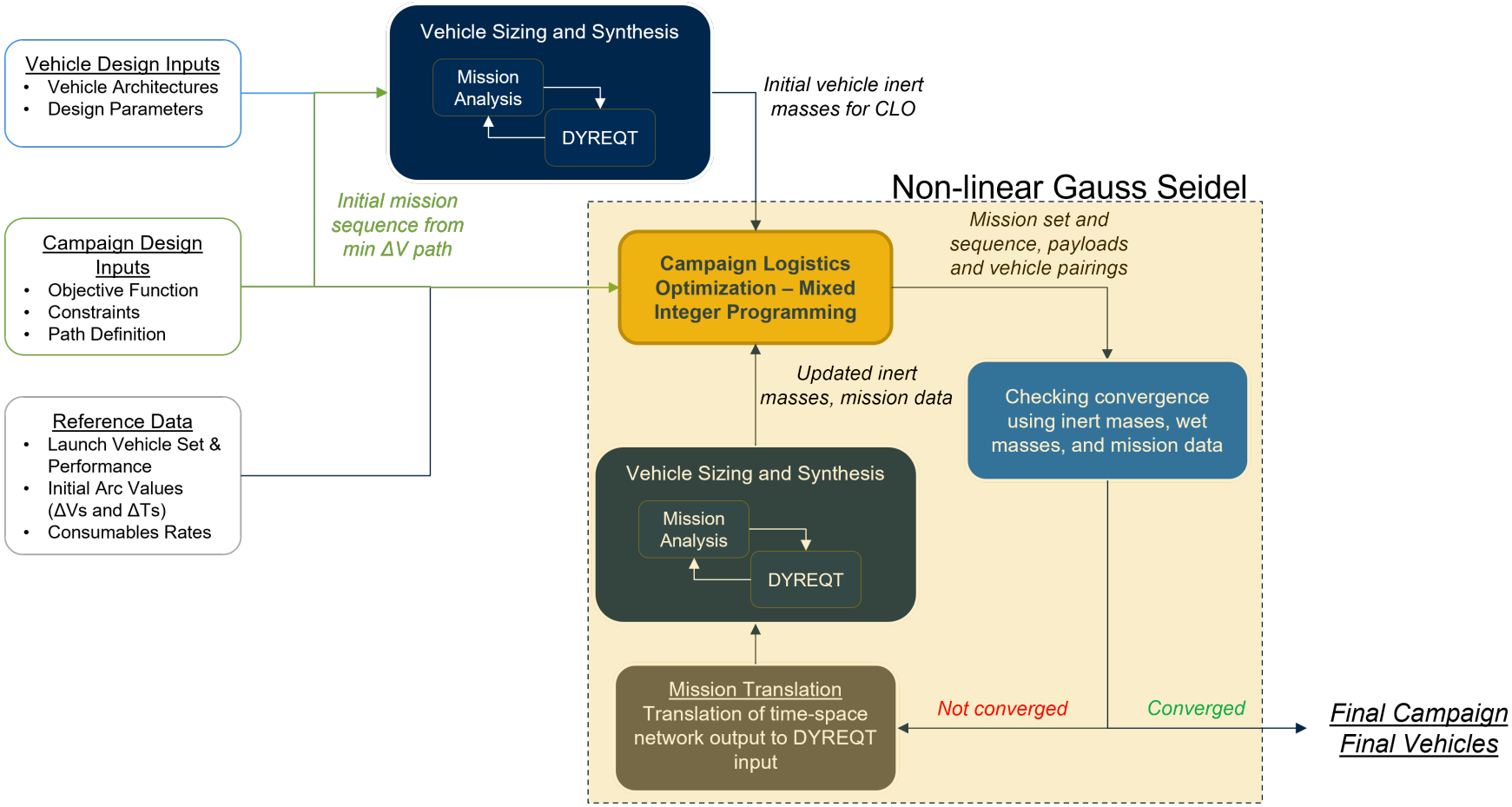

Figure 4.42: The process diagram of the final methodology, construct using results from experimentation.

Using reference data, the vehicle architecture definition, and the minimum ΔV path, the method is initialized using VSS, which provides an initial set of inert masses for the subsequent CLO run. If Equation 4.51 is below the tolerance, the solution has converged, and if not, the optimized mission set produced by CLO is given to VSS after some translation, and the process is run using NLGS iteration. A converged solution will produce a fully optimized campaign in the form of vehicle paths, payload paths, chosen launch vehicles as well as their launch dates, and vehicle mass histories of propellant, payloads, and consumables. Each vehicle will also have a subsystem mass breakdown due to the inclusion of the VSS process. The final HLS campaign solution found using this methodology and experimentation is presented in Appendix B while the following chapter will detail a larger-scale demonstration, while the validation of this method is presented in Appendix C.

5
MARS CAMPAIGN DESIGN AND TRADE STUDY

5.1 Overarching Experiment

The overarching hypothesis for this is restated below:

Overarching Hypothesis: If the CLO and VSS processes are integrated, the impacts of the vehicle and campaign trades on each other can be directly quantified.

With final methodology identified and assembled, the **Overarching Experiment** should test this hypothesis by applying the methodology at scale. Specifically, the experiment should show that integration of the two individual process allow for these trades to be conducted in a relatively short amount of time. Trade studies can be conducted at the campaign and vehicle levels to show the impacts of their design sensitivities on each other. In this vain, with the lunar focus of experimentation, the overarching experiment can be executed using a crewed Mars exploration campaign, which is larger scale with longer timescales and higher number of overall elements.

5.2 Canonical Large-scale Campaign: DRA 5 NTP Crewed Mission

As the government reference HLS 2024 mission was used for the experimental apparatus, a larger, more complex campaign can be used to formally demonstrate the methodology. Though with mostly similar requirements as the smaller one, the key difference with this campaign is the addition of Mars within the network. Requirements of a relevant, crewed, large-scale Mars campaign with ample documentation for reference leads to NASA's long standing DRA 5, specifically Addendum 2, introduced in Chapter 1 [8]. Shown in Figure 5.1, this Mars campaign is a 900-day total duration, with 180-day transits and a 500-day

surface stay with 6 crew. For the purposes of an initial demonstration, only the first surface mission is considered.

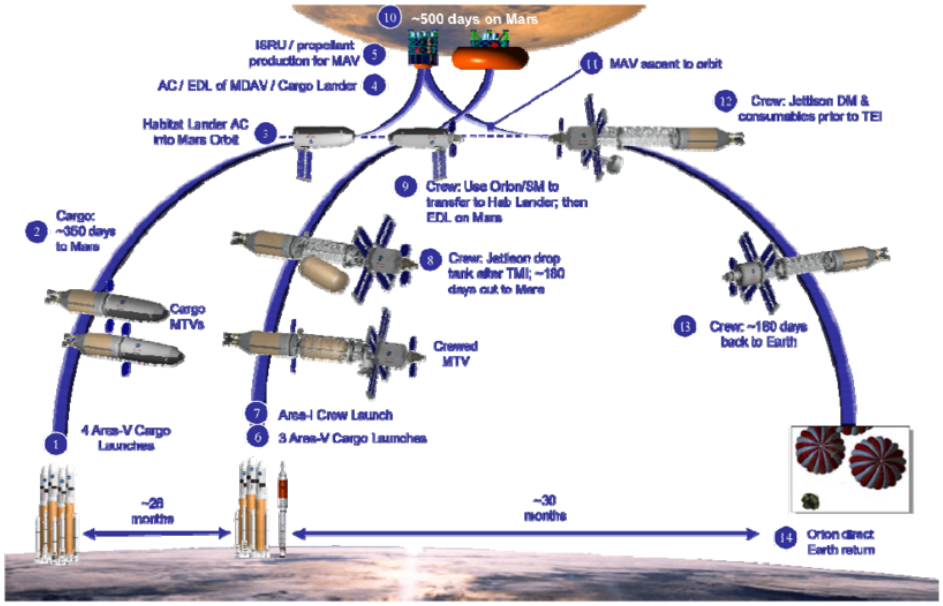

Figure 5.1: Mars DRA 5 ConOps for a nuclear thermal transportation system[8]

The significant increase in timescales and distance to destination is accompanied by an increase in number of launches and rendezvous operations. Prior to the first crew mission, two cargo missions are executed to deploy systems necessary for surface operations and the launch, aggregation and transit timelines are overlapping, depicted by the schedule in the top half of Figure 5.2.

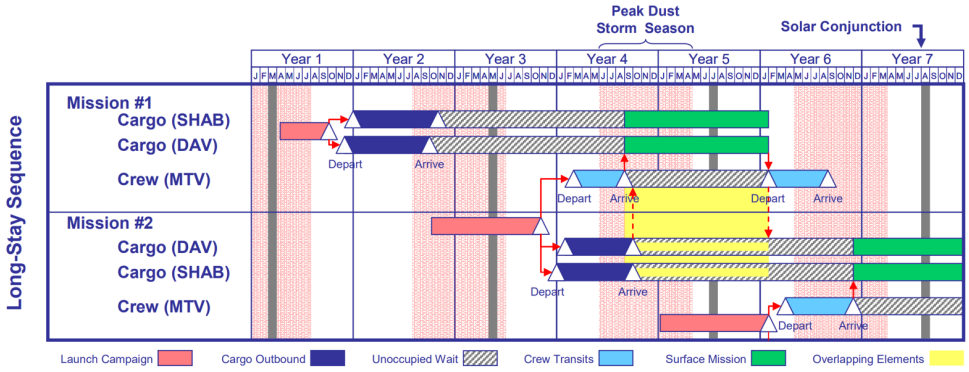

Figure 5.2: Mars DRA 5 timelines for the two crewed surface missions and four pre-deploy cargo missions [8].

The execution of the first two cargo payloads occur almost simultaneously, while the launch campaign for the following crew mission does not start until they arrive at Mars. Surface nuclear power, ISRU, and Mars Ascent Vehicle (MAV) land on Mars first, the former produces the propellant for the latter. The crew arrives and rendezvous in the Mars 1-sol parking with the surface habitat before landing on the surface themselves. For both crew and cargo, DRA 5 traded two propulsion architectures: all chemical and NTP, and this demonstration will only be considering the latter, with Liquid Hydrogen (LH_2) propellant. However, each individual cargo and crew missions require their own specific NTP vehicle, though the two cargo versions will be the same, shown in Figure 5.3.

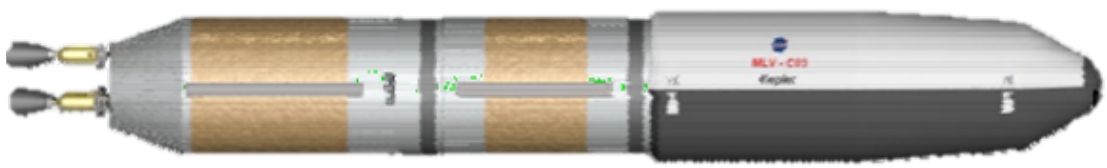

Figure 5.3: Fully assembled vehicle configuration of the DRA 5 NTP cargo vehicle [8].

Each one is made up of three individual elements: a core stage that houses some propellant and two Nuclear Thermal Rocket (NTR) engines, an inline LH_2 tank that houses more propellant, and the payload which includes the landing systems. The crewed vehicle is similar, but houses a much larger inline tank and a truss structure that is designed to house a drop tank and dock with the transit habitat and Orion. The fully aggregated crew transport vehicle configuration is shown in Figure 5.4, and is also referred to as the Mars Transit Vehicle (MTV).

Orion is used to transport the crew both to the vehicle in the LEO aggregation orbit and safely land them back on Earth after the Mars mission. A total of five SLS Block 2

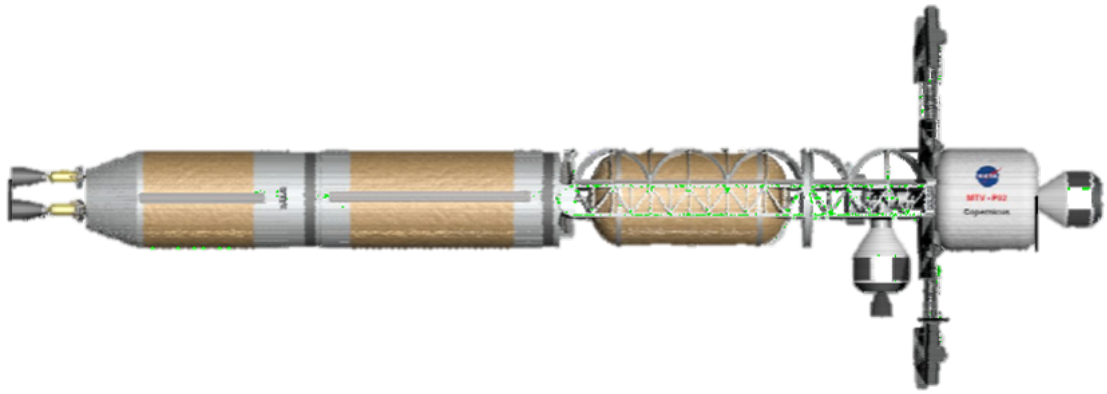

Figure 5.4: Fully assembled vehicle configuration of the DRA 5 NTP crew vehicle [8].

launches are required to assemble the two cargo vehicles, while only 4 are needed for the crewed version, with a separate Block 1 launch for the crew. The vehicle assembly and aggregation strategy for all vehicles is summarized in Figure 5.5.

5.3 Integrated Trade Study Definition

Now that the methodology has been constructed, it can be used to perform design a much larger, campaign and perform a integrated trade study. Given the Mars campaign from DRA 5, described in Section 5.2, the trade study can be split into two smaller ones to explicitly represent campaign and vehicle level trade variables in each one. This process can demonstrate how the sensitivities of changes in these variables affect the design of each other to test the overarching hypothesis of this research.

5.3.1 Vehicle-level Trade Study

Changes in vehicle design parameters can potentially have a significant impact on the design and execution of the campaign, especially for crewed Mars exploration. Notably, the propulsion system architecture and accompanying propellant are significant parameters in the design of vehicles or Mars transportation systems. DRA 5 down-selected to NTP with LH_2 propellant after building a campaign around it and an all-chemical transportation alternative. Hydrogen is typically the go-to propellant for NTP systems for its high I_{sp}s of about

Vehicle Assembly Timelines & ETO Delivery Manifest

	Launch Number	Launch Time Before TMI (days)	Launch Manifest	Shroud Length (m)	Launch Mass (t)
Cargo Mission (Two Vehicles)	Ares V Launches				
	1	-180	NTR TMI Core Stage 1	30.0	96.6
	2	-150	NTR TMI Core Stage 2	30.0	96.6
	3	-120	Twin In-Line LH2 Tank	30.0	93.2
	4	-90	Payload 1 (Cargo Land	30.0	103.0
	5	-60	Payload 2 (Hab Lander	30.0	103.0
		-60	TMI Window Allowance		
Total MTV Mass Delivered to Orbit					492.3
Crewed Mission	1	-150	NTR Core Stage	30.00	106.2
	2	-120	In-Line LH2 Tank	30.00	91.4
	3	-90	Truss & Drop Tank	30.00	96.0
	4	-60	Crew Payload Element	30.00	62.2
		-60	TMI Window Allowance		
	Ares I Launch (delivers astronauts to orbiting crew MTV)				
	1	-5	6 Mars Crew	n/a	0.6
Total MTV Mass Delivered to Orbit					356.4

Ares V launches:	9	Total IMLEO (t):	848.7

Figure 5.5: Vehicle assembly and aggregation strategies for the crew and cargo NTP vehicles in DRA 5 [8].

900s, at the cost of integrated CFM systems to keep the temperature low and minimize boiloff. Even then, the density of LH_2 is relatively low, at 70.85 kg/m^3, requiring many large tanks to store all of the propellant needed for a Mars mission. Since all space vehicles are constrained by the mass, and more often the volume, of LV fairings, there are potentially better options for NTP propellants that can reduce launch rates and leverage ISRU systems to refuel [139]. Irvine *et al.* specially shows the benefit of ammonia as propellant, with a much smaller vehicle stage [140]. NTP systems can theoretically use any propellant, as they operate by using the heat generated by the nuclear reactor to expand it out a nozzle to generate thrust. However, with ISRU systems being key to long-term space exploration, it is beneficial to explore propellant options that can be generated using them. Figure 5.6 shows the densities of different in-situ propellant at different temperatures.

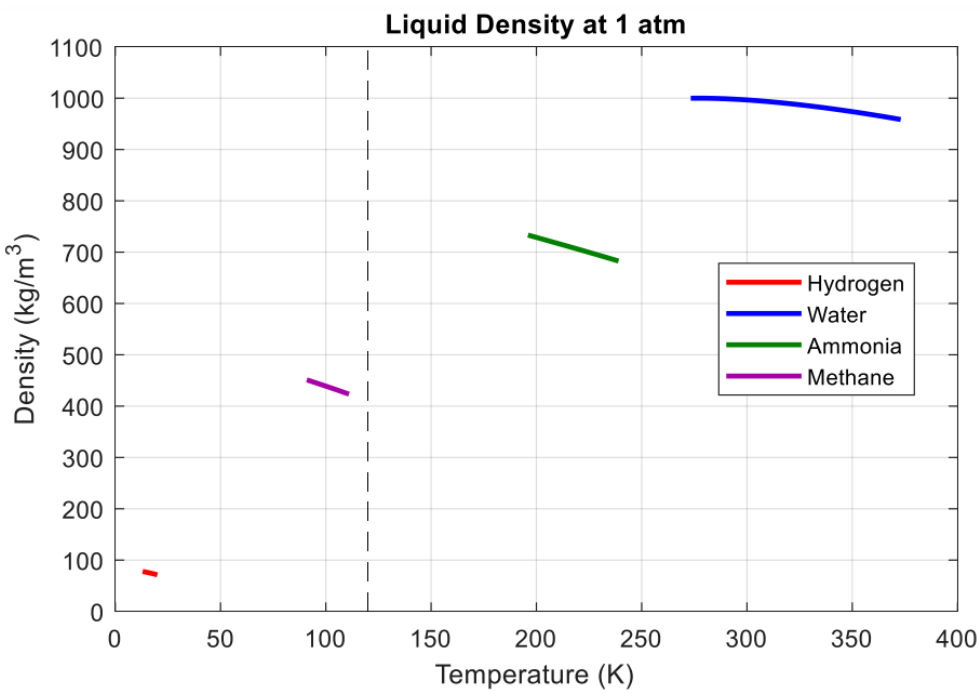

Figure 5.6: Densities of different in-situ, liquid propellant densities [139].

These other propellants not only are more dense, but have wider ranges of liquid temperature ranges, easing requirements on thermal control systems. Thus, the vehicle-level trade for the large-scale campaign application will trade these four propellant species for the two NTP vehicle designs in NASA's DRA 5.

5.3.2 Campaign-level Trade Study

Chapter 1 introduced the behavior of vehicle design choices being highly dependent on campaign goals, through Observation 2. A major campaign goal for Mars that has been discussed when developing mission strategies is the total duration and more importantly the surface stay duration. Although longer stays on Mars enable more science and exploration, they come with higher risk profiles and exposure to the deep space radiation environment. DRA 5 itself explored many different durations for both the transit and surface portions, ultimately selecting the long-stay mission of 540 days on Mars with a conjunction class trajectory. The amount of time spent on the surface of Mars drives the design of many

other elements of the campaign, from the trajectory design within and out of the Mars sphere, vehicle architecture selections, habitat design, and more [141]. Given the design of a vehicle is driven by its mission, surface stay duration can have a significant impact the vehicle mass and even vehicle configuration. This further drives the overall ConOps of the campaign, specifically the strategies for launch and aggregation of all of the vehicles prior to Earth departure. To directly assess these impacts, the campaign-level trade variable for the Mars campaign is the total stay duration on the surface of Mars.

5.4 DRA 5 Campaign Problem Definition

5.4.1 Campaign Logistics Optimization

Nodes and Arcs

To perform the two trade studies, the campaign description in Section 5.2 is decomposed to define the overall campaign problem and accompanying inputs. There are two cargo pre-deploy mission prior to the crew mission, occurring over the course of two opportunities. The main network information required to model DRA 5 are the interplanetary arc costs of ΔV and ΔT. Subsubsection 2.6.2 defined the use of porkchop plots for interplanetary mission design problems. For these trade studies, porkchop data is generated across the three Earth-Mars opportunities, separated into outbound and inbound. There are two outbound opportunities, 2033 and 2035, where the former is reserved for the two cargo missions while the latter for the crew. Although only the crew is returning from Mars, two inbound opportunities must be explored: one for the short stay alternative and another for long stay. For the short stay option, crew is allowed to return in the same opportunity they depart Earth from, in 2035, whereas they must wait until 2037 to return after a long stay. As the porkchop data depends on the specific dates of departure and arrival of a spacecraft, the campaign time domain is anchored at a date; that is, time $t = 0$ is set equal to a real date. Using porkchop data from DRA 5's documentation and accounting for similar launch

and aggregation campaigns, the anchor date for these campaigns is set as 7/4/2032. The campaign is capped on the other end based on 2037 inbound porkchop data, allowing time for the crew to return to Earth, if the optimizer chooses to take the last possible arc back.

Given the multi-year campaign, using single day timesteps would significantly increase the computational complexity of the CLO problem and the its runtime. Seven day timesteps are used for this trade study to allow the optimizer good enough play over when each missions are executed while also balancing that computational complexity. This comes with the caveat that smaller operations such as payload transfers and staging are modeled as occurring over the course of a week, which in reality may not be the case.

Using the previous time domain definition, data was generated using an open source, python framework, Poliastro, which solves the Lambert's targeting problem between two bodies [142]. For each opportunity, the solver is given a wide range of departure and arrival dates to create the largest allowable dataset that could then be constrained based on a maximum ΔV. Table 5.1 summarizes the inputs given to the Lambert's solver for each opportunity, where 39 7-day periods were given for each departure date and 96 for arrival date. Figure 5.7-Figure 5.10 are the resulting plots that show the C3 required for each opportunity, depicted by a 2-D contour plot where the red dashed lines indicate transfer time.

Table 5.1: Ranges of dates and opportunities used to generate porkchop data.

		2033	**2035**	**2037**
Outbound	Departure Date	10/31/2033	1/28/2035	-
	Arrival Date	2/13/2033	5/13/2035	-
Inbound	Departure Date	-	1/28/2035	4/12/2037
	Arrival Date	-	5/13/2035	7/26/2037

CLO is further given two additional ConOps level degrees of freedom in the Earth aggregation and Mars parking orbits. NASA's campaign aggregated all three vehicles in LEO and used a 1-sol Mars parking orbit. This trade study will add a HEO aggregation option as well as cover parking orbits from 1-sol to 7-sol and adding LMO. The HEO

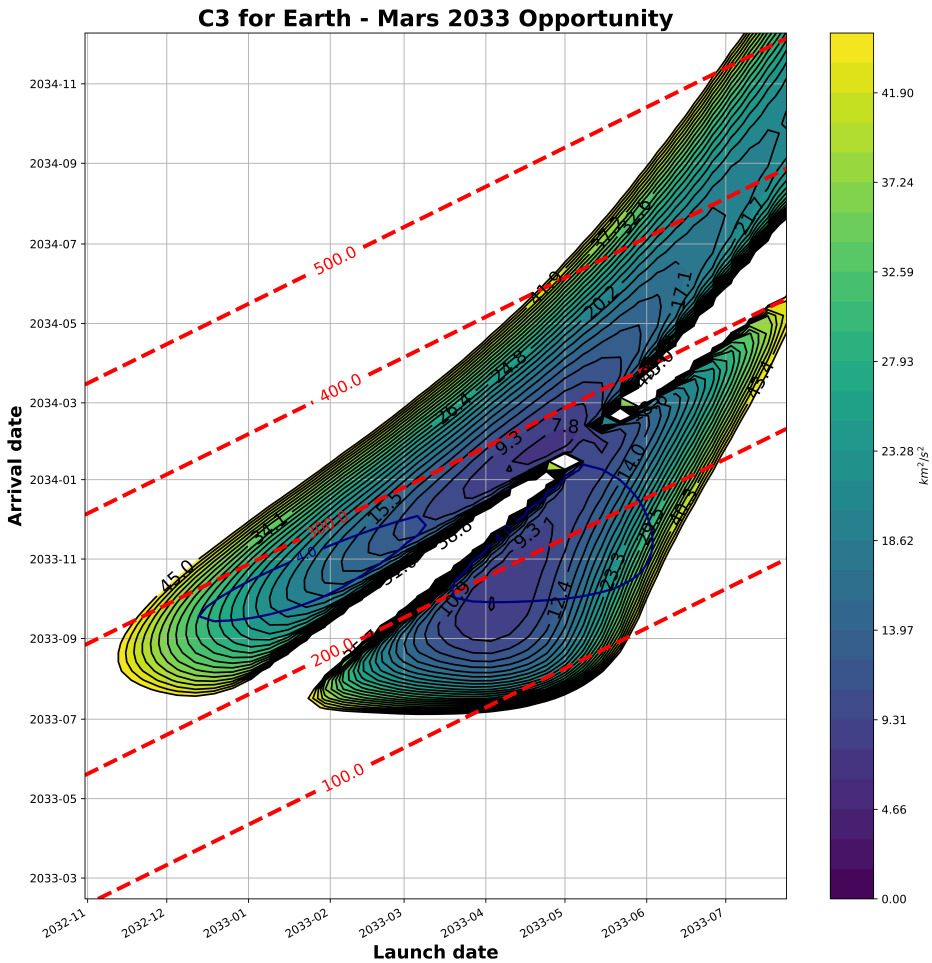

Figure 5.7: Porkchop plot for the outbound 2033 Earth-Mars opportunity.

aggregation option allows the optimizer to asses if more of a load can be put on the launch vehicles rather than the in-space transportation systems. With the node parameterization, the CLO process will consider the parking orbits as individual, n-sol and LMO nodes, with each representing a range of orbits, defined in Subsection 2.6.1. This gives a total 4 combinations of aggregation and parking orbits for each vehicle. However, the porkchop data now needs to be augmented as it assumes a direct transfer from Earth's sphere of influence to that of Mars. Depending on the departure and arrival orbits at either body, the spacecraft must perform an escape or capture burn in addition to the interplanetary transfer ΔV. With the porkchop data providing the departure and arrival hyperbolic excess

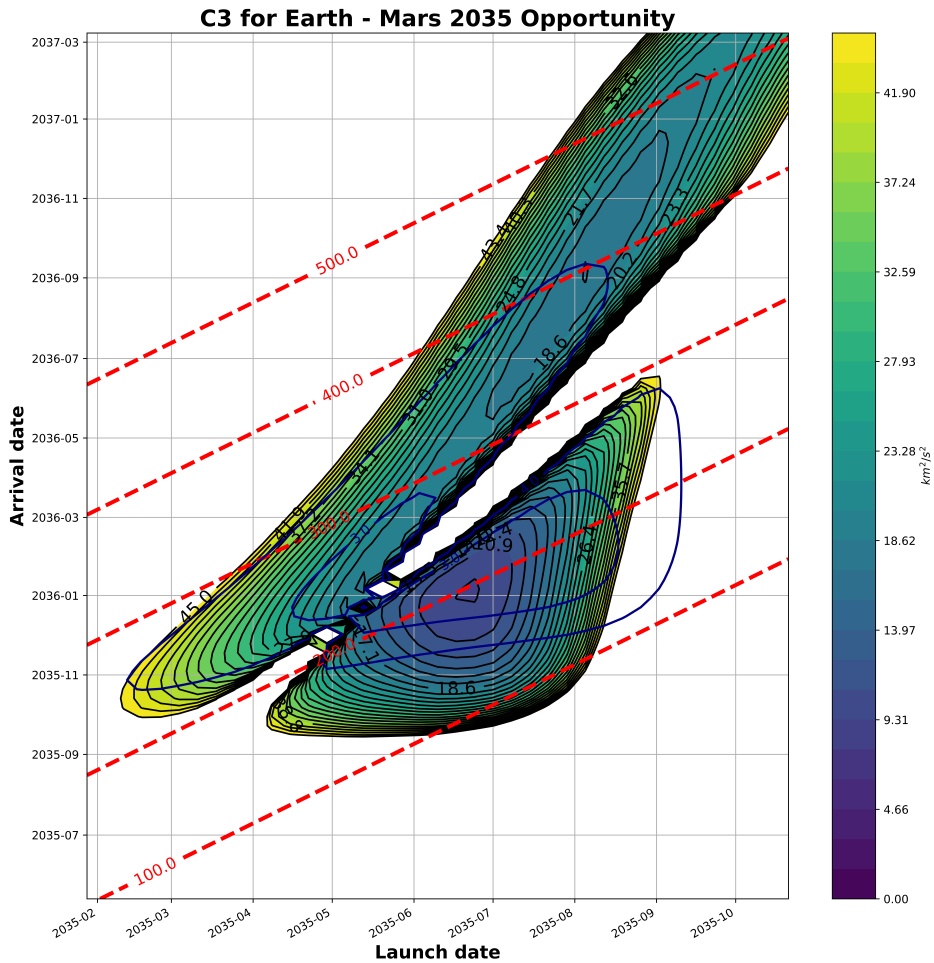

Figure 5.8: Porkchop plot for the outbound 2035 Earth-Mars opportunity.

velocities, $V_{\infty,dep}, V_{\infty,arr}$, the total ΔV from an orbit can be calculated using Equation 5.1 [88].

$$\begin{aligned}\Delta V_{total} = &\mid \sqrt{(V_{escape,body,dep})^2 + (V_{\infty,dep})^2} - V_{periapsis,orbit,dep} \mid + \\ &\mid \sqrt{(V_{escape,body,arr})^2 + (V_{\infty,arr})^2} - V_{periapsis,orbit,arr} \mid\end{aligned} \tag{5.1}$$

Cargo elements arriving at Mars use aerocapture to capture into Mars orbits, so the additional capture ΔV is assumed to be zero for those cases. The same is true for the MTV arriving at Earth, as capture is done via a Lunar Gravity Assist (LGA).

The number of interplanetary arcs are further reduced by filtering out ones that have extremely high ΔVs. Table 5.2 defines the limits assumed for the interplanetary ΔV's

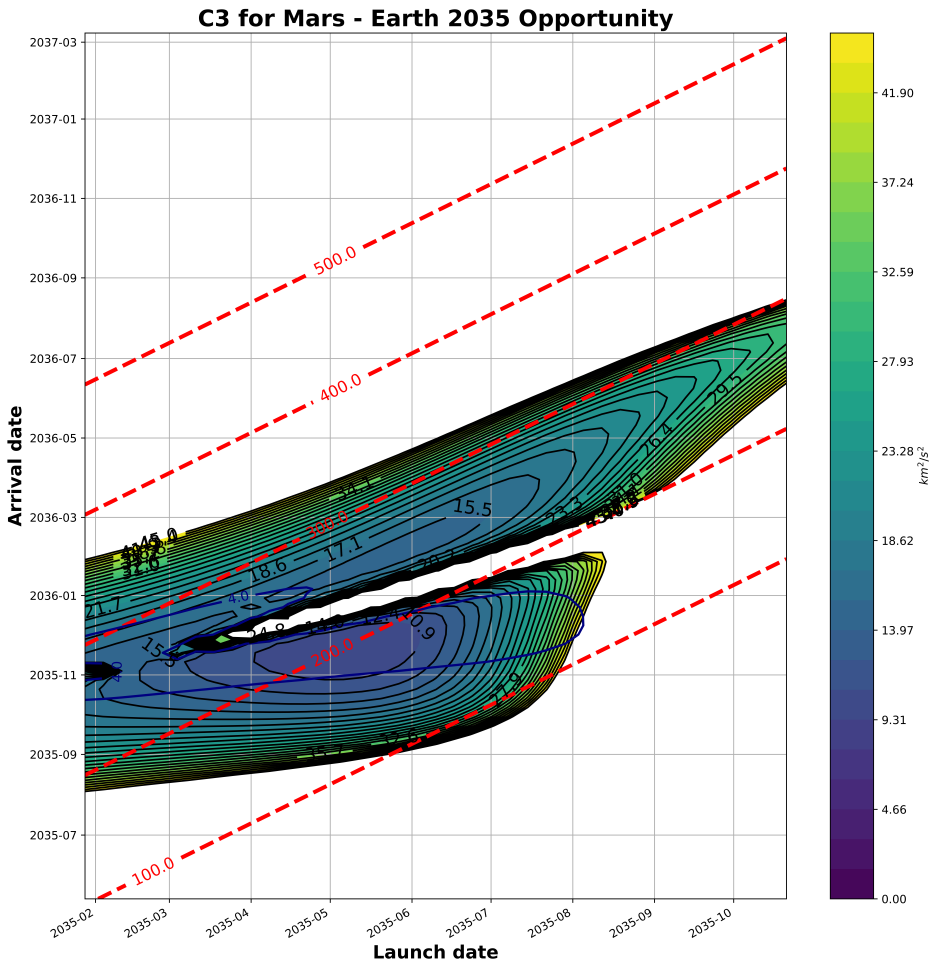

Figure 5.9: Porkchop plot for the inbound 2035 Mars-Earth opportunity.

for each opportunity and transfer direction, where values were chosen based on mission data from DRA 5. Launch arcs in the campaign are restricted based on the interplanetary departure dates from Earth to reduce computational complexity. A similar process is used for arcs towards Earth for Crew return. Figure 5.11 shows the full network of arcs and nodes used for the Mars campaign trade study, which serves as the basis for the path definition, detailed in the following section.

Table 5.2: Limits of interplanetary ΔV on arc generation depending on the opportunity and transfer direction.

	2033 [m/s]	**2035 [m/s]**	**2037 [m/s]**
Outbound	3,500	6,000	-
Inbound	-	6,000	3,500

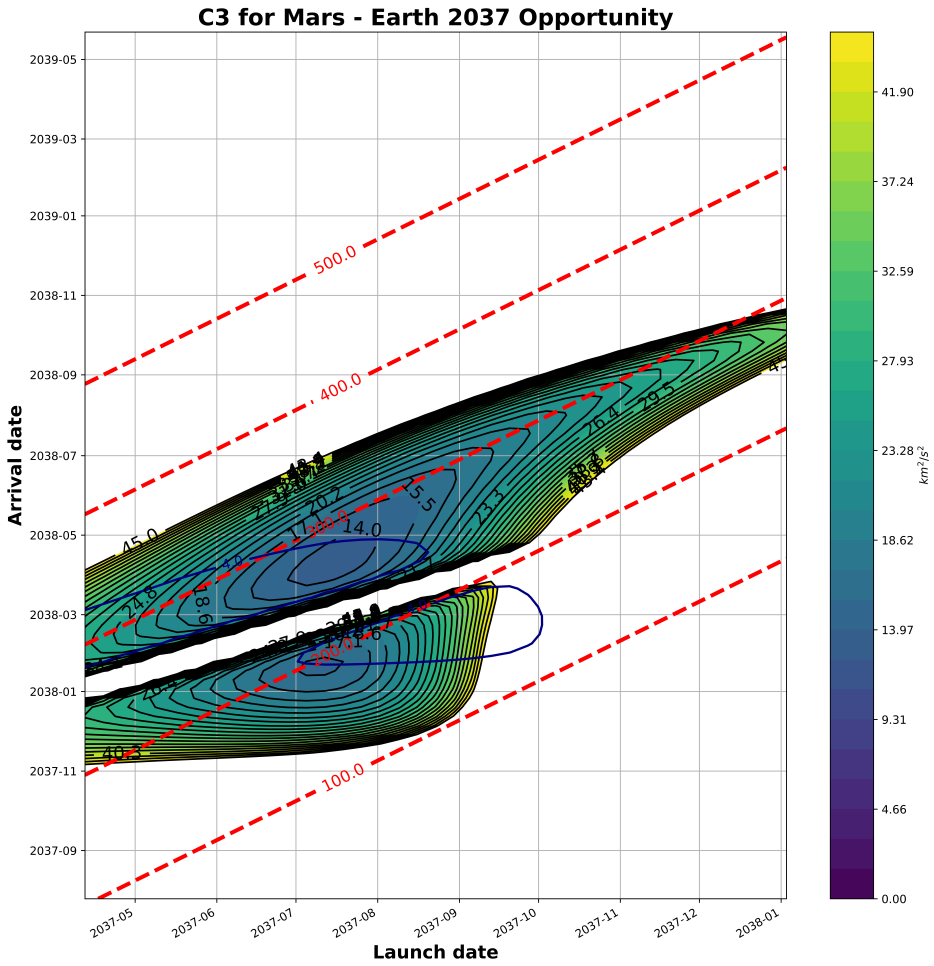

Figure 5.10: Porkchop plot for the inbound 2037 Mars-Earth opportunity.

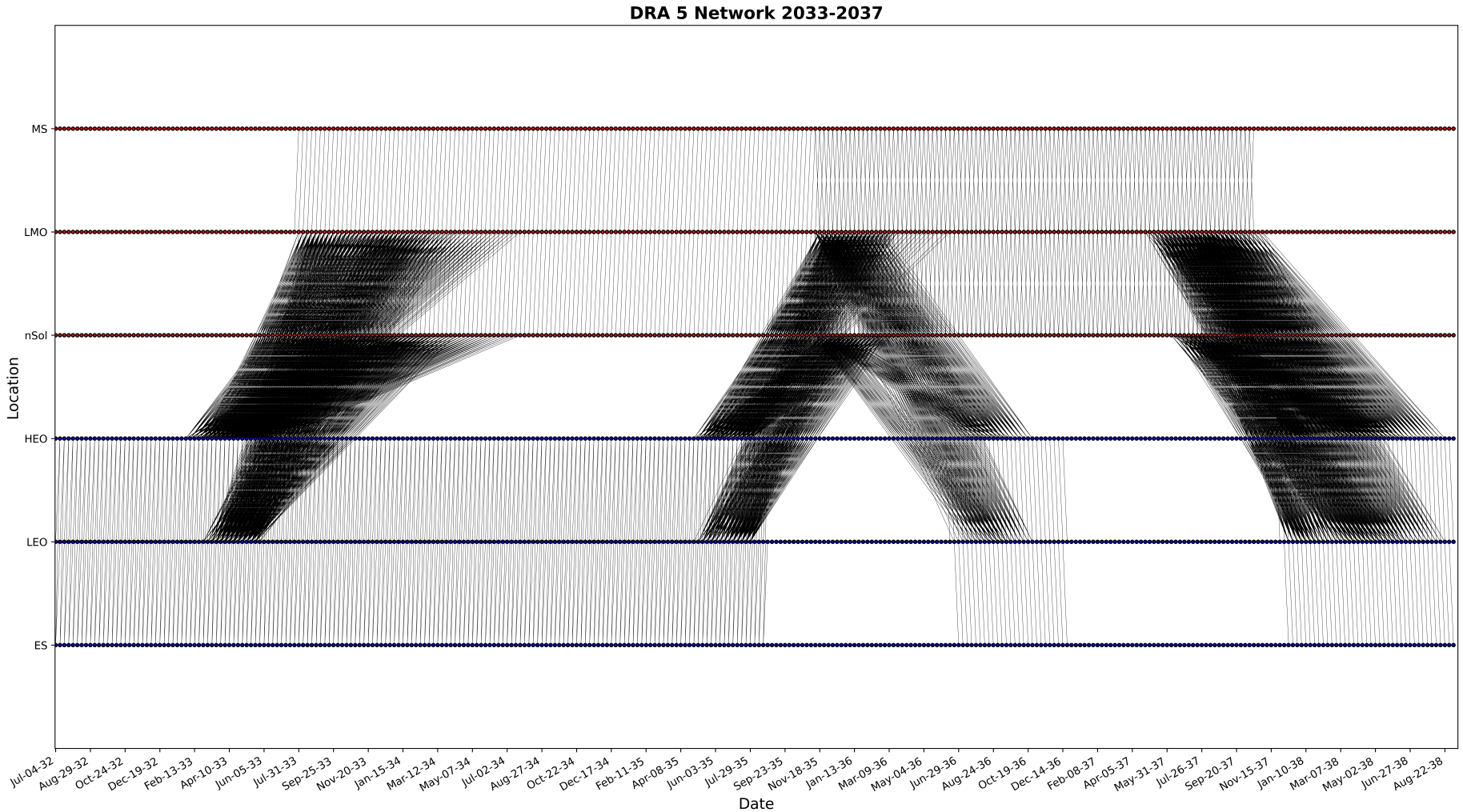

Figure 5.11: Full Mars campaign network used for the vehicle and campaign-level trade studies.

Vehicles and Other Elements

More than just the propulsive elements were modeled for this campaign in the network. Each vehicle, whether crew or cargo, has a core stage and an inline tank, at the minimum. The core stage has fuel tank for storage as well as the engines and accompanying subsystems, making it the main propulsive stage for each element. The inline tank mainly provides additional fuel storage for the core stage and is designed such that it is not discarded after being spent; it stays with the vehicle until the mission is completed, both for crew and cargo variants. Crew vehicles have an additional drop tank, design to be discarded immediately following the Earth-Mars transfer, and further requires a structural truss element as housing. There are several crew elements in the campaign, each providing a different function in the crew stack. The Transit Habitat (THAB) houses the 6 crew members during the outbound and inbound interplanetary transits, and an Orion is docked to it throughout the mission for additional habitable volume while also doubling as the Earth reentry vehicle. A shorter truss connects the propulsive elements to the THAB and houses a container of contingency consumables for the crew, as well as a docking module for another Orion that delivers the crew to the MTV, but does not go to Mars. It is assumed that the truss payload element also includes the mass of the shorter truss as the consumables container is modeled as a vehicle since it is staged prior to Mars departure.

For the cargo vehicles, the individual payload elements are modeled as fixed masses as well as the cargo aeroshell stages that carry them, and it is assumed that the masses of the latter include the propellant required Entry, Descent, and Landing (EDL) to descend to the Martian surface. Cargo 1 will carry the MAV, ISRU, and Fission Surface Power (FSP) required to power the ISRU, while Cargo 2 will carry the Surface Habitat (SHAB). Some of the payload elements are also modeled as vehicles to accurately model the flow of crew consumables throughout the network and limitations within the CLO process. Both the THAB and SHAB are modeled as such, but their masses are effectively zero as a vehicle to avoid double-counting with their payload counterparts. The MAV is also modeled as

a vehicle, as the crew is on board during ascent from the Martian surface, and its mass assumes that it has the appropriate amount of propellant to ascend to the parking orbit. Table 5.3-Table 5.5 list of all the elements, separated in to categories based on their function, included in the network, as well as their roles and main parameters.

Table 5.3: List of vehicle elements representing the cargo stacks, their roles within the network and initial design parameters.

Design Parameter	**Cargo Core**	**Cargo Inline**	**Payload Element**
Role	Propulsive Element	Propulsive Element	Fixed Vehicle
Inert Mass (kg)	37,200	12,500	115,000
Diameter (m)	10	8.9	10
Height (m)	26.6	16.3	30
Fuel	LH_2,NH_3,H_2O	LH_2,NH_3,H_2O	-
I_{sp} (s)	900,360,315	900,360,315	-
Boiloff$_{fuel}$ (kg/day)	0	0	0
Max Fuel Mass (kg)	1,000,000	1,000,000	1,000,000

Table 5.4: List of vehicle elements representing the crew stack, their roles within the network and initial design parameters.

Design Parameter	**Crew Core**	**Crew Inline**	**Crew Drop Tank**	**Truss**	**Consumables Container**	**Transit Habitat**
Role	Propulsive Element	Propulsive Element	Propulsive Element	Fixed Vehicle	Fixed Vehicle	Fixed Vehicle
Inert Mass (kg)	51,600	27,000	21,000	15,600	13,500	27,500
Diameter (m)	10	10	10	8.9	7.5	4.5
Height (m)	30	30	30	25	7	20
Fuel	LH_2,NH_3,H_2O	LH_2,NH_3,H_2O	LH_2,NH_3,H_2O	-	-	-
I_{sp} (s)	900,360,315	900,360,315	900,360,315	-	-	-
Boiloff$_{fuel}$ (kg/day)	0	0	0	0	0	0
Max Fuel Mass (kg)	1,000,000	1,000,000	1,000,000	-	-	-

Table 5.5: List of payload elements and their roles within the network and initial design parameters.

Design Parameter	**Surface Habitat**	**MAV**	**Orion 1**	**Orion 2**	**Crew**
Role	Fixed Vehicle	Fixed Vehicle	Fixed Vehicle	Fixed Vehicle	Fixed Payload
Inert Mass (kg)	-	-	14,000	14,000	600
Diameter (m)	7.6	4	4	4	0.5
Height (m)	3	4	4	4	0.5

NASA's DRA 5 concept launches several sets of multiple elements on a single Ares V vehicle, but due to further limitations in the CLO process, every individual element in this network must be launched separately. The full crew element of the THAB, Orion Two, Consumables Container, Short Truss, and Docking Module is launched separately rather than on one SLS Block 2B. The same is true for the crew drop tank and its large truss housing. This limitation comes with the added risk of more launches, but potentially using smaller, cheaper launch vehicles for those extra launches. Additionally, to facilitate a more apples to apples comparison between the results of using this methodology to that of generated by NASA in DRA 5, the cadence of SLS launches is reduced to 30 days, mimicking the capability that was expected of the Ares V.

Paths

Paths are used extensively to model the proper operations for the NTP vehicle for both of the vehicle and campaign level trade studies. Rather than defining one large path for each vehicle, many smaller paths are used to define parts of each vehicle's overall mission. Each path is also given a small time domain that the optimizer can choose from to further reduce computational complexity. Table 5.6 detail all paths that are defined for CLO and Table 5.7 list the inline and drop tank ranges given as options to open up higher energy transfer options. Each path input is repeated for the different number of tank configurations.

Table 5.6: Defined paths for the Mars campaign trade studies.

Path	Event Type	Arc Options	Timestep Range
Cargo 1 Aggregation and Departure	ΔV	Departure: LEO,HEO, Arrival: n-sol,LMO	238-329
Cargo 1 Arrival and EDL	ΔV	Departure: n-sol,LMO, Arrival: Martian surface	392-749
Cargo 2 Aggregation and Departure	ΔV	Departure: LEO,HEO, Arrival: n-sol,LMO	238-329
Crew Aggregation and Departure	Δm ΔV	Crew from Orion 1 to THAB Departure: LEO,HEO, Arrival: n-sol,LMO	1022-1113 -
Crew Mars Ops 1	Δm	Crew from THAB to SHAB	1232-1442
Crew Surface Ops	ΔV ΔT ΔV	Departure: n-sol,LMO, Arrival: Martian Surface 504 days Departure: Martian Surface, Arrival: n-sol,LMO	1253-1463 - -
Crew Mars Ops 2	Δm ΔV	Crew from SHAB to THAB Departure: n-sol,LMO, Arrival: LEO,HEO	1785-1972 -
Crew Return Ops	Δm ΔV	Crew from SHAB to Orion 2 Departure: LEO,HEO, Arrival: Earth Surface	1988-2240 -

Table 5.7: List of different tank configurations given to the optimizer to trade as a range [min,max].

	LH_2 (Long Stay)	**NH_3**	**H_2O**	**Short Stay**
Cargo Inline	1	1-2	2-3	1
Crew Drop Tanks	1	10-15	20-25	2-4

For paths with multiple drop tanks or multiple propellant sources, it is assumed that over the course of a single arc and single burn, the amount of propellant burned is split evenly amongst those elements. Further, spent elements are not discarded until the after the transfer, rather than being discarded immediately after being spent. These two points are key limitations within the CLO process, identified as points of departure for future work.

5.4.2 Vehicle Sizing and Synthesis

As with the HLS campaign example, only the propulsive elements are sized by the VSS process for the crew and cargo vehicles. Table 5.8 lists the subsystems used for each of these propulsive elements and what part of the vehicle they are modeling. The core, inline, and drop stages largely have similar architectures, and the only difference between them being the inclusion of engines on the core. If a stack requires more than one inline or drop tanks, they use exactly the same architecture definition as the original. For the vehicle-level trade study, although the architecture definitions are identical between the different propellant species, the main difference in the fuel tank models would be the inclusion of active CFM systems for the LH_2 NTP option compared to H_2O and NH_3. Table 5.9 detail the main design parameters used in VSS for the main propulsive elements, and a 15% MGA was used across all subsystems.

Table 5.8: List of crew vehicle elements and the subsystems that were modeled for each of them in VSS.

	Core Stage	**Inline Stage**	**Drop Tank**
Propulsion	NTP Fuel Tank NTR RCS	NTP Fuel Tank - RCS	NTP Fuel Tank - RCS
Avionics	Sensors Comms	Sensors Comms	Sensors Comms
Structures	Structures	Structures	Structures
Power	Power	Power	Power
Thermal	Radiator	Radiator	Radiator

Table 5.9: Key design parameters used in VSS for each of the propulsive elements across the different alternative campaigns: [LH_2-Long Stay, NH_3, H_2O, LH_2-Short Stay].

Subsystem	Design Parameter	Core Stage	Inline Stage	Drop Tank
Propulsion	Cryocooler	20K, none, none, 20K	20K, none, none, 20K	20K, none, none, 20K
	Tank l/d	1.4	1.4	1.4
	Tank Pressure [psi]	40	40	40
	Tank Temperature [K]	20, 245, 323, 20	20, 245, 323, 20	20, 245, 323, 20
	Tank Material	AL2195	AL219 5	AL2195
	Num Engines	3	0	0
	Engine Thrust [klbf]	25	0	0
	I_{sp}	900,360,315,900	900,360,315,900	900,360,315,900
	$T_{chamber}$ [K]	2,800	0	0
	$P_{chamber}$ [MPa]	3.5	0	0
Avionics	n_{gyros}	6	6	6
	$n_{sun\ senors}$	8	8	8
	$n_{star\ sensors}$	4	4	4
	$n_{horizon\ sensors}$	3	3	3
	Accuracy	1	1	1
	Comms Package	Deep Space	Deep Space	Deep Space
Structures	Structures Fraction	0.30	0.30	0.30
RCS	RCS Fraction	0.20	0.20	0.20
Power	η_{cell}	0.33	0.33	0.33
	Array Density [kg/m^2]	18.2	18.2	18.2
	Operations Distance [AU]	1.5	1.5	1.5
	Battery specific capacity [W*hr/kg]	125	125	125
	Depth of Discharge	0.5	0.5	0.5

The VSS process handles the mission level degrees of freedom for the problem, which in this cases is the semimajor axis, or orbital energy of the two parking node options at Mars. The valid ranges are shown below in Table 2.7. A notional rubberized MAV is included the VSS optimization problem to properly assess the split between the in-space and ascent transportation systems. Though not being fully sized at the subsystem-level, excluding this element from this part of the problem would only unintentionally force the optimizer to push the orbit up as high as possible to reduce the load on the in-space systems. In other words, the MAV serves as a penalty function for the optimizer choosing higher orbits.

The MAV is represented as a scalable propulsive element with the 6 crew members serving as its payload. It is assumed to have a PMF of 0.6, and using Liquid Oxygen (LOx)/Liquid Methane (LCH_4) propellant with an I_{sp} of 340s. These two parameters are used to directly size the MAV using the propellant mass calculated using the ideal rocket equation and the resulting ΔV from mission analysis, as shown in Equation 5.2. This process is included regardless if CLO decides to choose an n-sol or LMO Mars parking node.

$$m_{inert} = m_{prop} * \frac{1}{PMF - 1} \tag{5.2}$$

5.4.3 Process Parameters

Given the increased computational complexity of the Mars campaign design compared to that of HLS, the maximum runtime of CLO is increased to 24 hours. The MIP gap for the Gurobi optimizer is set to 0.001 and the convergence tolerance is still set at 5%. The maximum number of iterations is set to 20. With the inclusion of tank configuration degrees of freedom and interplanetary arcs, the objective function presented in Subsection 2.6.8 should be augmented to minimize both. The deep space time term is formulated as:

$$\frac{w_{dst}}{1000} \sum_{a \in A_{LEO,ES}} t_{departure} * b_{orion_2,a} - \sum_{a \in A_{interplanetary,outbound}} t_{departure} * b_{orion_2,a} \tag{5.3}$$

which replaces the execution time objective term. Further, the tank configuration choice can be minimized by adding a term for the number of launches:

$$\frac{w_{n_{launches}}}{n_{tanks,max}} \sum_{lv \in LV} \sum_{v \in V} b_{lv,v} \tag{5.4}$$

Table 5.10 shows the weights used for the CLO problem.

Table 5.10: Objective weights for the Mars campaign CLO problem.

Objective Term	Weight	Max Value
Propellant Mass	0.25	80,000
Number of Burns	0.22	10
Number of Launches	0.15	30
Deep Space Time	0.23	1,000
Launch Costs	0.15	4,100,000,000

5.5 Vehicle Trade Study Results

Solutions generated by the integrated methodology are defined by large datasets given the full campaign and vehicle design processes. Each vehicle-propellant species option is a fully optimized campaign with vehicle ConOps, payload paths, and vehicle mass histories. Table 5.11 lists the total runtimes to generate the campaign and vehicles for each of the 3 propellant options. VSS provides a subsystem-level mass breakdown for each vehicle that was included in the sizing, in this case the core, inline, and drop stages for each campaign option. In addition to the three options explored, NASA's own DRA 5 results are presented in order to compare how the method performs comparatively. DRA 5 provides sets of alternatives for its NTP architectures across a series of Earth-Mars opportunities, but to offer a fair comparison with the results generated for this research, only campaigns and

vehicles designed for the same 2033-2035 opportunities were included. The convergence performance for each solution is presented in Section D.1.

Table 5.11: Runtimes to produce each integrated solution in the vehicle-level trade study.

Propellant Option	CLO [d]	VSS [s]	Total [d]
LH_2	4	385	4.00445
NH_3	4	424	4.00491
H_2O	4	481	4.00557

A comparison of the total campaign mass for each option is shown in Figure 5.12 as an initial campaign comparison. Between the three new options generated by the methodology, the LH_2 option is significantly less massive than those of the non-cryogenic propellants of NH_3 and H_2O. Given the exponential nature of the ideal rocket equation, the propellant mass required to execute the same missions will be more than 3x higher than that required with LH_2.

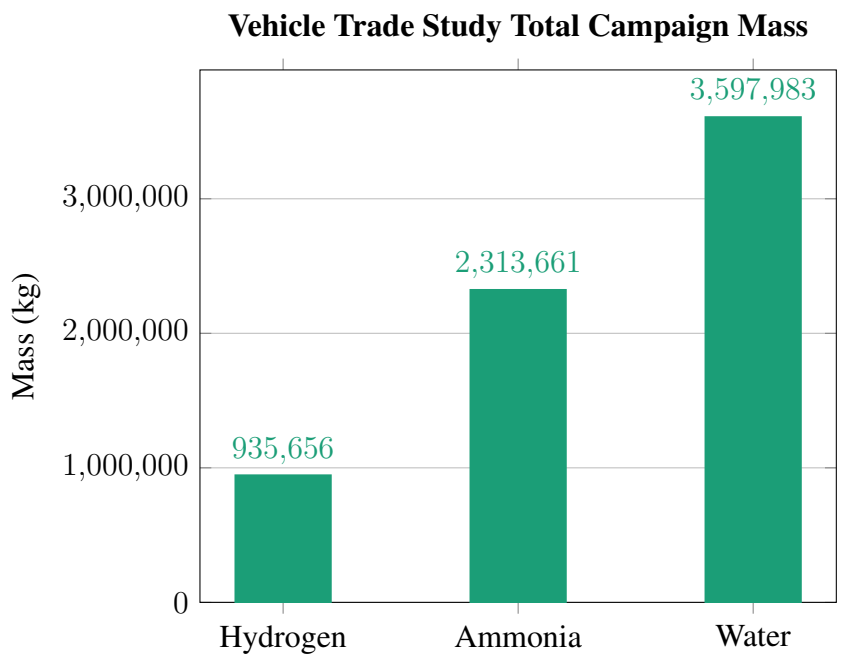

Figure 5.12: Total mass required to execute each campaign alternative.

The primary differences in mass between the alternatives can be further broken down into propellant and inert masses, as shown in Figure 5.14. Expected trends in propellant

requirements based on the differences in I_{sp} is clear in this figure. Comparing the propellant masses, labeled as (1), using ammonia requires an increase of almost 1,400t, or 4x more fuel, than LH_2, and using water requires another 1,200t. One of the primary purposes of considering these two propellants in addition to the better performing LH_2 is the investigation of how much the inclusion of active CFM systems affect the inert mass of the LH_2 alternative. Although the propellant masses for water and ammonia are significantly higher, Figure 5.14 also shows through label (2) that the inert mass required does not increase at the same rate. The inert mass for ammonia is only nearly 10t higher than that for LH_2 which is only a 1.6% difference.

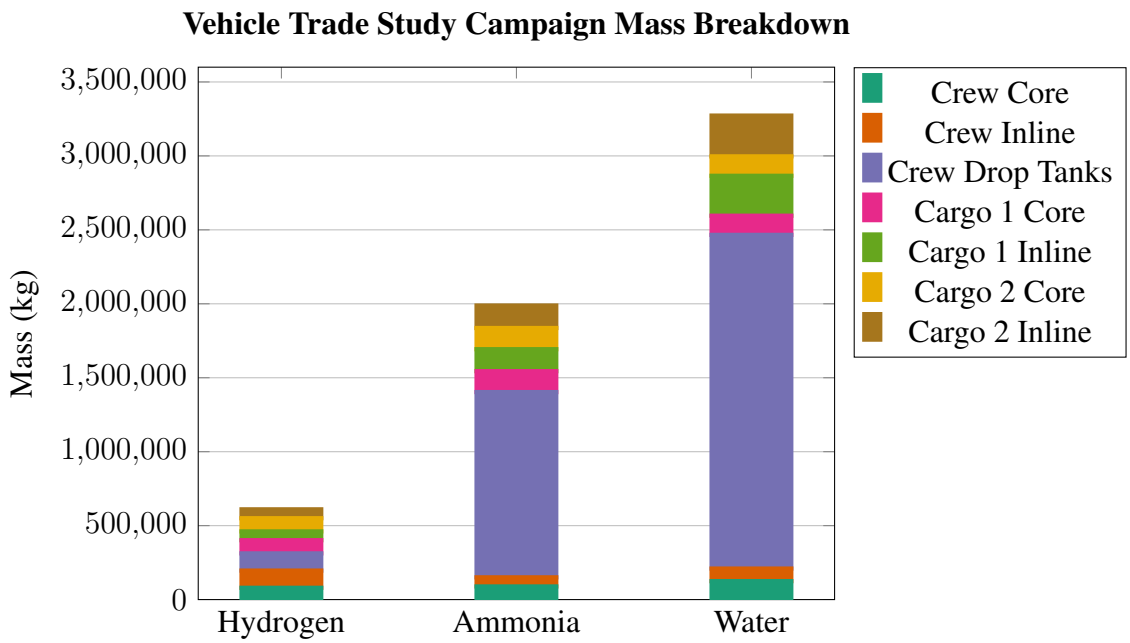

Figure 5.13: Total mass required to execute each campaign alternative.

Another way to assess the efficiency of the size of these elements between each alternative campaign is the ratio of inert mass to required propellant mass, or a measure of how much hardware is necessary to carry the propellant. This can be calculated using Figure 5.13, where it shows the value is significantly higher for the LH_2 campaign than that of the other two propellants. For the former, at a value of 1.41, the inert mass contributes more to the overall campaign mass than the propellant, where the opposite is true for ammonia

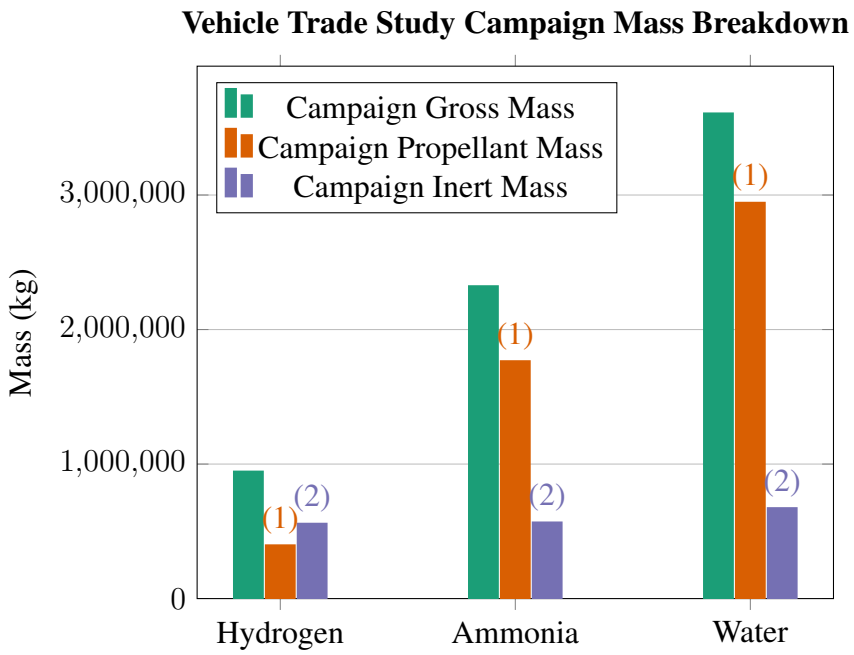

Figure 5.14: Breakdown of campaign mass into propellant and inert masses.

and water. The jump is most significant between LH_2 and ammonia, and using water over ammonia does not offer as much of a benefit.

Figure 5.15 and Figure 5.16 show the launch counts and launch costs, respectively, for each campaign alternative. For the three new campaigns generated, only four separate launch vehicles were chosen: NASA's SLS 1B and 2B, and SpaceX's Falcon Heavy and Starship. Distribution of launches between the three campaign alternatives are very similar, with a very Starship driven launch strategy. Given the price to performance ratio of Starship as well as the dimensions of its fairing, this is expected behavior. However, SLS 2B is still used for larger and more massive elements. Figure 5.16 shows the launch costs expectedly follows the same trends as the counts, and each campaign costs is dominated by the use of SLS 2B even though the number of Starship launches is much more. Figure 5.17 depicts the dollar launch costs per unit campaign mass for campaign option showing that the lower I_{sp} propellants are much more costs effective. By itself, this may indicate it is a feasible alternative, but the new methodology provides the capability to assess many different parts of the campaign, telling the whole story. In this case the financial costs are accompanied by

a significant increase in launch and element counts, potentially increasing risk with more points of failure.

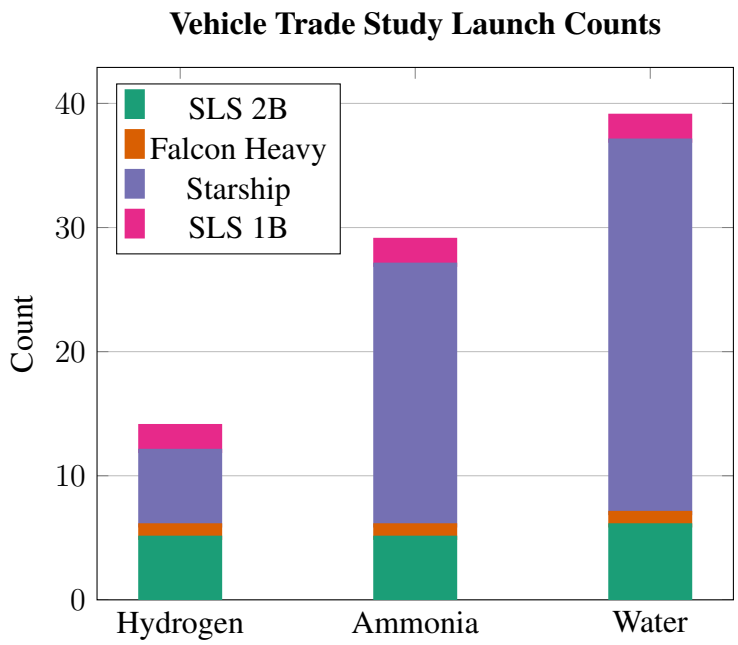

Figure 5.15: Total launch counts required to execute each campaign alternative.

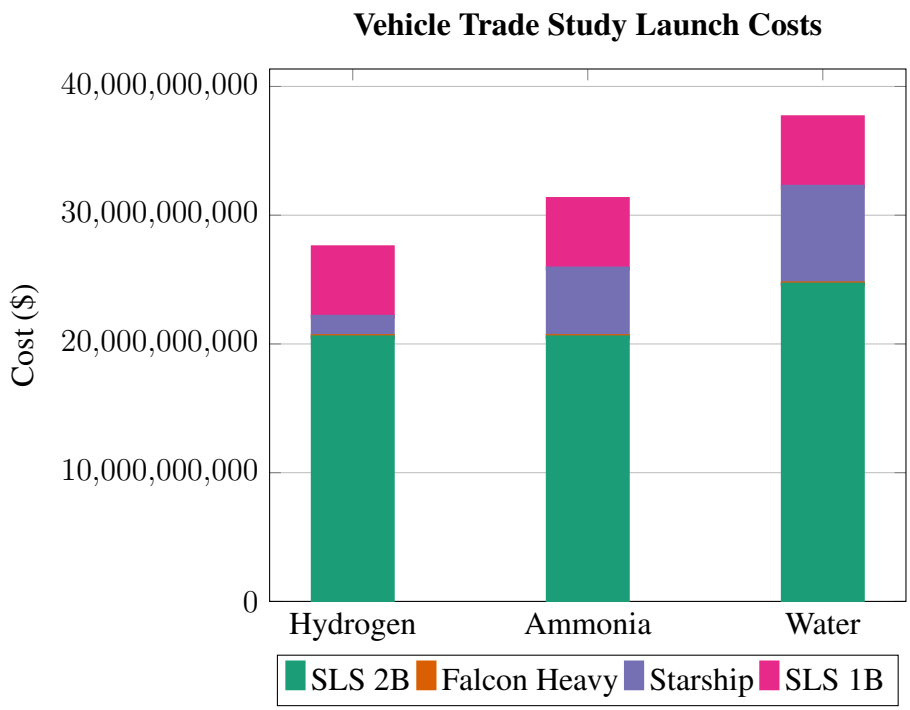

Figure 5.16: Total launch costs required to execute each campaign alternative.

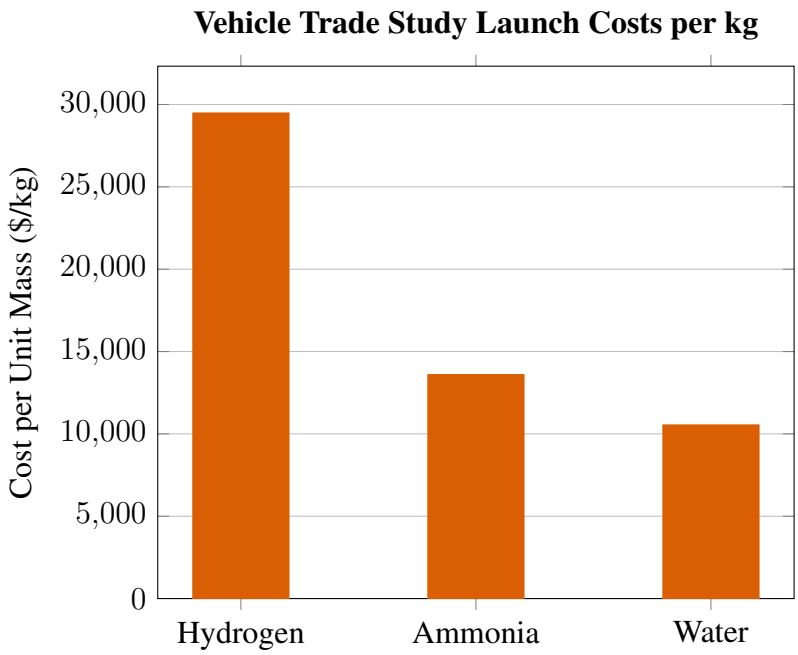

Figure 5.17: The launch costs per unit campaign mass for each campaign alternative.

With the CLO process, the ConOps and missions for each campaign can be compared directly; where Figure 5.18-Figure 5.20 show the vehicle paths for each alternative. Table 5.12 supplements the paths with the accompanying dates and ΔV data for those alternatives. Both show that the integrated methods closes on the same interplanetary mission for all three propellant species. For the 504-day long-stay mission, all campaigns have the same departure dates for both cargo missions and the subsequent crew missions. All campaigns have both crew and cargo vehicles departing from LEO and parking at LMO. Cargo 1 departs on May 1st, 2033 and arrives at Mars 273 days later on January 19th, 2034, with Cargo 2 only a week behind at both ends. As Cargo 1 stages its propulsive elements and descents immediately to setup necessary surface systems, Cargo 2 stages its and waits in LMO for the crew to arrive. After MTV aggregation and crew rendezvous, the crew transfer from Orion to the THAB and depart towards Mars on June 24th, 2035 with an outbound flight time of 203 days. The MTV stages its drop tanks and the crew transfers to Cargo 2 for descent to the Martian surface. They then transfer to the MAV after a 504-day surface exploration phase which takes them back to the MTV, just in time for a Mars departure

date of July 29th, 2037. The crew transfer to the pre-docked Orion after a 266-day transfer which returns them to Earth with a splashdown date of April 11th, 2038. This mission results in a total deep space time for the crew of 1,022 days, or nearly 3 years.

Table 5.12: Summary of dates and transit times produced by the new methodology and DRA 5.

		New Methodology
	Earth Aggregation	LEO
	Mars Parking	LMO (271km x 271km)
Cargo 1	Earth Departure Date	5/1/2033
	Mars Arrival Date	1/29/2034
	Time of Flight [days]	273
Cargo 2	Earth Departure Date	5/8/2033
	Mars Arrival Date	2/5/2034
	Time of Flight [days]	273
Crew	Earth Departure Date	6/24/2035
	Mars Arrival Date	1/13/2036
	Outbound ToF [days]	203
	Mars Stay Time [days]	532
	Surface Stay Time [days]	504
	Mars Departure Date	7/19/2037
	Earth Arrival Date	4/11/2038
	Inbound ToF [days]	266
	Splashdown Date	4/25/2038
	Total Deep Space Time [days]	1022

Although the mission profiles are the same for each campaign alternatives, the main differences lie in each of their vehicle configuration and subsequent aggregation timelines. Differences in the I_{sp} for each propellant option is reflected in the overall propellant required for the campaign and further affects the number of required inline and propellant tanks. The final count of each of them are shown in Table 5.13. For both cargo missions, ammonia and water options require one and two more inline tanks than that of LH_2, respectively. The MTV requires significantly more drop tanks for its ammonia and water options, increasing

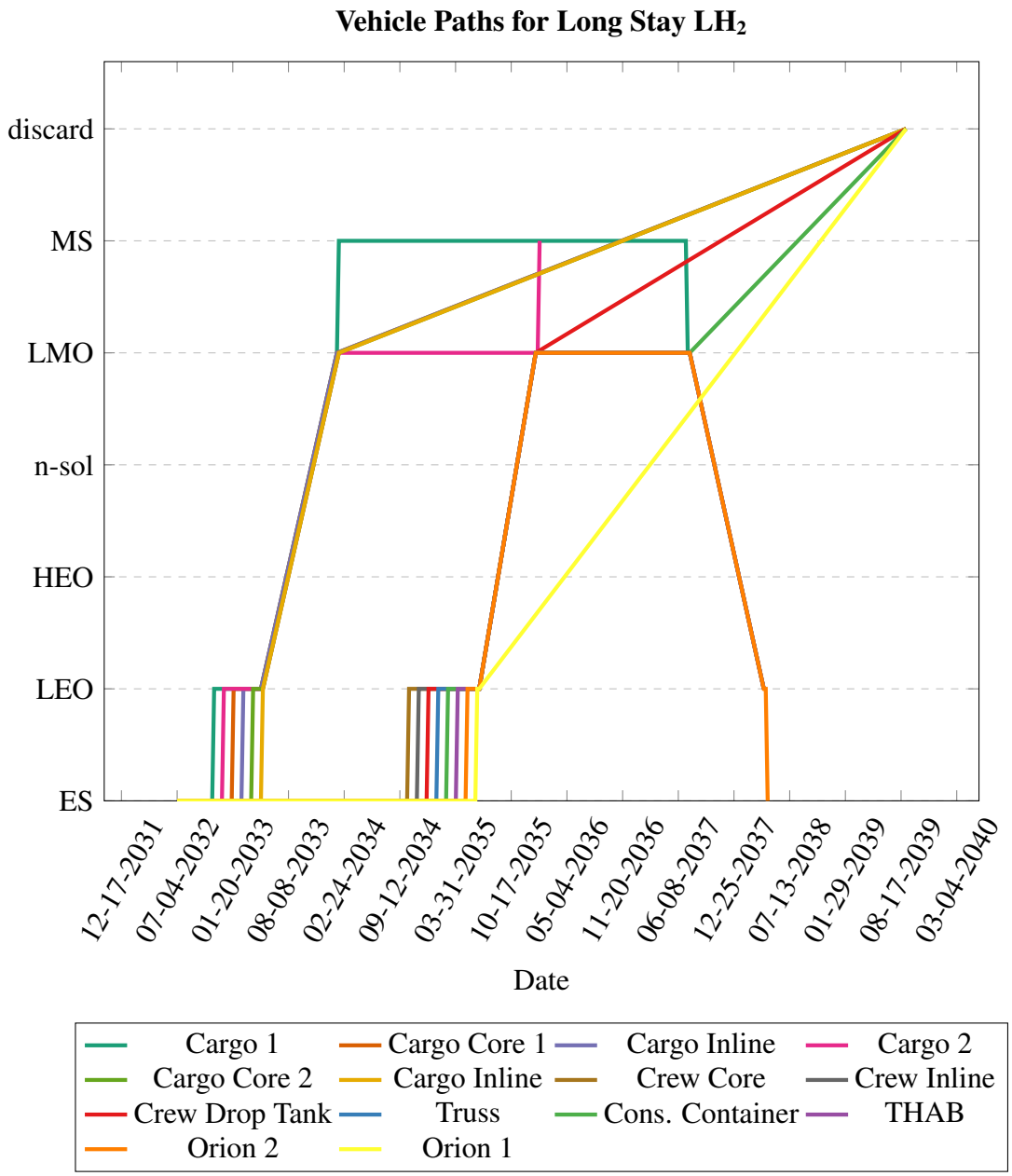

Figure 5.18: Vehicle paths for the long stay LH_2 NTP campaign option.

from just a single to 14 for the former and 22 for the latter. The I_{sp} change further propagates down to the launch and aggregation strategy, as seen in Figure 5.18-Figure 5.20, and further detailed in Table 5.15 and Table 5.14. Compared to the LH_2 option, the ammonia campaign requires an additional two launches for the two extra cargo inline tanks, which pushes the assembly start date from October 8th, 2034 to July 10th, 2033. This means the MTV assembly must start before either cargo vehicle has arrived at Mars to be able to depart by

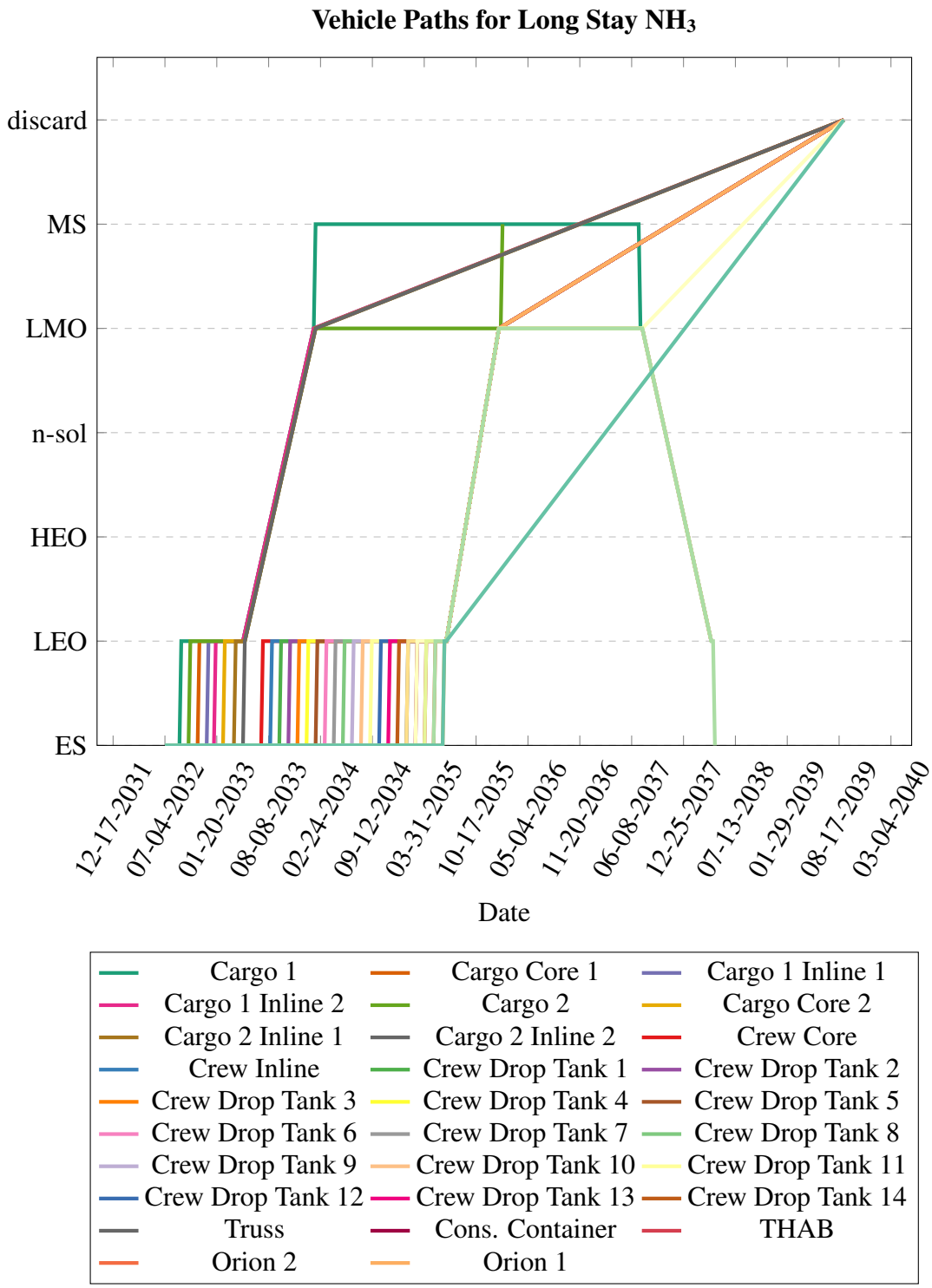

Figure 5.19: Vehicle paths for the long stay NH_3 NTP campaign option.

June 24th 2035, potentially increasing the risk of the overall mission in the event one of those missions fail. For water, the campaign time domain anchor date was pushed back to

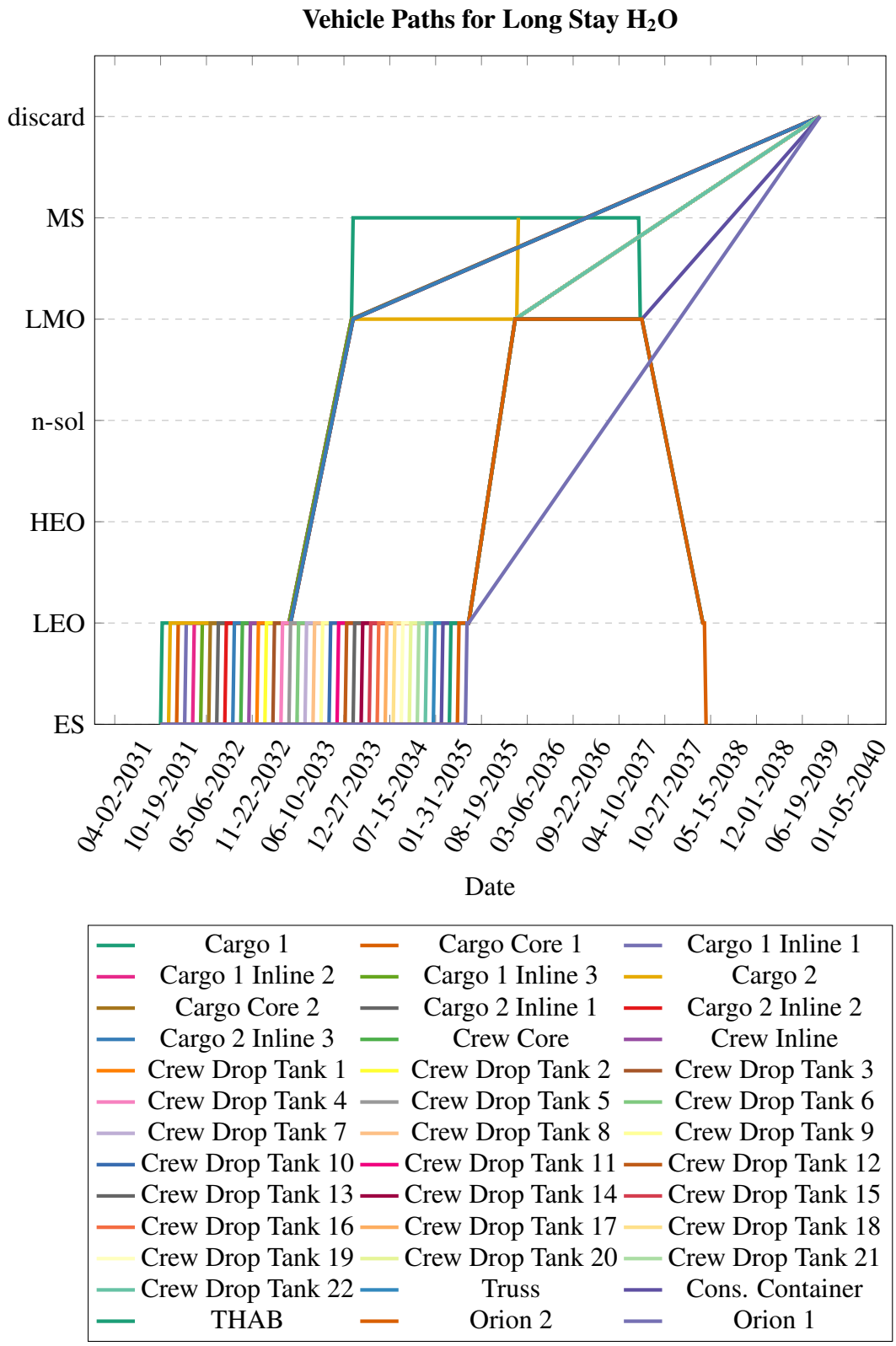

Figure 5.20: Vehicle paths for the long stay H_2O NTP campaign option.

allow for the 22 crew drop tanks and 6 total cargo inline tanks to be launched while still being properly constrained by launch vehicle capabilities. The spacing between the cargo and crew vehicle assembly timelines is non existent as every launch opportunity is taken to assemble all elements in time for their Earth departure dates.

Table 5.13: Tank counts for each campaign alternative.

	LH_2	**NH_3**	**H_2O**
Crew Inline	1	1	1
Crew Drop Tanks	1	14	22
Cargo 1 Inline	1	2	3
Cargo 2 Inline	1	2	3

CLO calculates the consumables required on both habitats to support the crew throughout the mission. Figure 5.21 and Figure 5.22 show the mass histories of food, water, oxygen on the THAB and SHAB throughout the campaign as well as indicating when the crew is on board. The THAB requires slightly less consumables than the SHAB as the crew spends more time on the surface than in transit, a difference of 95 days. Notice the consumables mass only decreases on each element during periods when the crew is on board.

The subsystem mass breakdowns in Figure 5.23-Figure 5.25 shows the inert masses are similar across each element type. Core stages, labeled as (1) are dominated by the massive size of the NTP engines and are several times more massive than the inline or drop tank engines, regardless of the propellant species. Ammonia and water do not require active CFM systems and the masses between them and LH_2 reflects a significant difference. The inline and drop tanks for ammonia and water are very mass efficient, the ammonia crew inline tank reaching as low as 5t, labeled as (2).

5.6 Campaign Trade Study Results

Short stay focused campaigns are expected to have very different mission profiles compared to that of longer stay options due to the Earth-Mars synodic cycle. The former typically targets a crew return in the same opportunity that they departed from, otherwise would be

Table 5.14: Launch dates for every element in each campaign alternative.

	LH_2	NH_3	H_2O
Crew Core	10/8/2034	7/10/2033	10/3/2032
Crew Inline Tank	11/12/2034	8/14/2033	11/7/2032
Crew Drop Tank 1	12/17/2034	9/18/2033	12/12/2032
Crew Drop Tank 2		10/23/2033	1/16/2033
Crew Drop Tank 3		11/27/2033	2/20/2033
Crew Drop Tank 4		1/1/2034	3/27/2033
Crew Drop Tank 5		2/5/2034	5/1/2033
Crew Drop Tank 6		3/12/2034	6/5/2033
Crew Drop Tank 7		4/16/2034	7/10/2033
Crew Drop Tank 8		5/21/2034	8/14/2033
Crew Drop Tank 9		6/25/2034	9/18/2033
Crew Drop Tank 10		7/30/2034	10/23/2033
Crew Drop Tank 11		9/3/2034	11/27/2033
Crew Drop Tank 12		10/8/2034	1/1/2034
Crew Drop Tank 13		11/12/2034	2/5/2034
Crew Drop Tank 14		12/17/2034	3/12/2034
Crew Drop Tank 15			4/16/2034
Crew Drop Tank 16			5/21/2034
Crew Drop Tank 17			6/25/2034
Crew Drop Tank 18			7/30/2034
Crew Drop Tank 19			9/3/2034
Crew Drop Tank 20			10/8/2034
Crew Drop Tank 21			11/12/2034
Crew Drop Tank 22			12/17/2034
Truss	1/21/2035	1/21/2035	1/21/2035
Cons. Container	2/25/2035	2/25/2035	2/25/2035
TransHab	4/1/2035	4/1/2035	4/1/2035
Orion Two	5/6/2035	5/6/2035	5/6/2035
Orion One	6/10/2035	6/10/2035	6/10/2035
Cargo 1 - MAV & ISRU	11/7/2032	8/29/2032	10/19/2031
Cargo 2 - SHAB	12/12/2032	10/3/2032	11/23/2031
Cargo 1 Core	1/16/2033	11/7/2032	12/28/2031
Cargo 1 Inline 1	2/20/2033	12/12/2032	2/1/2032
Cargo 1 Inline 2	-	1/16/2033	3/7/2032
Cargo 1 Inline 3	-		4/11/2032
Cargo 2 Core	3/27/2033	2/20/2033	5/16/2032
Cargo 2 Inline 1	5/1/2033	3/27/2033	6/20/2032
Cargo 2 Inline 2		5/1/2033	7/25/2032
Cargo 2 Inline 3			8/29/2032

Table 5.15: Launch vehicles selected for every element in each campaign alternative.

	LH_2	NH_3	H_2O
Crew Core	Starship	Starship	SLS 2B
Crew Inline Tank	SLS 2B	Starship	Starship
Crew Drop Tank 1	SLS 2B	Starship	Starship
Crew Drop Tank 2		Starship	Starship
Crew Drop Tank 3		Starship	Starship
Crew Drop Tank 4		Starship	Starship
Crew Drop Tank 5		Starship	Starship
Crew Drop Tank 6		Starship	Starship
Crew Drop Tank 7		Starship	Starship
Crew Drop Tank 8		Starship	Starship
Crew Drop Tank 9		Starship	Starship
Crew Drop Tank 10		Starship	Starship
Crew Drop Tank 11		Starship	Starship
Crew Drop Tank 12		Starship	Starship
Crew Drop Tank 13		Starship	Starship
Crew Drop Tank 14		Starship	Starship
Crew Drop Tank 15			Starship
Crew Drop Tank 16			Starship
Crew Drop Tank 17			Starship
Crew Drop Tank 18			Starship
Crew Drop Tank 19			Starship
Crew Drop Tank 20			Starship
Crew Drop Tank 21			Starship
Crew Drop Tank 22			Starship
Truss	SLS 2B	SLS 2B	SLS 2B
Cons. Container	Starship	Starship	Starship
TransHab	FH	FH	FH
Orion Two	SLS 1B	SLS 1B	SLS 1B
Orion One	SLS 1B	SLS 1B	SLS 1B
Cargo 1 - MAV & ISRU	SLS 2B	SLS 2B	SLS 2B
Cargo 2 - SHAB	SLS 2B	SLS 2B	SLS 2B
Cargo 1 Core	Starship	SLS 2B	SLS 2B
Cargo 1 Inline 1	Starship	Starship	Starship
Cargo 1 Inline 2		Starship	Starship
Cargo 1 Inline 3			Starship
Cargo 2 Core	Starship	SLS 2B	SLS 2B
Cargo 2 Inline 1	Starship	Starship	Starship
Cargo 2 Inline 2		Starship	Starship
Cargo 2 Inline 3			Starship

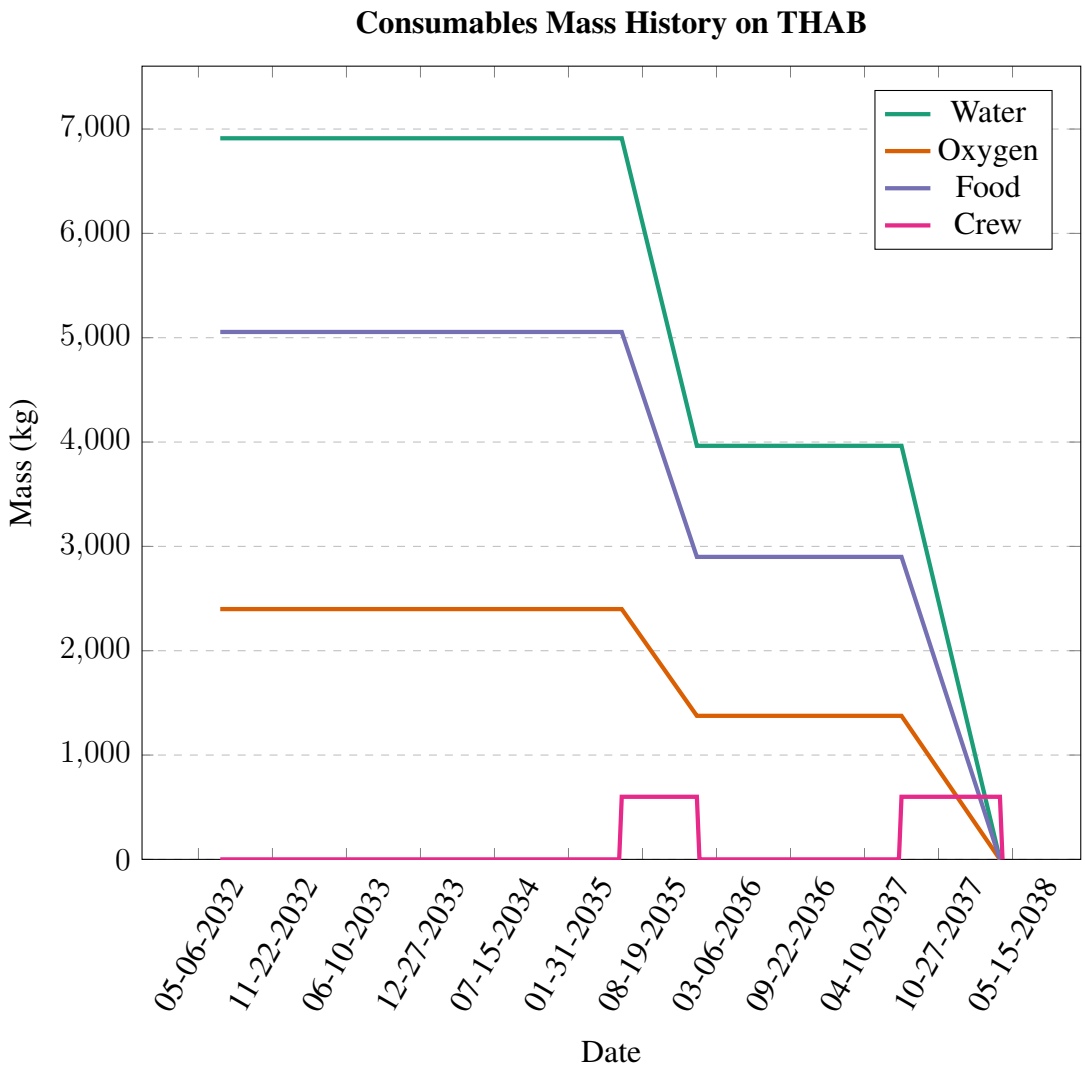

Figure 5.21: Consumables mass history on the THAB for the long stay campaigns.

stranded near Mars waiting for the next one 26 months later. Pushing this quick return increases energy, or ΔV requirements on the in-space transportation systems. For this trade study, the crew departure and return opportunities occur during the 2035 opportunity, immediately following the cargo missions in 2035 and both stay options will use LH_2 to reduce the number of variables. The long stay campaign option with a target of 500 days is the same solution provided in the previous section for the LH_2 NTP option. Shorter stays at Mars are typically between 30-50 days, and so this trade study will explore a 28 day option to potentially identify a lower bound on the design space and keep consistent

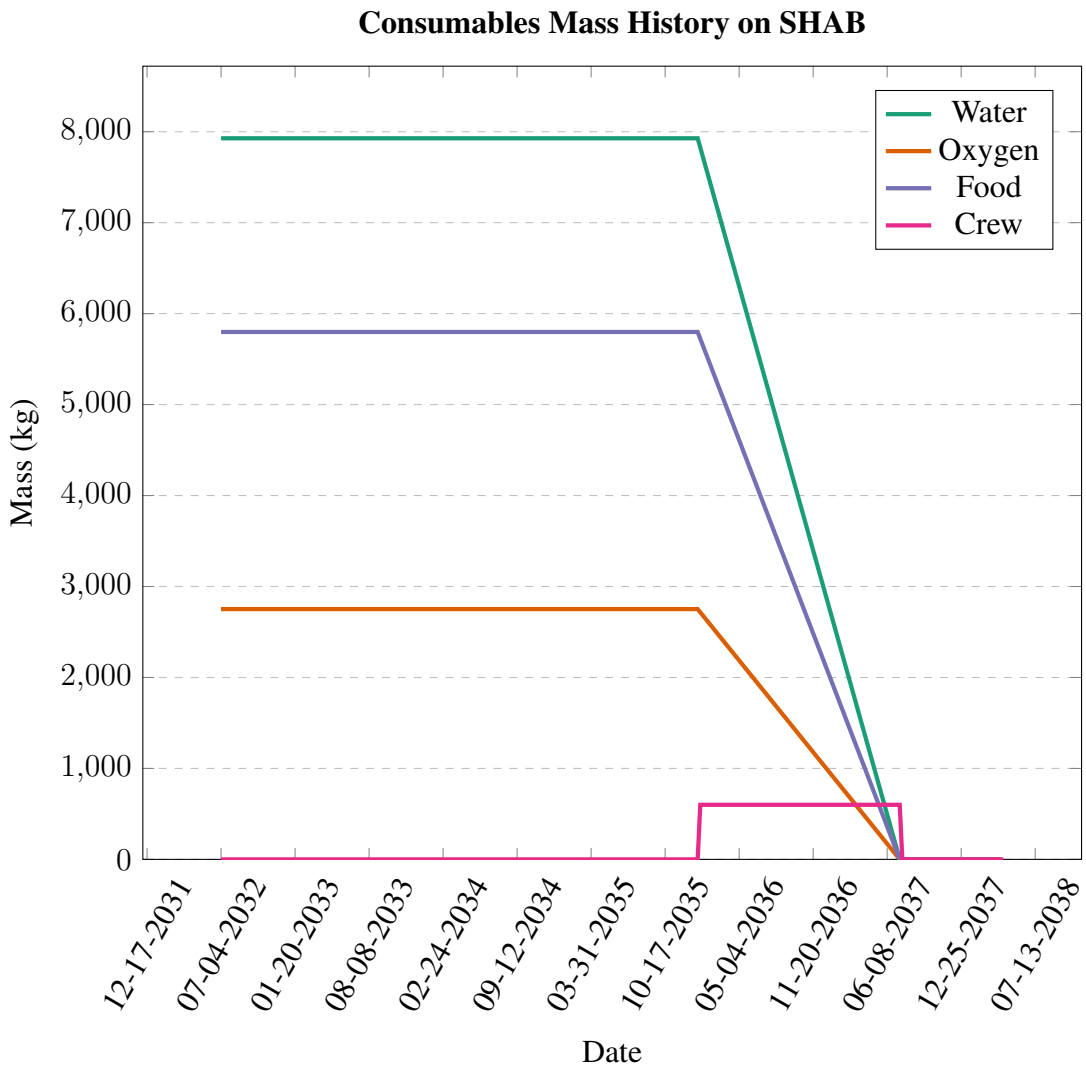

Figure 5.22: Consumables mass history on the SHAB for the long stay campaigns.

with the 7-day timesteps of the network. NASA has not detailed a full short stay campaign within DRA 5 and so it will not be use in the comparison. A key architecture change for the short stay option is the removal of a SHAB and its transportation system as the MAV has the capabilities to house the crew for the short stay time [8]. The short stay option took a total of 3.003113 days to close, after 3 iterations. The convergence performance for each solution is presented in Section D.2.

Figure 5.26 shows the overall campaign mass for each alternative is very similar in magnitude to each other. Although it is expected that the shorter stay missions require

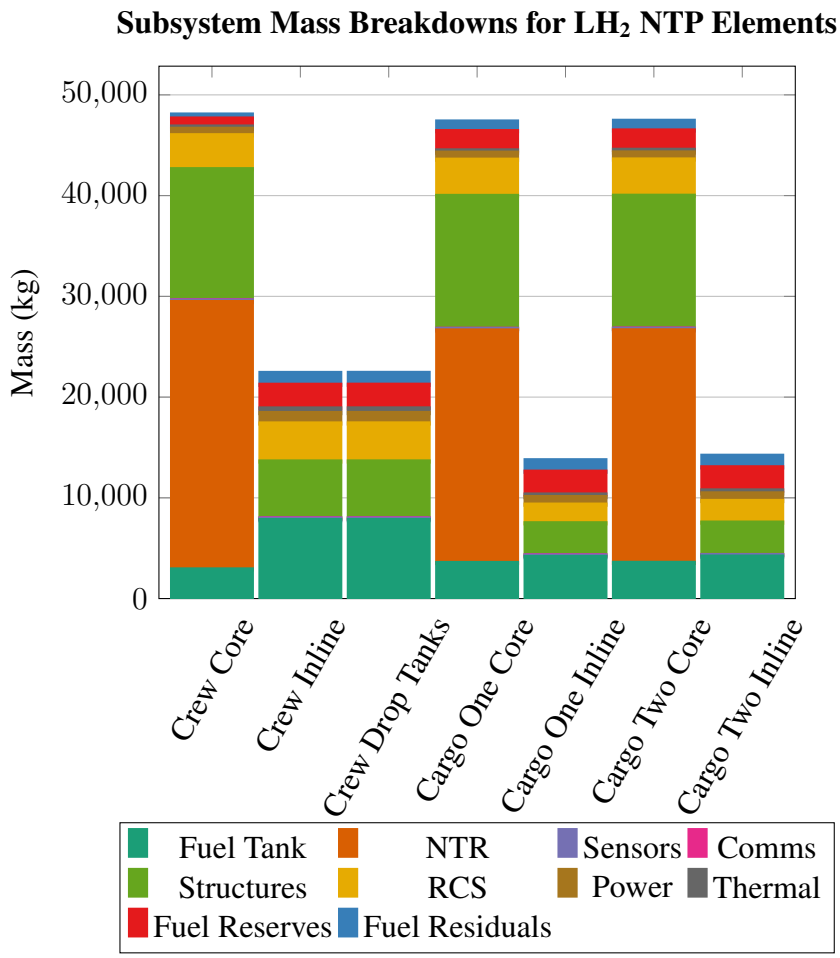

Figure 5.23: Subsystem-level mass breakdown for vehicles in LH_2 long stay campaign.

more propellant, the added mass is offset by the remove of an entire cargo pre-deploy mission. Investigating further with Figure 5.27, which shows that the mass growth of the propulsive elements is significant, meaning most of the savings is due to the removal of the massive 115t payload. Figure 5.28 further supports this observation showing that although the propellant mass required is significantly higher for the short stay alternative, its inert mass is actually lower.

Figure 5.29, Figure 5.30, and Figure 5.31 tell an interesting story regarding the launch strategy between the two surface stay options. The long stay campaign leans heavily on Starship to launch its elements, whereas the short stay solution added an SLS 2B, which

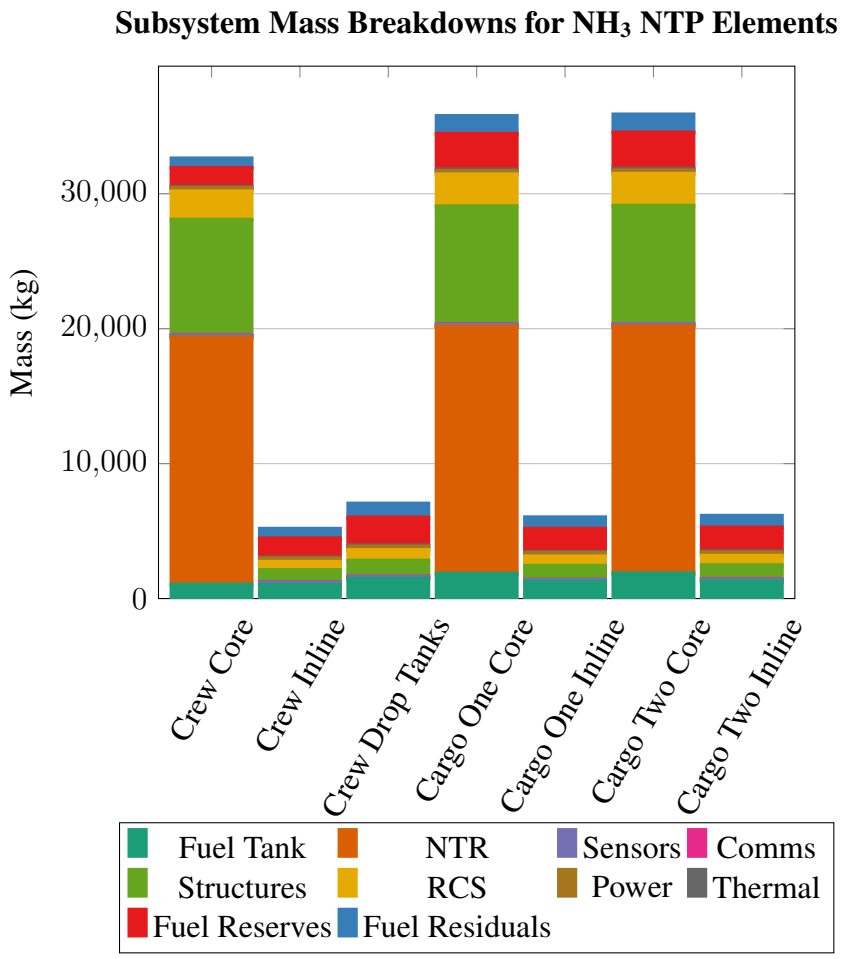

Figure 5.24: Subsystem-level mass breakdown for vehicles in NH_3 long stay campaign.

increases the costs enough to overtake the launch costs for the longer stay option. This results in a higher costs per unit mass for the short stay option.

For the short stay campaign depicted in Figure 5.32, the crew departs Earth on June 10th, 2035 and arrive at Mars just 182 days later on December 9th, 2035, with an outbound ΔV of 5,666 m/s. After transferring to the MAV for descent and 28-day surface stay, the crew ascends and transfers back to the THAB, departing from Mars on February 3rd, 2036. The crew then arrive at Earth 245 days later on October 10th, 2036 with a splashdown date exactly 2 weeks later. The inbound transfer has a ΔV value of 5,145 m/s. Although the second cargo mission is not executed, the MTV requires 2 additional drop tanks to perform the higher energy short stay mission. The launch dates and chosen launch vehicles for

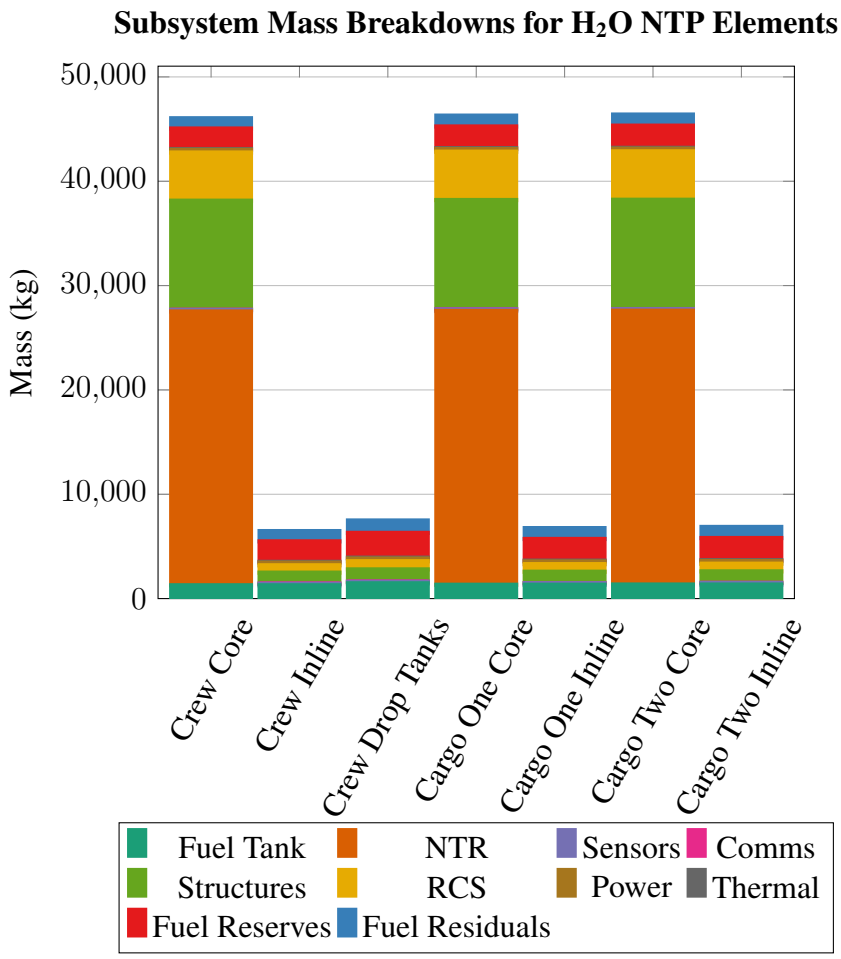

Figure 5.25: Subsystem-level mass breakdown for vehicles in H_2O long stay campaign.

the short stay campaign, as compared to the long stay option are shown in Table 5.16 and Table 5.17.

Figure 5.33 shows the subsystem-level breakdown of the inert mass for each propulsive element in the short stay campaign. These results line up well the previous sets with the core stages being more massive than others, due to the NTRs themselves. The short stays impact only affects the crew elements with the higher outbound and inbound ΔVs. The single cargo mission takes the same opportunity as it does for the long stay missions, as their transit times are independent of that of the MTV.

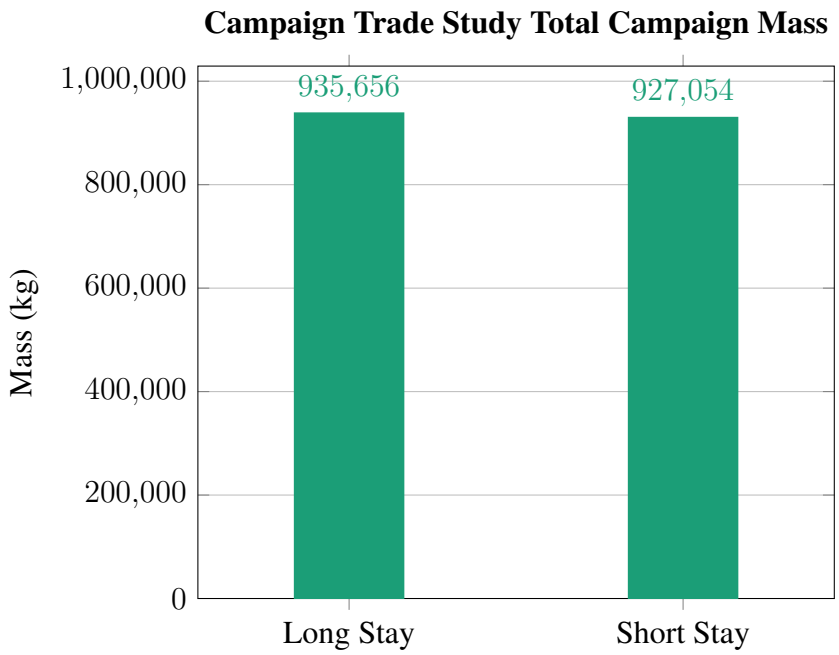

Figure 5.26: Total mass required to execute each surface stay campaign alternative.

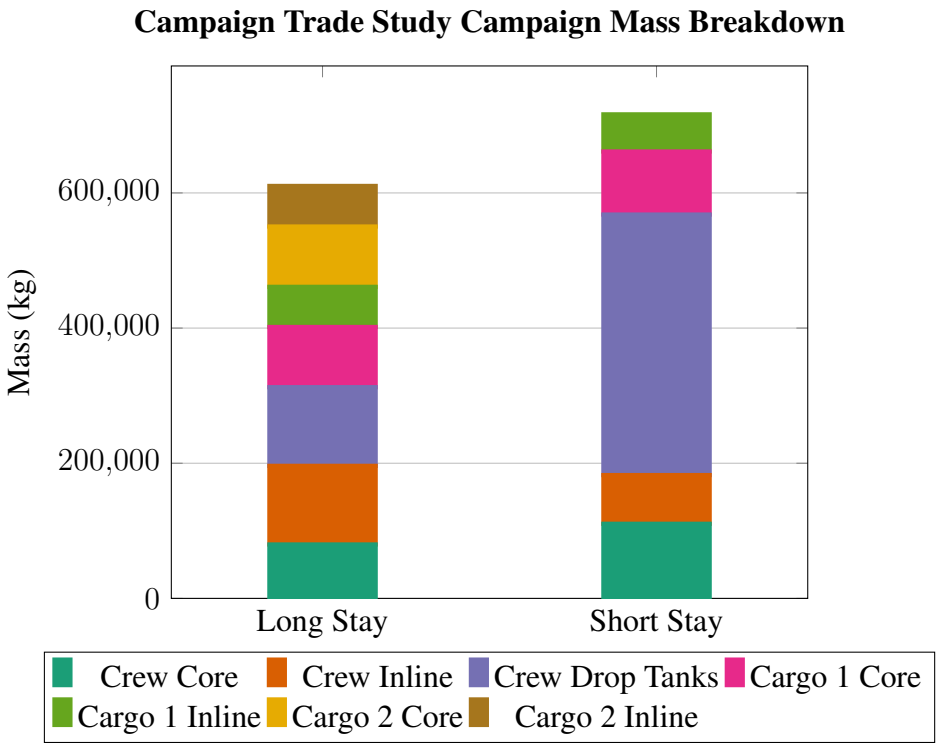

Figure 5.27: Breakdown of campaign mass by propulsive elements.

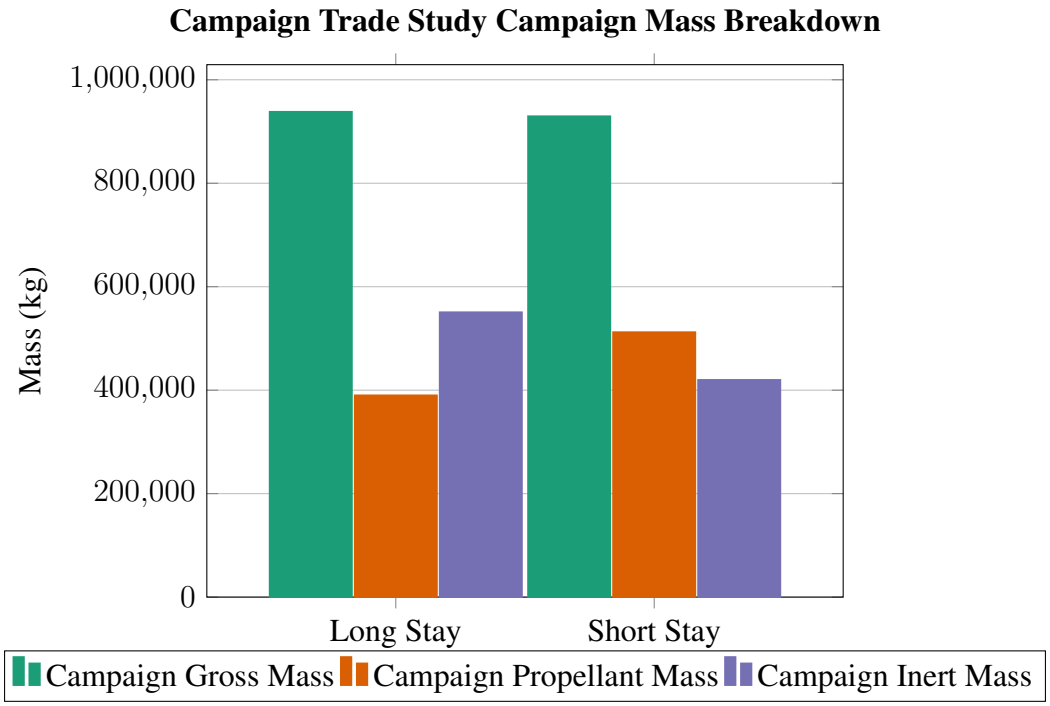

Figure 5.28: Breakdown of campaign mass into propellant and inert masses for the long and short stay alternatives.

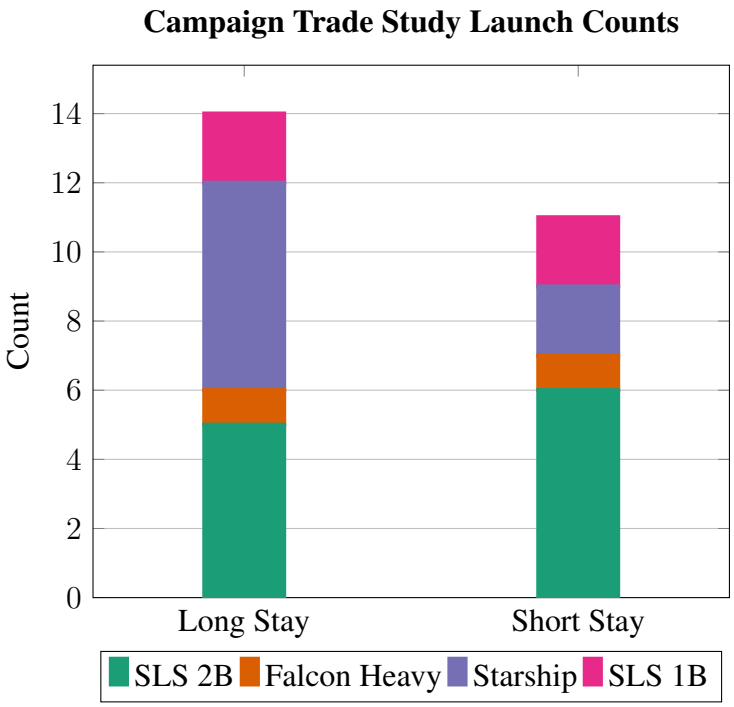

Figure 5.29: Launch counts distribution for each campaign-level trade option.

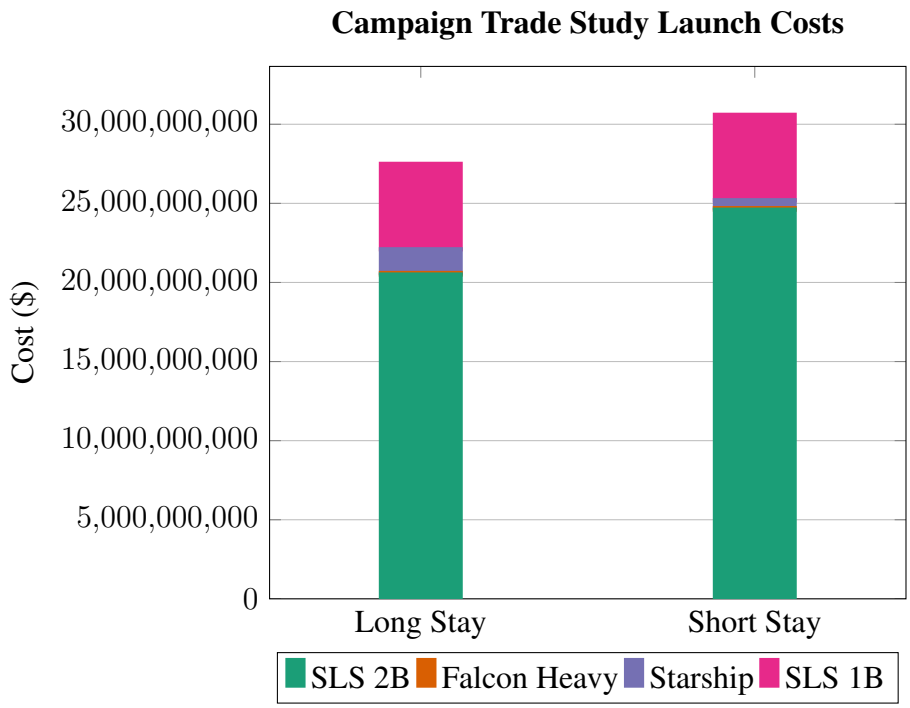

Figure 5.30: Launch costs distribution for each campaign-level trade option.

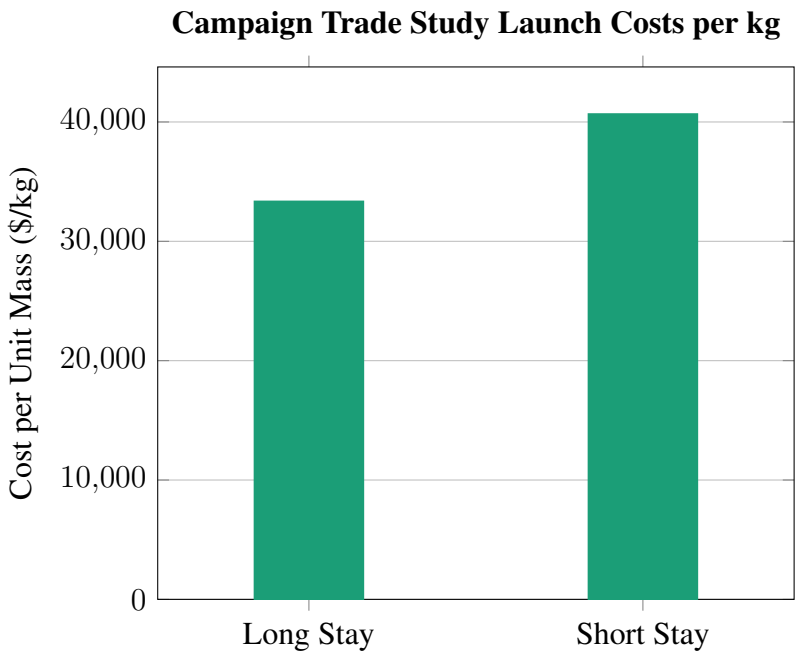

Figure 5.31: The launch costs per unit campaign mass for each surface stay campaign alternative.

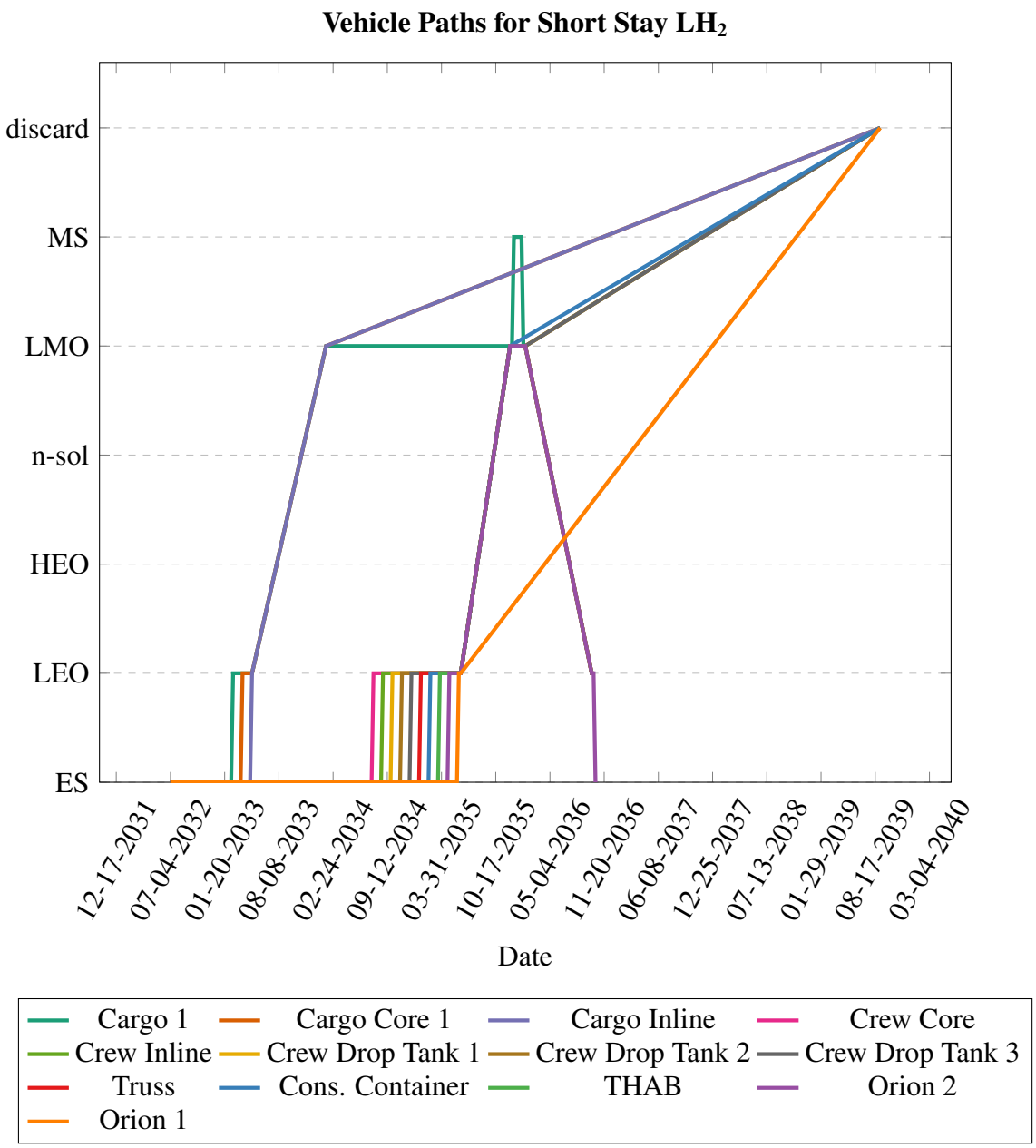

Figure 5.32: Vehicle paths for the short stay LH_2 NTP campaign option.

Table 5.16: Launch dates for every element in each surface stay campaign alternative.

	LH_2 Long Stay	**LH_2 Short Stay**
Crew Core	10/8/2034	7/16/2034
Crew Inline Tank	11/12/2034	8/20/2034
Crew Drop Tank 1	12/17/2034	9/24/2034
Crew Drop Tank 2		10/29/2034
Crew Drop Tank 3		12/3/2034
Truss	1/21/2035	1/7/2035
Cons. Container	2/25/2035	2/11/2035
TransHab	4/1/2035	3/18/2035
Orion Two	5/6/2035	4/22/2035
Orion One	6/10/2035	5/27/2035
Cargo 1 - MAV & ISRU	11/7/2032	2/13/2033
Cargo 2 - SHAB	12/12/2032	
Cargo 1 Core	1/16/2033	3/20/2033
Cargo 1 Inline 1	2/20/2033	4/24/2033
Cargo 2 Core	3/27/2033	
Cargo 2 Inline 1	5/1/2033	

Table 5.17: Launch vehicle selections for every element in each surface stay campaign alternative.

	LH_2 Long Stay	**LH_2 Short Stay**
Crew Core	Starship	SLS 2B
Crew Inline Tank	SLS 2B	Starship
Crew Drop Tank 1	SLS 2B	SLS 2B
Crew Drop Tank 2		SLS 2B
Crew Drop Tank 3		SLS 2B
Truss	SLS 2B	SLS 2B
Cons. Container	Starship	Starship
TransHab	FH	FH
Orion Two	SLS 1B	SLS 1B
Orion One	SLS 1B	SLS 1B
Cargo 1 - MAV & ISRU	SLS 2B	SLS 2B
Cargo 2 - SHAB	SLS 2B	
Cargo 1 Core	Starship	Starship
Cargo 1 Inline 1	Starship	Starship
Cargo 2 Core	Starship	
Cargo 2 Inline 1	Starship	

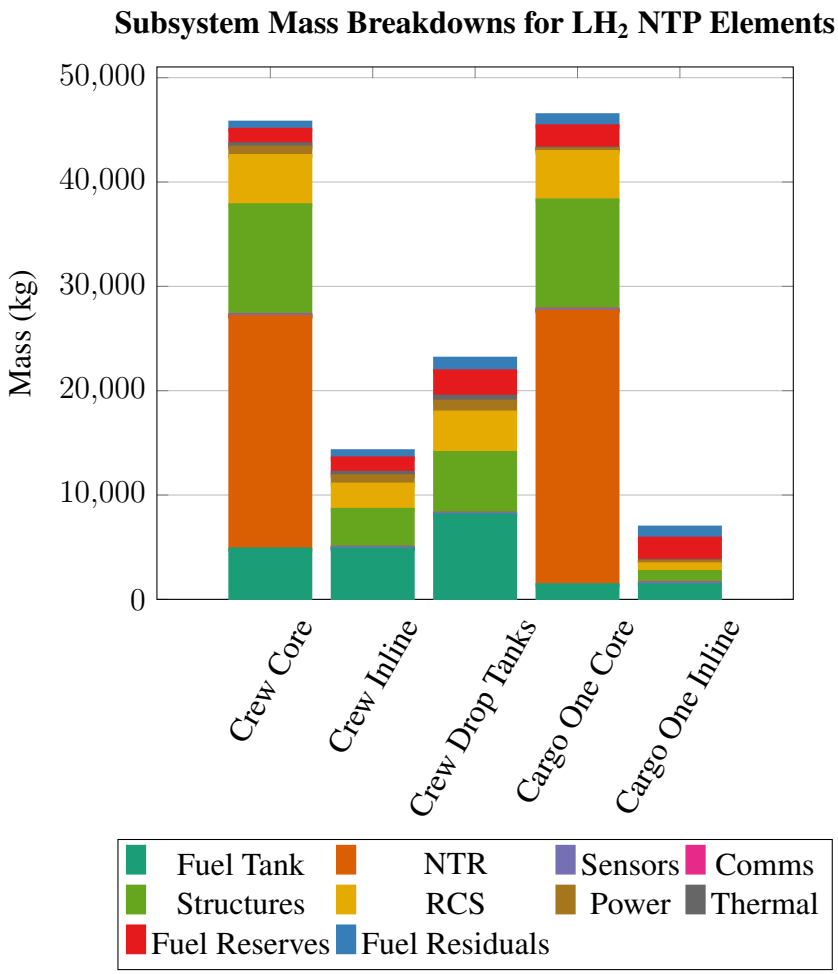

Figure 5.33: Subsystem-level mass breakdown for vehicles in LH_2 short stay campaign.

5.7 Analysis and Discussion

With these results, the main point to address is how they fill the gaps identified in the first three chapters and if they prove the overall hypothesis proposed by this research, restated below:

Overarching Hypothesis: If the CLO and VSS processes are integrated, then impacts of the vehicle and campaign trades on each other can be directly quantified.

Many effects between the different parts of the campaign and vehicle design problems that were identified through running the Mars campaign trade studies with this methodology. The chosen interplanetary missions affect the sizing of each individual subsystems, which also affect each other. These sizes not only affect the front end of the campaign, but that front end also affects the sizes themselves as all vehicles are constrained by what capability launch vehicles have. Depending on the campaign objective function, it may prefer larger, more expensive vehicles to reduce the number of launches with bigger vehicles or tend towards more, smaller launches. These questions are now answered in the loop with the direct integration and the large set of results; discussion from the previous two sections show that claim in the **Overarching Hypothesis** is supported.

As found during literature review, this iterative process is executed in the state-of-the-art, but the campaign and vehicle design processes are disintegrated and each one is run separately, limiting the ability to run trades in a relatively short amount of time. Further, although the set of results produced by CLO were also produced by DRA 5, sizing for the vehicles in DRA 5 was done at the system-level, meaning their NTP solution did not have a subsystem-level mass breakdown. Any vehicle trades performed using their method would not include the effects on the rest of the vehicle. That is a propellant species change would only show impacts on the mission and the overall system mass; it would be difficult to show how it affects the design of the tanks, the accompanying power, structural, and

more. Figure 5.34 is an n^2 diagram of the crewed mission VSS problem, showing all of the different design variables across the problem and their connections. Including these variables within CLO would likely significantly increase the runtime and by solving the vehicle MDAO problem externally, these subsystem-level sizing solutions can found more quickly. Other CLO formulations presented in Chapter 2 have the same limitations, as typically they do not represent the vehicle at the subsystem-level. The methodology proposed by Isaji *et al.* does integrate the vehicle MDAO problem and though it was stated that higher fidelity subsystem models could be integrated in a similar manner, but given the formulation itself, more complex ConOps like the ones found in DRA 5 may be harder to include.

With this integrated method, there is more information available even at this early stage of design, enabling more informed decision making. The relative speed in generating these solutions is another key improvement as these four alternative solutions with their detailed campaign and vehicle design information was generated over the course of 15 days. As mentioned in Chapter 2, NASA's took many months and hundreds of employees to build DRA 5, which still lacked some information at both, the campaign and vehicle levels. Tweaks in either design processes or running an additional trade can be done relatively quickly.

Since the primary input to VSS is the mission sequence and vehicle ConOps, if the optimal missions were known a priori, the VSS process could be used to find these solutions in more quickly. However, the only way to know the mission set is optimal is if you explored many of the available options, which is exactly what the CLO process is doing, but in a more algorithmic manner. It provides the optimal interplanetary transfers, launch and aggregation strategy, and even trading between the number of drop tanks and their size. Although it may be feasible to manually find this solution using only VSS, it may not be viable. The two processes are synergistic with each other and their integration improves the way campaign and vehicle design is done.

As the data from the vehicle and campaign-level trade studies supports it, **the Overarching Hypothesis can be accepted**, thereby achieving the **Research Objective** and filling the **Key Gap**.

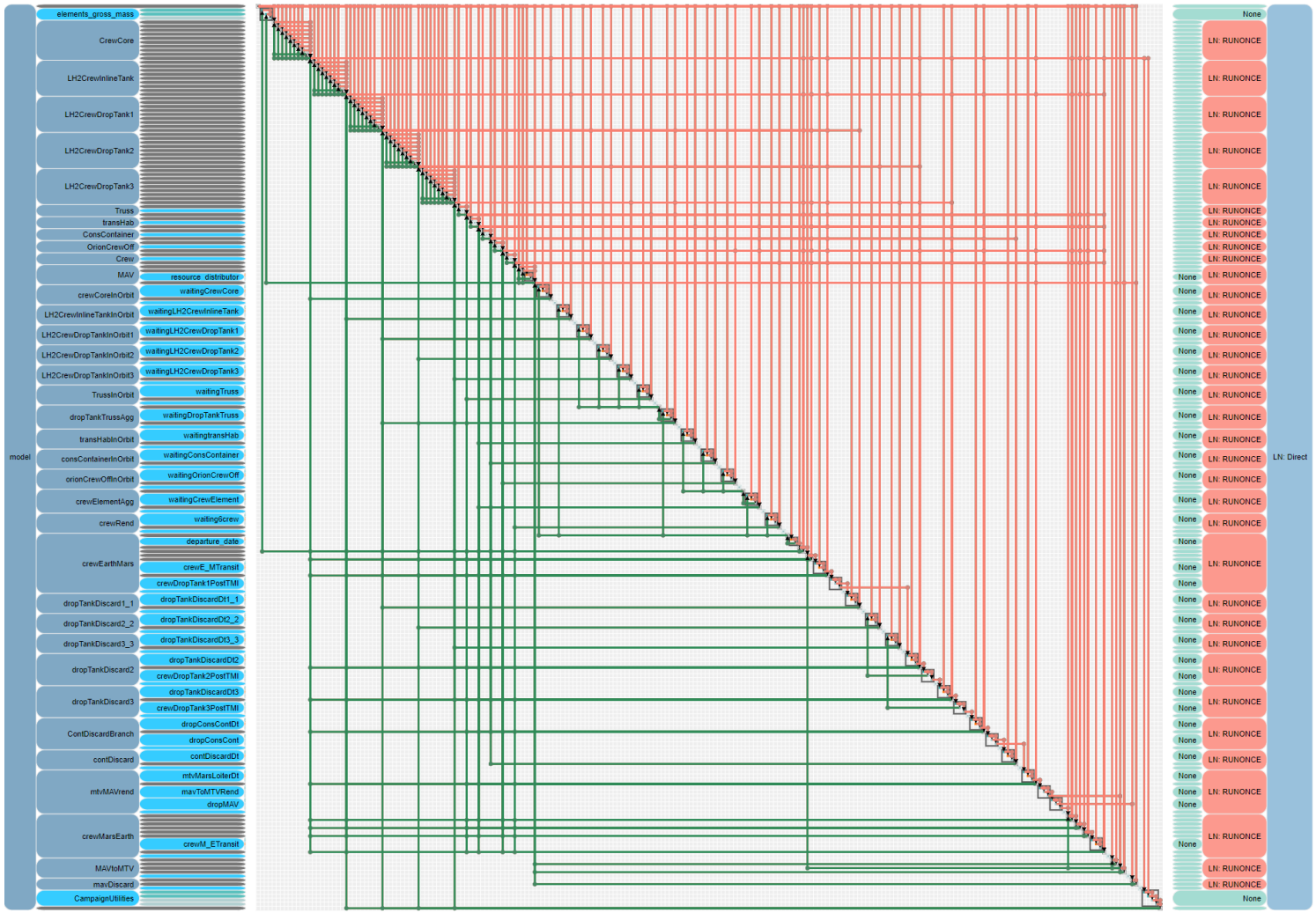

Figure 5.34: An n^2 diagram of the VSS problem for the short stay crew mission with LH_2.

6
CONCLUSIONS

With the goal of offering decision makers more information earlier on the SEC design process, the research objective was to establish a methodology for the concurrent design of SECs and transportation systems, enabling trade space exploration.

Fully integrated, the process is iterative in nature, where the converged solution is a final campaign, optimized for its goals, and each vehicle sized optimally at the subsystem level for its individual mission in the campaign. Integrating the two processes enables concurrent trade space exploration of the campaign and vehicle, where the impacts of changes in either can be directly assessed. The inclusion of VSS enables the assessment changes in subsystem level parameters on not only other subsystems on the vehicle, but the overall campaign and overall ConOps. Different campaign goals in this methodology could be implemented in CLO, which changes the mission set and sequence and further changes the sizes of the vehicles within. Ultimately, this methodology enables the generation of many different campaign alternatives in a relatively quick amount of time. Each vehicle in the campaign is supported by sizing of vehicles at the subsystem level, all of which provides decision makers more information up front to help make more informed down-selections.

The detailed state of the current state of the art was explored through a deep dive literature review to identify pieces that could be used to construct this methodology. The campaign design problem was found to be a complex, logistics optimization problem that can be represented through a TEGMCF. Paths enabled the modeling of complex ConOps of vehicle stacks and payload transfer in the campaign. By representing SEC as a space logistics network, the design problem could solved using mixed-integer programming to identify the optimal flow of resources throughout, and by extension, the optimal set and sequence of missions in the campaign. This solution drives the design of each vehicle in the

campaign, where each complex MDAO problem of transportation systems design is solved using a VSS process.

The final process structure of the integrated methodology was constructed by identifying the three main research questions and subsequent hypotheses and experiments. Through the first experiment, it was found that a NLGS solver performs better than Jacobi iterations by solving in fewer iterations. **Experiment 2** showed that for the problem to be considered fully converged, both vehicle and mission coupling variables should be used as the convergence criteria. That is, a valid solution must be both below the allowable tolerance on the mission and vehicle side. Before addressing **Hypothesis 3** directly, it was decomposed into two smaller research questions. From these two, it was found that solving the VSS problem first with a path guess that minimizes ΔV performs best for the overall methodology. With these results and the previous formulations identified from literature, the final process structure for the methodology was constructed in Figure 4.42.

Two trade studies were conducted at scale on a multi-year Mars campaign based on NASA's DRA 5. The NTP propellant species was used as the vehicle-level trade parameter, while surface stay duration was used for the campaign-level. Three propellants were explored: LH_2, NH_3, and H_2O, while a long stay of 504 days and short stay of 28 days were used as the campaign-level parameters. The vehicle trade study showed the drastic increase in mass required to used the higher density propellants, due to their much lower I_{sp}. The short-stay campaign was found to require a similar amount of mass to execute compared to the long-stay option, but with higher costs. All of the data exhibited expected behaviors showed that the methodology was successfully able to show the design sensitivities of campaigns and vehicles on each other, therefore resulting the acceptance of the overall hypothesis. The overall, fully decomposed structure of this research is presented in Figure 6.1.

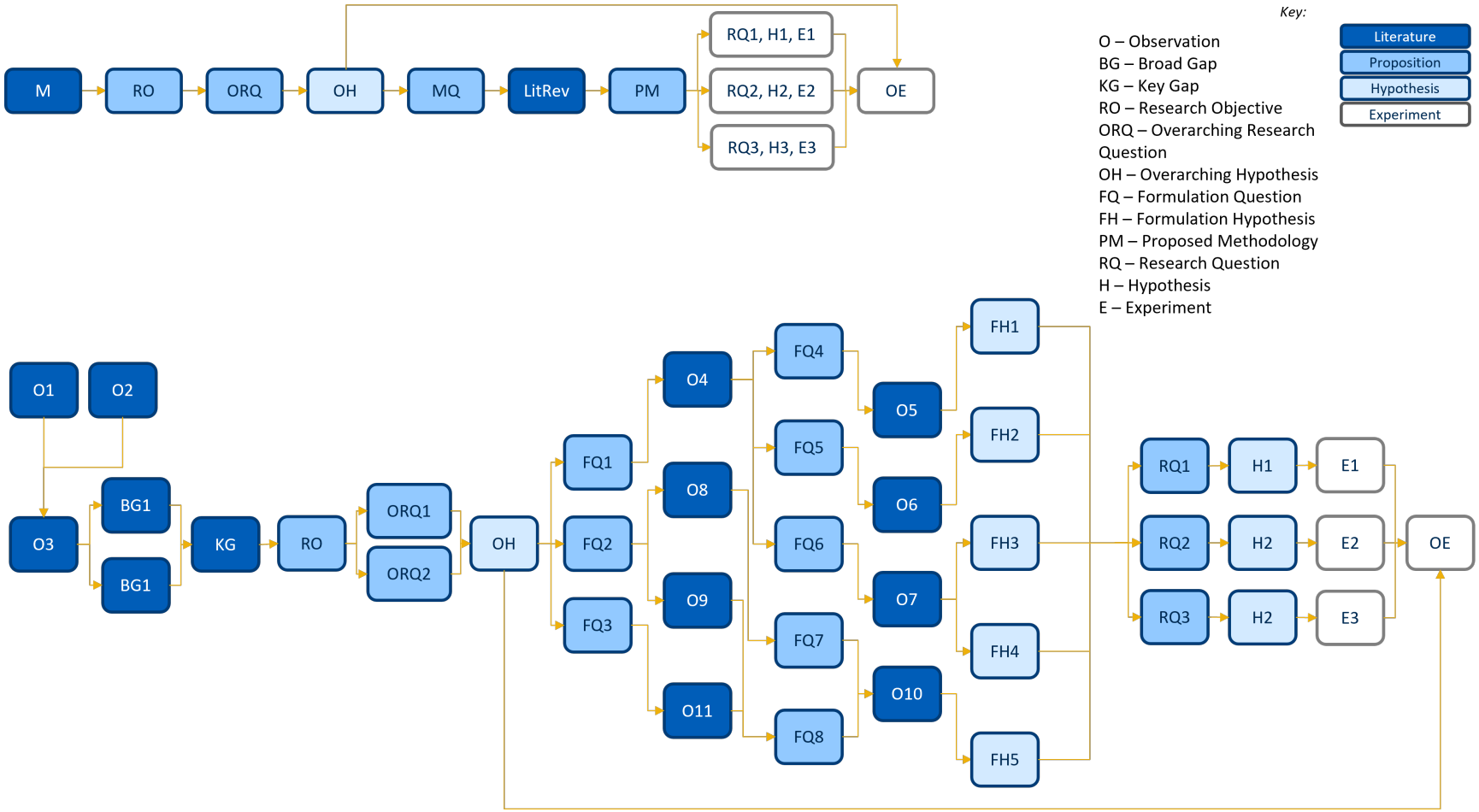

Figure 6.1: Fully formulated logic structure for this thesis.

6.1 Summary of Research Contributions

The primary contribution of this research is the methodology proposed to enable concurrent trade space exploration of campaigns and vehicles. Integrating these two individual processes allows decision makers to develop campaigns at the conceptual-level of design, but supported by sizing of individual transportation systems within at the subsystem-level. Not only does this mean this methodology provides more information earlier on in the design process, but because of the runtimes, any changes or trades can be conducted in a relatively quick amount of time. By formulating the campaign design problem as a logistics network to optimize, each solution produced can be considered the best strategy, given some objective. Inclusion of the VSS further means that each vehicle in the campaign is optimized for the specific mission it flies and changes in subsystem=level parameters can be propagated up to the campaign-level.

Although this research used the foundation of previous space logistics formulations, the specific implantation of CLO in this methodology includes the addition of nodal parameterization. Instead of representing each node as a fixed orbit, they represent a range of orbits, grouped by their orbital energy rather than a distance measurement. This way, launch arcs can also be parameterized to include a continuous function for the throw capabilities of each LV which allows each payload to be thrown as far as possible. For fixed node locations, if a payload mass is only slightly above the throw limit to a node, it is bumped down to a lower node, even though it may not be the optimal one. The nodal parameterization also enables the VSS to find the best orbit for each vehicle being sized. Higher fidelity trajectory analyses could be integrated through surrogate models to enable more mission-level trades that impact both the campaign and vehicle designs.

This specific implementation of CLO includes several features that model in-space operations that are key to looking at the campaign design problem with a more transportation centric approach. The concept of vehicle stacks was introduced with the previously es-

tablished idea of paths, which enabled the investigation of more complex campaigns and ConOps. Modeling payload transfers also enable proper modeling of crew and other dynamic payloads that are not simply sent to a single destination.

6.1.1 Expected Publications

The research proposed is expected to be the basis of a journal paper and a few conference publications that describe the methodology and specific technical contributions to the field. Improving the state of the art for SEC design by including VSS is the primary contribution that will be documented in a journal and conference paper. They will motivate the need for this capability and describe how each individual process was selected, implemented and eventually integrated for the methodology while also providing the results of the Mars campaign trade study. As a supplement, an additional paper can be written on the translation of campaign goals and mission scenarios for each lunar and Mars canonical example into the CLO formulation. Although an initial trade study for the Mars campaign was done, further studies can be performed using other trade variables and additional degrees of freedom, such as the vehicle architectures in Figure 1.8, as well as apply quantitative technology assessments. The same could be done for the lunar campaign, providing an independent assessment of the different HLS options to identify potential areas of improvement. Both papers will describe the CLO formulation as well as the subsystem level modeling used to generate the vehicle point designs.

6.1.2 Future Work

Technical improvements should directly contribute to adding capability or fidelity to the different design processes. Although vehicle stacks and payload transfers were added to the CLO process, some assumptions potentially limit the type of campaigns that could be assessed with this methodology. A key assumption is that any staged elements are done so at the end of an arc conflicting with the ideal operation of staging spent elements

immediately. This significantly affects modeling vehicles with many drop tanks used over the course of a single transfer, just like the ones shown in the previous chapter. For example, for the outbound opportunity, if four drop tanks are required for the burn, all 4 burn at the same time, rather than burning one and staging immediately. This is because a single arc requires the propellant load for the entire ΔV that arc requires. In other words, it would be beneficial to investigate how to break up large transfers into smaller ones for proper staging. A directly related limitation is the assumption that those large propellant burns are split evenly amongst the elements performing the burn.

Further blurring the line between how vehicles and payloads are modeled within CLO may not only help in addressing the previously mentioned limitation, but could enable exploration of more complex campaign strategies. Currently, due to the underlying different assumptions, variables, and constraints between a vehicle and payload, modeling specific architectures may required creative path definitions and other external constraints. By defining what moves through the campaign as a generic element, these elements can be utilized or built up in different ways much like the ontology defined in DYREQT. Fundamentally, this makes sense as more and more complicated vehicle architectures require resource sharing across elements in a stack, which is further exacerbated with crew, ISRU, or regular resupply missions. The combination of a more general definition of an element and paths may offer more flexibility in what campaigns can be modeled and what more trades can be conducted. Smaller fidelity improvements include: multi-element launches, path-enabled auto resupply logic from multiple locations, and ISRU refueling.

Although a rudimentary translation tool is integrated between CLO and VSS, a more robust solution is necessary for full automation. Currently, the translation tool must be setup for each problem, but runs automatically til convergence. To improve runtimes, the technical variables and constraints in Chapter 2 could be consolidated and refined so as to be sure none are overlapping.

Appendices

APPENDIX A

SUBSYSTEM MODEL DESCRIPTIONS

A.1 Avionics

Avionics subsystems are modeled and sized primarily by user defined component set, divided into the main groups of: Actuators, Sensors, Communications, and other miscellaneous devices. Sizing algorithms are mainly sourced from [112] and are used to estimate the mass and power draws for every component. Miscellaneous devices require a user input count, unit mass, and unit power. It is assumed that 90% of the power required by all avionics equipment is waste heat that needs to be rejected by the thermal subsystem.

A.1.1 Actuators

There are three main actuators considered for the avionics subsystems for in-space transportation systems: reaction wheels, Control Moment Gyros (CMG), and Magnetic Torquers (MT). Both the mass and power of each component is estimated using a piecewise linear approximating function, a general form shown in Equation A.1, where the dependent variable is the overall system mass. The slope and intercept for this approximating function depends on the actual component, and a list is shown in Table A.1

$$m_{avionics} = n_{component} * \begin{cases} \frac{y_{comp,max} - y_{comp,min}}{10000} * m_v + y_{comp,min} & \text{if } m_v < 10000 \\ y_{comp,max} * m_v & \text{if } m_v \geq 10000 \end{cases} \tag{A.1}$$

Table A.1: List of coefficients for estimating the mass of actuators as a linear approximation.

	Component	y_{min}	y_{max}
Mass	Reaction Wheels	2	20
	CMGs	0.1	10
	MTs	0.4	50
Power	Reaction Wheels	10	100
	CMGs	90	150
	MTs	0.6	16

A.1.2 Sensors

The sensors follow the same model as the actuators, of a linear approximating function, but the dependent variable here is the accuracy required. There are a total of six sensor components considered, listed below in Table A.2, along with their linear coefficients.

Table A.2: List of coefficients for estimating the mass of sensors as a linear approximation.

	Component	y_{min}	y_{max}
Mass	Gyros	0.1	15
	Sun Sensors	0.1	2
	Star Sensor (Scanner)	2	5
	Star Sensor (Fixed)	1	4
	Horizon Sensor	0.5	3.5
	Magnetometer	0.3	1.2
Power	Gyros	0.6	16
	Sun Sensors	0	3
	Star Sensor (Scanner)	0.6	16
	Star Sensor (Fixed)	5	10
	Horizon Sensor	0.3	5
	Magnetometer	0	1

A.1.3 Communications

The mass and power estimation of communications equipment is done via simple Master Equipment List (MEL) aggregation. That is, the total mass of equipment is the sum of the number of equipment and their mass densities, again sourced from [112]. The power required calculation is handled the same way. A table of the considered communications

equipment and their mass densities are listed in Table A.3, while the power densities are listed in Table A.3.

Table A.3: List of unit mass values used to estimate the total mass of communications equipment.

Component	Unit Mass [kg/count]
S-Band Transponder	3.5
S-Band Diplexer	0.2
S-Band Cables	3
S-Band Antenna	0.4
X-Band Transmitter	0.2
X-Band Cables	0.2
X-Band Antenna	0.2
X-Band Transponder	3
X-Band TWTA	2.5
X-Band Diplexer	0.6
X-Band Switching Network	0.75
X-Band Cables (Deep Space)	5
X-Band Low Gain Antenna	0.7
X-Band Med Gain Antenna	1.5
X-Band High Gain Antenna	6
Ka-Band Exciter	0.3
Ka-Band TWTA	2.8
Ka-Band Waveguide	3
Ka-Band Antenna	2.5
Ka-Band Oscillator	1.3
Wireless Sensors	Input

A.2 Propulsion

A.2.1 Tanks

The tanks subsystem model sizes many different components related to propellant storage and distribution, all for a single tank. For vehicles with multiple tanks, this subsystem model is called multiple times. Based on the inputs and amount of propellant required, the geometry of each tank is calculated and used to estimate the bare dry mass. Additional

Table A.4: List of unit power values used to estimate the total power required of communications equipment.

Component	Unit Power [W/count]
S-Band Transponder	22
S-Band Diplexer	0
S-Band Cables	0
S-Band Antenna	0
X-Band Transmitter	0
X-Band Cables	0
X-Band Antenna	0
X-Band Transponder	0
X-Band TWTA	25
X-Band Diplexer	0
X-Band Switching Network	0
X-Band Cables (Deep Space)	0
X-Band Low Gain Antenna	0
X-Band Med Gain Antenna	0
X-Band High Gain Antenna	0
Ka-Band Exciter	1.5
Ka-Band TWTA	40.5
Ka-Band Waveguide	0
Ka-Band Antenna	0
Ka-Band Oscillator	2.5
Wireless Sensors	Input

mass is added to account for any propellant management devices, as well as active and passive thermal control systems.

Geometry

The geometry of the tank is driven primarily by an input l/d ratio and the total propellant required calculated using the sizing mission. Given the density of the propellant in the tank, the diameter of the tank can be calculated analytically using Equation A.2-Equation A.4. The length of the tank is then simply the product of the diameter and the l/d ratio. If the ratio is 1, the length of the tank is zero as the tank is a sphere.

$$V_{prop,total} = ullage * ((m_{prop,required} + m_{prop,trapped})/\rho_{prop}) \tag{A.2}$$

$$d_{tank} = \begin{cases} (12 * V_{prop,total}/(\pi * (3(l/d) - 1)))^{1/3} & \text{if } l/d \geq 1 \\ (24 * V_{prop,total}/(\pi * (l/d) * (3 + (l/d)^2)))^{1/3} & \text{if } l/d < 1 \end{cases} \tag{A.3}$$

$$l_{tank} = \begin{cases} l/d * d_{tank} & \text{if } l/d \geq 1 \\ 0 & \text{if } l/d < 1 \end{cases} \tag{A.4}$$

Hardware Mass

To estimate the bare dry mass of the tank, the thickness of the tank is calculated using the set tank pressure and the structural properties of the material. The mass can then be calculated using the material density, surface area and thickness of the tank, all shown below.

$$t = \frac{pk_{safety}d}{4\sigma} \tag{A.5}$$

$$m_{tank} = A_{surface,tank} * t * \rho_{material} \tag{A.6}$$

$$m_{separator} = 0.2m_{tank} \tag{A.7}$$

$$m_{misc,hardware} = 0.05 * m_{tank} \tag{A.8}$$

$$m_{lad} = 0.537 * m_{tank} \tag{A.9}$$

$$m_{total} = m_{tank} + m_{separator} + m_{lad} + m_{misc,hardware} + m_{mli} + m_{pressurant,sys} + m_{crycooler} \tag{A.10}$$

Thermal Control Systems Mass

Both passive and active thermal control systems are accounted for in this subsystem. Spray On Foam Insulation (SOFI) and Multi-Layer Insulation (MLI) are the primary drivers of passive systems, with the main inputs being SOFI thickness and the number of MLI layers. The sizing algorithms are shown below:

$$A_{surface,mli} = 2\pi(d_{tank}/2)^2 + (\pi d_{tank} l_{tank}) \tag{A.11}$$

$$m_{mli} = 1.1 * A_{surface,mli} * 0.018 * n_{mli} \tag{A.12}$$

$$l_{tank,out} = l_{tank} + 2t \tag{A.13}$$

$$d_{tank,out} = d_{tank} + 2t \tag{A.14}$$

$$R_c = d_{tank,out}/2 \tag{A.15}$$

$$H_c = l_{tank,out} - d_{tank,out} \tag{A.16}$$

$$R_d = d_{tank,out}/2 \tag{A.17}$$

$$H_d = d_{tank,out}/2 \tag{A.18}$$

$$V_0 = \pi R_c^2 H_c + 4.0 R_d^2 * H_d/3.0 \tag{A.19}$$

$$R_c = R_c + t_{sofi} \tag{A.20}$$

$$R_d = R_d + t_{sofi} \tag{A.21}$$

$$H_d = H_d + t_{sofi} \tag{A.22}$$

$$V_f = \pi R_c^2 H_c + 4.0 * R_d^2 * H_d/3.0 \tag{A.23}$$

$$m_{sofi} = (V_f - V_0) * \rho_{sofi} \tag{A.24}$$

Given the use of cryogenic propellants for both campaigns considered for this thesis, it is important to establish a process for estimating the mass of active CFM systems. This starts with estimating the thermal penetration into the tank based on the environment it is operating in. The heat absorbed by the spacecraft from the sun, reflected heat from the orbiting body, and radiated heat from the orbiting body are calculated as: [143]

$$Q_{sun} = \frac{1,368}{(d_{sun})^2} \tag{A.25}$$

$$Q_{body,reflected} = albedo * viewfactor * Q_{sun} \tag{A.26}$$

$$Q_{body,radiated} = k_b * viewfactor * (T_{body})^4 \tag{A.27}$$

$$\tag{A.28}$$

The heat penetrating the MLI of the tank is estimated using: [144]

$$T_c = T_{tank} \tag{A.29}$$

$$T_h = ((\frac{\alpha_{mli}}{k_b \epsilon_{mli}}) * (Q_{sun} + Q_{body,reflected} + \tag{A.30}$$

$$\frac{\epsilon_{mli}}{\alpha_{mli}} Q_{body,radiated}) * (\frac{A_{cross,tank}}{A_{surface,mli}}))^{0.25} \tag{A.31}$$

$$\tag{A.32}$$

$$\begin{aligned} Q_{mli} = 3 * (A_{surface,mli} * (2.4e-4 * (.017 + 7e-6 * (800 - (T_h - T_c)/2) + \\ .0228 * log((T_h - T_c)/2)) * 10^{2.63} * (T_h - T_c) + \\ 4.944e-10 * \epsilon_{mli} * (T_h^{4.67} - T_c^{4.67}))/n_{mli}) \end{aligned} \tag{A.33}$$

Using the estimate of heat penetrating the MLI layers, the cryocooler power and the boiloff rate can be calculated using Equation A.34 and Equation A.35, taken from [145].

$$\begin{aligned} Q_{cryocooler} = Q_{mli} \\ P_{cryocooler} = 7.0677 * \frac{\delta p_{bac}}{p_{inlet}} + (8.435 Q_{cryocooler} - 14.83) \end{aligned} \tag{A.34}$$

$$rate_{boiloff} = \frac{0.15 Q_{mli}}{h_{vap,prop}} \tag{A.35}$$

Finally, the mass of the cryocoolers are estimated using a scaling function based off of ongoing test elements from [146], with a 50% margin included:

$$m_{crycoolers} = 1.5 * \frac{26}{208} * 0.15 * Q_{mli} \tag{A.36}$$

A.2.2 Chemical Engines

Chemical engines are sized using first principle physics-based relationships. The main inputs for this model are the number of engines to size, thrust, I_{sp}, and the engine Thrust to Weight Ratio (T2W). The dry mass is simply calculated using:

$$m_{engines} = n_{engines} \frac{T_{max,engine}}{g_0 \frac{T}{W}} \tag{A.37}$$

A.2.3 Nuclear Thermal Rockets

Sizing of NTRs are critical to this thesis given their use in the final case study. This model estimates the mass of the engine assembly, nuclear reactor, radiation shield, and accompanying structures for an NTR, adapted from [147].

A.2.4 RCS

Sizing of RCS is typically performed similarly to main chemical propulsion systems, including engines and tanks. However, since RCS burns are not modeled in CLO, there are no equivalent burns in the sizing missions in VSS. Therefore, the previous models cannot be used. Instead, for the purposes of this research, the RCS for each vehicle is modeled as a fraction of the inert mass, in this case as 20%. The fraction includes the propellant itself, as well as storage and distribution systems and engines.

A.3 Structures

Estimating the mass of the structural components of a spacecraft can be very challenging due its dependence on the configuration. Creating a general sizing algorithm for this subsystem that is valid for many different types of transportation systems is even more challenging. As a result, the structural mass of each vehicle considered in this method

will be estimated as a fraction of the total inert mass of the vehicle. The specific ratio is dependant on the problem, and furthermore the vehicle, and so it is user input.

A.4 Thermal

For this research, the thermal subsystem only sizes the radiators required to reject heat loads from the spacecraft. Systems for propellant thermal control are sized by the tank subsystem model. Radiators are sized using an input area mass density, which should include the mass of any hardware for plumbing of coolants in the radiator systems. The radiator area is calculated using Equation A.38 below, where the temperature space is assumed to be 3K and the surface temperature of the radiator is 250K.

$$A_{rad} = \frac{Q_{rej}}{k_b \epsilon_{rad} \eta_{fin} (t_{rad}^4 - t_{space}^4)} \tag{A.38}$$

$$m_{rad} = \rho_{rad} A_{rad} \tag{A.39}$$

A.5 Power

The power subsystem sizing model includes power generation, distribution, and storage. Generation of power in-space is assumed to be sourced fully by solar energy and therefore requiring photovoltaic systems. The sum of all power requirements on the system is treated as peak power, and the average power is used to size the solar array. Based on input solar cell efficiencies, degradation, and eclipse time, the power generation required is defined by Equation A.40

$$P_{array} = \frac{(\frac{P_{req} t_{ecllpse,max}}{0.8 \eta_{transmission}}) + (\frac{P_{req}(t_{period} - t_{eclipse,max})}{0.8})}{t_{period} - t_{eclipse,max}} \tag{A.40}$$

The solar energy available depends on the distance from the sun, scaled using the inverse square law, anchored to 1,368 W/m^2 at 1 AU. Using the solar flux, the beginning of life power, P_{BOL}, can be calculated using the cell efficiency, as shown in Equation A.41.

$$P_{BOL} = \eta_{cell} * \frac{1,368}{(d_{sun})^2} \tag{A.41}$$

Given the mission duration and cell degradation rate, the end of life power can then be estimated, in Equation A.42

$$P_{EOL} = P_{BOL} * \frac{1 - deg_{cell}}{100}^{t}_{mission} \tag{A.42}$$

Finally, the required solar array area and subsequent mass is calculated using:

$$A_{array} = P_{array}/P_{EOL} \tag{A.43}$$

$$m_{array} = \rho_{array} A_{array} \tag{A.44}$$

Batteries are assumed for power storage, sized based on a given depth of discharge, energy density, and eclipse time, as shown in Equation A.47

$$cap_{batt} = P_{req} * \frac{t_{ecllpse,max}}{dod\eta_{transmission}} \tag{A.45}$$

$$m_{batt} = \frac{cap_{batt}}{\rho_{batt}} \tag{A.46}$$

Finally, the power distribution system mass is estimated using:

$$m_{pmad} = \frac{0.17}{0.83}(m_{array} + m_{batt}) \tag{A.47}$$

The waste heat is estimated just as a fraction of the power generation required of the subsystem.

APPENDIX B

HLS CAMPAIGN SOLUTION

Though the objective of this research is to establish an integrated design methodology as the main contribution, the results produced by it can be investigated as well. Figure B.1 shows the optimized mission sequence for the HLS campaign, or set of arcs that each of the three propulsive elements take. The AE is launched first on a SpaceX Falcon Heavy at 0, and takes the 100 day slow transfer to NRHO for aggregation. A SpaceX Starship launches the DE on day 30, which also takes the slow transfer to NRHO. When the TE launches at Day 101, the AE will have arrived in NRHO, while DE will have not, meaning it is the last to arrive at the aggregation location. Since Orion and the Crew are constrained to launch after all three elements have aggregated, they are launched at Day 130. Once the Crew arrive after a fast transfer, two of them transfer to the AE over the course of a day, before the whole stack descents to LLO and the TE is spent. The DE performs the descent burn and is spent on the surface. After the 7 day surface stay the Crew ascends back to NRHO through LLO, to transfer back to Orion for departure. Figure B.2 show the transfer of the two sets of crew between the AE and Orion, and can also be seen in the mass history of both vehicles. Orion then performs a lunar flyby to return to Earth on Day 156.

Figure B.1: Vehicle paths for the HLS campaign solution with objective value of 0.724.

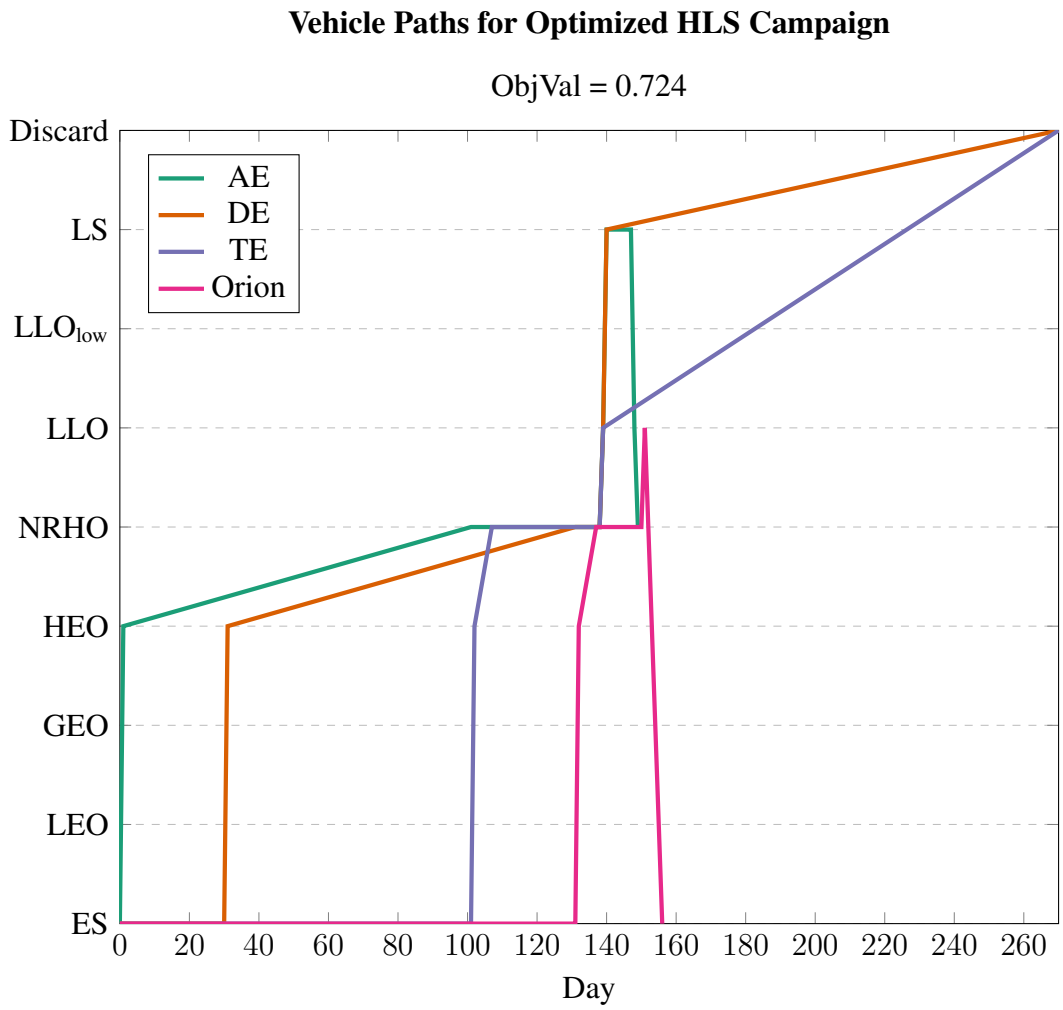

Figure B.2: Optimized paths for the Gateway and Surface Crews for the three element HLS campaign, showing the two transfers between the AE and Orion.

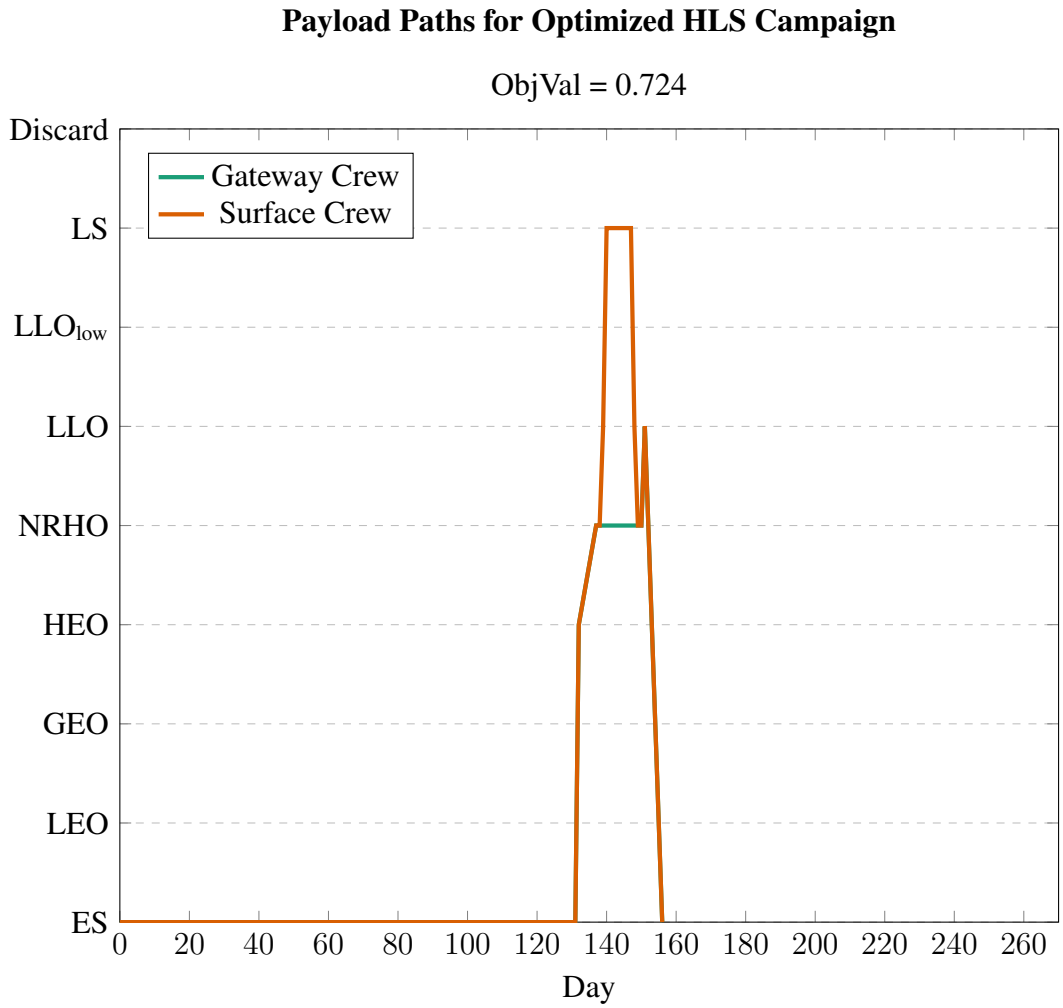

Figure B.3-Figure B.5 show the mass histories of each vehicle, including the propellants, payloads, and any consumables. Since the AE is the only element with active CFM systems, its propellant masses do not passively decrease over time, reflected in the flat slopes after launch. In contrast, both the TE and DE have nonzero slopes between their'' transfers. With the implementation of stacks in the CLO process, the propellant mass histories properly reflect the difference between the passive and active elements. For example, at time 138, the TE burns nearly all of its propellant before discarding itself and immediately after, the DE does the same. Table B.2 summarizes the final, optimized ΔV splits for each vehicle and Table B.1 summarizes the launch architecture.

Table B.1: Table summarizing the launch architecture for the optimized HLS campaign.

Vehicle	**Launch Vehicle**	**Launch Day**	**Launch Cost**
AE	SpaceX Falcon Heavy	0	$97,000,000
DE	SpaceX Starship	30	$250,000,000
TE	SpaceX Falcon Heavy	101	$97,000,000
Orion	SLS 1B	131	$3,000,000,000

Table B.2: Table of optimized cislunar ΔVs [m/s] for the final HLS campaign, where row headers are departure locations and column headers are arrival locations.

	NRHO	**LLO**	**$\mathbf{LLO_{low}}$**	**LS**
NRHO	0	393.75	1,750	0
LLO	656.25	0	0	1,636.25
$\mathbf{LLO_{low}}$	1,750	0	0	870
LS	0	1,636.25	870	0

With each of the three elements represented as a collection of subsystems, the VSS process can provide a subsystem mass breakdown for each one, shown in Table B.3. The AE has the highest inert mass, primarily driven by the 1.1t crew cabin that it carries. The DE and TE have very similar mass breakdowns, which is expected as they perform very similar missions. Tanks on the DE are slightly more massive than those on the TE as its propellant load is higher.

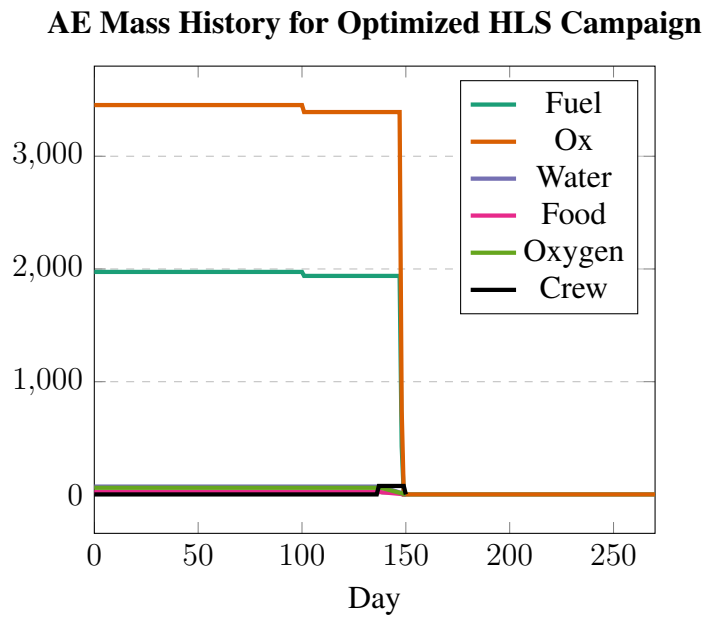

Figure B.3: Mass history of the AE in the optimized HLS campaign.

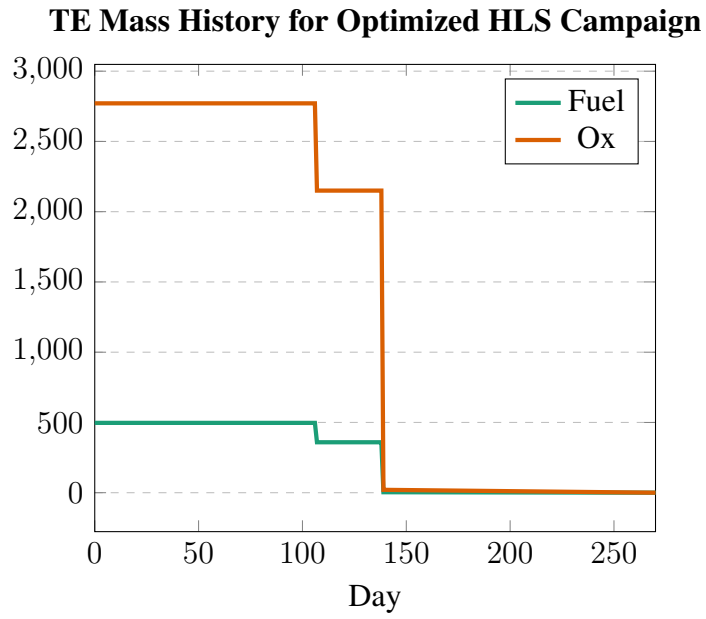

Figure B.4: Mass history of the TE in the optimized HLS campaign.

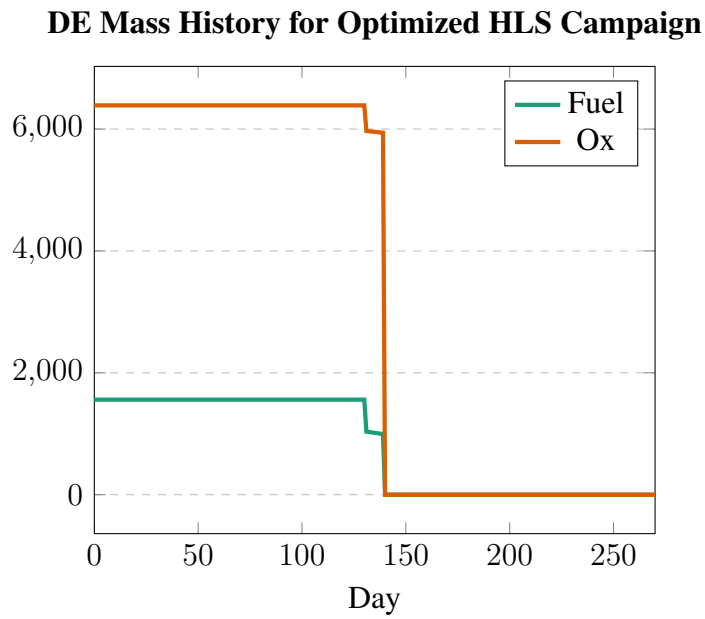

Figure B.5: Mass history of the DE in the optimized HLS campaign.

Table B.3: Table summarizing the launch architecture for the optimized HLS campaign.

Subsystem	AE [kg]	DE [kg]	TE [kg]
Fuel Tank 1	95.89	101.29	94.88
Fuel Tank 2	95.89	101.29	94.88
Ox Tank 1	99.40	95.73	91.03
Ox Tank 2	99.40	95.73	91.03
RCS	497.11	857.26	862.42
Engines	72.60	72.60	72.60
Sensors	10.13	10.13	10.13
Comms	95.89	101.29	94.88
Structures	1,395.52	1,061.37	1,067.76
Power	209.65	134.54	210.83
Thermal	52.97	100.01	57.73
Crew Cabin	1,136.00	0	0
Propellant Reserves	277.21	404.56	163.12
Propellant Residuals	138.60	8202.28	81.56
Total	**5,307.53**	**4,536.93**	**4,198.14**

APPENDIX C

METHOD EXECUTION PROCEDURE AND VALIDATION - HLS BASELINE

Though experimentation in Chapter 4 produced a final methodology structure and campaign solution for HLS, it is important to ensure the data produced by the methodology is accurate. The HLS solution in Appendix B was produced independently through experimentation, but the reference campaign presented by Trent and Edwards and reproduced by Zhu *et al.* can be considered as the baseline. In this campaign, the overall ConOps are very similar to the one presented in Chapter 4 but all three elements take a fast transfers to NRHO. To see if this methodology can reproduce these results, the degrees of freedom on the mission and ConOps are removed. All other assumptions and inputs are the same, including the network, vehicle subsystem definition, and vehicle design parameters. Since the launch vehicle selection was not presented in the government reference architecture, only the differences in masses for each vehicle are assessed. This validation will also serve as a description of steps required to execute the overall methodology.

C.1 Step 1: Campaign Problem Definition

Define the Network

Definition of the campaign network is driven primarily by defining the spatial nodes being considered as well as the time domain and timesteps. The latter could also be anchored to a specific date for campaigns that need that information, for example, interplanetary transfers. For this HLS problem, the following spatial nodes are chosen: Earth Surface, LEO, HEO, NRHO, LLO, and the Lunar Surface. With these nodes, a valid set of arcs is generated entirely by the user, with the main set of inputs to support them being a dataset of ΔV and ΔT costs for them, as shown in Table 4.2. In other words, it is entirely on the

user to generate the full set of arcs that model the types of transfers being considered. For this problem, launch arcs cover connections from to Earth LEO and HEO, and transfers to NRHO are can only be done through HEO. Since all three elements in the reference architecture use a fast transfer only minimum energy data is required. Transfers between NRHO and LLO occur at every timestep and in both directions, and descent arcs to the Lunar Surface from LLO are the same. However, ascents from the Lunar surface to LLO occur once every 7 timesteps, to model the phasing required into NRHO

Define the Vehicles and Payloads

Vehicles in the CLO problem are split into two groups: in-space and launch. Launch vehicles are defined by the parameters listed in Table 4.5 and Table 4.6, while in-space vehicles are defined as in Table 4.4. Further, for in-space vehicles, all stacks being considered must be defined as a set of the elements that they comprise of. In this case, the HLS stack is made up of the three propulsive elements: AE, DE, and TE. Though Orion is considered in the network, it stays in NRHO for the duration of the surface mission. Payloads are defined in a similar manner, as defined in Subsection 2.6.5.

Define the Paths

With the vehicles, payloads, and network defined, paths can be defined as a series of events of five types: ΔV, ΔT, ΔM, aggregate, or launch. For ΔV events that have stacks, the operating stack must be defined, as well as the active or propulsive element. Orion is pathed to launch on an SLS 1B with both the surface and gateway crews, but all other elements' launches are not. For this problem, the HLS path starts with aggregation of all four elements in NRHO, followed immediately by the surface crew transferring from Orion to the AE. Afterwards, the HLS stack descends to LLO using the TE as the active element, which is then staged. For vehicles that are staged, a staging location must be defined, or otherwise defaults to a discard node at the final timestep. Similarly, the DE performs the descent burn

to the lunar surface and is staged there. After the surface stay, the AE ascends to NRHO through LLO where the crew transfers back to Orion, which performs a lunar flyby on its way to Earth.

Define Campaign Optimization Problem

The code behind the methodology will generate the corresponding MIP variables for the defined problem, but it is necessary to define any additional, external constraints on the problem beyond in the ones detailed in Subsection 2.6.7. This is in addition to any more objective terms that may be necessary to properly model the campaign goals. Finally, specific Gurobi parameters can be set to constrain the runtime, set the tolerance, and flag any input or output files to save.

C.2 Step 2: Vehicle Problem Definition

Establish Vehicle Architectures and Design Parameters

The main set of inputs for the VSS problem is the breakdown of vehicles into the subsystems that are being modeled. Since DYREQT primary purpose is to be the synthesis tool, it is entirely on the user to bring in subsystem sizing models in the form of python code to integrate within. For this problem and others considered for this research, the subsystem models are described in Appendix A. Accompanying the subsystem models, listed in Table 4.9, will be the design parameters for each one, which for this problem are the same as listed in Table 4.10.

Define Mission Translation

The main purpose of the mission translation is to convert the data output format of the CLO process to the data input format of DYREQT. Due to the complexity between path definition and mission input definition, this translation procedure must be user defined per problem; there is no catch all translation. However, the writing of inputs to each individual

problem is already built; that is, based on the output values, those values are written to the appropriate locations for each problem. For example, once each vehicle is sized by VSS, code is already built to take those values and write them to the vehicle input file for CLO. Therefore, the primary purpose of mission translation is to update the sizing missions for VSS as solved by CLO.

Define Mission Analysis Optimization Problem

Since the use of parameterized orbital nodes is problem dependent, the setup of the mission analysis optimization problem is also problem dependent. That is, based on what nodes in the problem should be parameterized, those nodes should be defined as design variables and the accompanying objective function should be constructed. As the problem being considered for this chapter is a validation case, no nodes are parameterized and so there are no mission degrees of freedom. For the HLS problem used for experimentation, the parameterized nodes and the accompanying ranges for mission analysis are presented in Subsection 4.2.3.

With all of this defined, a final convergence tolerance can be set, but the default is 5%. Based on the input paths, the method will initialize the vehicle problem by identifying the path with the minimum ΔV. If the mission translation is written correctly, this process should then require no user interaction, and will either produce a converged this result or diverge. This process can be repeated for each campaign that is being considered, as well as each trade variable.

C.3 Validation

For the HLS baseline mission used here, the reference ConOps is depicted in Figure C.1 and the final solution is detailed in Table C.1. Since modeling of RCS burns and subsequent propellant is not being considered for this thesis, in order to model total propellant usage in line with the reference, it was assumed that 5% of the total propellant in the reference

solution is RCS. It is then bookkept in the inert mass just as it is in both the CLO and VSS processes. The methodology was able to converge on a solution in the first iteration, and the mass results for both the initialized VSS problem as well as the subsequent solution found by CLO with those vehicle masses are also listed in Table C.1. Validation of the subsystem models was performed by Trent in [18]. All errors are either at or below 5%, which is sufficient for this research. The largest difference in masses occurs in the descent element, which is likely due to the difference in how boiloff is modeled between the reference and VSS. Over the course of the entire campaign, even small difference in boiloff rates can be significant.

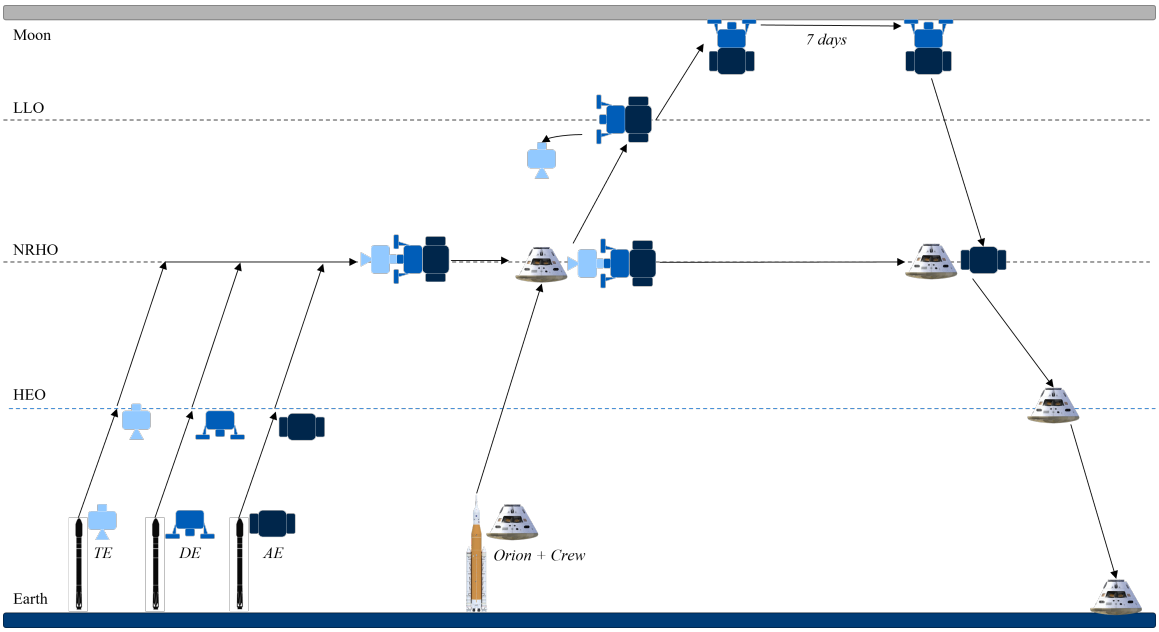

Figure C.1: Reference ConOps for the HLS baseline mission used for validation, adapted from [148].

Table C.1: Table showing the comparison of results between the methodology and reference HLS architecture [148, 126].

	Mass Type (kg)	**Reference**	**VSS**	**CLO**	**Error Between VSS and Reference**	**Error Between CLO and Reference**
Ascent Element	Inert	5,173	5,210	5,210	1%	1%
	Propellant	7,621	7,674	7,664	1%	1%
	Gross	12,794	12,884	12,874	1%	1%
Descent Element	Inert	5,784	5,567	5,567	4%	4%
	Propellant	10,547	11,067	11,045	5%	5%
	Gross	16,331	16,634	16,612	2%	2%
Transfer Element	Inert	5,473	5,356	5,356	2%	2%
	Propellant	9,490	9,256	9,253	2%	2%
	Gross	14,963	14,612	14,609	2%	2%

APPENDIX D

MARS TRADE STUDIES CONVERGENCE PERFORMANCE

D.1 Vehicle-level Trade Study

D.1.1 LH_2 NTP

Figure D.1: Errors for the vehicle inert masses per iteration for the LH_2 NTP option.

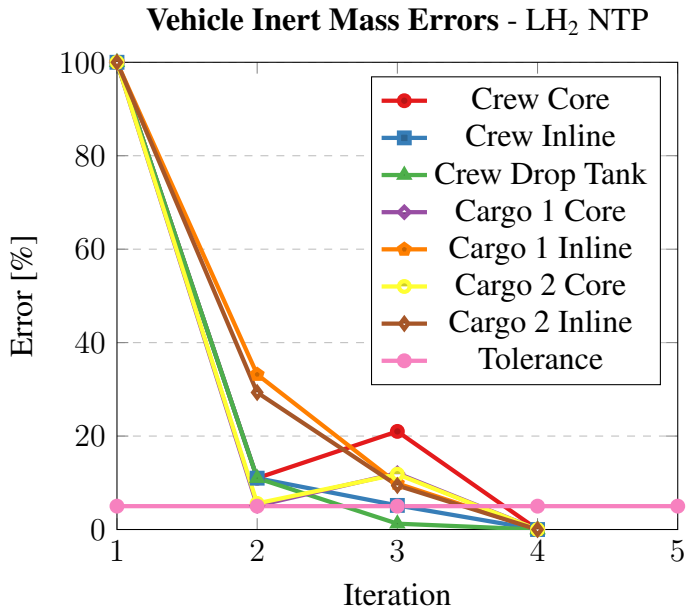

Figure D.2: Errors for the vehicle gross masses per iteration for the LH_2 NTP option.

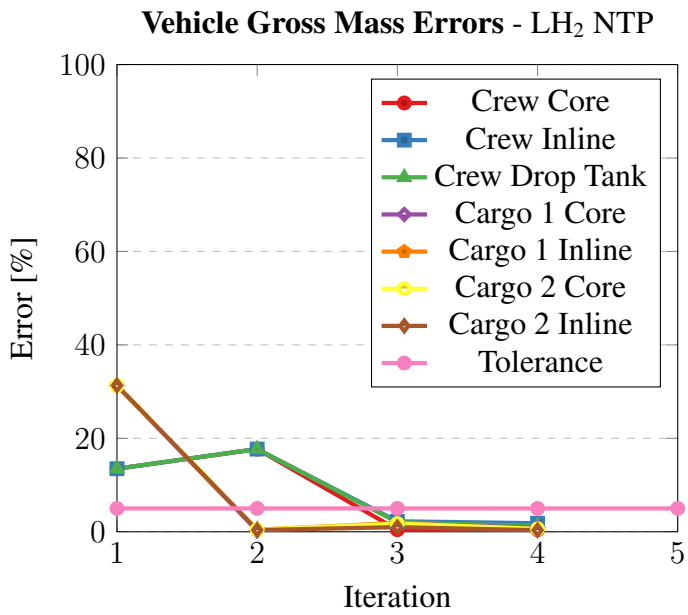

D.1.2 NH_3 NTP

Figure D.3: Errors for the vehicle inert masses per iteration for the NH_3 NTP option.

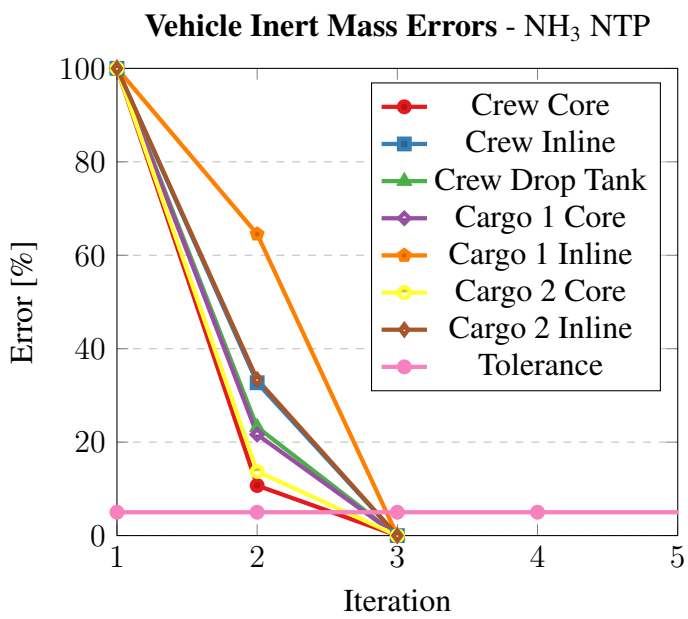

Figure D.4: Errors for the vehicle gross masses per iteration for the NH_3 NTP option.

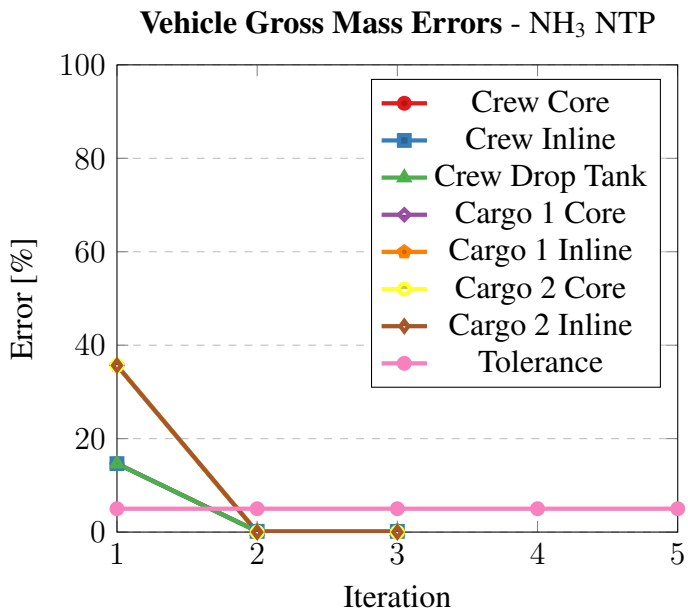

D.1.3 H_2O NTP

Figure D.5: Errors for the vehicle inert masses per iteration for the H_2O NTP option.

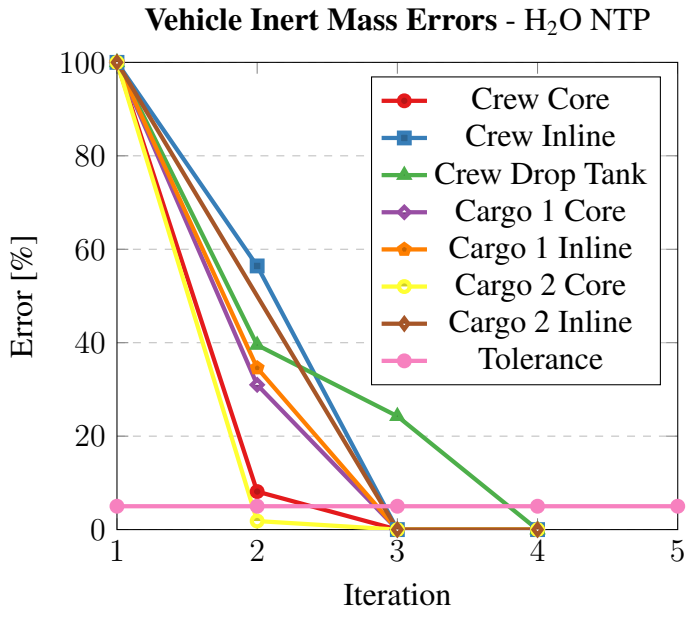

Figure D.6: Errors for the vehicle gross masses per iteration for the H_2O NTP option.

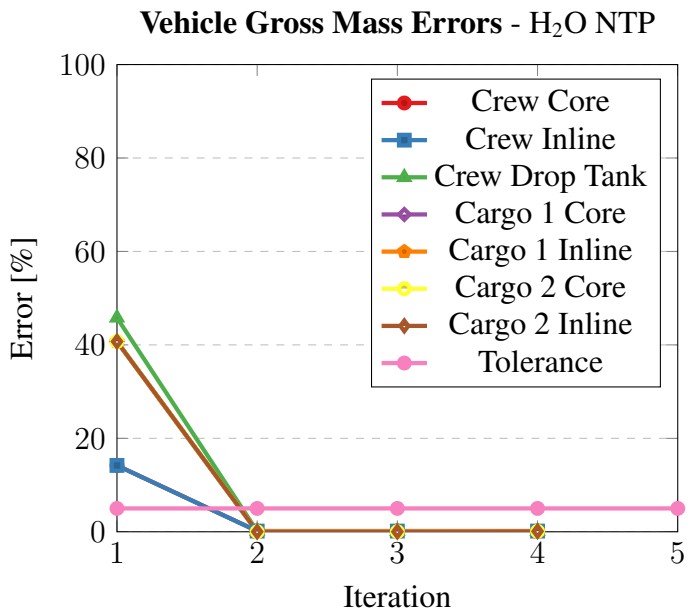

D.2 Campaign-level Trade Study

D.2.1 Long Stay

See Section D.1.

D.2.2 Short Stay

Figure D.7: Errors for the vehicle inert masses per iteration for the LH_2 NTP short stay option.

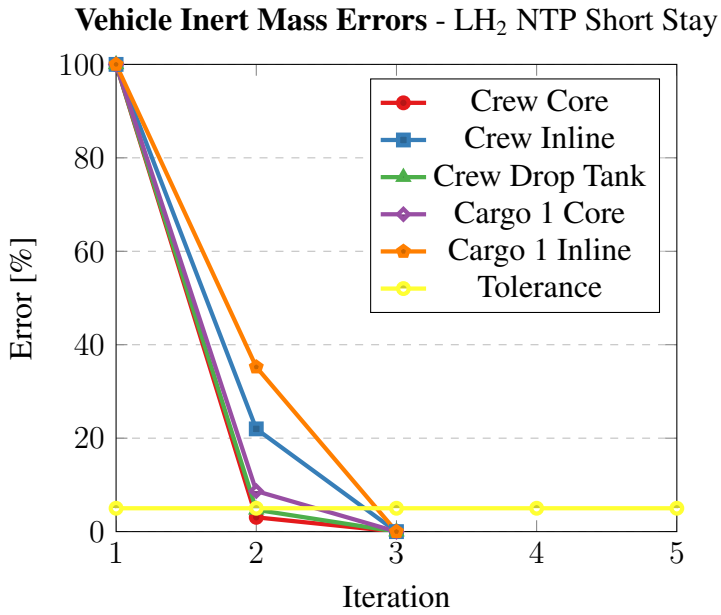

Figure D.8: Errors for the vehicle gross masses per iteration for the LH_2 NTP short stay option.

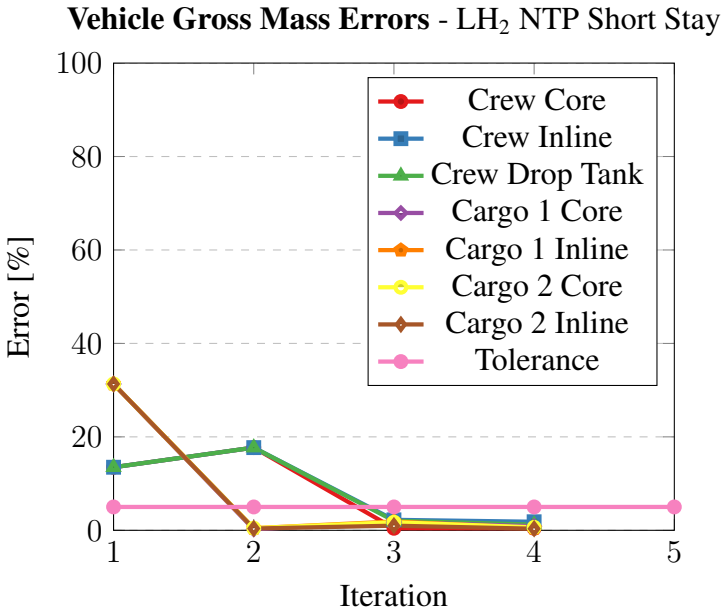

REFERENCES

[1] F. Wild, "What is the international space station," 2020.

[2] D. J. Trump, "Space policy directive 1: Reinvigorating america's human space exploration program," 2017.

[3] K. Northon, "Nasa unveils sustainable campaign to return to moon, on to mars," 2018.

[4] "Forward to the moon: Nasa's stretegic plan for human exploration," 2019.

[5] O. of the Chairman of the Joint Chiefs of Staff, *DOD Dictionary of Military and Associated Terms*. United States Department of Defense, 2021.

[6] M. W. O. Dictionary, *Campaign*. 2021.

[7] *NASA Systems Engineering Handbook*. NASA, 2007.

[8] Mars Architecture Steering Group and B. G. Drake, "Human exploration of mars design reference architecture 5.0," 2009.

[9] H. Price, J. Baker, and F. Naderi, "A minimal architecture for human journeys to mars," *New Space*, vol. 3, no. 2, 2015.

[10] B. Braun, "Investments in our future: Exploring space through innivation and technology," NASA, Tech. Rep., 2011.

[11] C. Lafleur, "Costs of us piloted programs," *The Space Review*, 2010.

[12] T. Heppnheimer, *The Space Shuttle Decision: NASA's Search for a Reusable Space Vehicle*. NASA, 1999.

[13] "Forward to the moon: Nasa's stretegic plan for human exploration," 2019.

[14] "Sls carries deep space potential," 2012.

[15] J. F. Kennedy, *Address to joint session of congress*, 1961.

[16] T. Ishimatsu, O. L. De Weck, J. A. Hoffman, and Y. Ohkami, "Generalized multicommodity network flow model for the earth-moon-mars logistics system," *Journal of Spacecraft and Rockets*, vol. 53, no. 1, pp. 25–38, 2016.

[17] W. M. Cirillo *et al.*, "Strategic Analysis Overview," pp. 1–17, 2006.

[18] D. J. Trent, "Integrated Architecture Analysis and Technology Evaluation for Systems of Systems Modeled at the Subsystem Level," Ph.D. dissertation, 2017.

[19] S. J. Edwards, M. J. Diaz, D. N. Mavris, and D. J. Trent, "A model-based framework for synthesis of space transportation architectures," in *2018 AIAA SPACE and Astronautics Forum and Exposition*, 2018, ISBN: 9781624105753.

[20] *Navigating the twists and turns steering sls development - nasaspaceflight.com*, https://www.nasaspaceflight.com/2018/10/navigating-twists-turns-steering-sls-development/, (Accessed on 04/09/2021).

[21] K. Goodliff, W. Cirillo, B. Mattfeld, C. Stromgren, and H. Shyface, "Comparison of human exploration architecture and campaign approaches," *AIAA SPACE 2015 Conference and Exposition*, pp. 1–21, 2015.

[22] D. C. Arney *et al.*, "Sustaining human presence on mars using isru and a reusable lander," in *AIAA SPACE 2015 Conference and Exposition*. eprint: https://arc.aiaa.org/doi/pdf/10.2514/6.2015-4479.

[23] C. Taylor and O. L. de Weck, "Integrated Transportation System Design Optimization," Ph.D. dissertation, 2007, pp. 1–16.

[24] H. Chen and K. Ho, "Integrated Space Mission Planning and In-Orbit Infrastructure Design with Mixed-Integer Nonlinear Programming," in *AIAA SPACE 2016*, 2016, pp. 1–33.

[25] D. S. F. Portree, "Humans to Mars: Fifty Years of Mission Planning, 1950–2000 127," Tech. Rep. 1970, 2001, pp. 18–19.

[26] A. Platoff, "Eyes on the Red Planet: Human Mars Mission Planning, 1952-1970," Tech. Rep. 1970, 2001.

[27] D. A. Craig, N. B. Herrmann, and P. A. Troutman, "The evolvable mars campaign - study status," in *2015 IEEE Aerospace Conference*, 2015, pp. 1–14.

[28] W. M. Cirillo *et al.*, "Strategic Analysis Overview," Tech. Rep., 2008, pp. 1–17.

[29] W. Cirillo *et al.*, "Analysis of logistics in support of a human lunar outpost," in *7th International Workshop on Modeling and Applied Simulation, MAS 2008, Held at the International Mediterranean Modeling Multiconference, I3M 2008*, 2008, pp. 148–157.

[30] ISECG, "The Global Exploration Strategy : The Framework for Coordination," Tech. Rep. April, 2007, pp. 1–24.

[31] A. S. L. T. Committee, *Space logistics*.

[32] T. E. Harris and F. S. Ross, "Fundamentals of a Method for Evaluating Rail Net Capacities," The RAND Corporation, Santa Monica, CA, Tech. Rep., 1955.

[33] G. B. Dantzig, L. R. Ford, and D. R. Fulkerson, "A Primal-Dual Algorithm," The RAND Corporation, Santa Monica, CA, Tech. Rep., 1956.

[34] *National football league scheduling - gurobi*, (Accessed on 07/29/2021).

[35] R. R. Craig, B. J. Lunday, R. R. Hill, and P. A. Nesbitt, "The military theater distribution network design problem," in *IIE Annual Conference and Expo 2015*, 2015, pp. 28–37, ISBN: 9780983762447.

[36] L. J. Ruckle, "Approaches To Solving the Express Shipment Service Network Design Problem," Ph.D. dissertation, 2018.

[37] D. K. Smith, R. K. Ahuja, T. L. Magnanti, and J. B. Orlin, *Network Flows: Theory, Algorithms, and Applications.* 11. 1994, vol. 45, p. 1340.

[38] B. Chachuat, *Mixed-Integer Linear Programming (MILP): Model Formulation*, 2019.

[39] C. R. Sergeant, M. S. Bazaraa, and J. J. Jarvis, *Linear Programming and Network Flows*, 5. 1978, vol. 29, p. 510, ISBN: 9780470462720.

[40] L. V. Kantorovich, "Mathematical Methods of Organizing and Planning Production," *Management Science*, vol. 6, no. 4, pp. 366–422, 1960.

[41] G. Dantzig, "Linear Programming and Extensions," Tech. Rep. August, 2018.

[42] V. Klee and G. Minty, "How good is the simplex algorithm," 1970.

[43] T. D. Hansen and U. Zwick, "An improved version of the random-facet pivoting rule for the simplex algorithm," in *Proceedings of the Forty-Seventh Annual ACM Symposium on Theory of Computing*, ser. STOC '15, Portland, Oregon, USA: Association for Computing Machinery, 2015, pp. 209–218, ISBN: 9781450335362.

[44] D. Bertsimas and T. J., *Introduction to Linar Optimization*, A. Scientific, Ed. Athena Scientific, 1997.

[45] G. Cornuéjols, *The ongoing story of gomory cuts*, 2012.

[46] R. Gomory, "Outline of an algorithm for integer solutions to linear programs and an algorithm for the mixed integer problem," in Jan. 2010, pp. 77–103, ISBN: 978-3-540-68274-5.

[47] R. Gomory, “An algorithm for the mixed integer problem,” 1960.

[48] ——, “An algorithm for integer solutions to linear programs,” 1958.

[49] R. Gomory, “Early integer programming,” *Operations Research*, vol. 50, pp. 78–81, Feb. 2002.

[50] A. Land and A. Doig, “An automatic method of solving discrete programming problems,” *Econometrica*, vol. 28, p. 497, 1960.

[51] K. Kianfar, “Branch-and-Bound Algorithms,” *Wiley Encyclopedia of Operations Research and Management Science*, no. February, 2011.

[52] H. A. Eiselt and C.-L. Sandblom, “Branch and Bound Methods,” *Integer Programming and Network Models*, pp. 205–228, 2000.

[53] D.-S. Chen, R. Batson, and Y. Dang, “Branch-and-cut approach,” in Sep. 2011, pp. 305–333, ISBN: 9780470373064.

[54] R. Anand, D. Aggarwal, and V. Kumar, “A comparative analysis of optimization solvers,” *Journal of Statistics and Management Systems*, vol. 20, no. 4, pp. 623–635, 2017.

[55] *Gurobi - the fastest solver - gurobi*, https://www.gurobi.com/, (Accessed on 07/10/2021).

[56] *Cplex optimizer — ibm*, https://www.ibm.com/analytics/cplex-optimizer, (Accessed on 07/10/2021).

[57] *Fico xpress solver — optimization solver — fico*, https://www.fico.com/en/products/fico-xpress-solver, (Accessed on 07/10/2021).

[58] D. C. Arney, “Rule-Based Graph Theory to Enable Exploration of the Space System Architecture Design Space,” Ph.D. dissertation, 2012.

[59] O. L. De Weck *et al.*, “SpaceNet v1.3 User’s Guide,” 2007.

[60] T. Ishimatsu, P. Grogan, and O. de Weck, “Interplanetary trajectory analysis and logistical considerations of human mars exploration,” *Journal of Cosmology*, pp. 3588–3600, Jan. 2010.

[61] *Spacenet 2.5*, http://spacenet.mit.edu/spacenet_2-5.php.

[62] K. Ho, O. L. De Weck, J. A. Hoffman, and R. Shishko, "Dynamic modeling and optimization for space logistics using time-expanded networks," *Acta Astronautica*, vol. 105, no. 2, pp. 428–443, 2014.

[63] A. Prasad, M. J. Diaz, and D. N. Mavris, "Integrated framework to enable design space exploration of in-space transportation architectures," in *Accelerating Space Commerce, Exploration, and New Discovery Conference, ASCEND 2020*, 2020, pp. 1–18, ISBN: 9781624106088.

[64] Z. Chen, H. Chen, and K. Ho, "Analytical model of space infrastructure staged deployment strategy in space logistics," *AIAA SPACE and Astronautics Forum and Exposition, SPACE 2017*, no. 203999, 2017.

[65] H. Chen, K. Ho, B. M. Gardner, and P. T. Grogan, "Built-in flexibility for space logistics mission planning and spacecraft design," in *AIAA SPACE and Astronautics Forum and Exposition, SPACE 2017*, 2017, ISBN: 9781624104831.

[66] H. Chen, H. W. Lee, and K. Ho, "Space transportation system and infrastructure design for regular interplanetary cargo missions," in *AIAA SPACE and Astronautics Forum and Exposition, SPACE 2017*, 2017, pp. 1–11, ISBN: 9781624104831.

[67] H. Chen, A. Lapin, C. Lei, K. Ho, and T. Ukai, "Optimization for large-scale multi-mission space campaign design by approximate dynamic programming," *2018 AIAA SPACE and Astronautics Forum and Exposition*, no. September, pp. 1–12, 2018.

[68] H. Chen and K. Ho, "Hierarchical reinforcement learning framework for space exploration campaign design," in *AIAA Propulsion and Energy Forum and Exposition, 2019*, 2019, pp. 1–18, ISBN: 9781624105906.

[69] H. Chen, T. S. du Jonchay, L. Hou, and K. Ho, "Multi-fidelity space mission planning and space infrastructure design framework for space resource logistics," in *AIAA Propulsion and Energy Forum and Exposition, 2019*, 2019, pp. 1–21, ISBN: 9781624105906.

[70] H. Chen, T. Sarton Du Jonchay, L. Hou, and K. Ho, "Multifidelity space mission planning and infrastructure design framework for space resource logistics," *Journal of Spacecraft and Rockets*, vol. 58, no. 2, pp. 538–551, 2021. arXiv: 1910.04265.

[71] K. McBrayer, N. Daniel, M. Deguignet, A. Velte, B. Robertson, and D. N. Mavris, "A network flow-based formulation to optimize campaign alternatives for a reference lunar surface base," in *Proceedings of the International Astronautical Congress, IAC*, vol. 2019-Octob, 2019, pp. 21–25.

[72] J. Bridenstine and B. Gerstenmaier, "HUMAN LANDING SYSTEM BAA INDUSTRY FORUM Agenda Topics Speakers NASA Affiliation Moon to Mars and Human Landing System (HLS) Remarks," Tech. Rep., 2019.

[73] G. Chavers, L. Watson-Morgan, M. Smith, N. Suzuki, and T. Polsgrove, "Nasa's human landing system: The strategy for the 2024 mission and future sustainability," in *2020 IEEE Aerospace Conference*, 2020, pp. 1–9.

[74] M. Isaji, Y. Takubo, and K. Ho, "Multidisciplinary design optimization approach to integrated space mission planning and spacecraft design," *Journal of Spacecraft and Rockets*, vol. 59, no. 5, pp. 1660–1670, 2022. eprint: https://doi.org/10.2514/1.A35284.

[75] M. Mane, W. A. Crossley, and Nusawardhana, "System-of-systems inspired aircraft sizing and airline resource allocation via decomposition," in *Journal of Aircraft*, vol. 44, 2007, pp. 1222–1235.

[76] G. C. Bower and I. M. Kroo, "Multi-objective aircraft optimization for minimum cost and emissions over specific route networks," *8th AIAA Aviation Technology, Integration and Operations (ATIO) Conference*, no. August, 2008.

[77] N. Davendralingam and W. A. Crossley, "Concurrent aircraft design and variable resource allocation in large scale fleet networks," in *9th AIAA Aviation Technology, Integration and Operations (ATIO) Conference, Aircraft Noise and Emissions Reduction Symposium (ANERS)*, 2009, ISBN: 9781563479809.

[78] L. Siqueira, V. Loureiro, and B. Mattos, "The suited airliner for an existing airline network," in *50th AIAA/ASME/ASCE/AHS/ASC Structures, Structural Dynamics, and Materials Conference*. eprint: https://arc.aiaa.org/doi/pdf/10.2514/6.2009-2206.

[79] M. Braun, K. Wicke, A. Koch, and T. Wunderlich, "Analysis of natural laminar flow aircraft based on airline network design and fleet assignment," Sep. 2011.

[80] N. Davendralingam and W. Crossley, "Robust optimization of aircraft design and airline network design incorporating economic trends," in *11th AIAA Aviation Technology, Integration,and Operations (ATIO) Conference, including the AIAA Balloon Systems Conference and 19th AIAA Lighter-Than-Air Technology Conference*, 2011, ISBN: 9781600869419.

[81] ——, "Robust approach for concurrent aircraft design and airline network design," *Journal of Aircraft*, vol. 51, no. 6, pp. 1773–1783, 2014.

[82] J. T. Hwang and J. R. Martins, "Parallel allocation-mission optimization of a 128-route network," 2015.

[83] ——, “Allocation-mission-design optimization of next-generation aircraft using a parallel computational framework,” 2016.

[84] S. Roy and W. A. Crossley, “An EGO-like Optimization Framework for Simultaneous Aircraft Design and Airline Allocation,” 2016.

[85] J. Alexandre, T. G. Fregnani, B. S. De Mattos, and J. A. Hernandes, “An innovative approach for integrated airline network and aircraft family optimization,” *Chinese Journal of Aeronautics*, vol. 33, no. 2, pp. 634–663, 2020.

[86] Y. Choi, “A Framework for Concurrent Design and Route Planning Optimization of Unmanned Aerial Vehicle Based Urban Delivery Systems,” vol. 8, no. 5, p. 55, 2019.

[87] Y. Choi, B. Robertson, Y. Choi, and D. Mavris, “A multi-trip vehicle routing problem for small unmanned aircraft systems-based urban delivery,” *Journal of Aircraft*, vol. 56, no. 6, pp. 2309–2323, 2019. eprint: https://doi.org/10.2514/1.C035473.

[88] R. Bate, D. Mueller, and J. White, *Fundamentals of Astrodynamics*, ser. Dover Books on Aeronautical Engineering Series. Dover Publications, 1971, ISBN: 9780486600611.

[89] Y. Shin, S. Yoon, Y. Seo, H. Jin, and J. Seon, “Radiation effect for a cubesat in slow transition from the earth to the moon,” *Advances in Space Research*, vol. 31, Jan. 2015.

[90] E. M. Ramos, P. Mishra, S. Edwards, and D. Mavris, “Response surface regressions for low-thrust interplanetary mission design,” 2016.

[91] Thomas G. Roberts, *Popular Orbits 101 - Aerospace Security*, 2020.

[92] B. Mattfeld, C. Stromgren, H. Shyface, D. R. Komar, W. Cirillo, and K. Goodliff, “Trades between opposition and conjunction class trajectories for early human missions to mars,” *AIAA SPACE 2014 Conference and Exposition*, pp. 1–17, 2014.

[93] P. D. Wooster, R. D. Braun, J. Ahn, and Z. R. Putnam, “Mission design options for human Mars missions,” *Citation: Mars*, vol. 3, pp. 12–28, 2007.

[94] C. B. Reynolds, C. R. Joyner, T. Kokan, D. J. Levack, and B. J. Musek, “Ntp robustness for mars conjunction and opposition class missions,” *Accelerating Space Commerce, Exploration, and New Discovery Conference, ASCEND 2020*, 2020.

[95] R. C. Woolley and C. W. Whetsel, “On the nature of earth-mars porkchop plots,” *Advances in the Astronautical Sciences*, vol. 148, pp. 413–426, 2013.

[96] L. Hastings, D. Plachta, L. Salerno, and P. Kittel, "An overview of nasa efforts on zero boiloff storage of cryogenic propellants," *Cryogenics*, vol. 41, no. 11, pp. 833–839, 2001, 2001 Space Cryogenics Workshop.

[97] M. Deguignet, "Development of a Methodology for Technology Requirement Assessment for Space Habitats," Ph.D. dissertation, Georgia Institute of Technology, 2020, pp. 1–9, ISBN: 9789896540821.

[98] D. W. Plachta and M. C. Guzik, "Cryogenic boil-off reduction system," *Cryogenics*, vol. 60, pp. 62–67, 2014.

[99] *Nasa has begun a study of the sls rocket's affordability [updated] — ars technica*, https://arstechnica.com/science/2021/03/nasa-has-begun-a-study-of-the-sls-rockets-affordability/, (Accessed on 07/20/2021).

[100] NASA Office of Inspector General, "NASA's Management of Space Launch System Program Costs and Contracts," 2020.

[101] *Capabilities & services*, Released by SpaceX, 2022.

[102] *Starship sn15*, Released by SpaceX, 2022.

[103] *New glenn*, Released by Blue Origin, 2021.

[104] *Space launch system*, NASA Website, 2022.

[105] *Rocket rundown: A fleet overview*, Released by ULA, 2022.

[106] *Closing the Loop: Recycling Water and Air in Space*, 2000.

[107] *Aircraft Engine Design*, June. 2002, ISBN: 9780072483116.

[108] B. Bagdatli, F. Karagoz, K. Reilley, and D. Mavris, "Mbse-enabled interactive environment for aircraft conceptual sizing and synthesis," 2019.

[109] J. Roskam, *Airplane Design: Preliminary sizing of airplanes*. DARcorporation, 1985, ISBN: 9780072483116.

[110] C. A. Perullo, J. Tai, and D. N. Mavris, "A New Sizing and Synthesis Environment for the Design and Assessment of Advanced Hybrid and Electric Aircraft Propulsion Systems," in *22nd International Society for Air Breathing Engines*, 2015.

[111] W. H. Allen, "Dictionary of technical terms for aerospace use," NASA Headquarters, Tech. Rep., 1965.

[112] J. R. Wertz, D. F. Everett, and J. J. Puschell, *Space Mission Engineering: The New SMAD*. 2015, p. 644.

[113] W. J. Larson and L. K. Pranke, *Human Spaceflight : Mission Analysis and Design*. 1999, p. 1035, ISBN: 9780072368116.

[114] C. D. Brown, *Elements of Spacecraft Design*. 2002.

[115] J. M. Lafleur and J. H. Saleh, "GT-FAST: A point design tool for rapid fractionated spacecraft sizing and synthesis," in *AIAA Space 2009 Conference and Exposition*, 2009, ISBN: 9781563479793.

[116] W. Hofstetter and D. Maschinenwesen, "Extensible Modular Landing Systems for Human Moon and Mars Exploration," *Arbeit*, 2004.

[117] J. M. Lafleur, C. I. Restrepo, and M. J. Grant, "Development, structure, and application of MAST: A generic mission architecture sizing tool," in *Collection of Technical Papers - AIAA/ASME/ASCE/AHS/ASC Structures, Structural Dynamics and Materials Conference*, vol. 3, 2006, pp. 1544–1554, ISBN: 1563478080.

[118] *Projects - zero point frontiers corp*, https://www.zeropointfrontiers.com/projects/, (Accessed on 08/03/2021).

[119] D. R. Komar, J. Hoffman, A. Olds, and M. Seal, "Framework for the parametric system modeling of space Exploration Architectures," in *Space 2008 Conference*, 2008, ISBN: 9781563479465.

[120] E. M. Ramos, B. E. Robertson, M. J. Diaz, and D. N. Mavris, "Development of a lunar lander modeling and simulation capability," in *AIAA SCITECH 2022 Forum*. eprint: https://arc.aiaa.org/doi/pdf/10.2514/6.2022-0380.

[121] B. Robertson, E. M. Ramos, M. J. Diaz, and D. Mavris, "A conceptual design study for an unmanned, reusable cargo lunar lander," *Proceedings of the International Astronautical Congress, IAC*, vol. 2019-Octob, no. October, pp. 21–25, 2019.

[122] D. Vallado, *Fundamentals of Astrodynamics and Applications*. 1997.

[123] N. L. Parrish, E. Kayser, S. Udupa, J. S. Parker, B. W. Cheetham, and D. C. Davis, "Survey of ballistic lunar transfers to near rectilinear halo orbit," in *Advances in the Astronautical Sciences*, vol. 171, 2020, pp. 1003–1022, ISBN: 9780877036654.

[124] P. Sloss, "Nasa launch services program outlines the alternative launcher review for em-1," *NASASpaceflight.com*, 2019.

[125] A. R. Collins, "Development of cislunar space logistics networks for satellite constellation support using event-driven generalized multi-commodity network flows," 2019.

[126] S. Zhu, C. Downs, B. E. Robertson, D. N. Mavris, and D. Trent, "Probabilistic modeling of a three-stage human landing system architecture," in *ASCEND 2021*, 2021, p. 4129.

[127] *Propulsion*, European Space Agency Website, 2022.

[128] *Orion*, Released by NASA, 2022.

[129] *Mon/mmh*, Encyclopedia Astronautica Website, 2019.

[130] *Nasa's management of the artemis missions*, Released by NASA Office of the Inspector General, 2021.

[131] B. German, *Multidisciplinary Design Optimization (MDO): Complex Systems and Introduction MDO Problems*, 2017.

[132] B. German and G. Lightsey, "Multidisciplinary Design Optimization (MDO): Single-Level and Multi-Level Methods Single-level MDO Approaches," *AE 6310: Optimization for the Design of Engineered Systems*, 2017.

[133] C. T. Kelley, *Iterative Methods for Linear and Nonlinear Equations*. 1995.

[134] J. V. Lambers, A. S. Mooney, and V. A. Montiforte, "Explorations in numerical analysis: Python edition," *Explorations In Numerical Analysis: Python Edition*, pp. 1–674, 2021.

[135] A. Muhammad and V. Zalizniak, "Solving Nonlinear Equations," in *Practical Scientific Computing*, 2011, pp. 73–88.

[136] A. B. Lambe and J. R. Martins, "Extensions to the design structure matrix for the description of multidisciplinary design, analysis, and optimization processes," *Structural and Multidisciplinary Optimization*, vol. 46, no. 2, pp. 273–284, 2012.

[137] Q. Yin, Y. Wu, and B. Wang, "A Method for Multidisciplinary System Analysis Based on Minimal Feedback Variables," *Mathematical Problems in Engineering*, vol. 2017, 2017.

[138] M. N. Vrahatis, G. D. Magoulas, and V. P. Plagianakos, "From linear to nonlinear iterative methods," in *Applied Numerical Mathematics*, vol. 45, 2003, pp. 59–77.

[139] D. Nikitaev, "In-Situ Alternative Propellants for Nuclear Thermal Propulsion Systems," in *NETS 2021 Conference*, 2021.

[140] A. Irvine, R. Hetterich, S. Edwards, and M. Rodriguez, "Design reference mission development for nuclear thermal propulsion enabled science missions," in *Accelerating Space Commerce, Exploration, and New Discovery Conference, ASCEND 2020*, 2020, ISBN: 9781624106088.

[141] D. C. Arney *et al.*, "The impact of mission duration on a mars orbital mission," in *AIAA SPACE and Astronautics Forum and Exposition, SPACE 2017*, 2017, ISBN: 9781624104831.

[142] J. L. C. Rodríguez *et al.*, *poliastro/poliastro: poliastro 0.17.0 (SciPy US '22 edition)*, version v0.17.0, Jul. 2022.

[143] T. M. Perrin and J. G. Casler, "Architecture study for a fuel depot supplied from lunar resources," in *AIAA SPACE 2016*. eprint: https://arc.aiaa.org/doi/pdf/10.2514/6.2016-5306.

[144] G. R. Cunnington, C. W. Keller, and A. P. M. Glassford, "Thermal performance of multilayer insulations," 2013.

[145] M. Haberbusch, B. Lawless, J. Ickes, and L. Walls, "Reduced gravity cryo-tracker system," in *47th AIAA Aerospace Sciences Meeting including The New Horizons Forum and Aerospace Exposition*. eprint: https://arc.aiaa.org/doi/pdf/10.2514/6.2009-1599.

[146] R. G. Ross and R. F. Boyle, "Nasa space cryocooler programs—an overview," in *Cryocoolers 12*, R. G. Ross, Ed. Boston, MA: Springer US, 2003, pp. 1–8, ISBN: 978-0-306-47919-9.

[147] W. J. L. Ronald W. Humble Gary N. Hendry, *Space Propulsion Analysis and Design*. Learning Solutions, 2007.

[148] D. Trent and S. J. Edwards, "Analysis of alternative architectures for a 2024 lunar sortie," in *ASCEND 2020*. eprint: https://arc.aiaa.org/doi/pdf/10.2514/6.2020-4087.